

AD A115166

DTIC FILE COPY

TECHNICAL REPORT

Volume 1

THE DEVELOPMENT OF PREDICTIVE ENGINEERING FORMULATIONS FOR DIVER HEATING

by

Charles E. Johnson, Ph.D., P.E.

and

James D. Collins, Ph.D.

Department of Mechanical Engineering and Materials Science  
Duke University

and

F.G. Hall Laboratory, Department of Anesthesiology  
Duke University Medical Center

for

Naval Medical Research and Development Command

and

Office of Naval Research

1982

DTIC  
SELECTED  
JUN 7 1982  
H  
DISTRIBUTION STATEMENT A  
Approved for public release  
Distribution Unlimited

82 05 03 024

TECHNICAL REPORT

THE DEVELOPMENT OF PREDICTIVE ENGINEERING FORMULATIONS FOR DIVER HEATING

by

Charles E. Johnson, Ph.D., P.E.

and

James D. Collins, Ph.D.

Department of Mechanical Engineering and Materials Science  
Duke University

and

F.G. Hall Laboratory, Department of Anesthesiology  
Duke University Medical Center

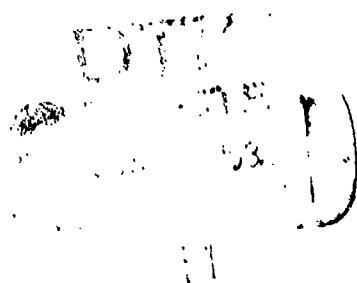
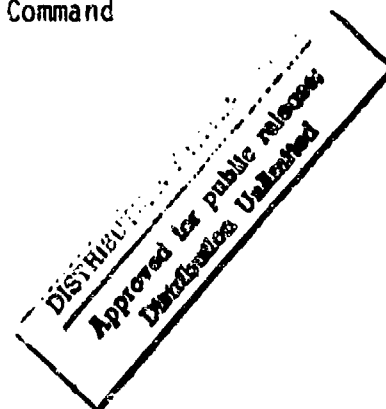
for

Naval Medical Research and Development Command

and

Office of Naval Research

1982



Accession For	
NTIS GRA&I	<input checked="" type="checkbox"/>
DTIC TAB	<input type="checkbox"/>
Unannounced	<input type="checkbox"/>
Justification	<i>for file</i>
By	
Distribution/	
Availability Codes	
Avail and/or	
Dist	Special
<i>A</i>	



# ABSTRACT

Predictive heat transfer equations have been developed to estimate the local supplementary heating necessary to support a resting diver. These formulations consider the diver's passive thermal protection in the form of a diving dress and the effects of his ambient environment upon the dress' thermal resistance. The mathematical model performs a numerical analysis on discrete composite layers comprised of the skin, dry protective suit, breathing gas mixture, and the surrounding fluid environment. The parametric properties associated with the heat transfer correlations were obtained from validated experimental heat flux and skin temperature data collected under specific environmental conditions.

The regional skin temperatures of this model are predicted by using a series of linear algebraic equations which have been derived from those of Kerslake and which predict the segmental skin temperatures of a quasi-euthermic diver having pronounced vasoconstriction. The equations were developed by numerically analyzing twelve segmental skin temperatures recorded from five resting subjects exposed to a 20 °C, 95% helium - 5% oxygen hyperbaric chamber environment pressurized to the equivalent of 200 meters of seawater. The independent variable of the basic correlation is an arbitrarily

defined mean skin temperature. The developed equations were authenticated by comparing the predicted normalized segmental temperature with the respective experimental normalized temperature obtained from several sets of physiological data which were collected during the evaluation of the Naval Coastal System Center's prototype Diver Thermal Protection garment. The results of these comparisons of non-dimensionalized temperatures indicated that the derived correlations should accurately predict the skin temperature of the principal segments as a function of mean skin temperature with a nominal error of no more than 15%.

The supplementary heating that is required to maintain a diver is obtained by determining the heat flux that would be lost were he not heated and subtracting from this the normal heat flux expected from a resting euthermic subject. Applying this principle to each of the regions, it is possible to predict the supplementary heating necessary to compensate for an excessive flux.

The mathematical model was written as an interactive computer program. The program collects information on the diver's posture and the ambient environment, and then generates estimates of the required regional supplementary heating. The program also allows the comparison of predicted temperatures, heat fluxes, overall heat transfer coefficients, normalized temperatures, and Biot numbers to values computed from experimental data.

## FOREWORD

Portions of this report have been excerpted from the original ONR Contract proposal of Dr. Charles E. Johnson and that contract's annual reports for 1980 and 1981. Most of Chapters III-V and part of Chapter VII have been presented at scientific meetings of the Undersea Medical Society and the American Society of Mechanical Engineers. The predictive skin temperature model (Chapter IV) was published in May of 1982 in Undersea Biomedical Research and the overall heat loss model is summarized in a paper accepted for publication in 1982 by the Journal of Biomechanical Engineering, a transaction of the American Society of Mechanical Engineers. This document, with the exception of the Addendum: Mixed Breathing Gas Interactive Model Program, was presented as the dissertation of James D. Collins in partial fulfillment of the requirements for the degree of Doctor of Philosophy in the Department of Mechanical Engineering and Materials Science in the Graduate School of Duke University.

Several terms which are used throughout this document have specially intended connotations. These terms are defined on the following pages for the benefit of the reader.

### Segment

Segment or segments is used when describing the twelve body segments (Fig. 2). Whenever segment appears in the text, it refers to these twelve body segments.

### Region

Region is used to describe the nine model man regions (Fig. 1) throughout all chapters, except Chapter IV where it is also used to describe Kerslake's eight regions. In general, any references to regions(s) refer to the nine region model man of Figure 1.

### Rate of Heat Loss/Flow

Rate of heat loss or flow is used to imply watts (joules/sec). Any reference to a rate of heat loss should be associated with the units of watts.

### Heat Flux

Heat flux refers to the rate of heat loss per unit of area ( $W/m^2$ ).

## Time Record

Time record is used to refer to the time moment associated with a single data event in the experimental data files. Each time record contains the event time, twelve segmental rates of heat loss or heat fluxes, twelve associated temperatures, and the ambient and rectal temperatures. (See Appendix A for details.).

## File

File refers to the individual experimental data files of Tables 2-4 (Chapter II). Each file contains multiple time records and represents a complete experiment. File is used to refer to both the individual subject and the composite subject data files.

We have conducted a comparative mathematical investigation of limited experimental data of skin temperature and heat flux obtained from subjects in various environments and states of thermal equilibrium. Except to delete obviously incongruous data points, the data that we used was accepted as being correct. The reader is referred to the Naval Medical Research and Development Command's Scientific Protocol for the Conduct of Thermal Physiology Experiments on Divers for a discussion of the potential error associated with diver thermal physiology experiments. Our investigation resulted in the proposed correlations to predict supplemental heating requirements to maintain

1

a resting subject in a state of euthermia in any ambient environment. The work is based upon the hypothesis of extrapolating empirical heat transfer formulations that are developed from known experimental data of one environment to another environment. This is an accepted modeling technique utilized with dimensionless heat transfer correlations that are derived from experimental studies and is a simpler alternative to modeling the entire thermal regulatory system.

This is not a definitive treatise of the topic, rather it is an introduction to the concept of developing empirical supplementary heating correlations for divers from experimental studies of diver heat loss and protective garment evaluations. We expect that the correlations suggested herein will be improved in accuracy as additional experimental data becomes available and that, ultimately, the technique will be extended for working divers when suitably controlled experiments have been conducted. Until these additional experimental studies are conducted, we recommend that the equations presented in this report be used by an engineer who is designing a regionally heated thermal protection garment for a resting diver.

Charles E. Johnson

James D. Collins

## ACKNOWLEDGMENTS

The research reported herein has been supported under Office of Naval Research Contract N00014-79-C-0379 with funds provided by the Naval Medical Research and Development Command (NMRDC). Personal thanks are extended to the consecutive Submarine and Diving Medicine Program Managers of NMRDC Captain James Vorosmarti, Jr., (MC)USN, and Captain Kristopher Greene, (MC)USN, for their interest and support of this research topic.

It would not have been possible to conduct the research reported herein without the assistance and cooperation of a number of people and organizations. Among the many people who have provided assistance, we would like to extend special thanks to the following:

Dr. Marshall L. Nuckols, Naval Coastal Systems Center, for the time he spent arranging our acquisition of the prototype Diver Thermal Protection garment evaluation studies and for personal consultations about the execution of the experimental studies. We also thank Dr. Nuckols for arranging an August 1980 visit of James D. Collins to the Navy Experimental Diving Unit of Panama City, Florida for the purpose of witnessing a Diver Thermal Protection garment evaluation study.

Dr. Claude Piantadosi for providing the respiratory heat loss studies that he performed while attached to the Navy Experimental Diving Unit of Panama City, Florida. Dr. Piantadosi was also extremely helpful in explaining the physiological phenomenon which are associated with this recorded skin temperature and heat flux data.

Mr. Shiangtai Tuan of the Duke University Computation Center, Mr. Steve Vickery of the Navy Experimental Diving Unit, and Dr. Larry Burton and Ms. Karen Shephard of the Department of Anesthesiology, Duke University Medical Center, for their help in the transfer of data files from the Navy Experimental Diving Unit's Hewlett-Packard 21MX computer to the Department of Anesthesiology's Digital Equipment Corporation 11/60 computer. We extend additional thanks to Ms. Karen Shephard for her help in our interacting with the Department of Anesthesiology's computer system.

Ms. Judy Milne and Ms. Melodie Feather for their time spent in entering and verifying the prototype Diver Thermal Protection garment data. Ms. Melodie Feather also typed and proofed this document and contributed many valuable editorial suggestions.

Cdr. John Zumrick (MC)USN of the Navy Experimental Diving Unit and Mr. Max Lippitt of the Naval Coastal Systems Center for the information they provided during the visit to the Navy Experimental Diving Unit in August 1980. Additional thanks are extended to Dr. Zumrick for acting as the official sponsor of this visit.

We are also very appreciative of the continued support of the following organizations:

The staff of the F.G. Hall Environmental Laboratory, Duke University Medical Center

The staff of the Department of Anesthesiology, Duke University Medical Center, especially the Anesthesiology computer group

The staff of the Department of Mechanical Engineering and Materials Science, especially Mrs. Pauline M. Roberts for editorial assistance in the preparation of reports and manuscripts

## TABLE OF CONTENTS

	<u>Page</u>
ABSTRACT	ii
FOREWORD	iv
ACKNOWLEDGMENTS	viii
LIST OF TABLES	xiii
LIST OF FIGURES	xviii
CHAPTERS	
I. INTRODUCTION	2
Problem Background, 2	
Objective, 4	
Approach, 4	
II. AVAILABLE EXPERIMENTAL DATA AND METHODS OF ANALYSIS APPLIED	14
Generation of an Example Average Subject File, 21	
Description of Data Groups, 75	
Summary, 83	
III. DEVELOPMENT OF THE DIVER MODEL	85
The Physical Model, 85	
The Model and Its Solution, 96	
IV. DEVELOPMENT OF PREDICTIVE SKIN TEMPERATURE CORRELATION	94
Development of Equations, 97	
Authentication of the Model, 119	

(Table of Contents, continued)

	<u>Page</u>
V. DEVELOPMENT OF OVERALL HEAT TRANSFER COEFFICIENT	132
Resistance of the Outer Boundary Layer, 133	
Undergarment Thermal Resistance, 142	
VI. THE INTERACTIVE MODEL PROGRAM	152
Main Program, 156	
REINIT, 157	
OHTC, 157	
F(T), 158	
CHTC, 159	
TR, 163	
PRED, 163	
TC, 163	
PLOTD, 164	
PLOTN, 164	
VII. MODEL VERIFICATION, CONCLUSIONS, AND RECOMMENDATION	166
Empirical Correlation of the Model, 166	
Discussion and Recommendation, 174	
APPENDICES	
A. ORGANIZATION OF THE DIRECT ACCESS EXPERIMENTAL DATA FILES	182
B. COMPOSITE DATA FILE LISTINGS FOR FILES RHL1AR1, DTP1ART, DTP2AR1, AND DTP3AR1	184
C. DETERMINATION OF THE VISCOSITY ( $\mu$ ), THERMAL CONDUCTIVITY (k), AND OTHER PROPERTIES FOR A 95% HELIUM - 5% OXYGEN GAS MIXTURE	205
D. INTERACTIVE PROGRAM DOCUMENTATION	213
E. INTERACTIVE PROGRAM FLOW CHART	269
F. INTERACTIVE PROGRAM LISTING	303
G. SAMPLE CALCULATION	344
REFERENCES	366
ADDENDUM: MIXED BREATHING GAS INTERACTIVE MODEL PROGRAM	371

# LIST OF TABLES

<u>Number</u>	<u>Title</u>	<u>Page</u>
1	Indices, Nomenclature, Abbreviations, and Surface Area Fractions for Hody's Twelve Segment Map	12
2	Respiratory Heat Loss Studies (RHL)	16
3	Diver Thermal Protection Garment Evaluations	17
4	Diver Thermal Protection Garment Evaluations	18
5	Model Man Dimensions	87
6	Comparison of Model Man and Hody's Man Regional Surface Area Percents	88
7	Kerslake's Curve Fitting Coefficients $A_i$	95
8	Comparison of Composite Experimental Temperatures Extracted From Figures 52-63 With Those Predicted With Kerslake's Equation (Eq. 7)	114
9	Comparison of Composite Experimental Temperatures Estimated by Means of Respective Linear Regression Equations Which Were Derived From Figures 52-63 With Those Predicted With Kerslake's Equation (Eq. 7)	115
10	Distribution Fractions for Predictive Skin Temperature Correlations	118
11	Percentage of the Total Number of Compared Points (56) Over the Span of 35 to 90 Minutes Which Have Absolute Temperature Differences $\leq 0.50^\circ\text{C}$ and $\leq 0.25^\circ\text{C}$	121

(List of Tables, continued)

<u>Number</u>	<u>Title</u>	<u>Page</u>
12	Time Averaged (Mean) Normalized Temperatures for Each of Hody's Twelve Segments Computed From the Mean Temperature Profiles of Experimental File RHL1AR1 and the Equivalent Predicted Normalized Temperature Which was Estimated by Equations 10 and 11	124
13	Time Averaged (Mean) Normalized Temperatures for Each of Hody's Twelve Segments Computed From the Mean Temperature Profiles of Experimental File DTP1ART and the Equivalent Predicted Normalized Temperature Which was Estimated by Equations 10 and 11	125
14	Time Averaged (Mean) Normalized Temperatures for Each of Hody's Twelve Segments Computed From the Mean Temperature Profiles of Experimental File DTP2AR1 and the Equivalent Predicted Normalized Temperature Which was Estimated by Equations 10 and 11	126
15	Time Averaged (Mean) Normalized Temperatures for Each of Hody's Twelve Segments Computed From the Mean Temperature Profiles of Experimental File DTP3AR1 and the Equivalent Predicted Normalized Temperature Which was Estimated by Equations 10 and 11	127
16	Model Man Region Names, Indices, and Corresponding Hody Segments	131
17	Empirical Convective Heat Transfer Correlations	141
18	Regional Allowable Heat Fluxes	154
19	$\alpha$ as a Function of Temperature	161
20	Thermal Conductivity of Water as a Function of Temperature	162
21	Time Averaged (Mean) Biot Numbers for Each Model Region (Fig. 1) Computed From the Composite Profiles of Experimental File DTP1ART and the Equivalent Predicted Biot Number	170
22	Time Averaged (Mean) Biot Numbers for Each Model Region (Fig. 1) Computed From the Composite Profiles of Experimental File DTP2AR1 and the Equivalent Predicted Biot Number	171

(List of Tables, continued)

<u>Number</u>	<u>Title</u>	<u>Page</u>
23	Time Averaged (Mean) Biot Numbers for Each Model Region (Fig. 1) Computed From the Composite Profiles of Experimental File DTP3AR1 and the Equivalent Predicted Biot Number	172
24	Mean Experimental and Predicted Biot Numbers Averaged From the Respective Biot Numbers of Tables 21, 22, and 23 From Files DTP1ART, DTP2AR1, and DTP3AR1, Respectively	173
25	Geometrical Data for the Thigh	177
B.1.A	Temperature C RHL1AR1	185
B.1.B	Rate of Heat Loss (Watts) RHL1AR1	188
B.2.A	Temperature C DTP1ART	191
B.2.B	Rate of Heat Loss (Watts) DTP1ART	193
B.3.A	Temperature C DTP2AR1	195
B.3.B	Rate of Heat Loss (Watts) DTP2AR1	197
B.4.A	Temperature C DTP3AR1	199
B.4.B	Rate of Heat Loss (Watts) DTP3AR1	202
C.1	Critical and Reduced Properties, and Compressibility Factor Values for a 95% Helium - 5% Oxygen Mixture at 295.30 °K and 20.89 ATA	206
C.2	Properties Substituted into Equations C.5 and C.6 for a 95% Helium - 5% Oxygen Mixture at 295.3 °K and 307.0 PSIA	209
C.3	Properties for Equations C.7 and C.8 for a 95% Helium - 5% Oxygen Mixture at 295.3 °K and 307.0 PSIA	211
C.4	Properties Necessary to Determine Grashof, Prandtl, and Nusselt Numbers for a 95% Helium - 5% Oxygen Mixture at 22.15 °C and 200 MSW	212
D.1	Production Mode Question Flow	233
D.2	Sample Production Mode Output	233

(List of Tables, continued)

<u>Number</u>	<u>Title</u>	<u>Page</u>
D.3	Research Mode Question Flow	234
D.4	Sample Research Mode Output	235
D.5	Experimental (T-EXPT) and Predicted (T-PRED) Temperature Values ( $^{\circ}\text{C}$ ) as a Function of Time as Plotted in Figure D.1	238
D.6	Experimental (Q-EXPT) and Uncorrected Predicted (Q-PRED) Heat Flux Values ( $\text{W}/\text{M}^2$ ) as a Function of Time as Plotted in Figure D.2	241
D.7	Experimental (U-EXPT) and Uncorrected Predicted (U-PRED) Overall Heat Transfer Coefficient Values ( $\text{W}/\text{M}^2\text{C}$ ) as a Function of Time as Plotted in Figure D.3	244
D.8	Experimental (TN-EXPT) and Predicted (TN-PRED) Normalized Temperature Values (Dimensionless) as a Function of Time as Plotted in Figure D.4	247
D.9	Experimental (BI-EXPT) and Uncorrected Predicted (BI-PRED) Biot Number Values (Dimensionless) as a Function of Time as Plotted in Figure D.5	250
D.10	Sample Research Mode Output With Corrected Overall Heat Transfer Coefficients	253
D.11	Experimental (T-EXPT) and Predicted (T-PRED) Temperature Values ( $^{\circ}\text{C}$ ) as a Function of Time as Plotted in Figure D.6	256
D.12	Experimental (Q-EXPT) and Corrected Predicted (Q-PRED) Heat Flux Values ( $\text{W}/\text{M}^2$ ) as a Function of Time as Plotted in Figure D.7	259
D.13	Experimental (U-EXPT) and Corrected Predicted (U-PRED) Overall Heat Transfer Coefficient Values ( $\text{W}/\text{M}^2\text{C}$ ) as a Function of Time as Plotted in Figure D.8	262
D.14	Experimental (TN-EXPT) and Predicted (TN-PRED) Normalized Temperature Values (Dimensionless) as a Function of Time as Plotted in Figure D.9	265

(List of Tables, continued)

<u>Number</u>	<u>Title</u>	<u>Page</u>
D.15	Experimental (BI-EXPT) and Corrected Predicted (BI-PRED) Biot Number Values (Dimensionless) as a Function of Time as Plotted in Figure D.10	268
G.1	A Production Mode Output Enhanced With Debug Information	345
G.2	Question Flow for Generation of Table G.1	346

## LIST OF FIGURES

<u>Number</u>	<u>Title</u>	<u>Page</u>
1	Average Diver Modeled as Connected Cylinders and Spheres	8
2	Hody's Twelve Segments	11
3	Segmental Subject Temperature Profiles for the Head (HEAD)	24
4	Segmental Subject Temperature Profiles for the Chest (CHST)	25
5	Segmental Subject Temperature Profiles for the Abdomen (ABD)	26
6	Segmental Subject Temperature Profiles for the Upper Back (UBAC)	27
7	Segmental Subject Temperature Profiles for the Lower Back (LBAC)	28
8	Segmental Subject Temperature Profiles for the Arm (ARM)	29
9	Segmental Subject Temperature Profiles for the Hand (WRST)	30
10	Segmental Subject Temperature Profiles for the Front Thigh (F-TH)	31
11	Segmental Subject Temperature Profiles for the Front Calf (FCLF)	32
12	Segmental Subject Temperature Profiles for the Rear Thigh (R-TH)	33

(List of Figures, continued)

<u>Number</u>	<u>Title</u>	<u>Page</u>
13	Segmental Subject Temperature Profiles for the Rear Calf (RCLF)	34
14	Segmental Subject Temperature Profiles for the Foot (FOOT)	35
15	Segmental Subject Rate of Heat Loss Profiles for the Head (HEAD)	37
16	Segmental Subject Rate of Heat Loss Profiles for the Chest (CHST)	38
17	Segmental Subject Rate of Heat Loss Profiles for the Abdomen (ABD)	39
18	Segmental Subject Rate of Heat Loss Profiles for the Upper Back (UBAC)	40
19	Segmental Subject Rate of Heat Loss Profiles for the Lower Back (LBAC)	41
20	Segmental Subject Rate of Heat Loss Profiles for the Arm (ARM)	42
21	Segmental Subject Rate of Heat Loss Profiles for the Hand (WRST)	43
22	Segmental Subject Rate of Heat Loss Profiles for the Front Thigh (F-TH)	44
23	Segmental Subject Rate of Heat Loss Profiles for the Front Calf (FCLF)	45
24	Segmental Subject Rate of Heat Loss Profiles for the Rear Thigh (R-TH)	46
25	Segmental Subject Rate of Heat Loss Profiles for the Rear Calf (RCLF)	47
26	Segmental Subject Rate of Heat Loss Profiles for the Foot (FOOT)	48
27	Segmental Subject-Averaged Temperature Profile for the Head (HEAD)	50

(List of Figures, continued)

<u>Number</u>	<u>Title</u>	<u>Page</u>
28	Segmental Subject-Averaged Temperature Profile for the Chest (CHST)	51
29	Segmental Subject-Averaged Temperature Profile for the Abdomen (ABD)	52
30	Segmental Subject-Averaged Temperature Profile for the Upper Back (UBAC)	53
31	Segmental Subject-Averaged Temperature Profile for the Lower Back (LBAC)	54
32	Segmental Subject-Averaged Temperature Profile for the Arm (ARM)	55
33	Segmental Subject-Averaged Temperature Profile for the Hand (WRST)	56
34	Segmental Subject-Averaged Temperature Profile for the Front Thigh (F-TH)	57
35	Segmental Subject-Averaged Temperature Profile for the Front Calf (FCLF)	58
36	Segmental Subject-Averaged Temperature Profile for the Rear Thigh (R-TH)	59
37	Segmental Subject-Averaged Temperature Profile for the Rear Calf (RCLF)	60
38	Segmental Subject-Averaged Temperature Profile for the Foot (FOOT)	61
39	Segmental Subject-Averaged Rate of Heat Loss Profile for the Head (HEAD)	63
40	Segmental Subject-Averaged Rate of Heat Loss Profile for the Chest (CHST)	64
41	Segmental Subject-Averaged Rate of Heat Loss Profile for the Abdomen (ABD)	65
42	Segmental Subject-Averaged Rate of Heat Loss Profile for the Upper Back (USAC)	66

(List of Figures, continued)

<u>Number</u>	<u>Title</u>	<u>Page</u>
43	Segmental Subject-Averaged Rate of Heat Loss Profile for the Lower Back (LBAC)	67
44	Segmental Subject-Averaged Rate of Heat Loss Profile for the Arm (ARM)	68
45	Segmental Subject-Averaged Rate of Heat Loss Profile for the Hand (WRST)	69
46	Segmental Subject-Averaged Rate of Heat Loss Profile for the Front Thigh (F-TH)	70
47	Segmental Subject-Averaged Rate of Heat Loss Profile for the Front Calf (FCLF)	71
48	Segmental Subject-Averaged Rate of Heat Loss Profile for the Rear Thigh (R-TH)	72
49	Segmental Subject-Averaged Rate of Heat Loss Profile for the Rear Calf (RCLF)	73
50	Segmental Subject-Averaged Rate of Heat Loss Profile for the Foot (FOOT)	74
51	Vertical Cylindrical Region Divided into Five Nodes (j=5)	90
52	Segmental Temperature Profile for the Head (HEAD) and the Body Mean Skin Temperature (HMST)	100
53	Segmental Temperature Profile for the Chest (CHST) and the Body Mean Skin Temperature (HMST)	101
54	Segmental Temperature Profile for the Abdomen (ABD) and the Body Mean Skin Temperature (HMST)	102
55	Segmental Temperature Profile for the Upper Back (UBAC) and the Body Mean Skin Temperature (HMST)	103
56	Segmental Temperature Profile for the Lower Back (LBAC) and the Body Mean Skin Temperature (HMST)	104
57	Segmental Temperature Profile for the Arm (ARM) and the Body Mean Skin Temperature (HMST)	105

(List of Figures, continued)

<u>Number</u>	<u>Title</u>	<u>Page</u>
58	Segmental Temperature Profile for the Hand (WRST) and the Body Mean Skin Temperature (HMST)	106
59	Segmental Temperature Profile for the Front Thigh (F-TH) and the Body Mean Skin Temperature (HMST)	107
60	Segmental Temperature Profile for the Front Calf (FCLF) and the Body Mean Skin Temperature (HMST)	108
61	Segmental Temperature Profile for the Rear Thigh (R-TH) and the Body Mean Skin Temperature (HMST)	109
62	Segmental Temperature Profile for the Rear Calf (RCLF) and the Body Mean Skin Temperature (HMST)	110
63	Segmental Temperature Profile for the Foot (FOOT) and the Body Mean Skin Temperature (HMST)	111
64	Linearized Abdominal (ABD) and Body Mean Skin (HMST) Temperatures	113
65	Log of Nusselt Number Versus Log of Grashof Number and Prandtl Number Product for Vertical Cylinder	136
66	Log of Nusselt Number Versus Log of Grashof Number and Prandtl Number Product for Horizontal Cylinder	137
67	Log of Nusselt Number Versus Log of Grashof Number and Prandtl Number Product for Sphere	138
68	Linear Relationship Describing the Undergarment's Specific Thermal Resistance Change as a Function of Change in Thickness	145
69	Percent Change in Thickness as a Function of Compressive Pressure	148
70	Percent Change in Thermal Resistance as a Function of Compressive Pressure	149
71	Lateral Mid-lines for Horizontal Cylinder and Sphere	153
72	Single Nodal Element for a Vertical Body Region and Multi-nodal Element for a Vertical Body Region	155
73	Representative Region Presented as a Truncated Cone	178

(List of Figures, continued)

<u>Number</u>	<u>Title</u>	<u>Page</u>
D.1	Plots of Experimental (T-EXPT) and Predicted (T-PRED) Temperatures ( $^{\circ}\text{C}$ ) for the Abdomen	237
D.2	Plots of Experimental (Q-EXPT) and Uncorrected Predicted (Q-PRED) Heat Flux ( $\text{W}/\text{M}^2$ ) for the Abdomen	240
D.3	Plots of Experimental (U-EXPT) and Uncorrected Predicted (U-PRED) Overall Heat Transfer Coefficient (OHTC in $\text{W}/\text{M}^2\text{C}$ ) for the Abdomen	243
D.4	Plots of Experimental Normalized (TN-EXPT) and Predicted Normalized (TN-PRED) Temperatures for the Abdomen	246
D.5	Plots of Experimental Biot (BI-EXPT) and Uncorrected Predicted Biot (BI-PRED) Numbers for the Abdomen	249
D.6	Plots of Experimental (T-EXPT) and Predicted (T-PRED) Temperatures ( $^{\circ}\text{C}$ ) for the Abdomen	255
D.7	Plots of Experimental (Q-EXPT) and Corrected Predicted (Q-PRED) Heat Flux ( $\text{W}/\text{M}^2$ ) for the Abdomen	258
D.8	Plots of Experimental (U-EXPT) and Corrected Predicted (U-PRED) Overall Heat Transfer Coefficient (OHTC in $\text{W}/\text{M}^2\text{C}$ ) for the Abdomen	261
D.9	Plots of Experimental Normalized (TN-EXPT) and Predicted Normalized (TN-PRED) Temperatures for the Abdomen	264
D.10	Plots of Experimental Biot (BI-EXPT) and Corrected Predicted Biot (BI-PRED) Numbers for the Abdomen	267

1

THE DEVELOPMENT OF PREDICTIVE ENGINEERING FORMULATIONS FOR DIVER HEATING

## CHAPTER I

### INTRODUCTION

#### Problem Background

There is virtually no situation in manned hyperbaric or hydrostatic operations where the effects of metabolic heat loss are not present. The extent and effect of metabolic heat loss from divers in various operational environments from temperate to arctic water conditions are highly documented [1-5]. The problems associated with cold and its physiological and psychological impairments are common to all forms of diving: salvage, free-swimming special warfare, tethered deep ocean, and surface supplied shallow water. Fatal mishaps in diving operations such as the Sealab III and the Link tragedies only remind us of the insidious influence of cold temperatures in the alien sea.

Scientists have been studying these problems for many years. As early as 1966, attempts were made to develop analytical models of the human thermal regulatory system [6,7]. In 1971 Payne and Austin [8] proposed a set of design guidelines for the thermal protection of divers. In 1976 the advisory and review group which evaluated thermal problems for the National Plan for

the Safety and Health of Divers in the Quest for Subsea Energy [9] placed the the highest priority on research involved in the prediction of and compensation for diver heat loss under various marine conditions. The primary recommendation of this committee was to establish a set of interim guidelines for human tolerance in hyperbaric conditions based upon a review of the existing literature. This was accomplished by Webb et al. [10] in 1976, with a revision appearing in 1980 [11]. However, both of these proposed guidelines for diver safety are expressed in purely physiological terms of maximum allowable heat loss quanta and minimum allowable skin temperatures and, thus, do not readily lend themselves to use by a designer of diver thermal protection equipment.

The second recommendation of the thermal committee for the National Plan [9] suggested a complete experimental and analytical study which would consist of:

A. A serious study of skin and respiratory heat exchange in divers to provide data that would be useful both operationally and in the design of thermal protection equipment. This data would perhaps enable the establishment of thermal limits for depth or duration of exposure either in water or in dry habitats.

B. An analytical approach to devise predictive equations based on accurate heat transfer data so that body heat loss and temperature can be predicted for any environment. A well-organized and comprehensive experimental program to develop and test such predictive equations is needed.

## Objective

The objective of this research has been to develop formulations for predicting the regional supplementary heating required to maintain a resting, nearly euthermic diver. Assuming that the respiratory heat loss is conserved, we hypothesized that the regional supplementary heating requirement could be estimated as the difference between the mandatory regional heat flux<sup>1</sup> due to metabolism and that predicted for an unheated immersed diver. Furthermore, we assumed that the predictive correlations for the regional heat flux could be developed by utilizing an overall heat transfer coefficient to describe the thermal behavior of the garment ensemble. We hypothesized that this coefficient could be developed by considering: a) the response of the garment's insulating materials to compression [12] and permeation [13] with conventional breathing gases and b) the geometrical parameters of individual body regions associated with three specific postures: standing, sitting, and prone. Pursuing the expressed hypothesis, we postulated that the resultant predictive correlations for diver regional heat flux could be corrected by using an empirically derived biasing factor. This factor would be obtained by comparing the respective predicted overall heat transfer coefficient with mean experimental values obtained from the U.S. Navy's prototype Diver Thermal Protection (DTP) garment evaluation studies.

## Approach

Traditionally, mathematical models attempting to predict physiological heat loss consider segments of the human body as cylindrical elements (head,

---

<sup>1</sup>See Foreword for connotations of region and heat flux.

torso, upper arm, lower arm, hand, thigh, etc). In the case of the immersed diver, heat is considered to be lost from the cylindrical surfaces, predominantly by convection. Metabolic heat is generated within the mass of each segment and is exchanged among the elemental cylinders by means of a modeled circulatory system. A portion of this heat is transported to the cylindrical surface by conduction through the tissue and by convective transport through a local circulatory system [6,7]. The various modes of transport approximating the physiological heat exchange process are interrelated by heat and mass transfer balances. The coefficients of local metabolic heat generation, tissue conductance, and circulatory transport are either arbitrarily assumed or empirically derived in such equations. Some progress has been made in identifying these parameteric coefficients by comparing the model to experimental data [14]. Body temperature and heat flux may then be predicted for conditions analogous to the experimental situation.

The accuracy of the discussed type of physiological heat exchange model is highly dependent upon the selection of heat distribution, transport, and generation parameters. However, these parameters vary quite significantly as a function of the state of thermal regulation, metabolic activity, and body region. For instance, tissue thermal conductance may vary by a factor of fifteen between the states of vasodilation and vasoconstriction [15]. Even the application of hot and cold stimuli to the peripheral limbs has been observed to cause changes in the vasomotor state of the upper respiratory system [16-18]. Thus, we infer that the variation of tissue conductance and the transport of heat by the local inter-regional circulation are quite difficult to predict as a function of either the thermal environment or some metabolic indicator (e.g., skin temperature or local heat flux).

A simpler alternative to modeling the entire thermal regulatory system and the thermal resistance imposed by the garment is to model only the heat

flux through the insulative garment. The thermal resistance imposed by this garment is a function of the ambient environment and the thermal state of the subject as reflected at the skin surface of each region. This concept relies heavily upon existing experimental data of regional skin temperature and heat flux obtained from subjects in various ambient environments and states of thermal equilibrium. Through a comparative mathematical analysis, the regional heat flux correlations would be developed. The predicted regional heat flux would then be used to estimate the regional supplementary heating required to maintain a subject in a state of eutheria. These heat fluxes could also be employed to predict the most prudent distribution of a limited amount of available supplementary heating while considering the limited heat conserving mechanisms of the human.

As noted above, this simpler approach relies heavily upon existing experimental data. An extensive search was performed to identify sources of experimental regional skin temperature and heat flux data. Unfortunately, the data available in the open literature was determined to be of limited value since most of the data is presented in terms of mean skin temperatures rather than the desired regional values or is presented in terms of experimental regional temperatures and computed, not experimental, heat fluxes. This lack of suitable regional experimental temperatures and heat fluxes prompted our requests to the U.S. Navy for diver experimental data recorded with calibrated instrumentation certified by the principal investigator. This request for only investigator certified instrumentation resulted from questions concerning the accuracy of certain commonly used heat flux transducers when only the manufacturer's calibration was employed [19,20]. Our request to the U.S. Navy identified two types of experimental studies. The first set of studies was performed by the Navy Experimental Diving Unit to investigate respiratory heat loss in a hyperbaric environment [21]. Sitting, nearly nude subjects were

exposed to hyperbaric helium-oxygen environments at a depth equivalent to 200 meters of seawater (MSW). These experiments consisted of resting dives at 15 °C and 20 °C ambient gas temperatures and working dives in a 20 °C environment.

The second series of studies was performed by the Naval Coastal Systems Center (NCSC), in conjunction with NEDU, to evaluate the Navy's prototype Diver Thermal Protection (DTP) garment [22]. Data of segmental<sup>2</sup> skin temperature and heat flux were recorded from prone immersed subjects breathing compressed air. This data was collected at two different depths, 3 and 21 meters but at essentially the same ambient temperature, 5 °C. During all of the experiments, the dry DTP garment was pressure compensated with compressed air.

The experimental data has been utilized to develop a model, in accordance with the stated hypothesis, for predicting regional heat flux and required supplementary heating. The modeled diver is comprised of connected cylinders for all regions except the head and hands which are treated as spheres (Fig. 1). The dimensions of this nine region man were selected to approximate those of the standard U.S. Air Force man [23] and to produce surface area fractions equivalent to the respective coefficients of the Hody mean skin temperature correlation [24,25].

Equation 1 estimates the regional rate of heat loss based on the regional skin surface area ( $S_i$ ), overall heat transfer coefficient ( $U_i$ ), and temperature difference between the skin surface ( $T_i$ ) and ambient ( $T_a$ ) temperatures.

$$\dot{Q}_i = U_i S_i (T_i - T_a) \quad (1)$$

---

<sup>2</sup>See Foreword for connotation of segment.

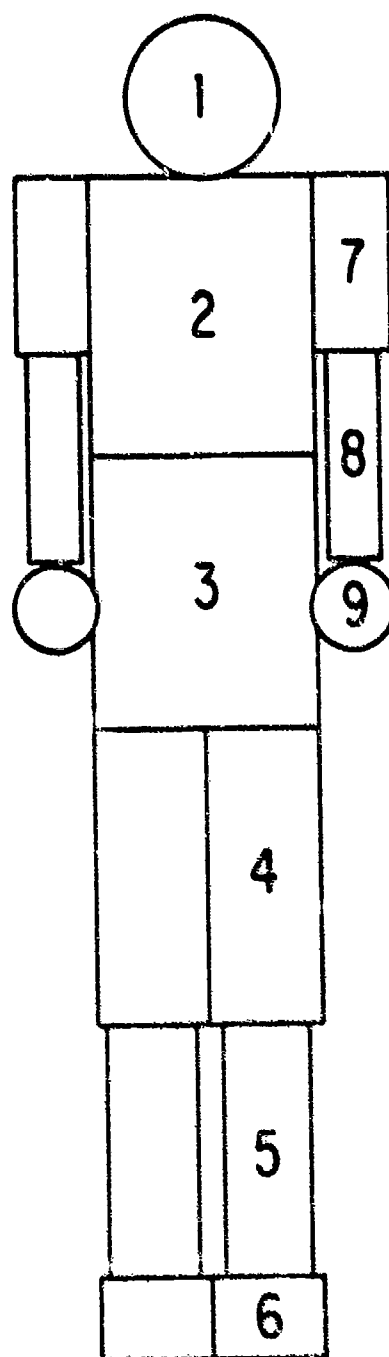


Figure 1. Average Diver Modeled as Connected Cylinders and Spheres. Numerals are arbitrary region reference numbers.

The regional skin temperature,  $T_{r_i}$ , is predicted with the Hody mean skin temperature [24,25] as the independent argument in a predictive correlation. This correlation was developed by adapting Kerslake's eight region predictive formula [2] to Hody's twelve segments by using the data of the first experimental series discussed [21]. The skin surface area is determined from the dimensions assigned to the cylindrical or spherical region of interest. The ambient temperature must be specified. A mean skin temperature is used as the independent argument of the predictive temperature formulations since the limits of diver thermal equilibrium are usually specified in terms of a minimum mean skin temperature, and the temperatures of the hand and foot [11].

The concept of mean skin temperature is predicated on: a) The true mean temperature is the mean of an infinite number of body temperature points, and the weighted mean of some finite number of these points provides a good estimate of the true value; and b) Local areas of the body may be assumed to be nearly homogeneous with respect to temperature. The sum of mean weighted regional temperatures is then assumed to be characteristic of the mean surface temperature of the human body. The weighting factors used with the various regions of the body are normally equivalent to the fraction of the total surface area comprised by the respective region [26]. Teichner [26] compared various methods which were cited in the literature for calculating mean skin temperature. He found that a six or seven point weighted system (Palmer and Park, and Burton, respectively) and an unweighted ten point mean estimated the mean skin temperature of man as well as more sophisticated schemes did. Teichner concluded that no more than six values are required to provide a good estimate of mean skin temperature and that little is gained when more than six are utilized. However, the statistical reliability of an estimate of true mean temperature is improved when additional points are considered.

The mean skin temperature, used as the independent variable in our predictive skin temperature correlation, is calculated by using the Hody correlation [24,25]. This twelve segment model was chosen over other formulae [26-29] since the segmental sensor sites specified in Hody's map (Fig. 2 and Table 1) matched those used by the Navy's thermal instrumentation system [30] in acquiring the experimental data.

A correlation for the overall heat transfer coefficient,  $U_i$  of Equation 1, was developed by modeling a composite garment ensemble after the Navy's prototype DTP garment. It will be shown that this formulation takes into account the garment entrapped gas, ambient temperature and depth, the effects of local hydrostatic compression of the garment, and the garment's external film coefficient of heat transfer. Experimental values of  $U_i$  to which the predicted values will be compared were obtained by averaging segmental skin temperatures and heat fluxes collected during the series of studies performed to evaluate the Navy's prototype Diver Thermal Protection garment.

The diver heat loss model has been written as an interactive FORTRAN computer program which has two modes of execution: production and research. The program allows the user in either mode to vary the garment's thermal properties and the assumed values of allowable regional heat flux. The user is also permitted to vary the assumed overall heat transfer coefficient ( $U$ ) biasing factors in either mode. These biasing factors will be shown to correct the non-dimensionalized values of predicted  $U$  such that in a comparison with non-dimensionalized experimental values the percent difference will be  $\leq 15\%$ . These options are provided to facilitate comparative investigation without requiring experimental studies.

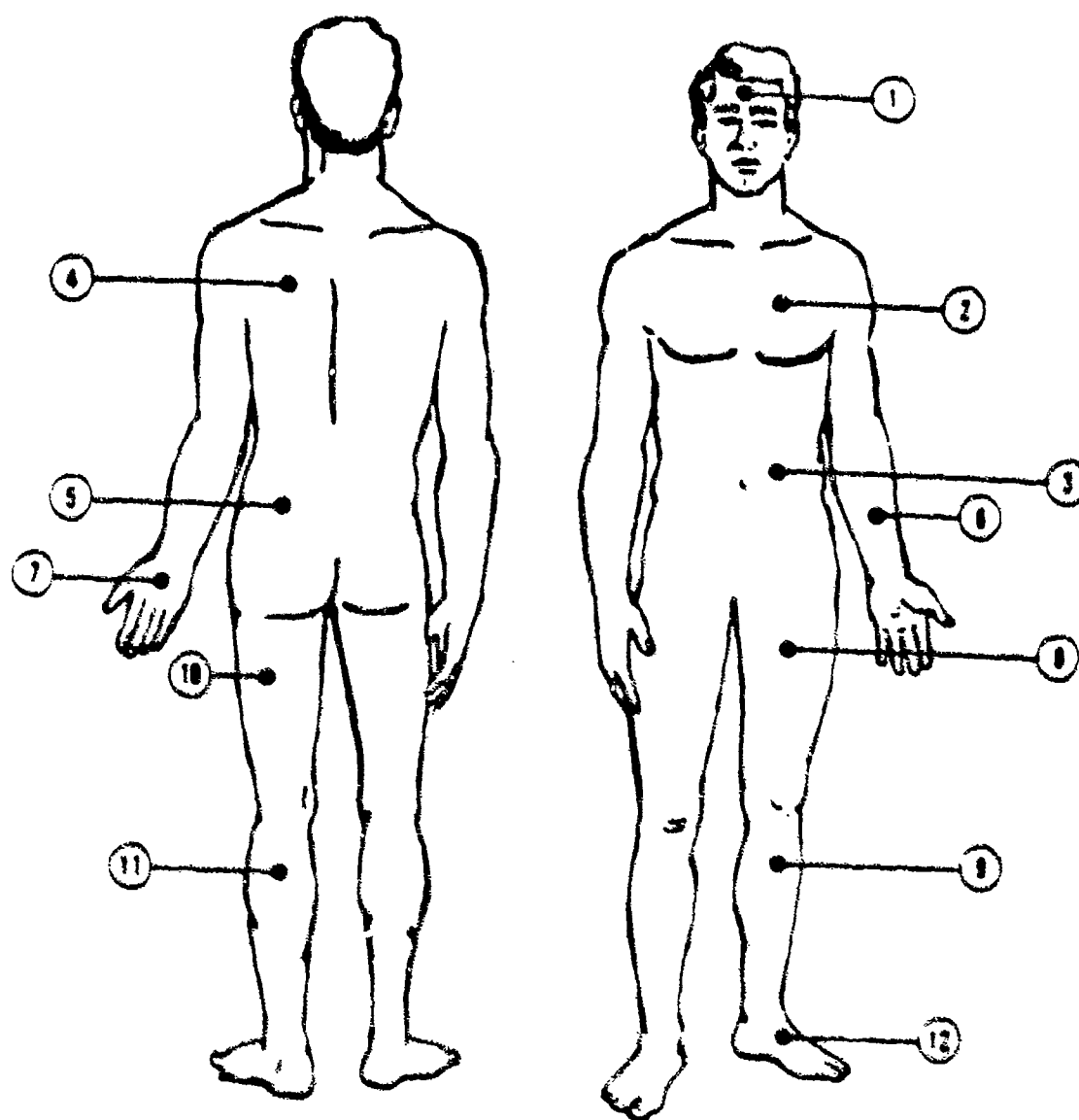


Figure 2. Body's Twelve Segments. (Adapted from reference 30)

Table 1

Indices, Nomenclature, Abbreviations, and Surface Area Fractions  
for Hody's Twelve Segment Map.<sup>†</sup>

<u>Segmental Index</u>	<u>Segmental Name</u>	<u>Abbreviation</u>	<u>Surface Area Fraction</u>
1	Head	HEAD	0.070
2	Chest	CHST	0.085
3	Abdomen	ABD	0.085
4	Upper Back	UBAC	0.090
5	Lower Back	LBAC	0.090
6	Arm	ARM	0.140
7	Hand	WRST	0.050
8	Front Thigh	F-TH	0.095
9	Front Calf	FCLF	0.065
10	Rear Thigh	R-TH	0.095
11	Rear Calf	RCLF	0.065
12	Foot	FOOT	0.070

<sup>†</sup>Data adapted from Zurrick [30]

The production mode is designed to produce estimates of the regional heat flux and required regional supplementary heating based on user supplied information. For this mode, the user must specify a mean skin temperature and the ambient temperature and depth. The value specified for the mean skin temperature indicates the desired thermal state of the subject. The research mode allows the comparison of experimental and predicted values of regional temperatures, heat fluxes, and overall heat transfer coefficients; the experimental mean skin and ambient temperatures are used in calculating the predicted data.

The computer code has been documented and flow charted, as well as internally documented with comment statements. The manner in which the interactive program has been written should allow a scientist versed both in programming with the FORTRAN language and in diver thermal protection principles to modify the program to consider new garment materials and suit configurations.

## CHAPTER II

### AVAILABLE EXPERIMENTAL DATA AND METHODS OF ANALYSIS APPLIED

As noted earlier, the experimental data available in the open literature was found to be of limited value. Most of the data is presented in terms of mean skin temperatures rather than the desired regional values or is presented in terms of experimental regional temperatures and computed, not experimental, heat fluxes. As a result, we requested diver experimental data which was recorded with investigator certified instrumentation from the U.S. Navy. Two types of studies were made available for our use. The first type of study was performed by the Navy Experimental Diving Unit (NEDU) to investigate respiratory heat loss in hyperbaric environments [21]. Sitting, nearly nude subjects were exposed to hyperbaric helium-oxygen environments at a depth of 200 meters of seawater (MSW) and ambient temperatures of 15 °C and 20 °C. The second type of study was performed by the Naval Coastal Systems Center (NCSC), in conjunction with NEDU, to evaluate the Navy's prototype Diver Thermal Protection (DTP) garment [13,22,31]. Prone, DTP clad subjects were exposed in water environments at depths of 3 and 21 meters and at an ambient temperature of 5 °C. In both cases studies were performed with both resting and working divers [21,13,22,31].

Table 2 describes the various experiments performed during the respiratory heat loss study while Tables 3 and 4 describe the DTP garment evaluation studies. Each table is organized with the resting dives listed first, followed by the working dives. If only a part of the resting subjects were used in the verification phases of our work, these subjects are listed first.

The usefulness of each of the experimental data files<sup>3</sup> shown in Tables 2-4 was evaluated by first determining the conditions under which the data was recorded. By examining the reports which describe the execution of the experimental studies [21,22], the data files were determined to be from either resting or working; prone, sitting, or standing; swim suited or DTP clad; and dry or immersed subjects who were breathing either a helium-oxygen mixture or air. From this information, the ambient temperature and pressure and the date of the study's execution, the data files were divided into similar groups.

To minimize the effects of individual subjects within a group and to give a degree of generality to our conclusions, it was decided to create average subject (composite) files. The average subject data was generated by averaging the data at each time increment from all of the selected subjects. This process was performed separately for each segment, thus producing twelve composite segmental temperature and twelve composite segmental rate of heat loss<sup>4</sup> profiles.

To reduce the possibility of basing our conclusions on unrealistic information, all of the subjects' segmental data was passed through filters before being plotted. The filter applied to the segmental temperature data

---

<sup>3</sup>See Foreword for the connotation of file.

<sup>4</sup>See Foreword for the connotation of rate of heat loss.

---

Table 2  
Respiratory Heat Loss Studies (RHL) [21]  
Data Provided by Navy Experimental Diving Unit, Panama City, Florida

Composite File Name	RHLXYZ <sup>1</sup> XYZ	Depth MSM	T <sub>amb</sub> °C	Ambient <sup>2</sup> Fluid	Attire <sup>3</sup>	Activity <sup>4</sup>	Posture <sup>5</sup>	Breathing <sup>2</sup> Gas	Comment
RHL1AR1	11R1	200	20	HeO <sub>2</sub>	SS	Rest	Sit	HeO <sub>2</sub>	Excluded from avg.
	12R1	200	20	HeO <sub>2</sub>	SS	Rest	Sit	HeO <sub>2</sub>	
	13R1	200	20	HeO <sub>2</sub>	SS	Rest	Sit	HeO <sub>2</sub>	
	14R1	200	20	HeO <sub>2</sub>	SS	Rest	Sit	HeO <sub>2</sub>	
	15R1	200	20	HeO <sub>2</sub>	SS	Rest	Sit	HeO <sub>2</sub>	
	16R1	200	20	HeO <sub>2</sub>	SS	Rest	Sit	HeO <sub>2</sub>	
RHL1AR2	12R2	200	15	HeO <sub>2</sub>	SS	Rest	Sit	HeO <sub>2</sub>	
	13R2	200	15	HeO <sub>2</sub>	SS	Rest	Sit	HeO <sub>2</sub>	
	14R2	200	15	HeO <sub>2</sub>	SS	Rest	Sit	HeO <sub>2</sub>	
	15R2	200	15	HeO <sub>2</sub>	SS	Rest	Sit	HeO <sub>2</sub>	
	16R2	200	15	HeO <sub>2</sub>	SS	Rest	Sit	HeO <sub>2</sub>	
	17R2	200	15	HeO <sub>2</sub>	SS	Rest	Sit	HeO <sub>2</sub>	
RHL1AG2	12G2	200	15	HeO <sub>2</sub>	SS	Rest	Sit	HeO <sub>2</sub> @20 °C	Breathed warm gas
	17G2	200	15	HeO <sub>2</sub>	SS	Rest	Sit	HeO <sub>2</sub> @20 °C	
RHL1AW1	11W1	200	20	HeO <sub>2</sub>	SS	W/C/50	Sit	HeO <sub>2</sub>	
	13W1	200	20	HeO <sub>2</sub>	SS	W/C/50	Sit	HeO <sub>2</sub>	
	14W1	200	20	HeO <sub>2</sub>	SS	W/C/50	Sit	HeO <sub>2</sub>	
	15W1	200	20	HeO <sub>2</sub>	SS	W/C/50	Sit	HeO <sub>2</sub>	
	16W1	200	20	HeO <sub>2</sub>	SS	W/C/50	Sit	HeO <sub>2</sub>	

1W = Group #; X = Subject #; Y = R(Rest), W(Work), G(Warm Gas); Z = Test #

2HeO<sub>2</sub> = 95% He, 5% O<sub>2</sub>

3SS = Swim Suit, DTP = Prototype Diver Thermal Protection garment

4Rest = Resting; W/C/50 = Working at a Constant rate of 50 watts; W/I/50 = Working Intermittently (work 6 min., rest 4 min.) at a constant work rate of 50 watts; W/I/Var = Working Intermittently (work 6 min., rest 4 min.) at an increasing work rate of 50, 100, 150 watts; R/LW = Rest/Light Work;

LW/MW = Light Work/Moderate Work; LW/R = Light Work followed by Rest

5Sit = Sitting, P = Prone, Sit/45 = Sitting with legs at 45° angle

Table 3  
Diver Thermal Protection Garment Evaluations [13,22]  
Data Provided by Naval Coastal Systems Center, Panama City, Florida

Composite File Name	DTPWXYZ <sup>1</sup> WXYZ	Depth MSW	T <sub>amb</sub> °C	Ambient <sup>2</sup> Fluid	Attire <sup>3</sup>	Activity <sup>4</sup>	Posture <sup>5</sup>	Breathing <sup>2</sup> Gas	Comment
DTP1AR	11RT	3	5	H <sub>2</sub> O	DTP	Rest	P	Air	
	12RT	3	5	H <sub>2</sub> O	DTP	Rest	P	Air	
	13RT	3	5	H <sub>2</sub> O	DTP	Rest	P	Air	
	14RT	3	5	H <sub>2</sub> O	DTP	Rest	P	Air	
DTP2AR1	21R1	3	5	H <sub>2</sub> O	DTP	Rest	P	Air	Suit flooded
	22R1	3	5	H <sub>2</sub> O	DTP	Rest	P	Air	
	23R1	3	5	H <sub>2</sub> O	DTP	Rest	P	Air	
	24R1	3	5	H <sub>2</sub> O	DTP	Rest	P	Air	
DTP2AW2	21W2	3	5	H <sub>2</sub> O	DTP	W/I/50	Sit	Air	
	22W2	3	5	H <sub>2</sub> O	DTP	W/I/50	Sit	Air	
	23W2	3	5	H <sub>2</sub> O	DTP	W/I/50	Sit	Air	
	24W2	3	5	H <sub>2</sub> O	DTP	W/I/50	Sit	Air	
DTP2AW3	21W3	3	5	H <sub>2</sub> O	DTP	W/I/Var	Sit	Air	
	22W3	3	5	H <sub>2</sub> O	DTP	W/I/Var	Sit	Air	
	23W3	3	5	H <sub>2</sub> O	DTP	W/I/Var	Sit	Air	
	24W3	3	5	H <sub>2</sub> O	DTP	W/I/Var	Sit	Air	

1W = Group #: X = Subject #; Y = R(Rest), W(Work), G(Warm Gas); Z = Test #

2HeO<sub>2</sub> = 95% He, 5% O<sub>2</sub>

3SS = Swim Suit, DTP = Prototype Diver Thermal Protection garment

4Rest = Resting; W/C/50 = Working at a Constant rate of 50 watts; W/I/50 = Working Intermittently (work 6 min., rest 4 min.) at a constant work rate of 50 watts; W/I/Var = Working Intermittently (work 6 min., rest 4 min.) at an increasing work rate of 50, 100, 150 watts; R/LW = Rest/Light Work;

LW/MW = Light Work/Moderate Work; LW/R = Light Work followed by Rest

5Sit = Sitting, P = Prone, Sit/45 = Sitting with legs at 45° angle

Table 4  
Diver Thermal Protection Garment Evaluations [22,31]  
Data Provided by Navy Experimental Diving Unit and Naval Coastal Systems Center, Panama City, Florida

Composite File Name	DTPWXYZ <sup>1</sup> WXYZ	Depth MSW	T <sub>ambient</sub> °C	Ambient <sup>2</sup> Fluid	Attire <sup>3</sup>	Activity <sup>4</sup>	Posture <sup>5</sup>	Breathing <sup>2</sup> Gas	Comment
DTP3AR1	33R1	21	5	H <sub>2</sub> O	DTP	Rest	P	Air	Excluded from avg.
	34R1	21	5	H <sub>2</sub> O	DTP	Rest	P	Air	
	35R1	21	5	H <sub>2</sub> O	DTP	Rest	P	Air	
	36R1	21	5	H <sub>2</sub> O	DTP	Rest	P	Air	
DTP3AW1	32W1	21	5	H <sub>2</sub> O	DTP	W/I/50	Sit	Air	
	33W1	21	5	H <sub>2</sub> O	DTP	W/I/50	Sit	Air	
	34W1	21	5	H <sub>2</sub> O	DTP	W/I/50	Sit	Air	
	37W1	21	5	H <sub>2</sub> O	DTP	W/I/50	Sit	Air	
	38W1	21	5	H <sub>2</sub> O	DTP	W/I/50	Sit	Air	
DTP4AR1	41R1	3	5	H <sub>2</sub> O	DTP	R/LW	P	Air	
	43R1	3	5	H <sub>2</sub> O	DTP	R/LW	P	Air	
	45R1	3	5	H <sub>2</sub> O	DTP	R/LW	P	Air	
DTP4XYZ	41W1	3	5	H <sub>2</sub> O	DTP	LW/MW	Sit	Air	Work at 50 watts {Alternating {Work/Rest Moderate activity {Rest with legs {at 45° angle Right hand flooded Flooded suit
	44RQ	3	5	H <sub>2</sub> O	DTP	LW/MW	Sit	Air	
	44RW	3	5	H <sub>2</sub> O	DTP	LW/MW	Sit	Air	
	48W2	3	5	H <sub>2</sub> O	DTP	LW/MW	Sit	Air	
	46R2	3	5	H <sub>2</sub> O	DTP	LW/R	Sit/45	Air	
	47R2	3	5	H <sub>2</sub> O	DTP	LW/R	Sit/45	Air	
	45RH	3	5	H <sub>2</sub> O	DTP	Rest	Sit	Air	
	48RF	3	5	H <sub>2</sub> O	DTP	Rest	Sit	Air	

1W = Group #; X = Subject #; Y = R(Rest), W(Work), G(Warm Gas); Z = Test #

2HeO<sub>2</sub> = 95% He, 5% O<sub>2</sub>

3SS = Swim Suit; DTP = Prototype Diver Thermal Protection garment

4Rest = Resting; W/C/50 = Working at a Constant rate of 50 watts; W/I/50 = Working Intermittently (work 6 min., rest 4 min.) at a constant work rate of 50 watts; W/I/Var = Working Intermittently (work 6 min., rest 4 min.) at an increasing work rate of 50, 100, 150 watts; R/LW = Rest/Light Work;

LW/MW = Light Work/Moderate Work; LW/R = Light Work followed by Rest  
5Sit = Sitting, P = Prone, Sit/45 = Sitting with legs at 45° angle

stipulated that the segmental temperature ( $^{\circ}\text{C}$ ) could not change by more than  $1.0^{\circ}\text{C}$  during one time increment. This was applied at each time increment after the first ten. The filter used with the segmental rate of heat loss data stipulated that the segmental change in the rate of heat loss (watts) should not be more than 15 watts during one time increment. This filter was used only after the fourth time increment. The delayed use of these filters was to allow for sudden changes in the temperatures and rates of heat loss at entry into the cold environment.

The selected subjects (mentioned above) were chosen from the available pool of subjects by producing a plot for each segment which superimposes the corresponding segmental profiles of each subject. Examination of the 24 segmental temperature and rate of heat loss plots indicated if any subject seemed to be significantly different from the rest of the subjects plotted. If an experimental subject appeared to be consistently different across all segments, then that subject was excluded from the segmental subject averages.

Using only the selected subjects, segmental subject averages,  $M(i)$ , were produced (at each time increment) with Equation 2.

$$M(i) = \frac{\sum_{j=1}^n S_j(i)}{n} \quad (2)$$

where:  $M(i)$  = Segmental subject average temperature or rate of heat flow at time  $i$

$S_j(i)$  = Segmental temperature or rate heat flow of subject  $j$  at time  $i$

$n$  = Number of selected subjects

$i$  = Time increment index

$j$  = Subject number index

A standard deviation [32],  $V(i)$  (Eq. 3), was also calculated for each segment at each time increment as the subject average was being determined.

$$V(i) = \left( \frac{\sum_{j=1}^n (S_j(i))^2 - \left( \frac{\sum_{j=1}^n S_j(i)}{n} \right)^2}{n - 1} \right)^{1/2} \quad (3)$$

where:  $V(i)$  = Segmental standard deviation about the segmental subject average,  $M(i)$

$S_j(i)$  = Segmental temperature or rate heat flow of subject  $j$  at time  $i$

$n$  = Number of selected subjects

$i$  = Time increment index

$j$  = Subject number index

The subject-averaged segmental skin temperatures and rates of heat loss were then plotted one segment per figure. By examining these mean plots, it was found that some of the subject data had been recorded out of time sequence. For example, a typical subject could have properly sequenced data recorded at 3 minute time increments from time zero to 27 minutes into the test. Then the next time record<sup>5</sup> might occur at a time of 29 minutes rather than the expected time of 30 minutes. From this point on, all of the data could remain out of sequence or another incorrect time increment could occur to cause the data to return to the initial time sequence. In either case, the subjects' mean plots would show a sawtooth appearance due to the time records of one subject being out of sequence with the other subjects. To eliminate this problem, all of the offset data was either arbitrarily shifted back into sequence or deleted from the averages. The choice of corrective method was

---

<sup>5</sup>See Foreword for connotation of time record.

based on the amount of data out of synchronization as well as a consideration of the limited number of subjects available in any group.

The mean (subject-averaged) segmental temperatures and rates of heat loss were then reproduced and stored in a new file. These stored values are representative of the data that would be expected from an average diver having a total body surface area similar to the average of the body surface areas of the selected subjects. Subsequently, all of the experimental data used to create and evaluate this model was taken from these average diver files. The decision to use average diver data is based on the desire to have the model represent a range of divers and to give the results a degree of statistical significance. Also, since the model predicts supplementary heating values based on average values of allowable regional heat flux, the use of this average man data should not cause any significant errors.

#### Generation of an Example Average Subject File

As an example of the procedure described in the previous section, the development of the average man file from the four subjects defined in files DTP21R1, DTP22R1, DTP23R1, and DTP24R1 will be shown. These experiments were performed by NCSC to evaluate the performance of a prototype DTP garment worn by resting, mostly prone divers in 5 °C water at a pressure equivalent to 3 MSW.

From the report describing these dives [22], it was discovered that subject number one's suit flooded early in the experiment. Since a wet subject is expected to have thermal parameters which are quite different from those of a dry diver, we decided to exclude the data of subject 1 (found in file DTP21R1) from the average man calculations. The remaining subjects were

then plotted one segment at a time on the same set of axes. Figures 3-14 show the segmental subject temperature profiles, and Figures 15-26 display the segmental subject rate of heat loss plots. Each figure displays three segmental profiles, one for each of the selected subjects. By examining the twelve temperature and twelve heat loss figures, it can be seen that, for the most part, the segmental profiles which were taken from three different subjects are quite similar. It was found that the data recorded from the head, hand, and foot was generally quite anomalous when compared to the other segments, but, for consistency, these segments were averaged.

The average subject data is now generated from the segmental data of the selected subjects. Figures 27-38 show the subject-averaged segmental temperature profiles which correspond to the segmental subject temperature data of Figures 3-14, and Figures 39-50 display the subject-averaged segmental rate of heat loss profiles derived from the segmental subject rate of heat loss data of Figures 15-26. All of the mean subject data was calculated with Equation 2. The dashed lines enclosing each of the segmental subject-averaged profiles represent  $\pm 1$  standard deviation (Eq. 3) about the mean value that is calculated at each time increment. The mean profiles of Figures 27-50 did not exhibit any unsynchronous times, thus no corrective measures were required. The segmental subject-averaged (composite) temperatures (Fig. 27-38) and rates of heat loss (Fig. 39-50) are stored in file DTP2AR1 in the format as described in Appendix A. The data stored in file DTP2AR1 represents a composite subject which was generated from the data of three different divers.

Figures 3-14. Segmental Subject Temperature Profiles. Each figure displays the three subject's temperature profiles for a specific segment. Figures 3-14 correspond to segments 1-12 of Figure 2 and Table 1.

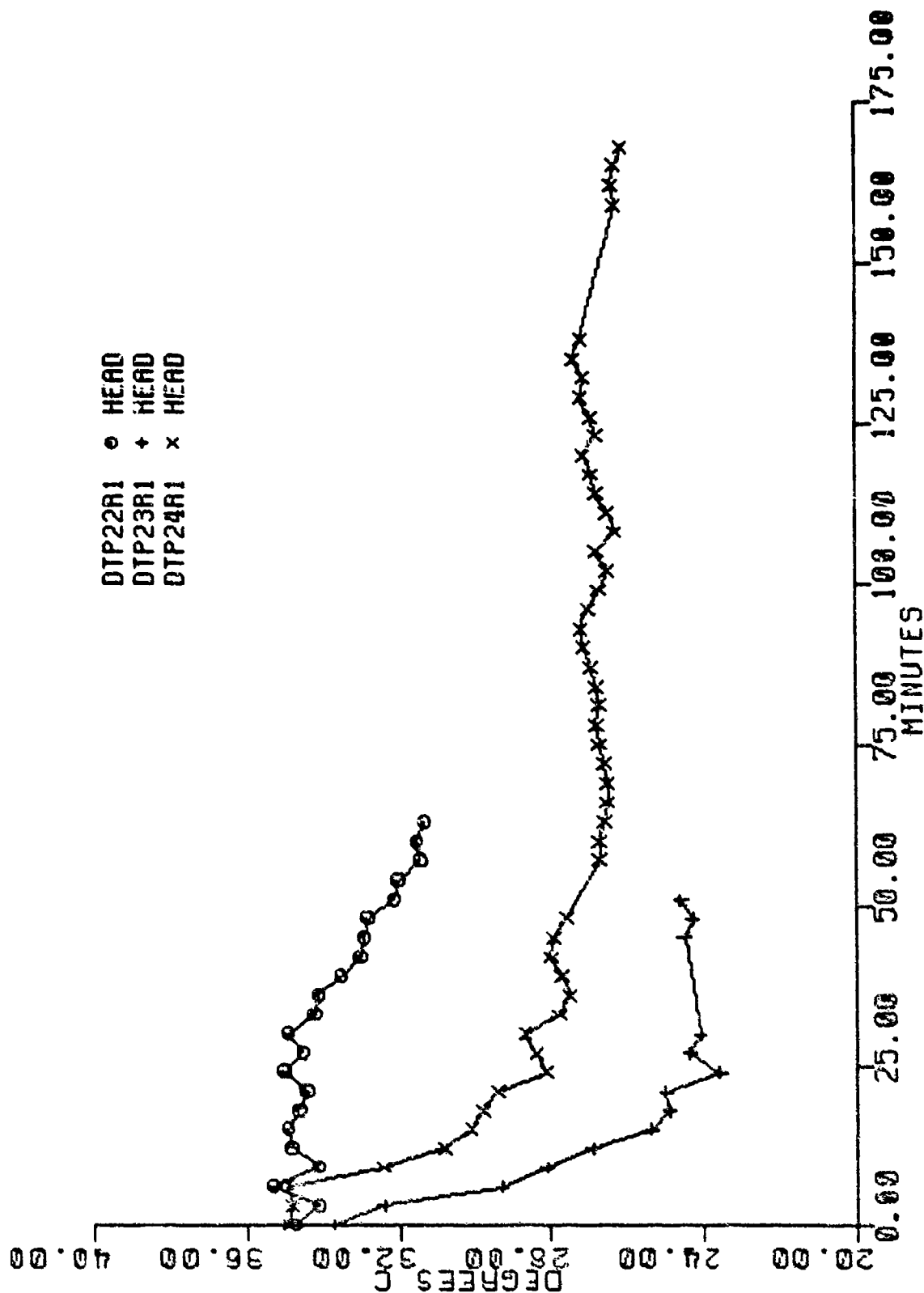


Figure 3. Segmental Subject Temperature Profiles for the Head (HEAD).

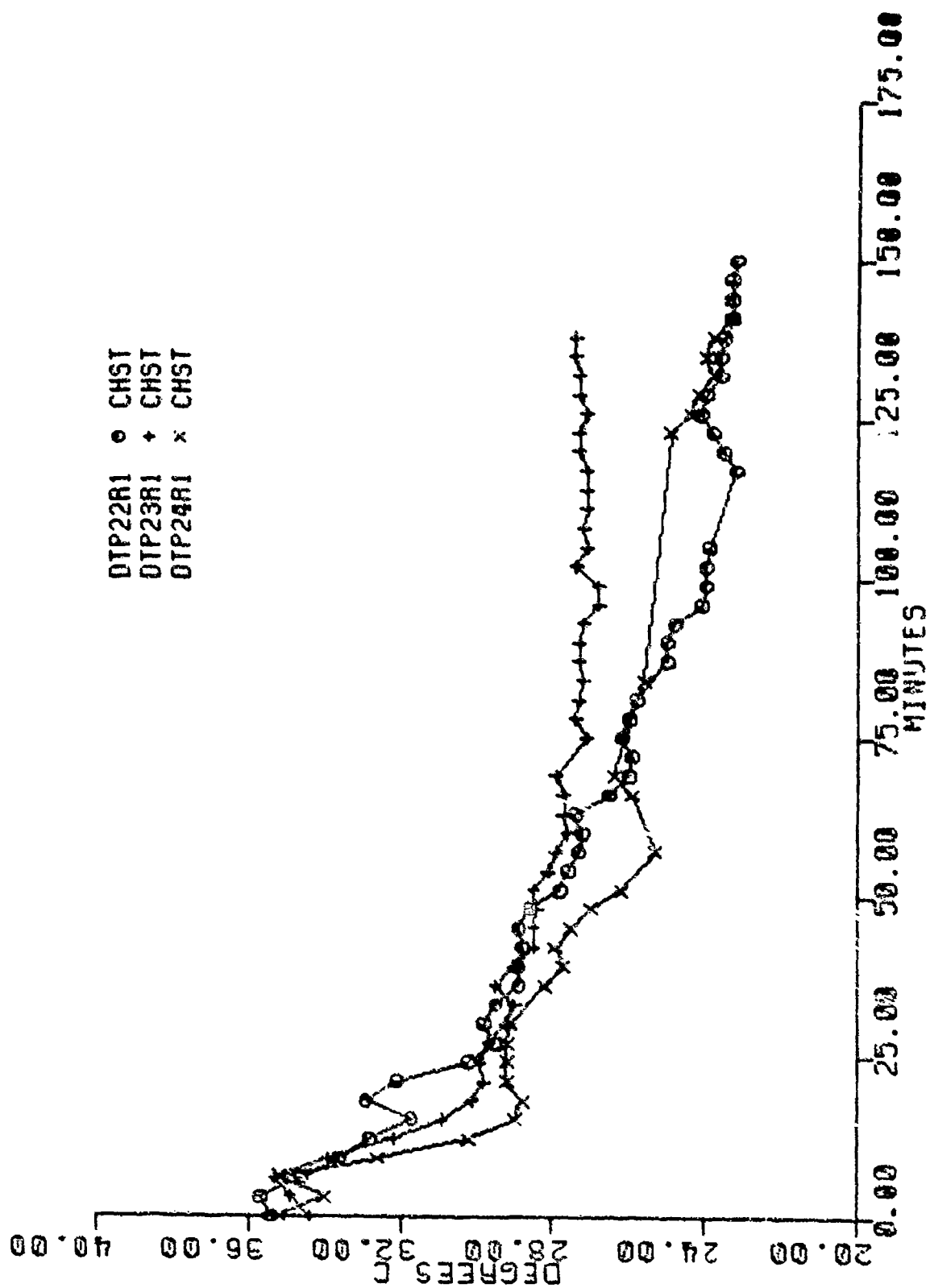


Figure 4. Segmental Subject Temperature Profiles for the Chest (CHST).

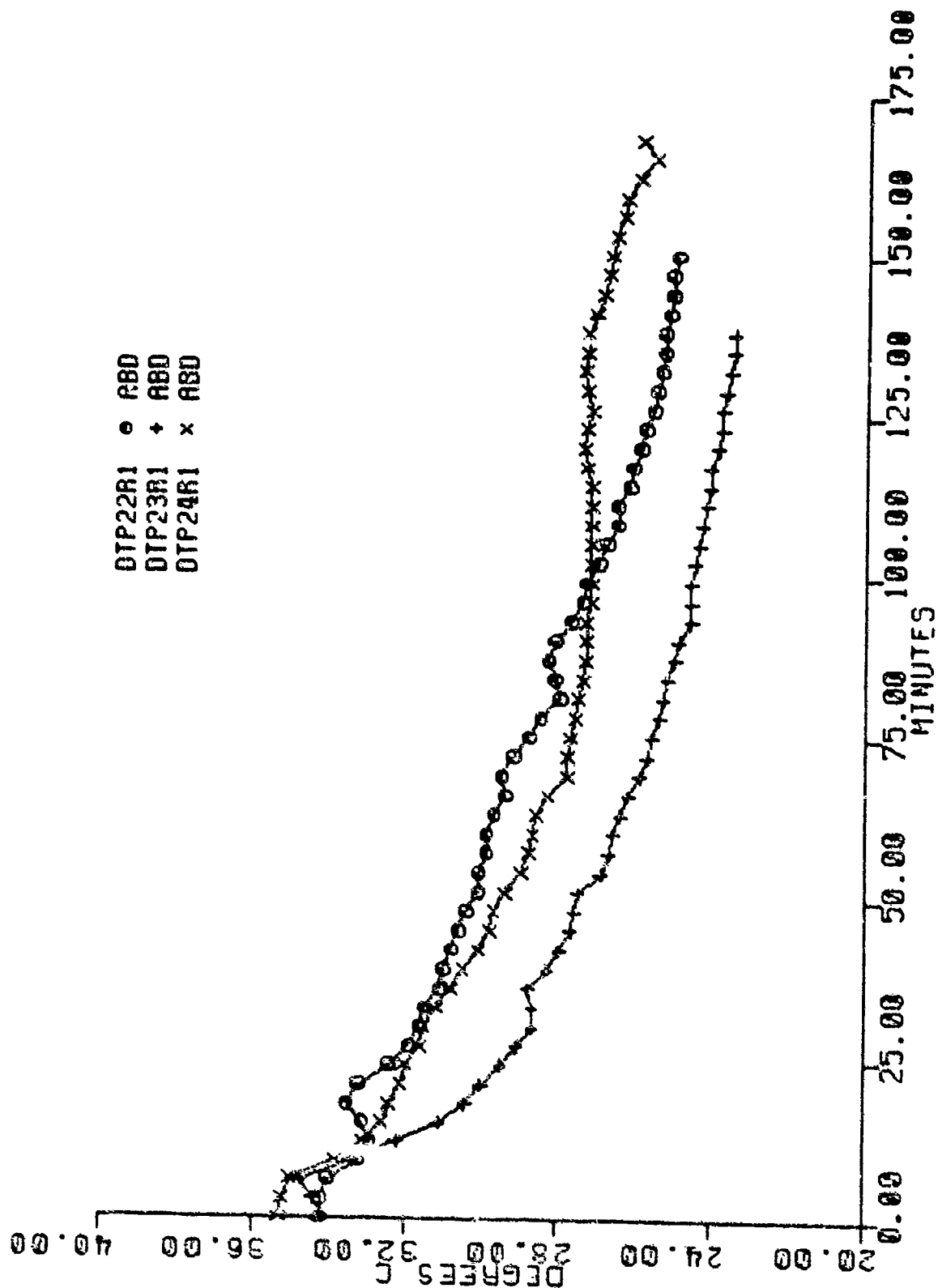


Figure 5. Segmental Subject Temperature Profiles for the Abdomen (ABD).

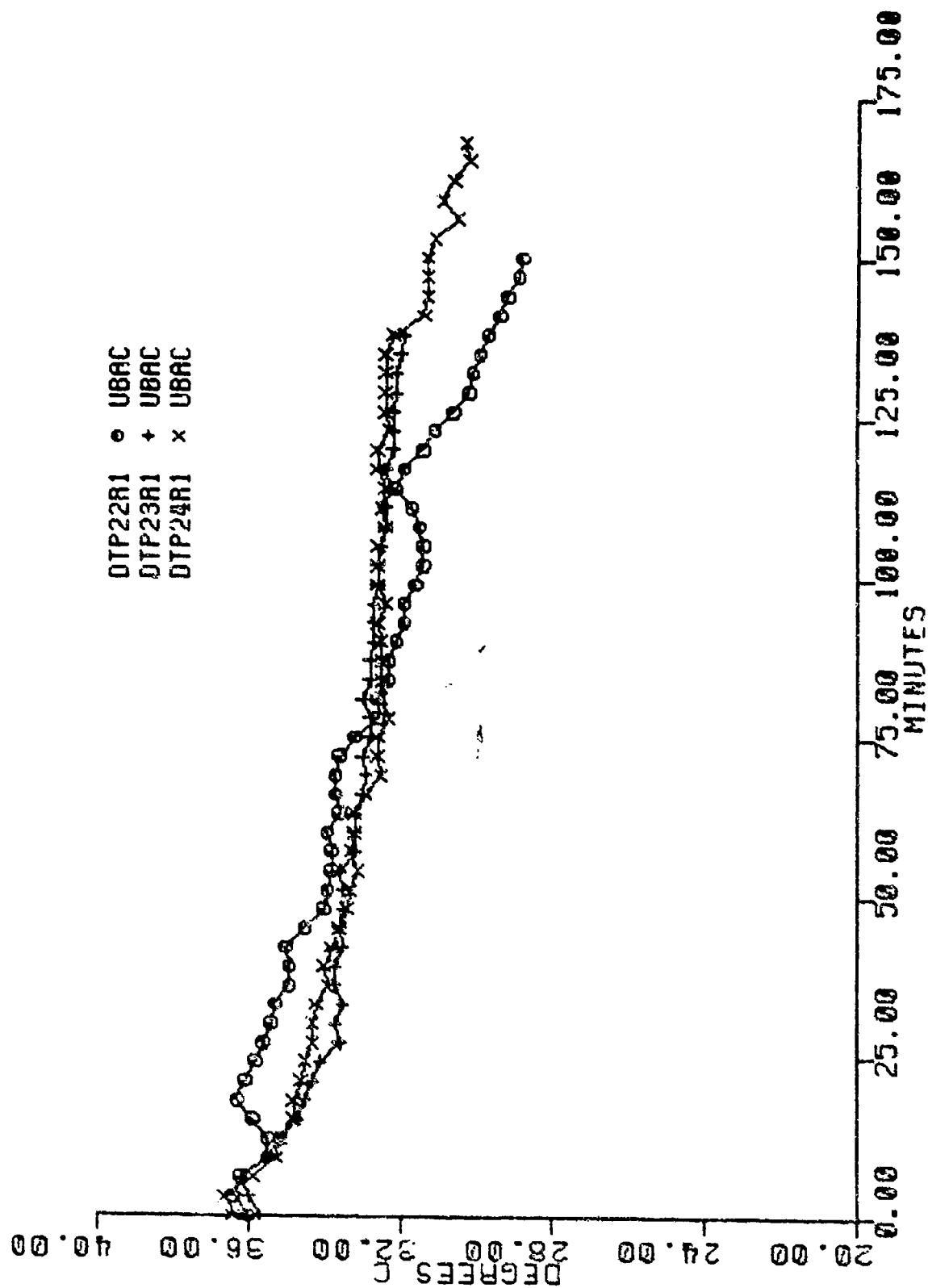


Figure 6. Segmental Subject Temperature Profiles for the Upper Back (UBAC).

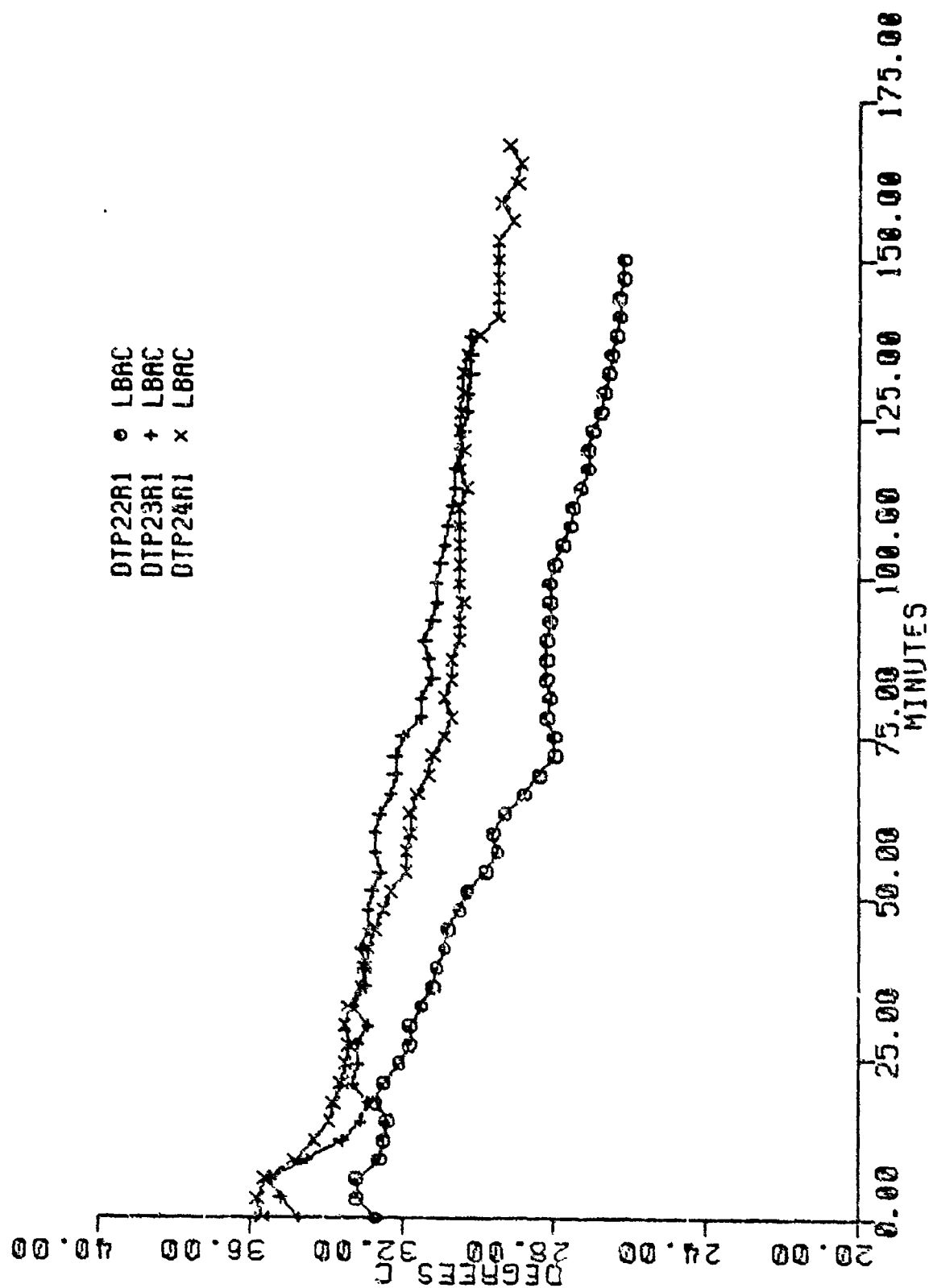


Figure 7. Segmental Subject Temperature Profiles for the Lower Back (LBAC).

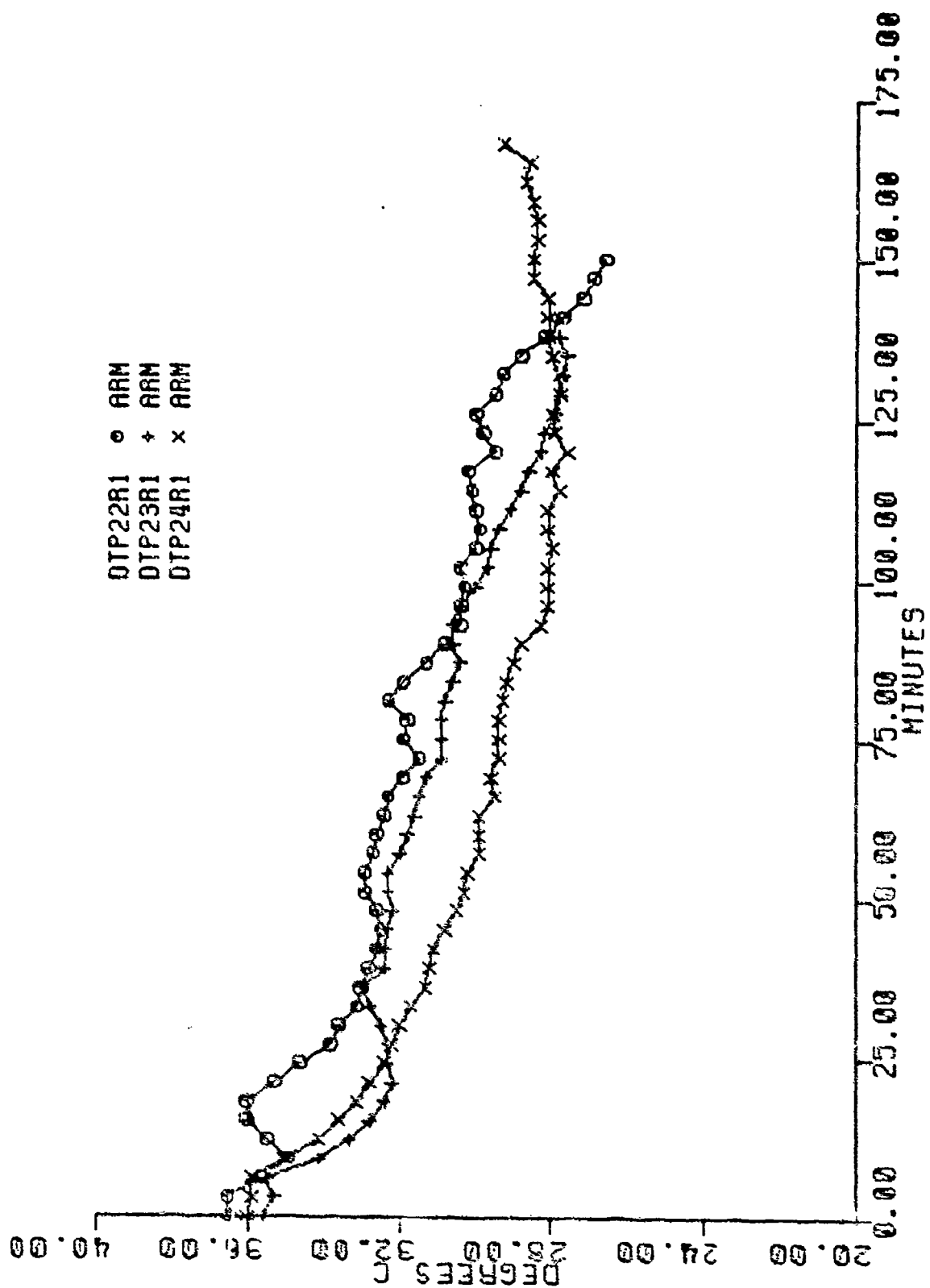


Figure 8. Segmental Subject Temperature Profiles for the Arm (ARM).

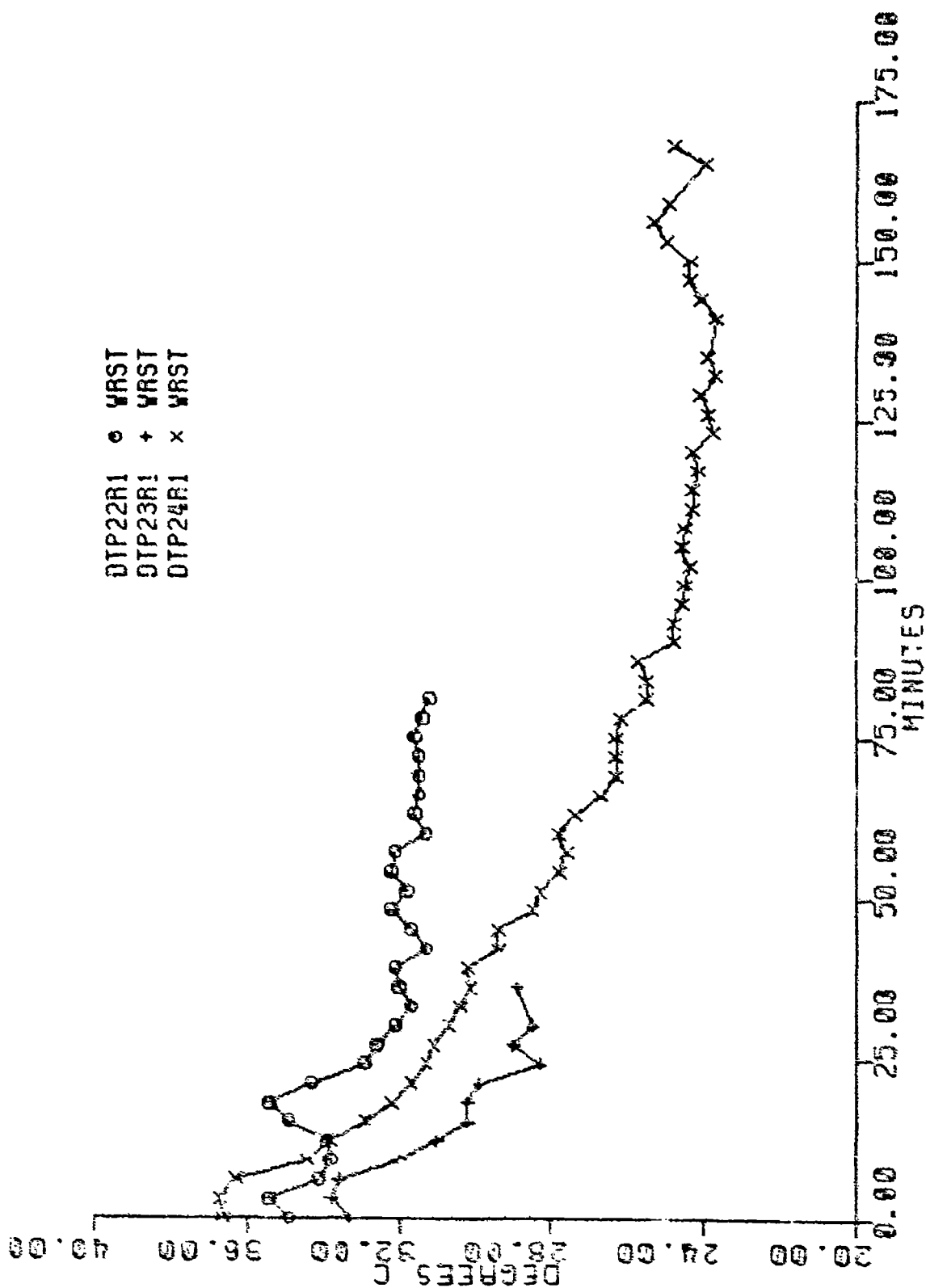


Figure 9. Segmental Subject Temperature Profiles for the Hand (WRST).

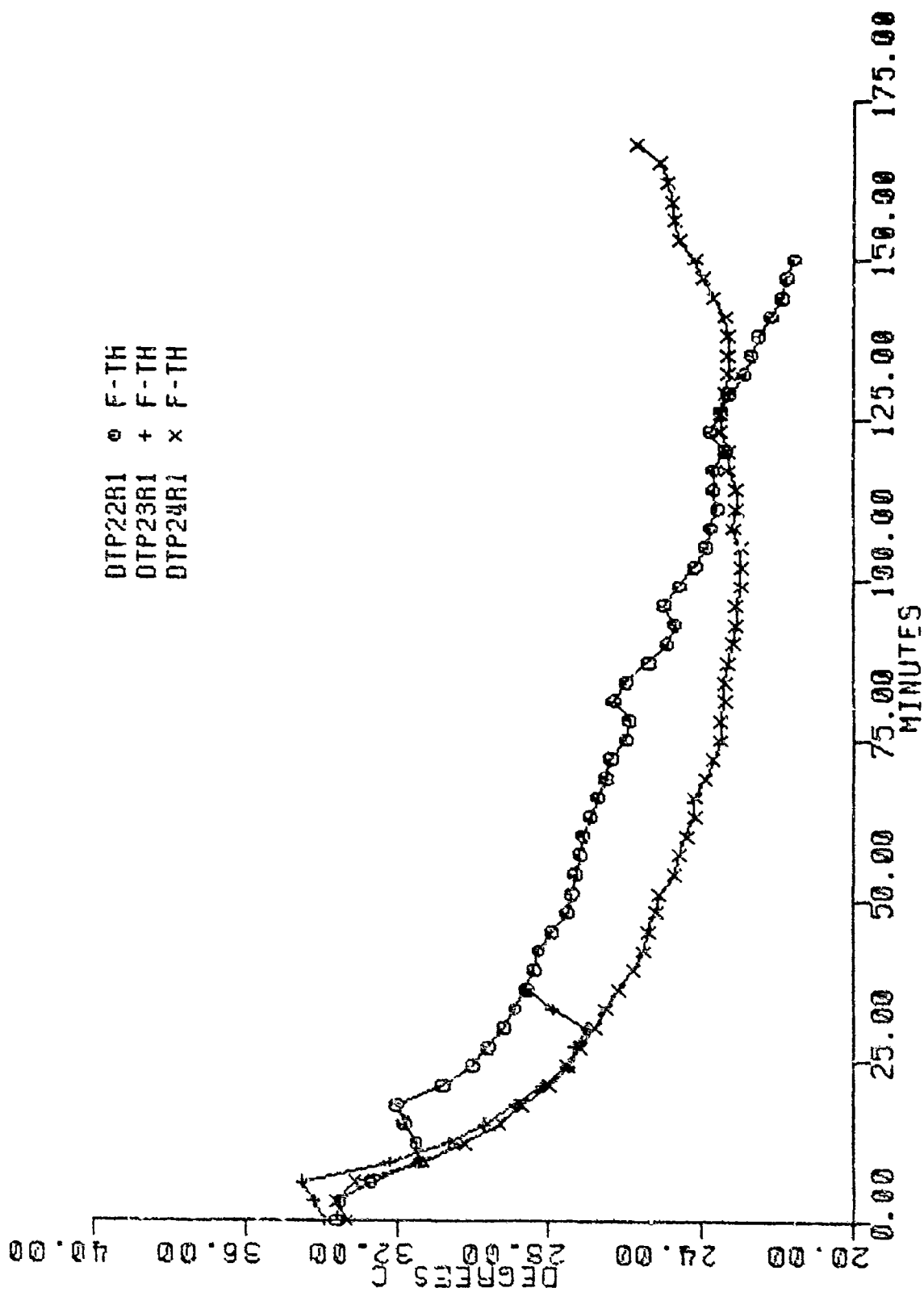


Figure 10. Segmental Subject Temperature Profiles for the Front Thigh (F-TH).

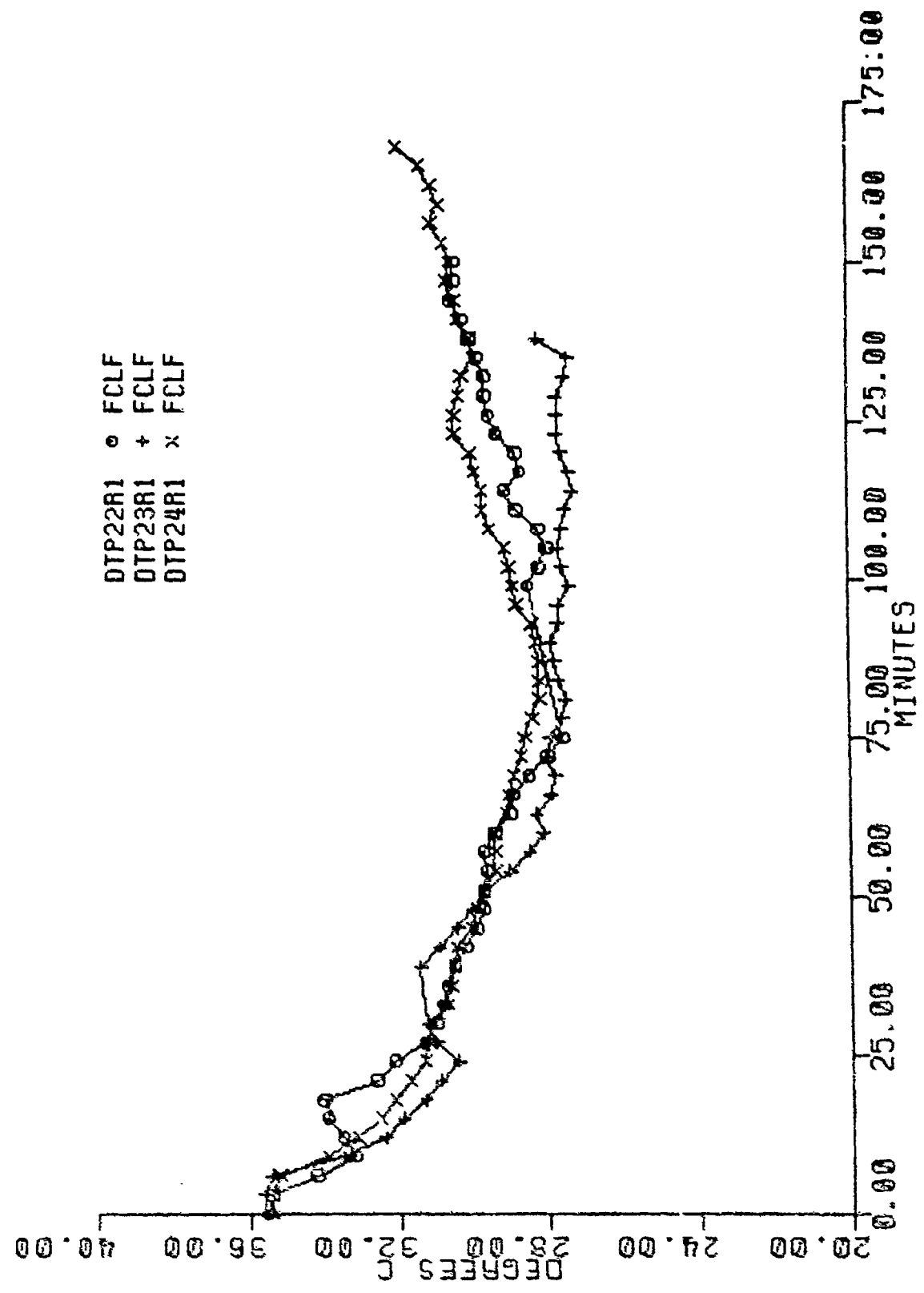


Figure 11. Segmental Subject Temperature Profiles for the Front Calf (FCLF).

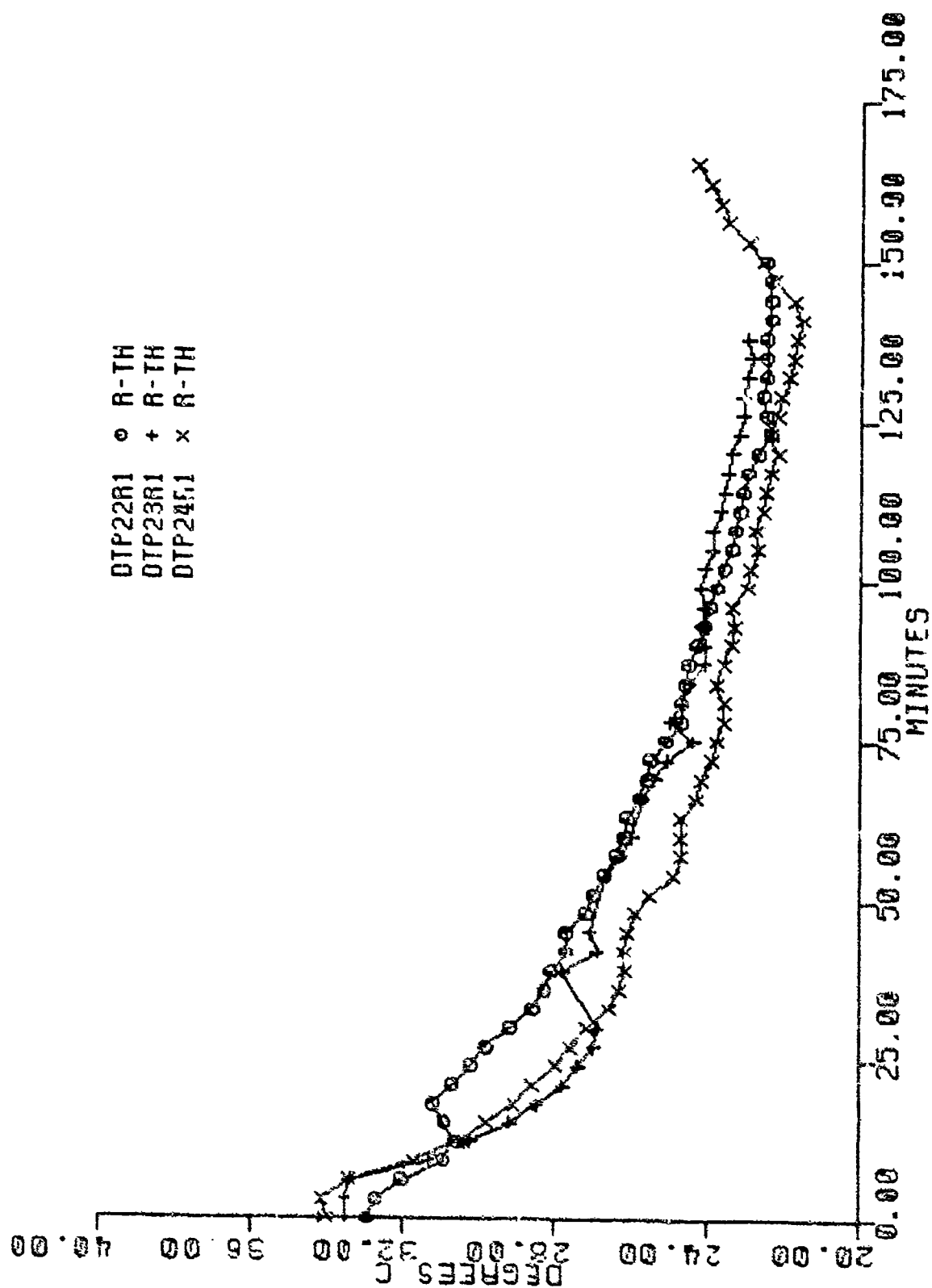


Figure 12. Segmental Subject Temperature Profiles for the Rear Thigh (R-TH).

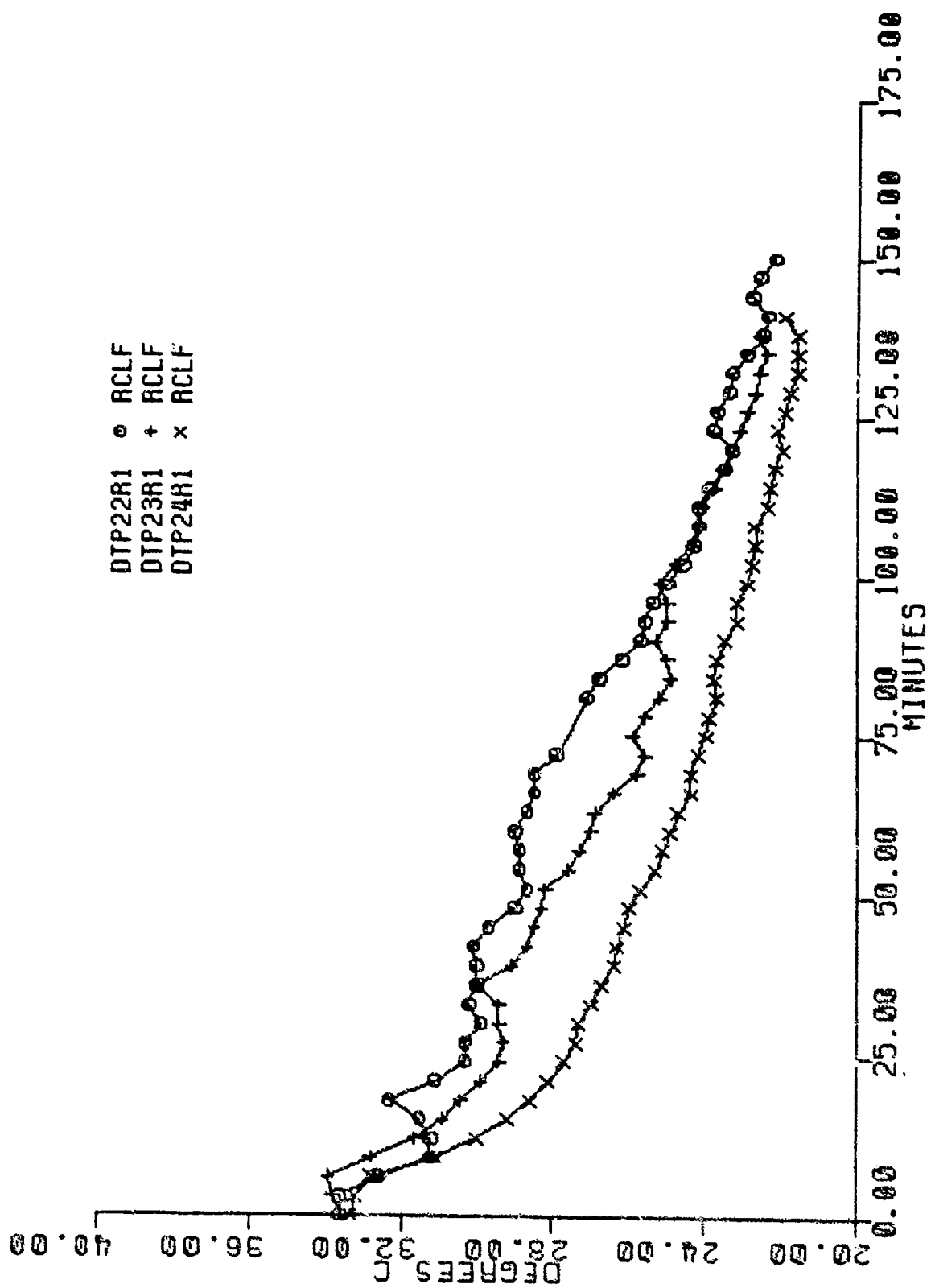


Figure 13. Segmental Subject Temperature Profiles for the Rear Calf (RCLF).

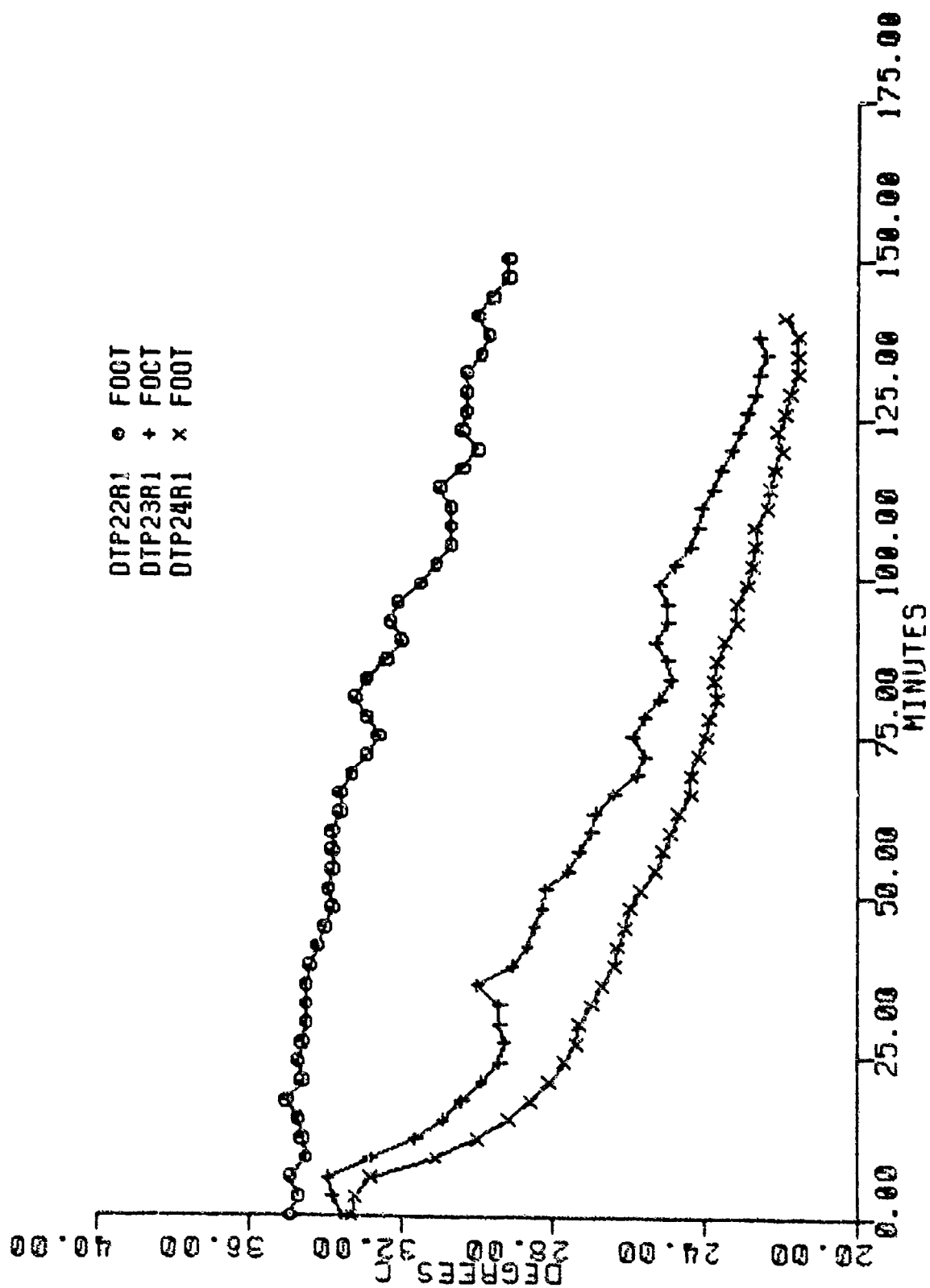


Figure 14. Segmental Subject Temperature Profiles for the Foot (F00T).

Figures 15-26. Segmental Subject Rate of Heat Loss Profiles. Each figure displays the three subject's rate of heat loss profiles for a specific segment. Figures 15-26 correspond to segments 1-12 of Figure 2 and Table 1.

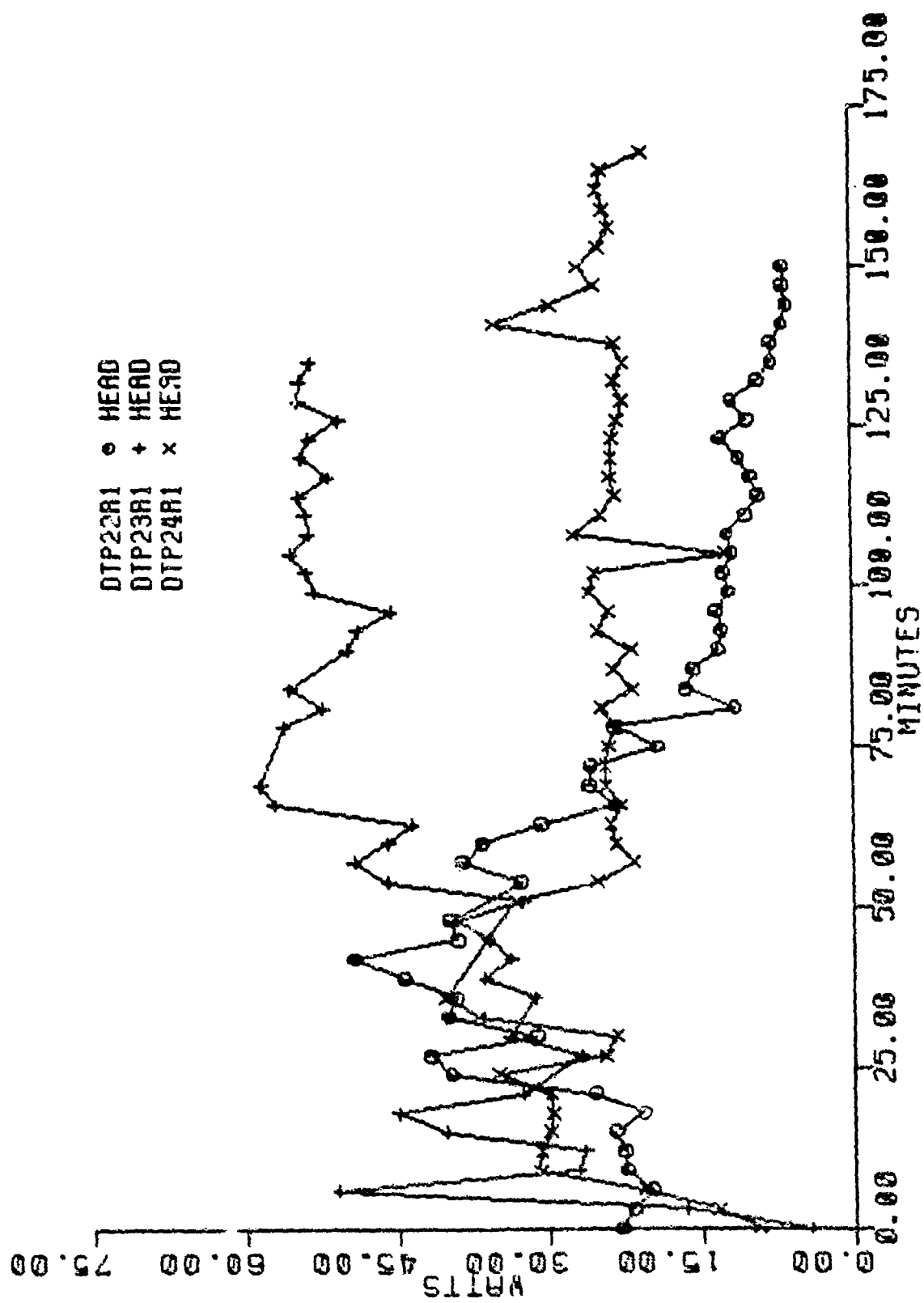


Figure 15. Segmental Subject Rate of Heat Loss Profiles for the Head (HEAD).

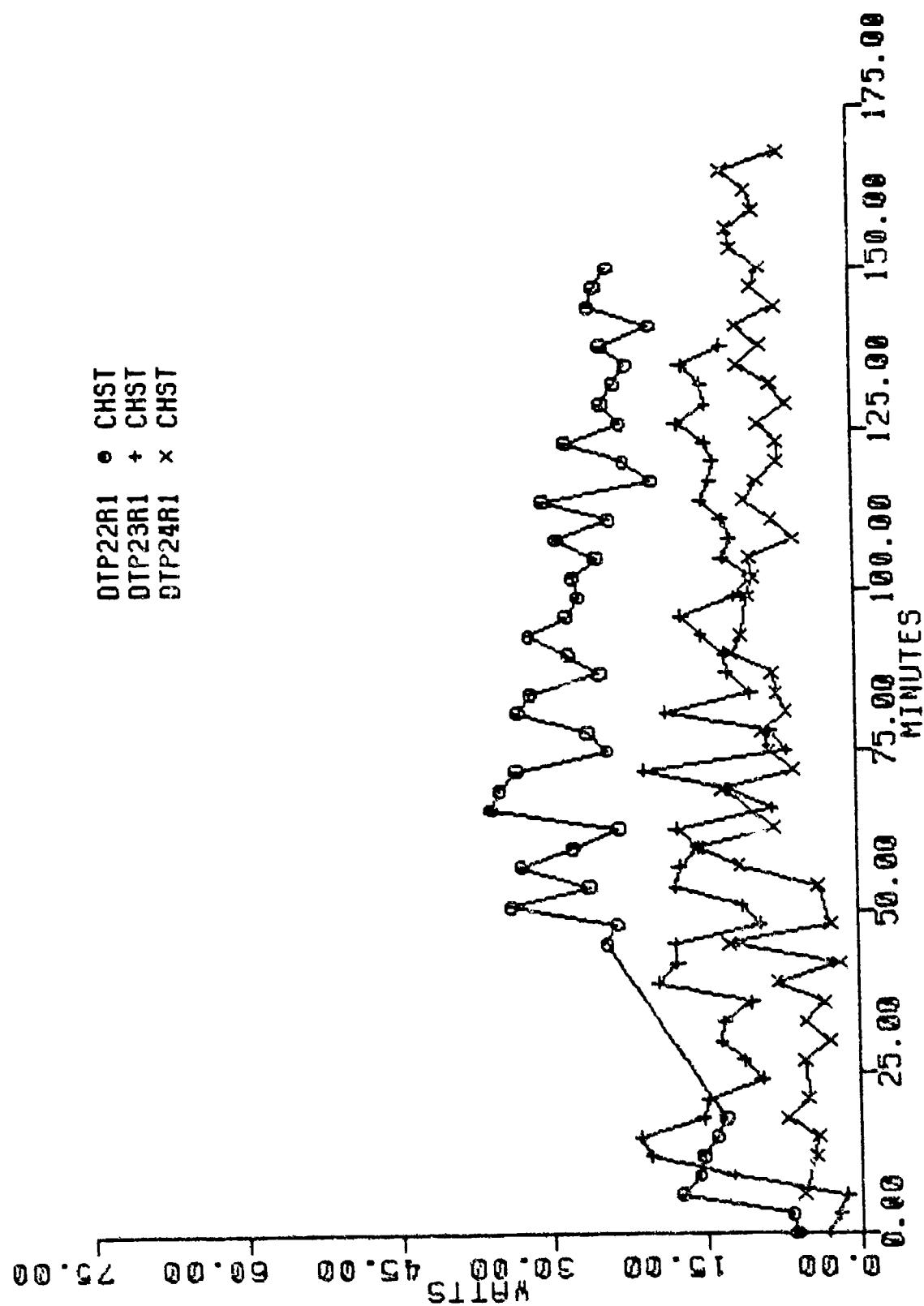


Figure 16. Segmental Subject Rate of Heat Loss Profiles for the Chest (CHST).

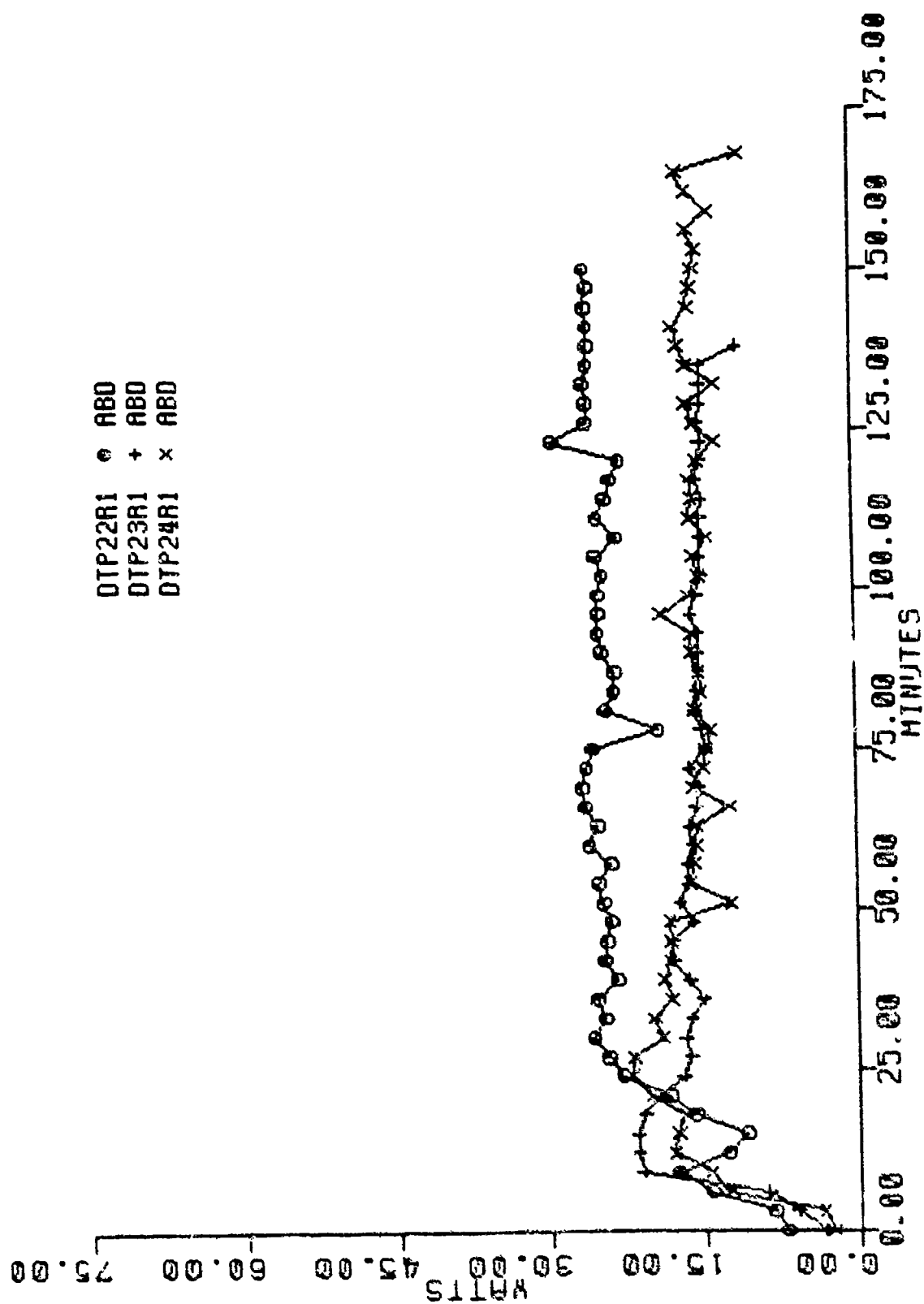


Figure 17. Segmental Subject Rate of heat Loss Profiles for the Abdomen (ABD).

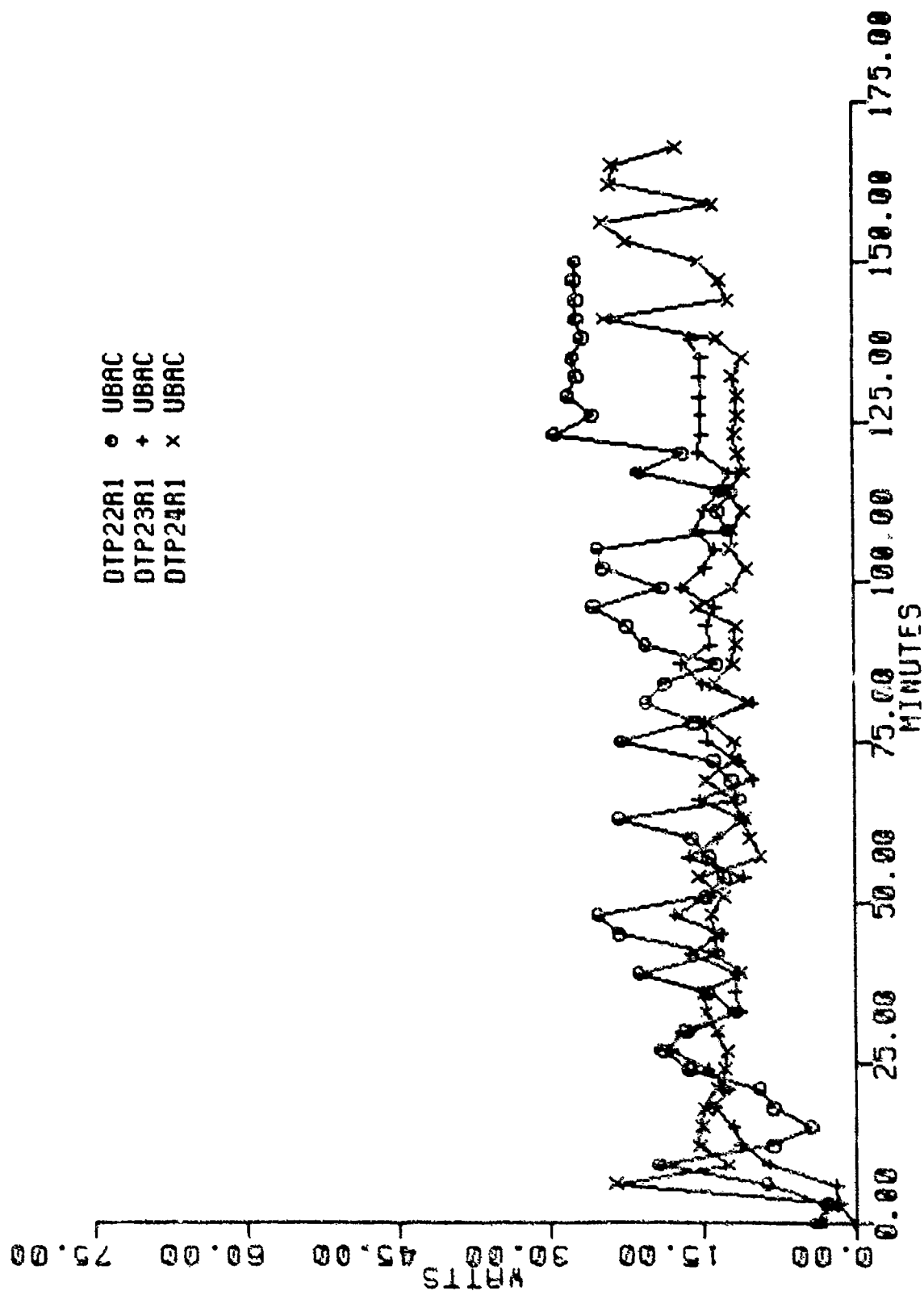


Figure 18. Segmental Subject Rate of Heat Loss Profiles for the Upper Back (UBAC).

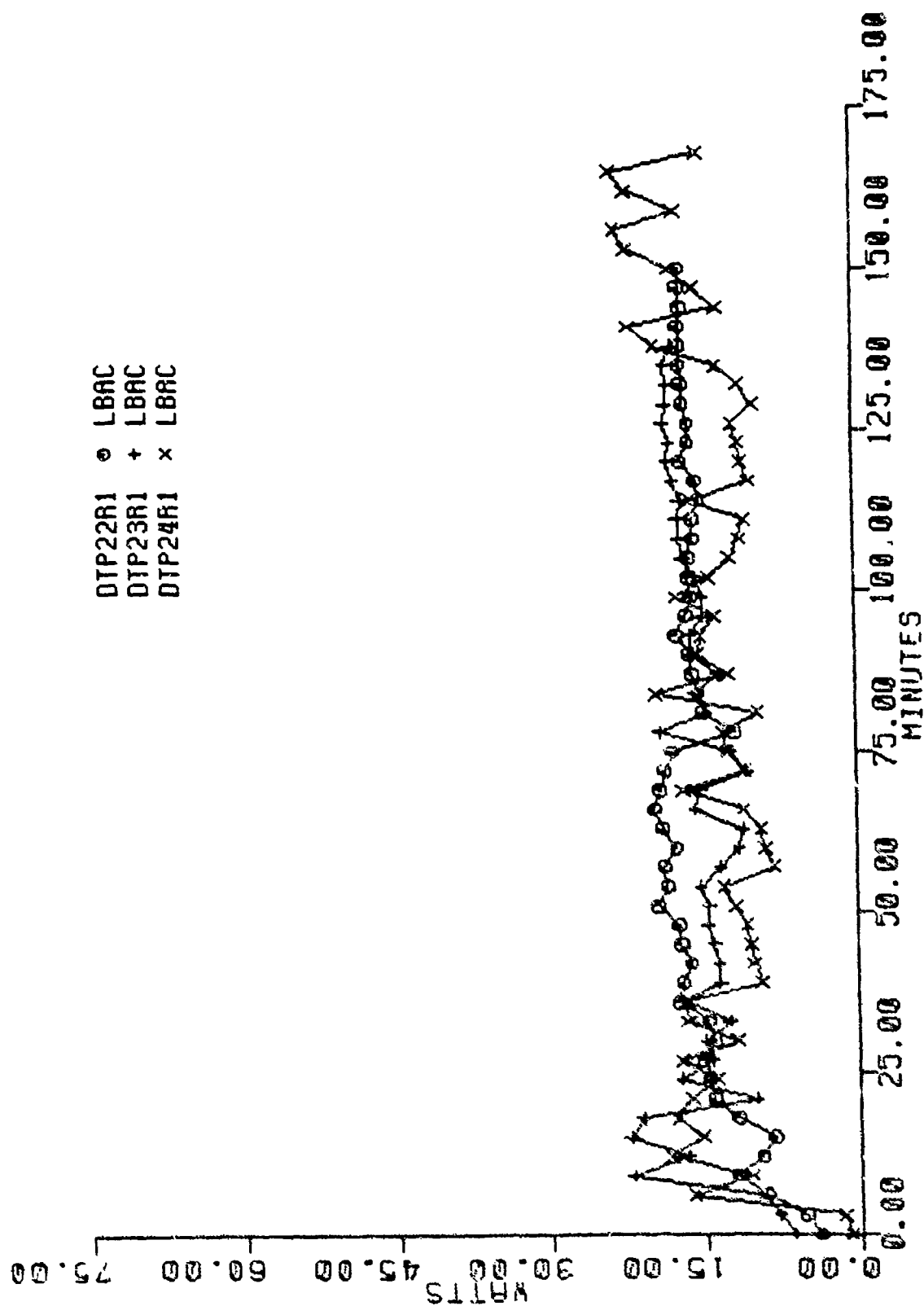


Figure 19. Segmental Subject Rate of Heat Loss Profiles for the Lower Back (LBAC).

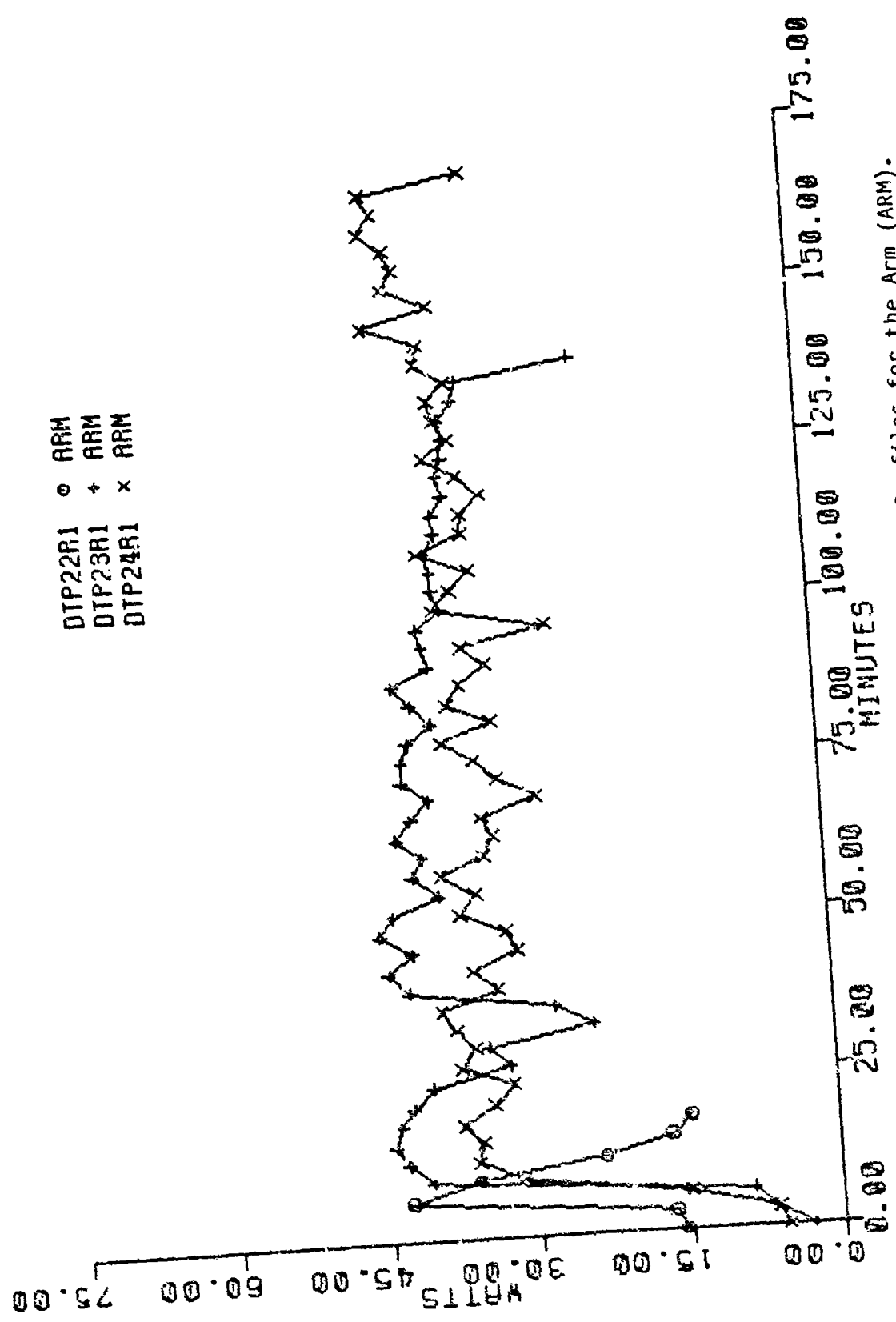


Figure 20. Segmental Subject Rate of Heat Loss Profiles for the Arm (ARM).

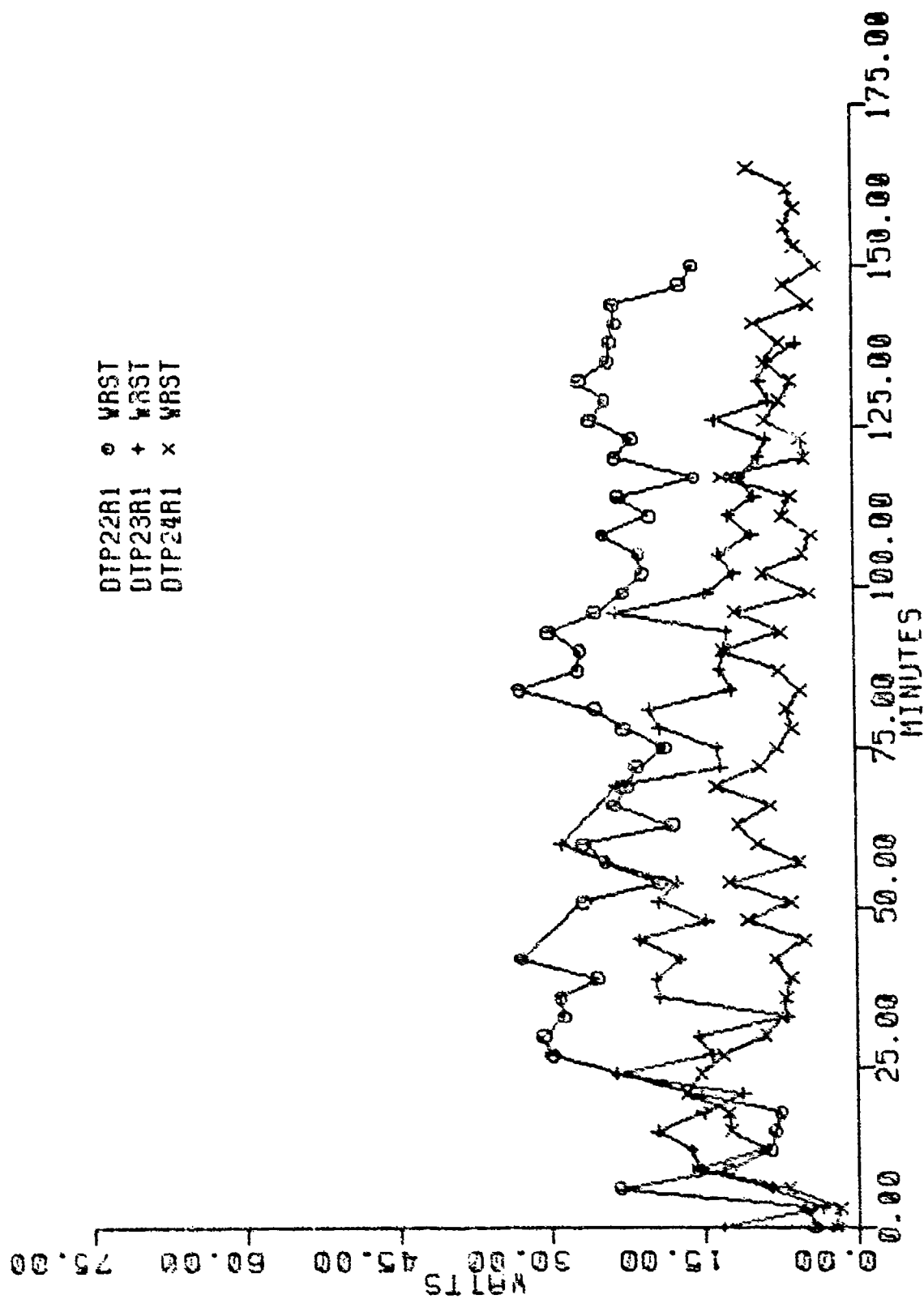


Figure 21. Segmental Subject Rate of Heat Loss Profiles for the Hand (WRST).

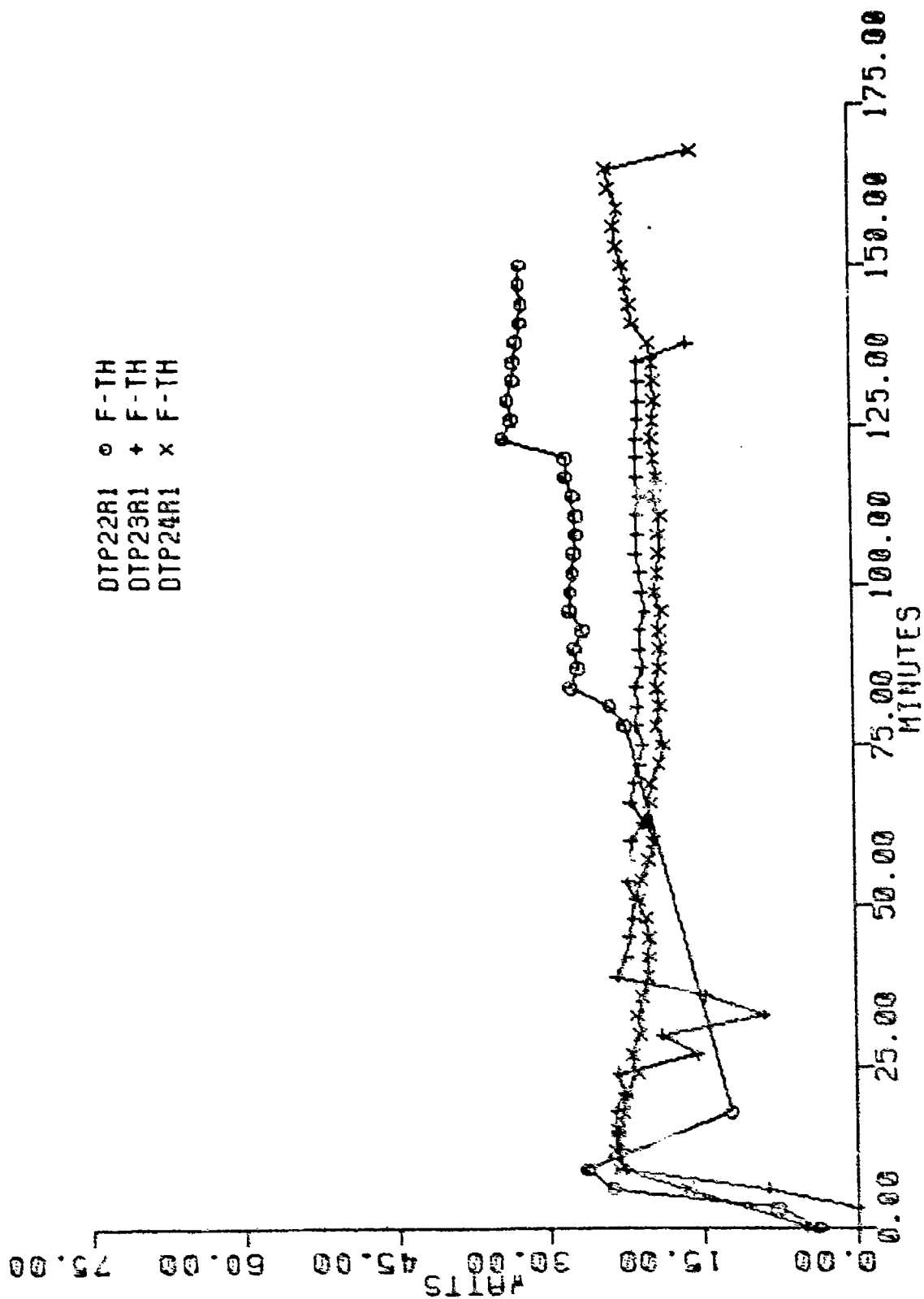


Figure 22. Segmental Subject Rate of Heat Loss Profiles for the Front Thigh (F-TH).

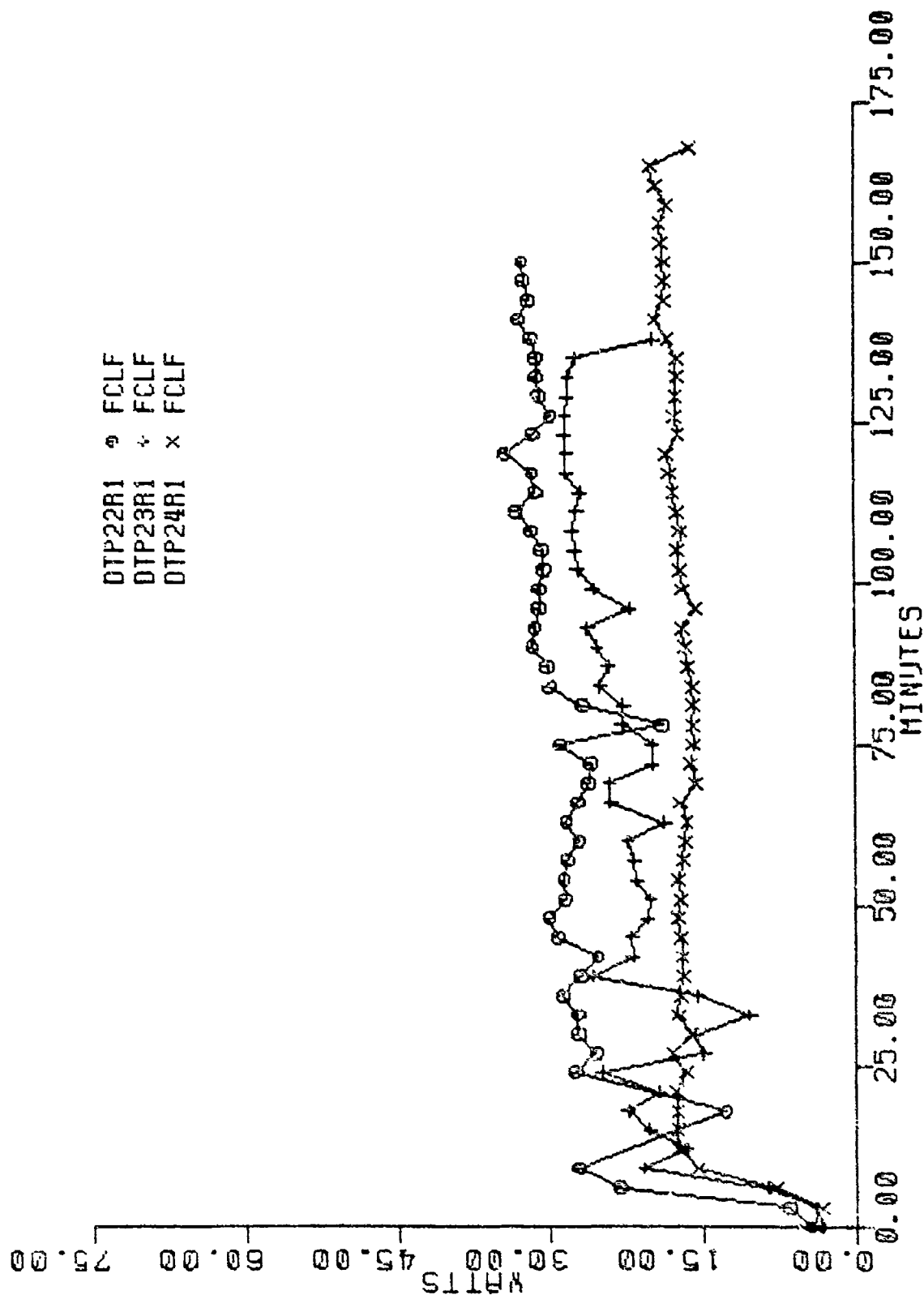


Figure 23. Segmental Subject Rate of Heat Loss Profiles for the Front Calf (FCLF).

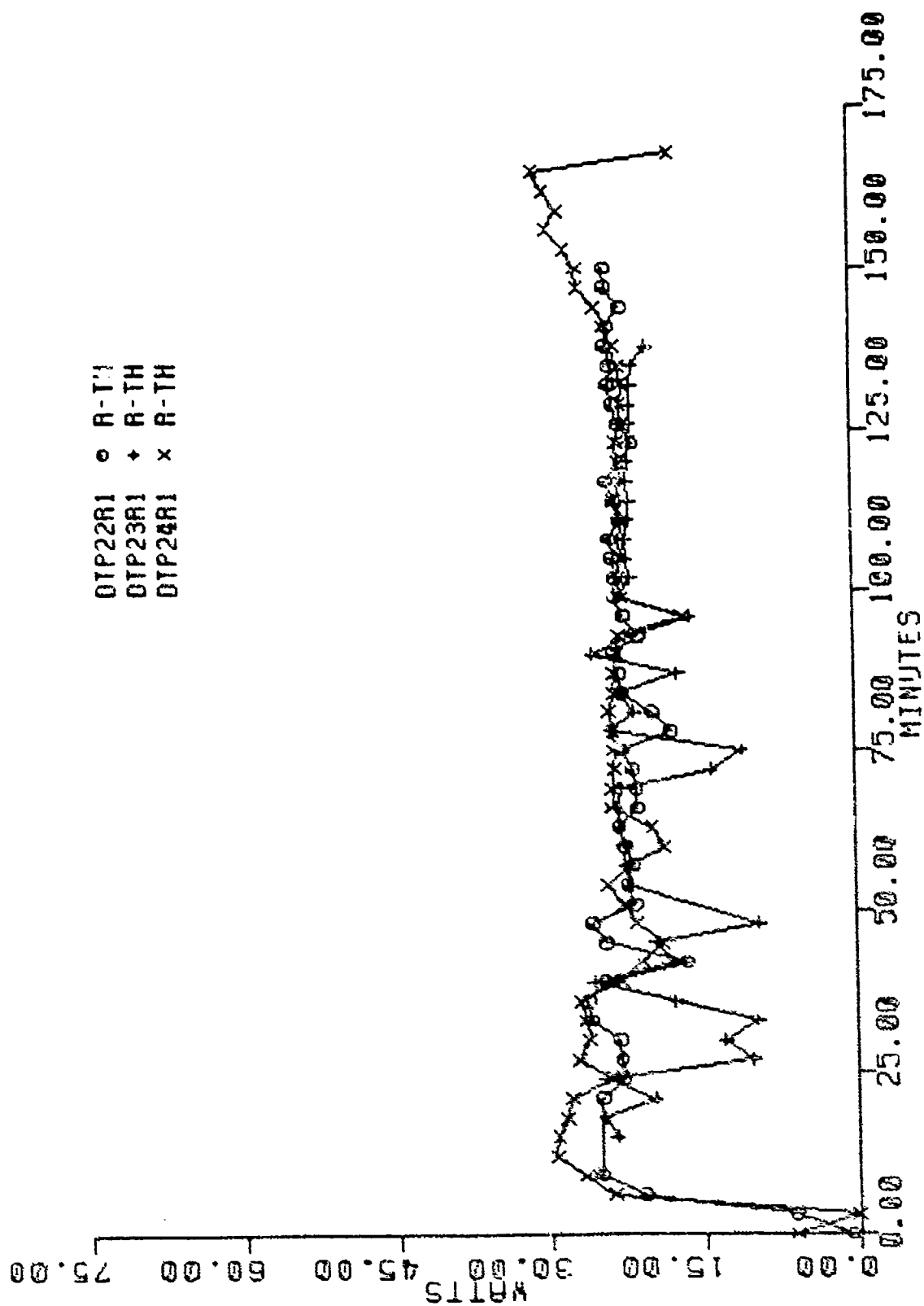


Figure 24. Segmental Subject Rate of Heat Loss Profiles for the Rear Thigh (R-TH).

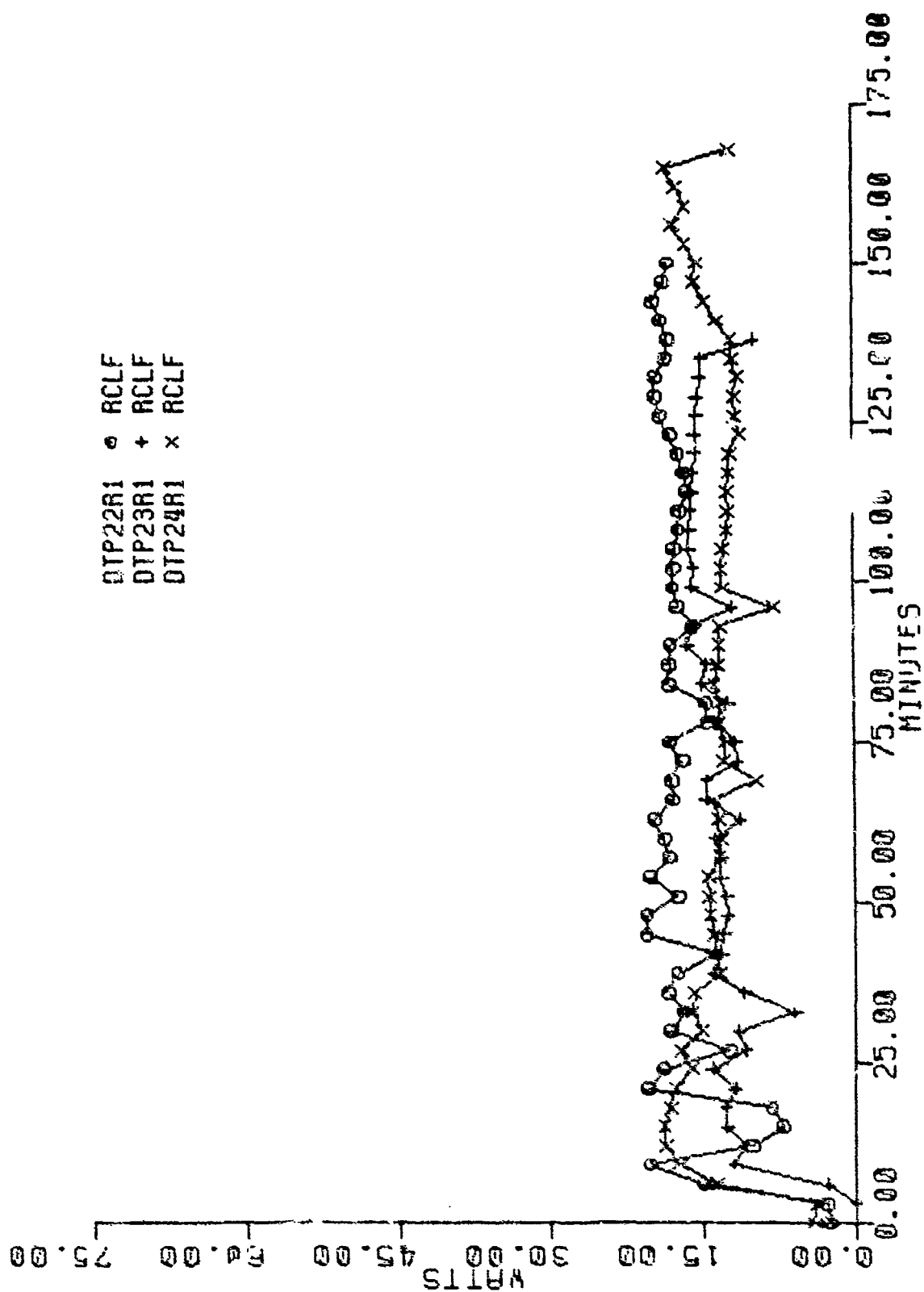


Figure 25. Segmental Subject Rate of Heat Loss Profiles for the Rear Calf (RCLF).

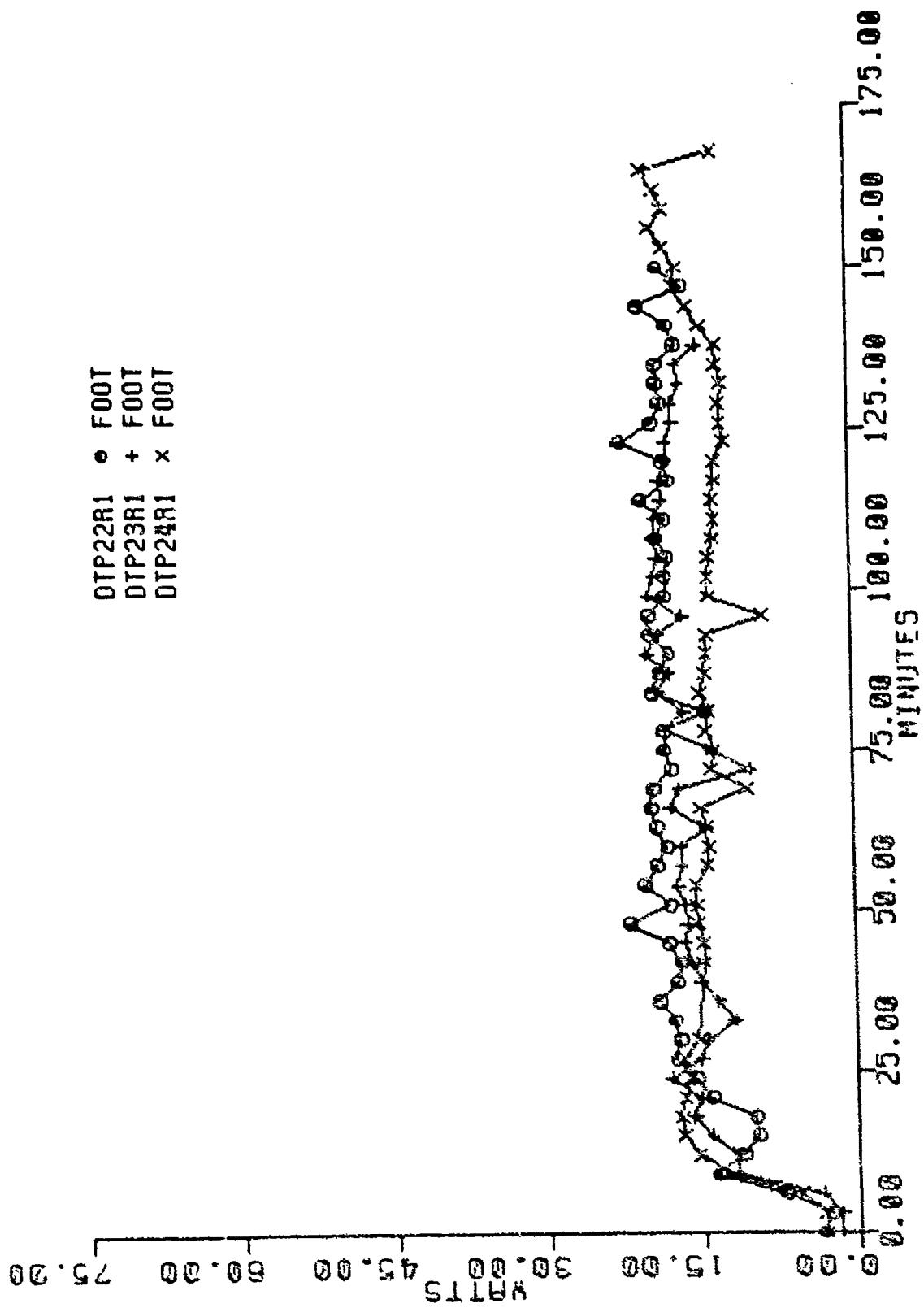


Figure 26. Segmental Subject Rate of Heat Loss Profiles for the Foot (F00T).

Figures 27-38. Segmental Subject-Averaged Temperature Profiles. Each figure displays a specific segment's mean temperature profile.

Figures 27-38 were developed from data of Figures 3-14 and correspond to segments 1-12 of Figure 2 and Table 1.

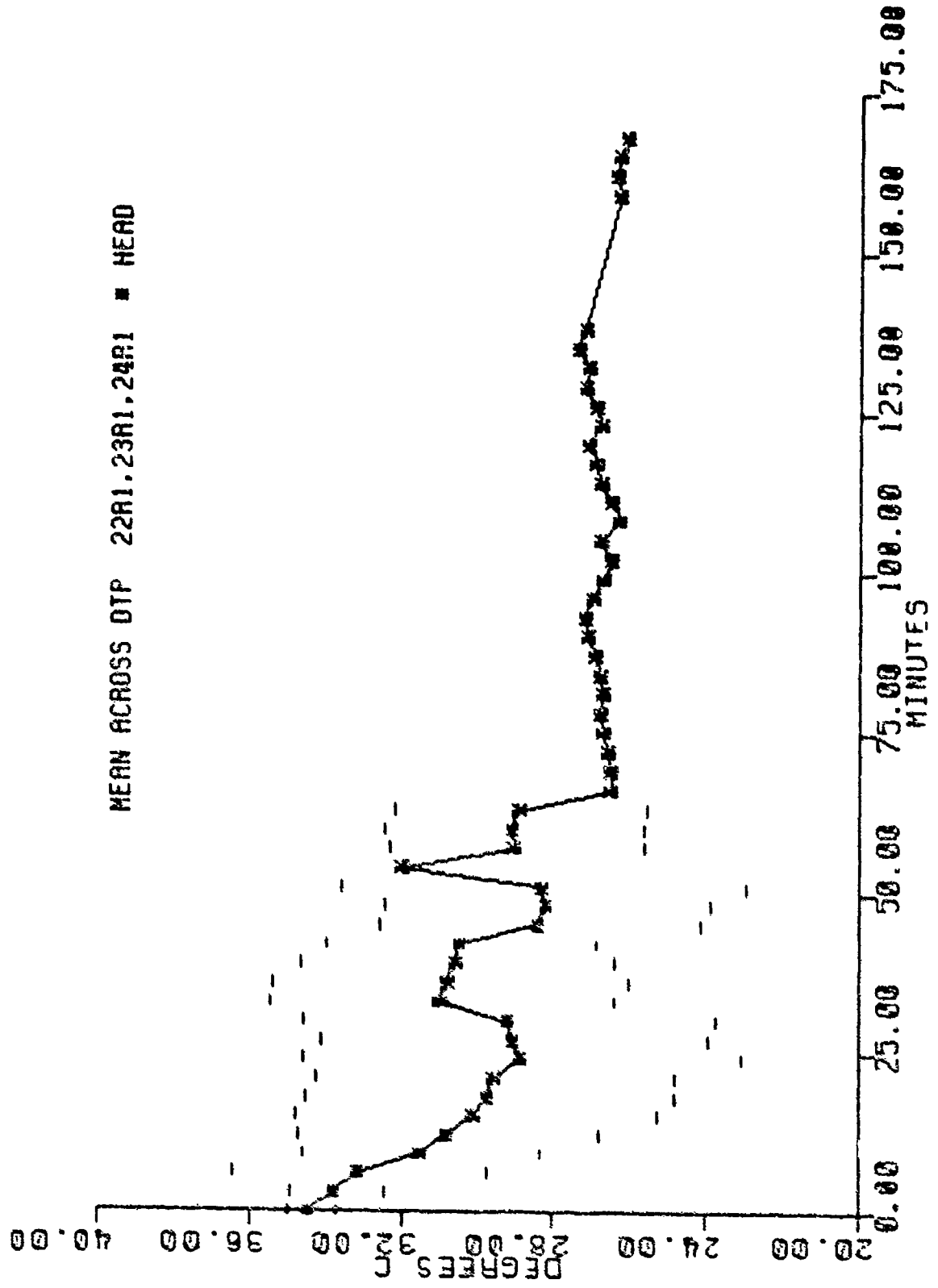


Figure 27. Segmental Subject-Averaged Temperature Profile for the Head (HEAD).

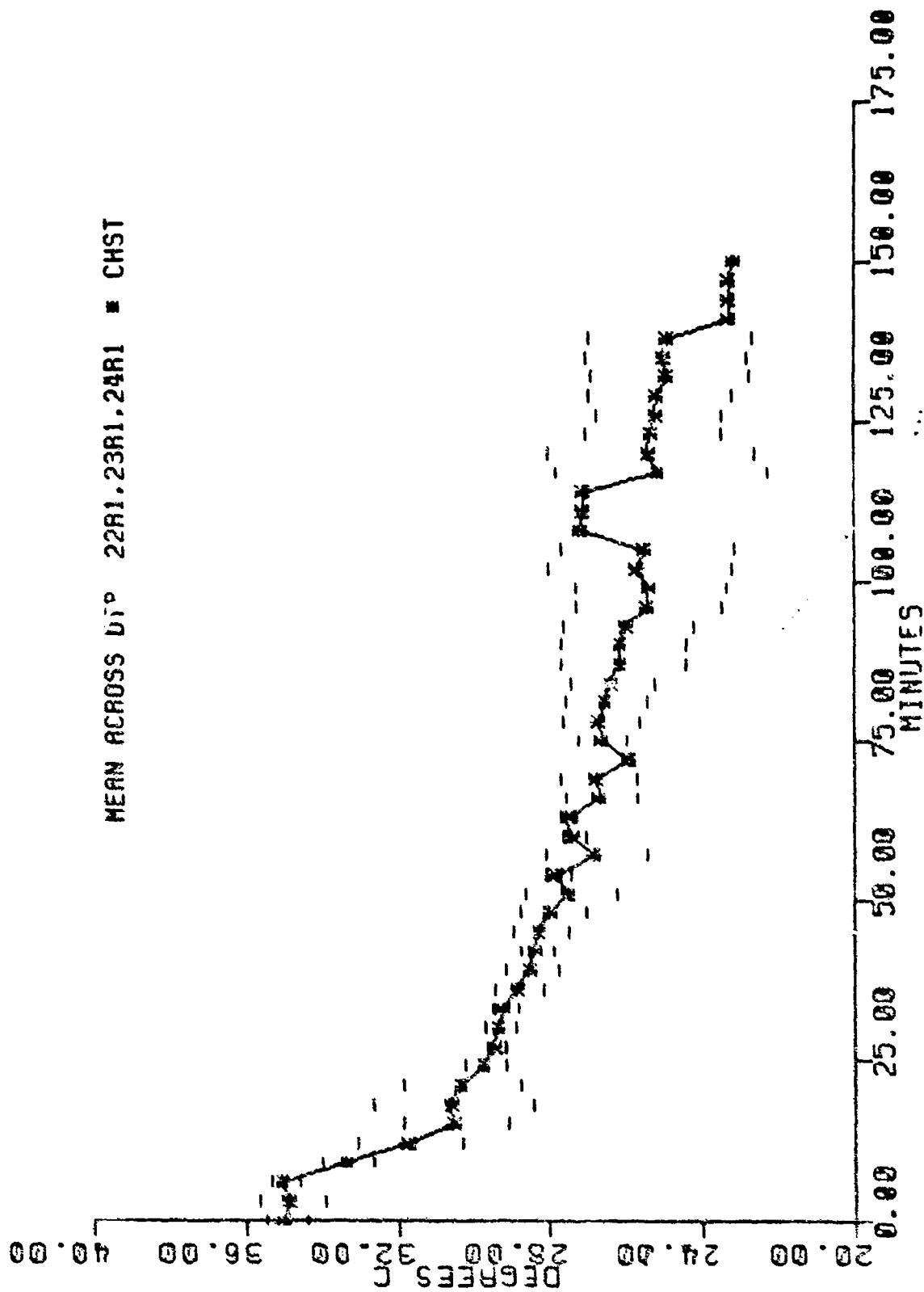


Figure 28. Segmental Subject-Averaged Temperature Profile for the Chest (CHST).

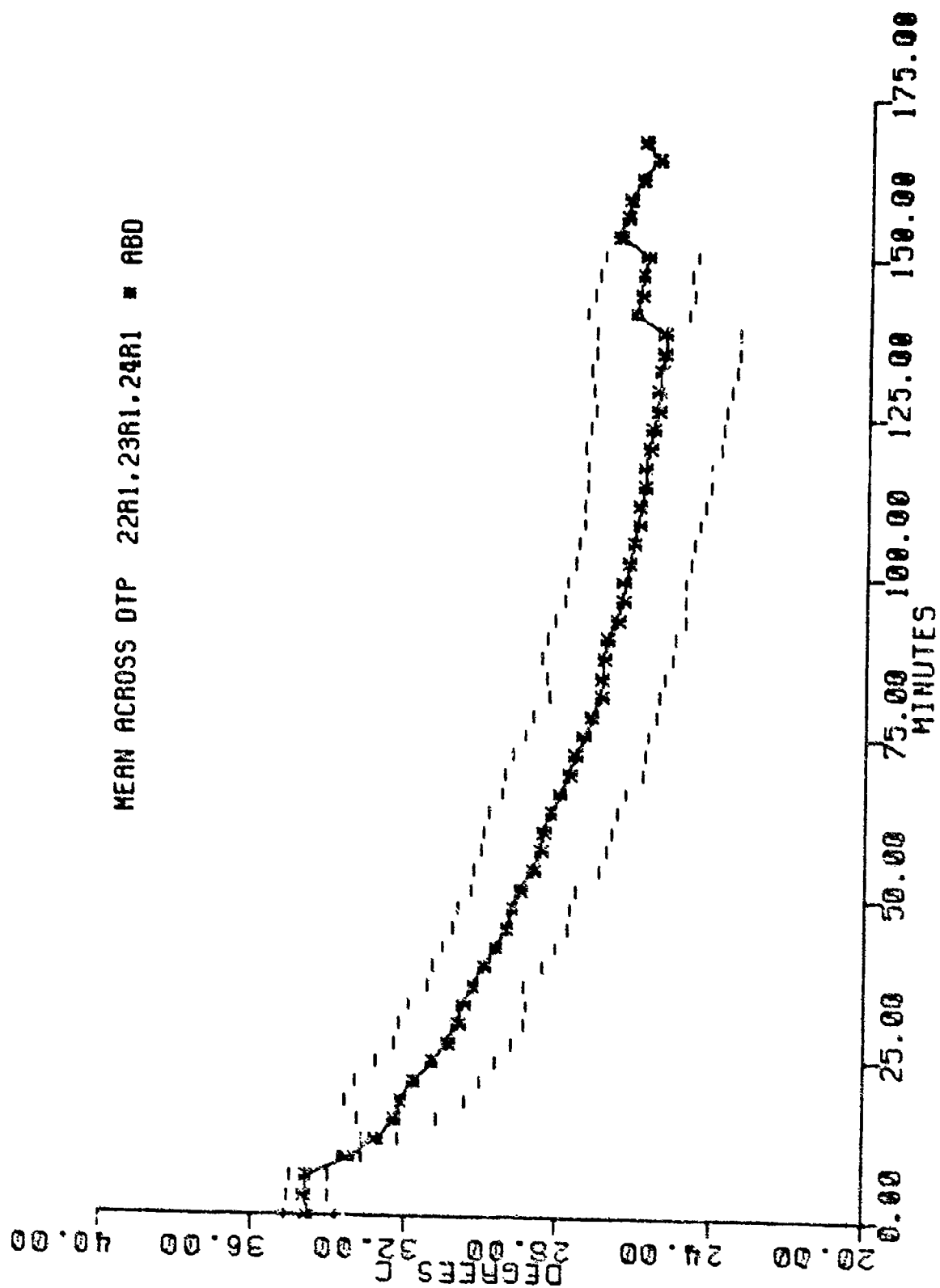


Figure 29. Segmental Subject-Averaged Temperature Profile for the Abdomen (ABD).

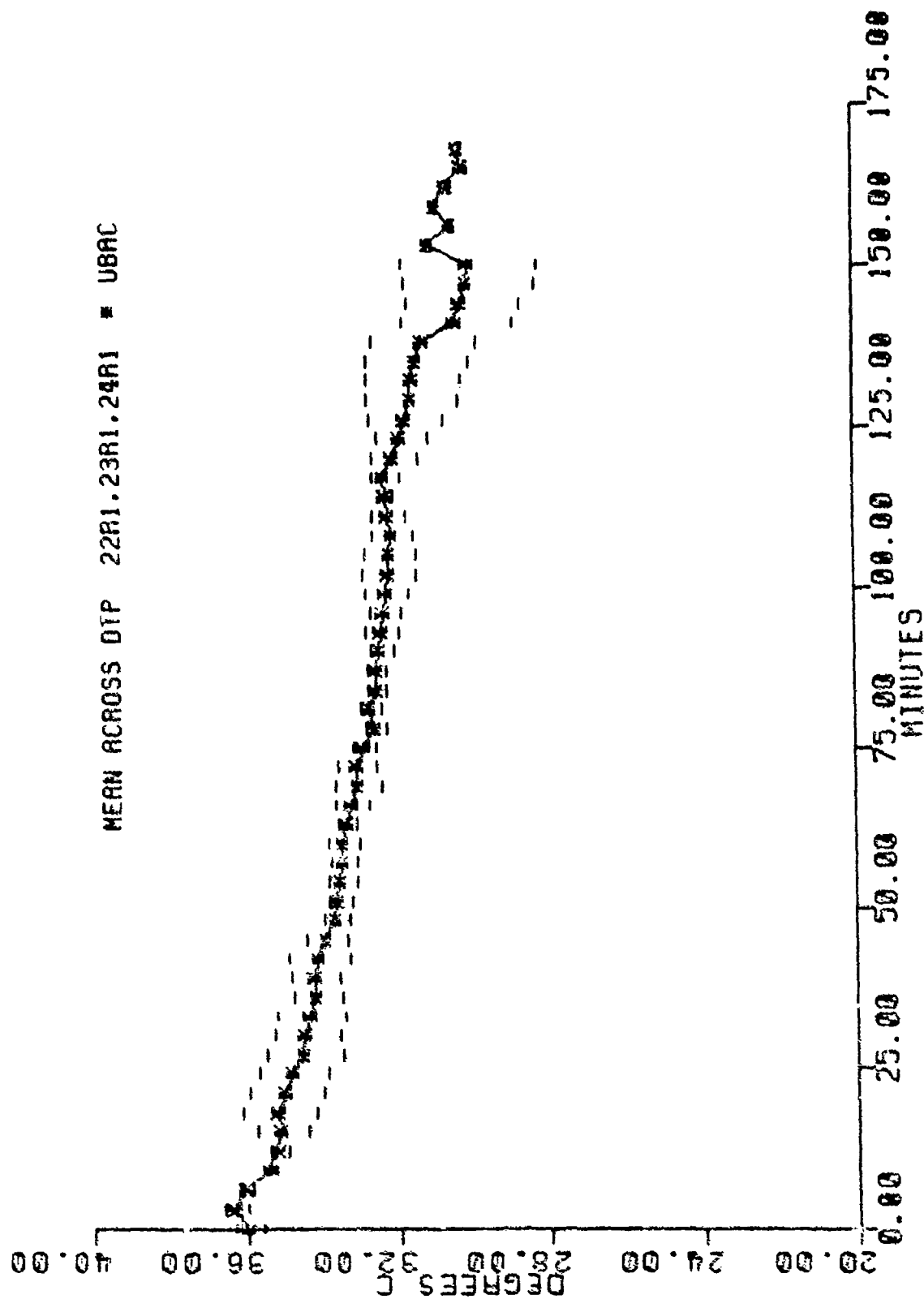


Figure 30. Segmental Subject-Averaged Temperature Profile for the Upper Back (UBAC).

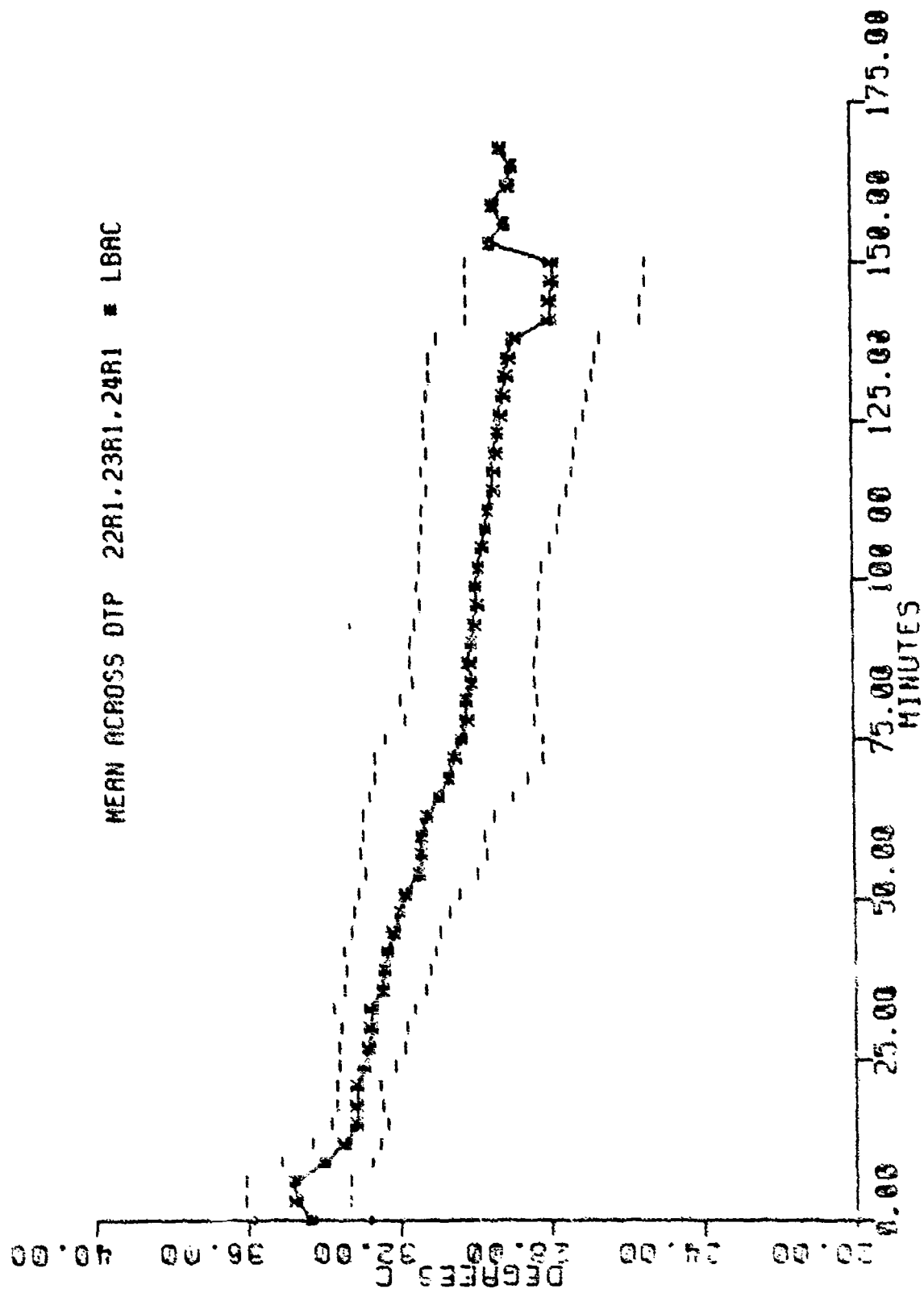


Figure 31. Segmental Subject-Aver ged Temperature Profile for the Lower Back (LBAC).

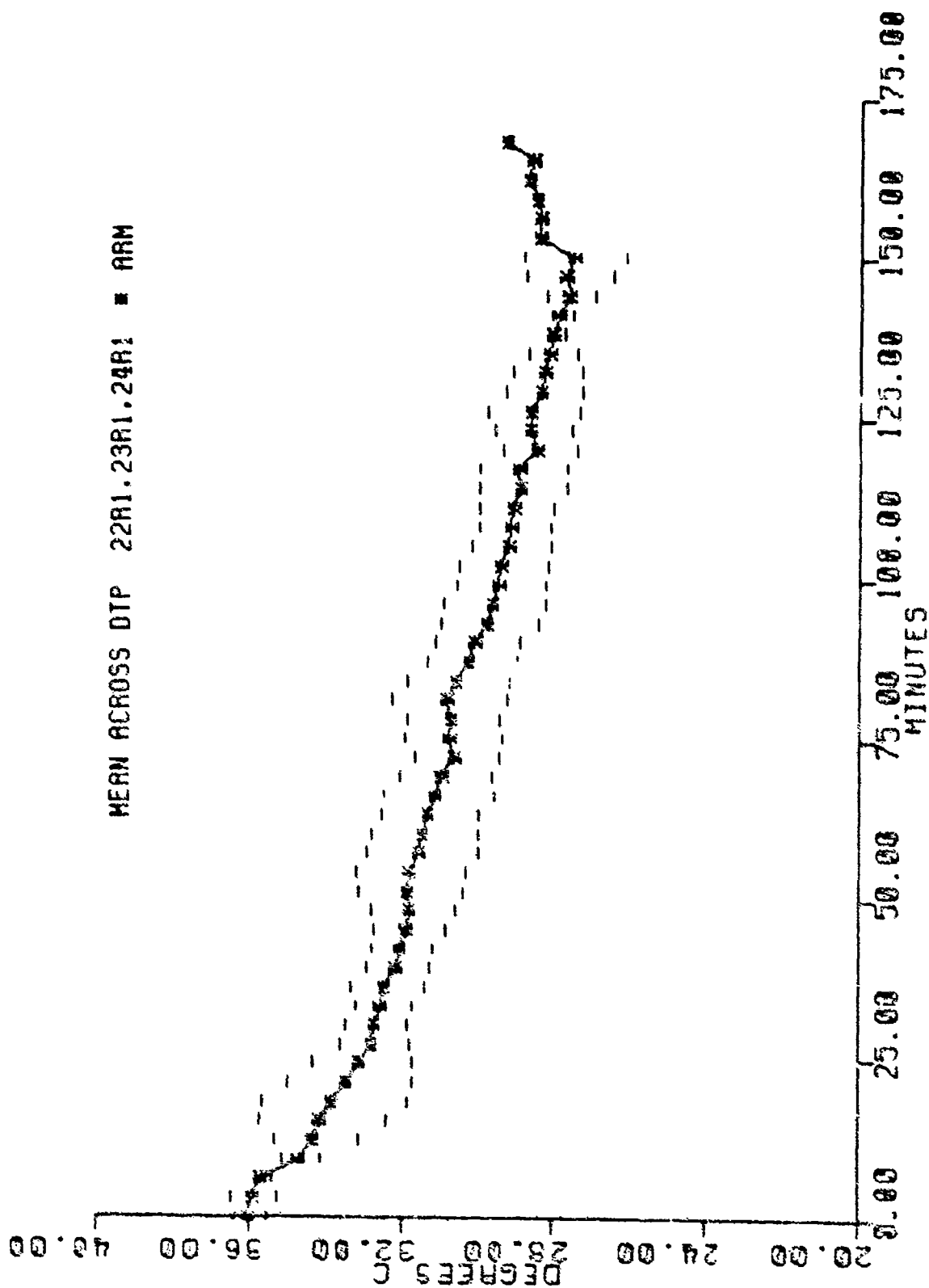


Figure 32. Segmental Subject-Averaged Temperature Profile for the Arm (ARM).

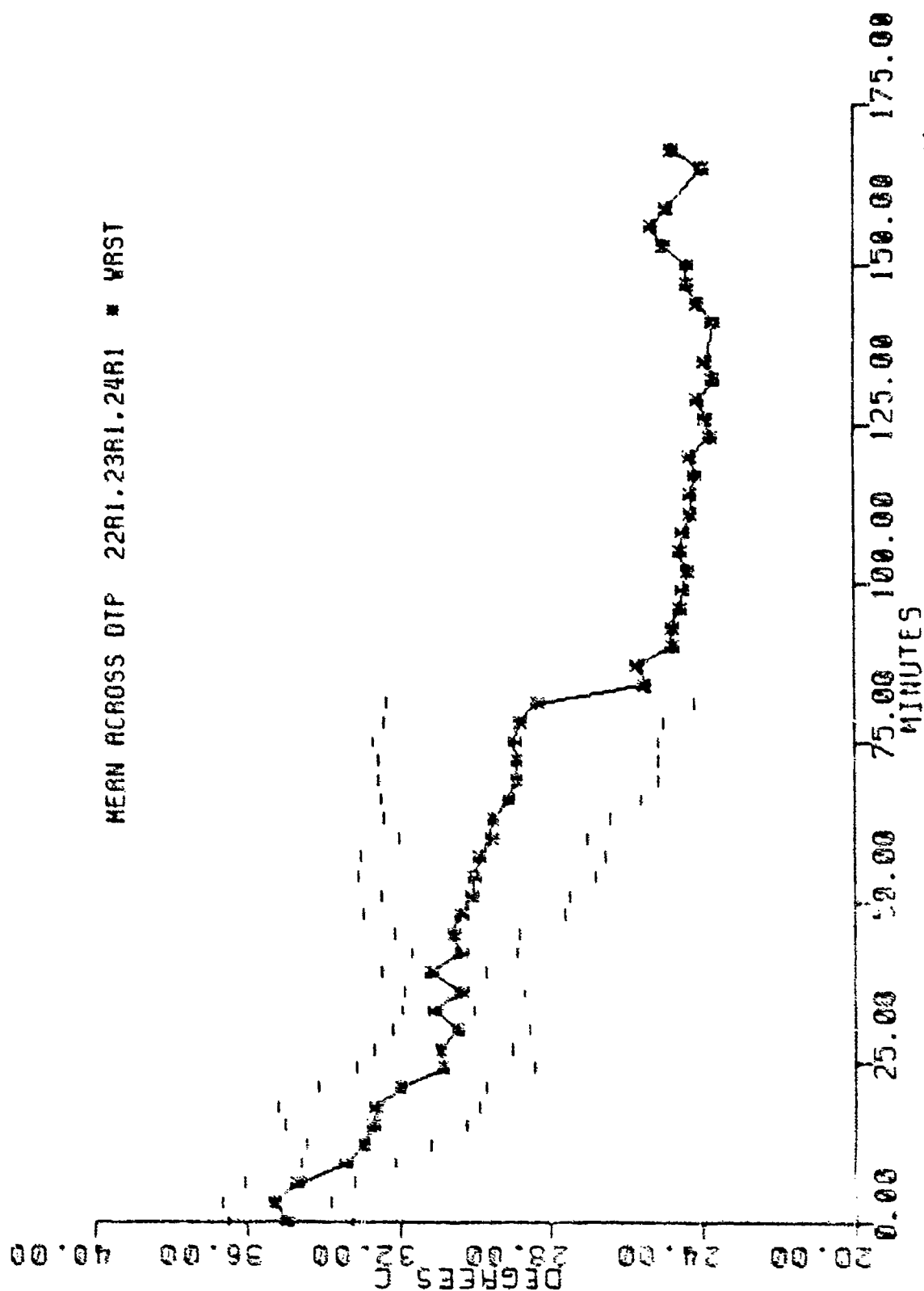


Figure 33. Segmental Subject-Averaged Temperature Profile for the Hand (WIST).

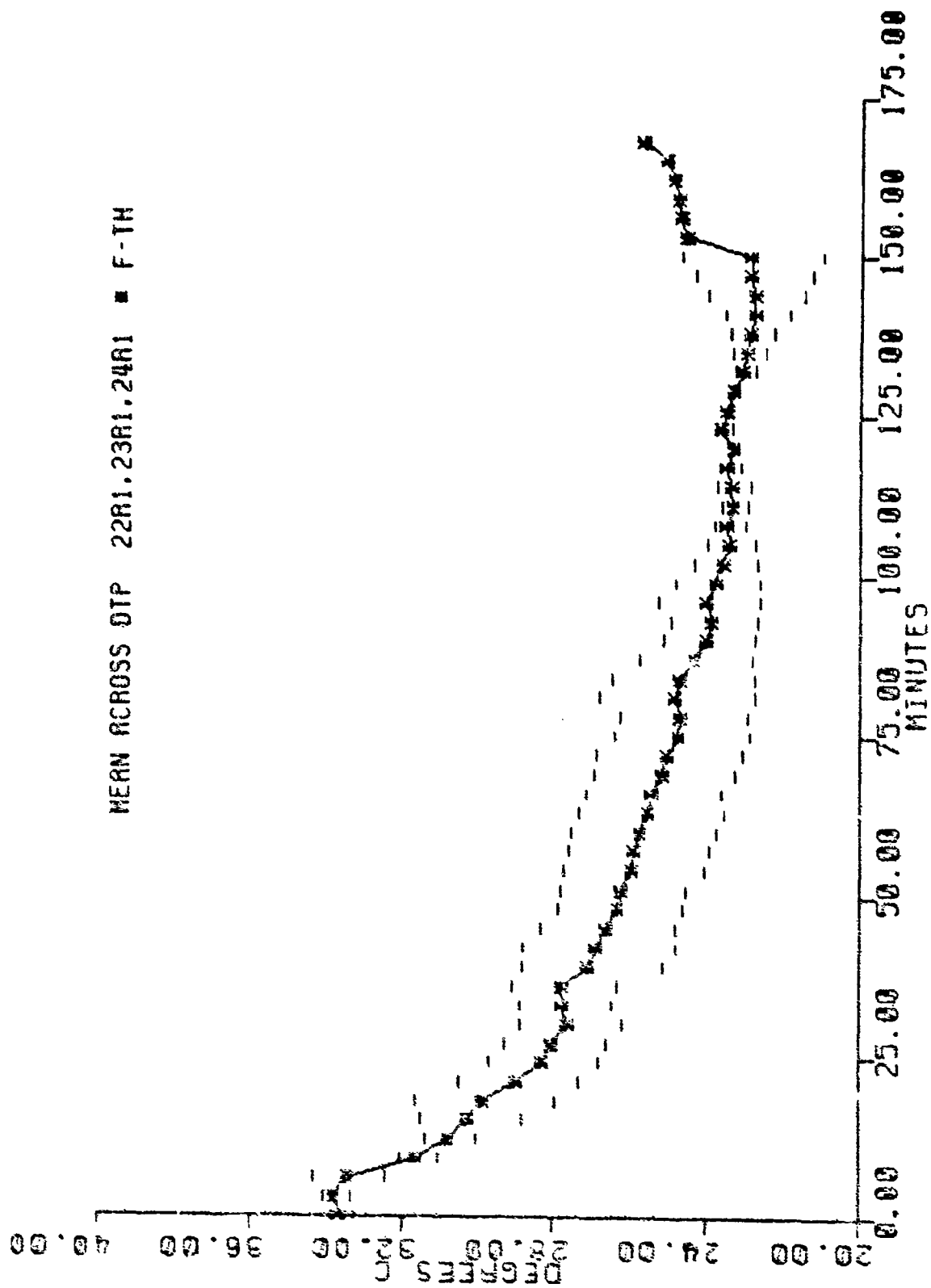


Figure 34. Segmental Subject-Averaged Temperature Profile for the Front Thigh (F-TH).

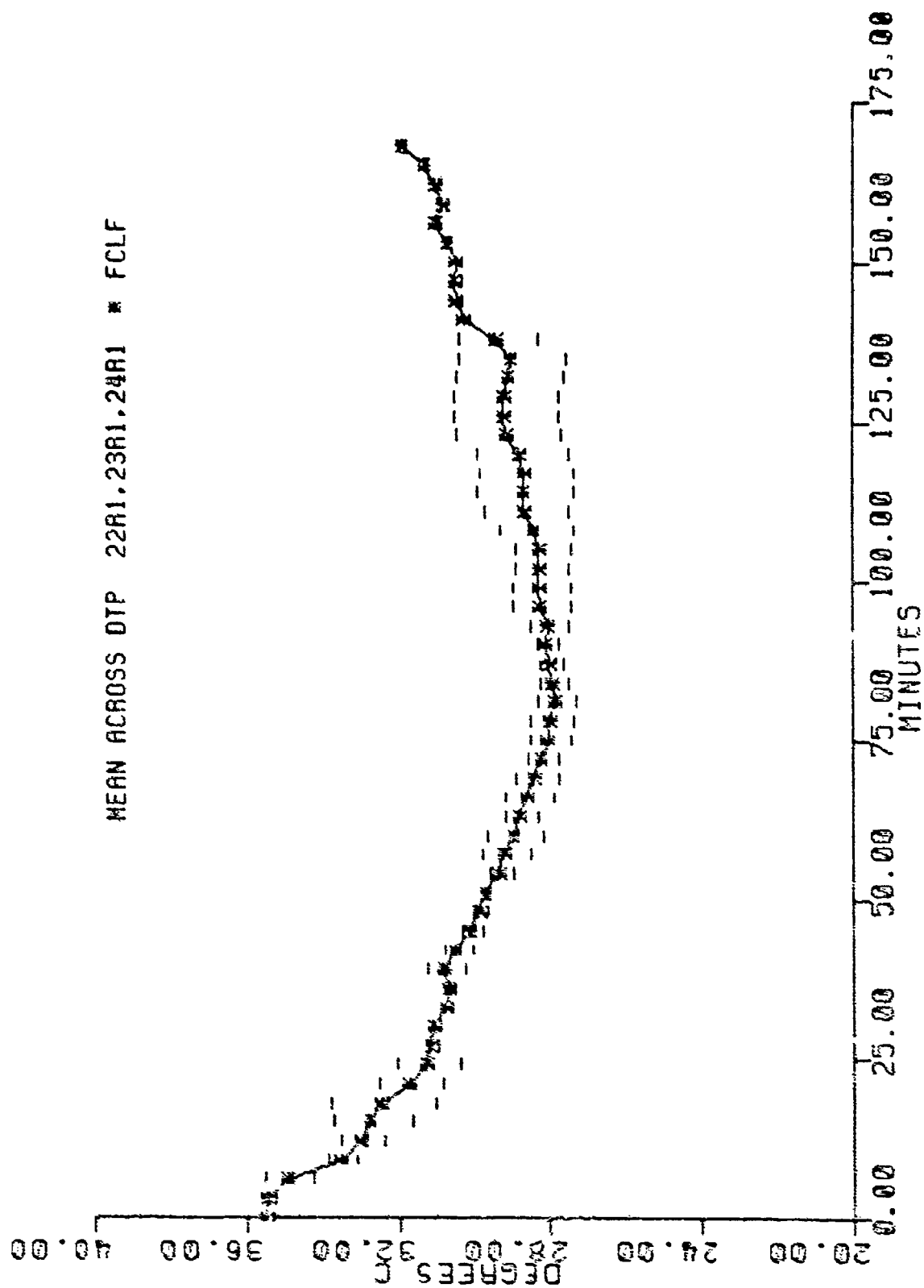


Figure 15. Segment 1 Subject-Averaged Temperature Profile for the Front Calf (FCLF).

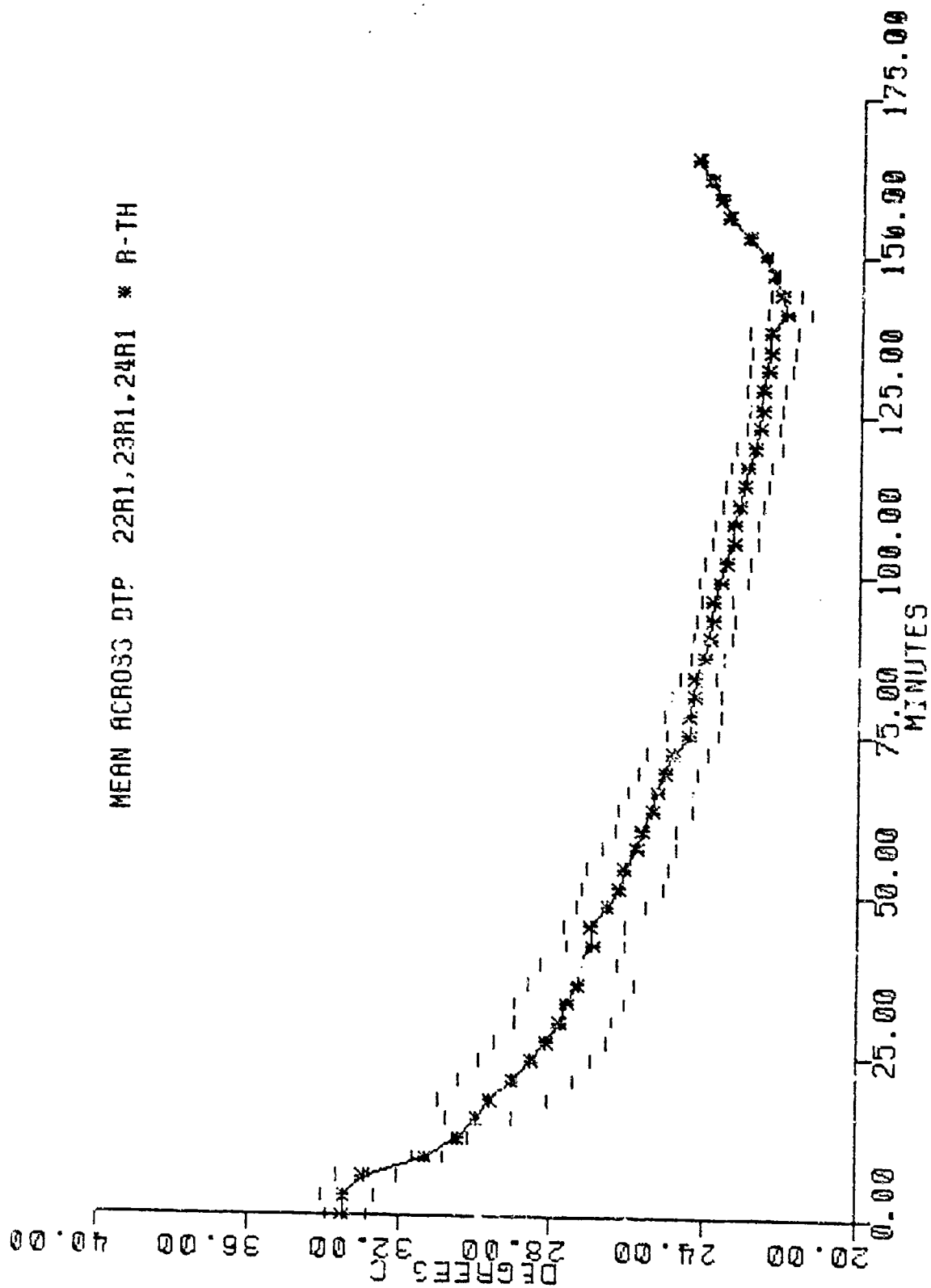


Figure 36. Segmental Subject-Averaged Temperature Profile for the Rear Thigh (R-TH).

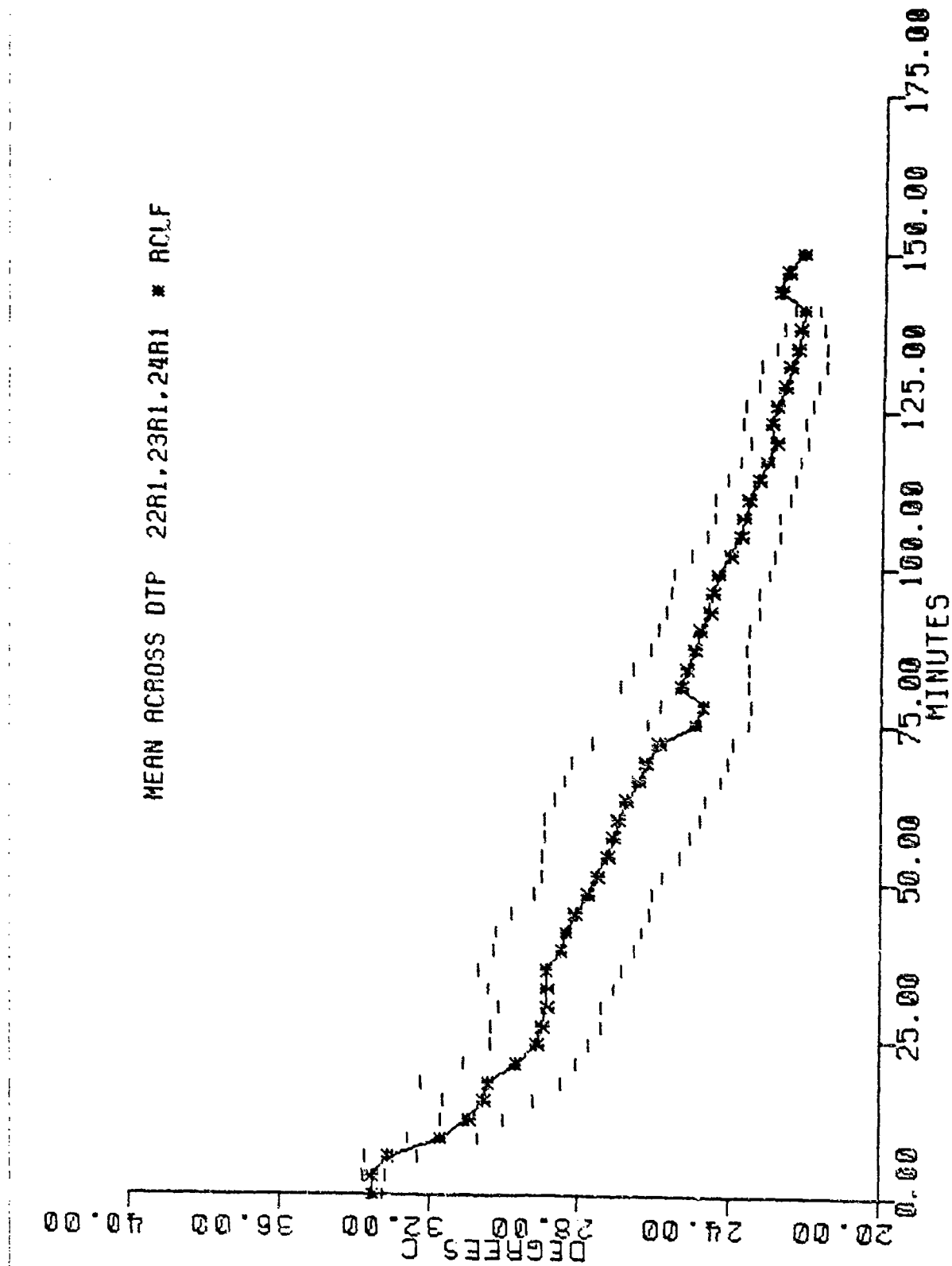


Figure 37. Segmental Subject-Averaged Temperature Profile for the Rear Calf (RCLF).

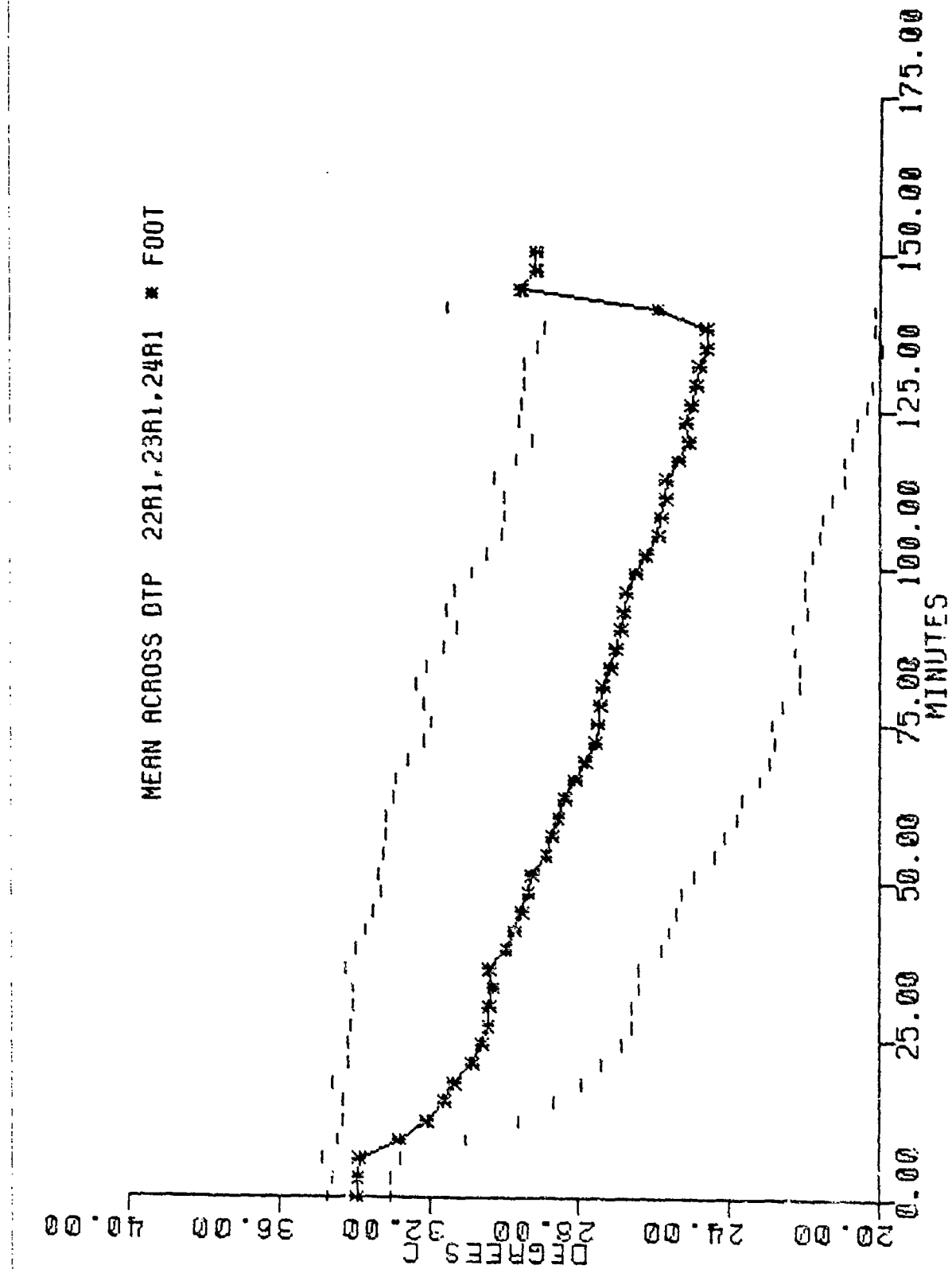


Figure 38. Segmental Subject-Averaged Temperature Profile for the Foot (FOOT).

Figures 39-50. Segmental Subject-Averaged Rate of Heat Loss Profiles. Each figure displays a specific segment's mean rate of heat loss profile. Figures 39-50 were developed from data of Figures 15-26 and correspond to segments 1-12 of Figure 2 and Table 1.

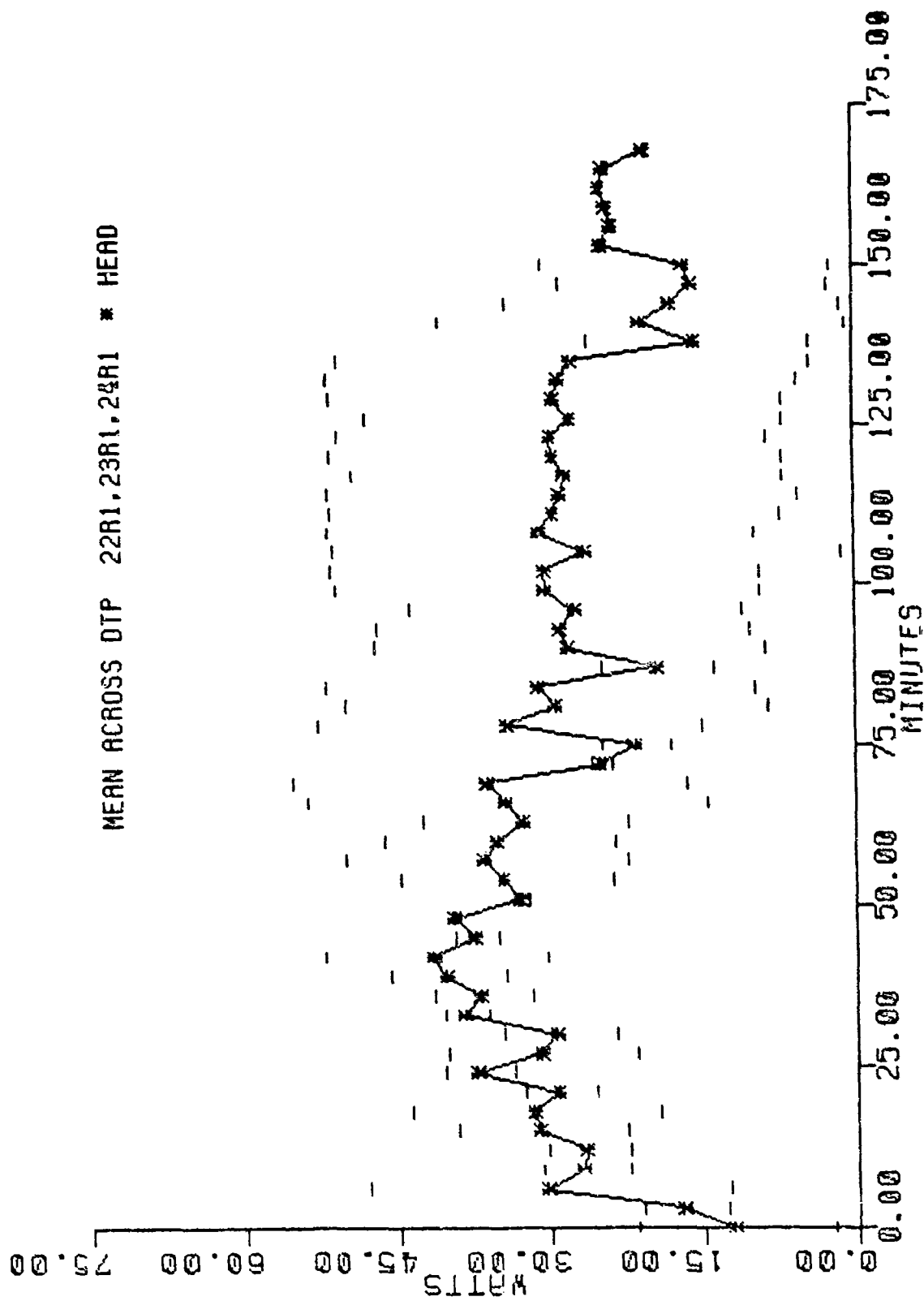


Figure 39. Segmental Subject-Averaged Rate of Heat Loss Profile for the Head (HEAD).

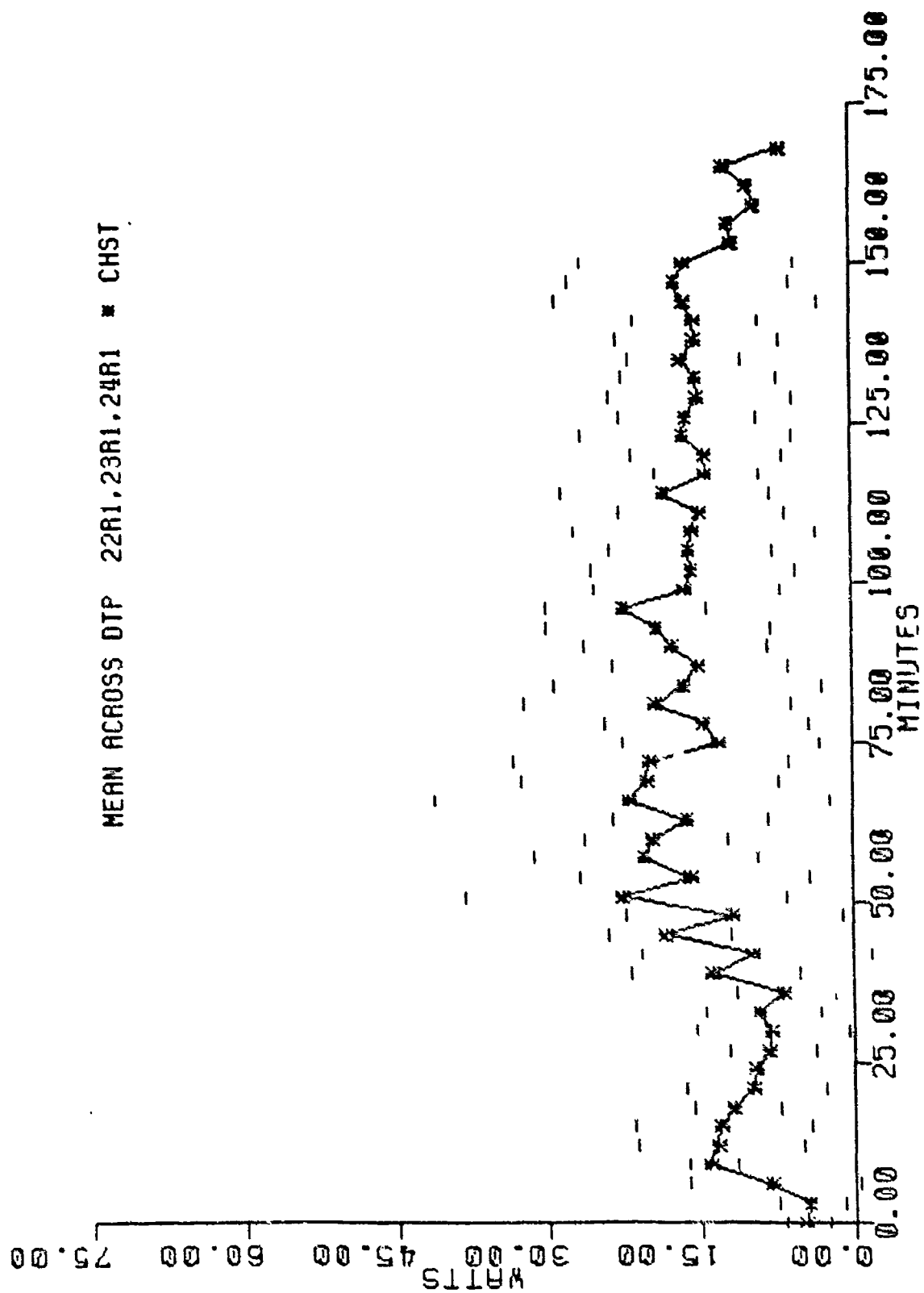


Figure 40. Segmental Subject-Averaged Rate of Heat Loss Profile for the Chest (CHST).

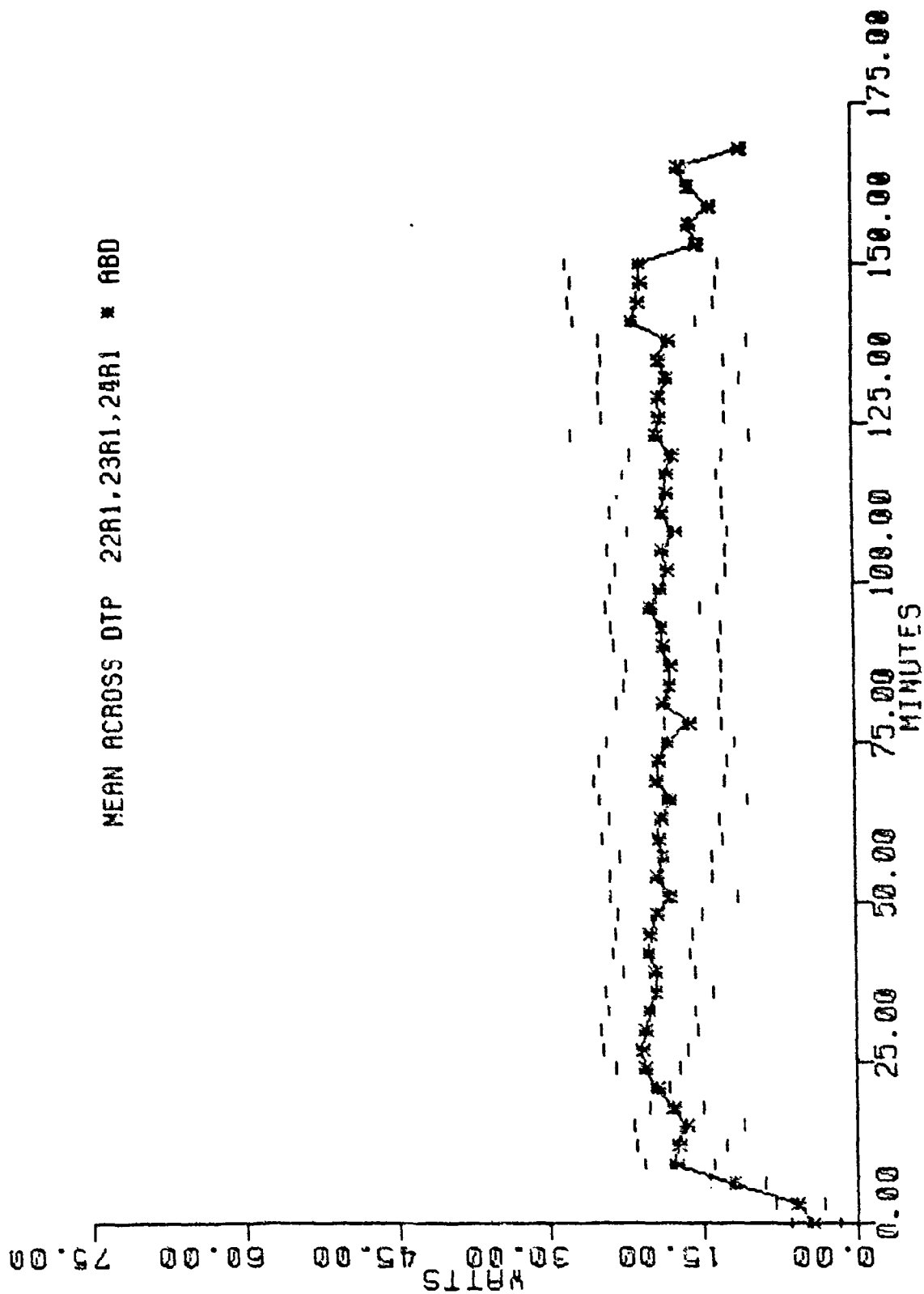


Figure 41. Segmental Subject-Averaged Rate of Heat Loss Profile for the Abdomen (ABD).

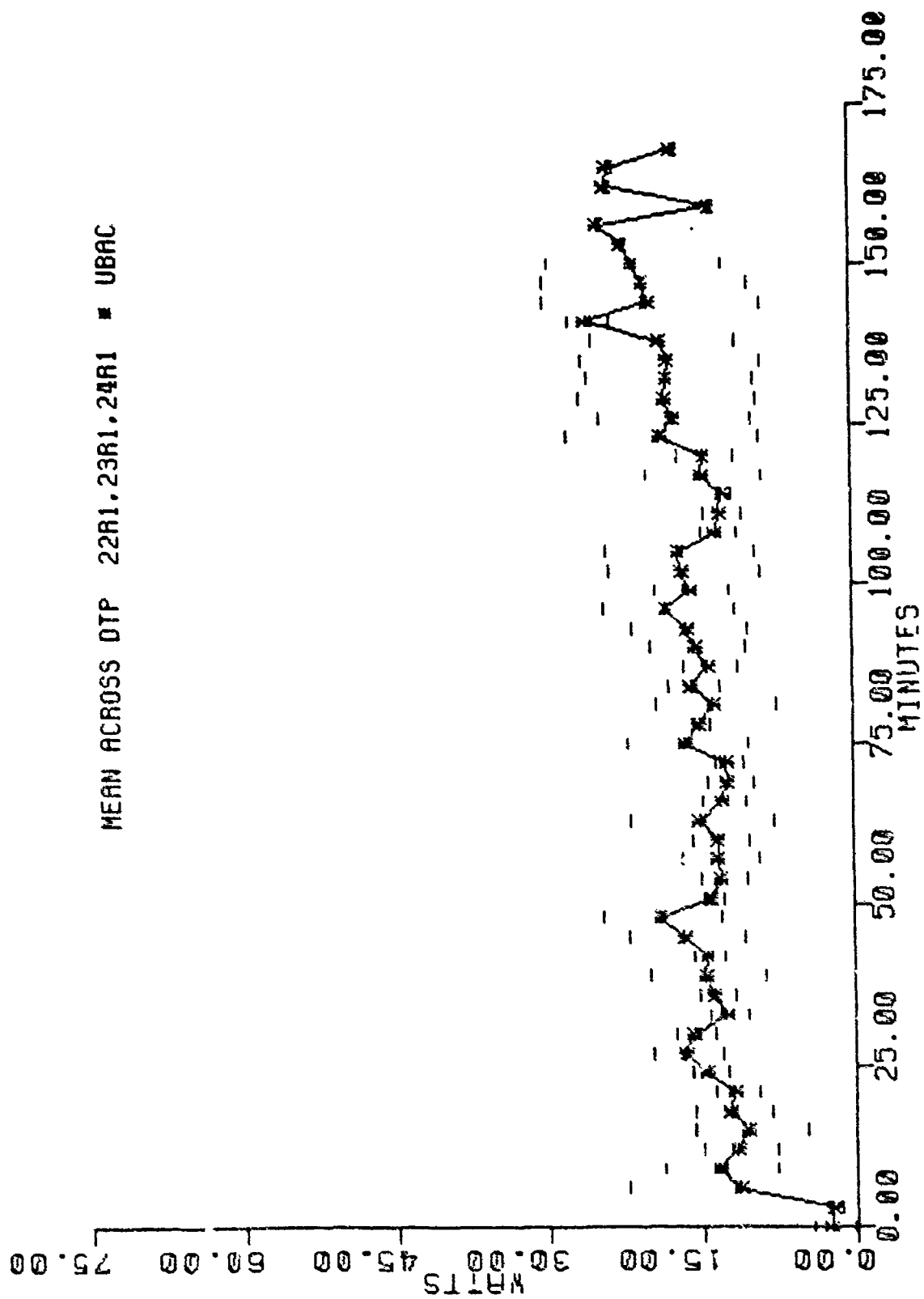


Figure 42. Segmental Subject-Averaged Rate of Heat Loss Profile for the Upper Back (UBAC).

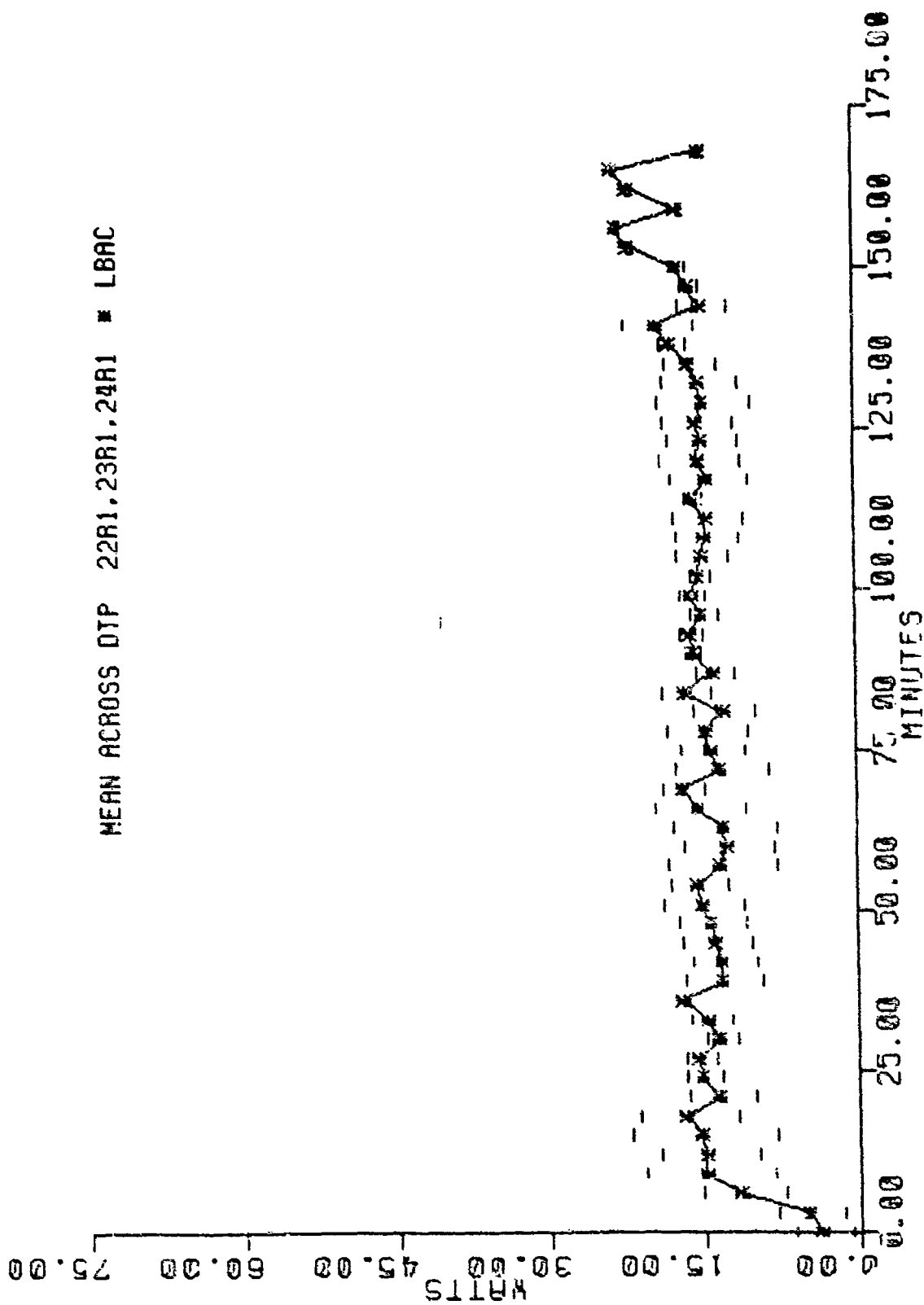


Figure 43. Segmental Subject-Averaged Rate of Heat Loss Profile for the Lower Back (LBAC).

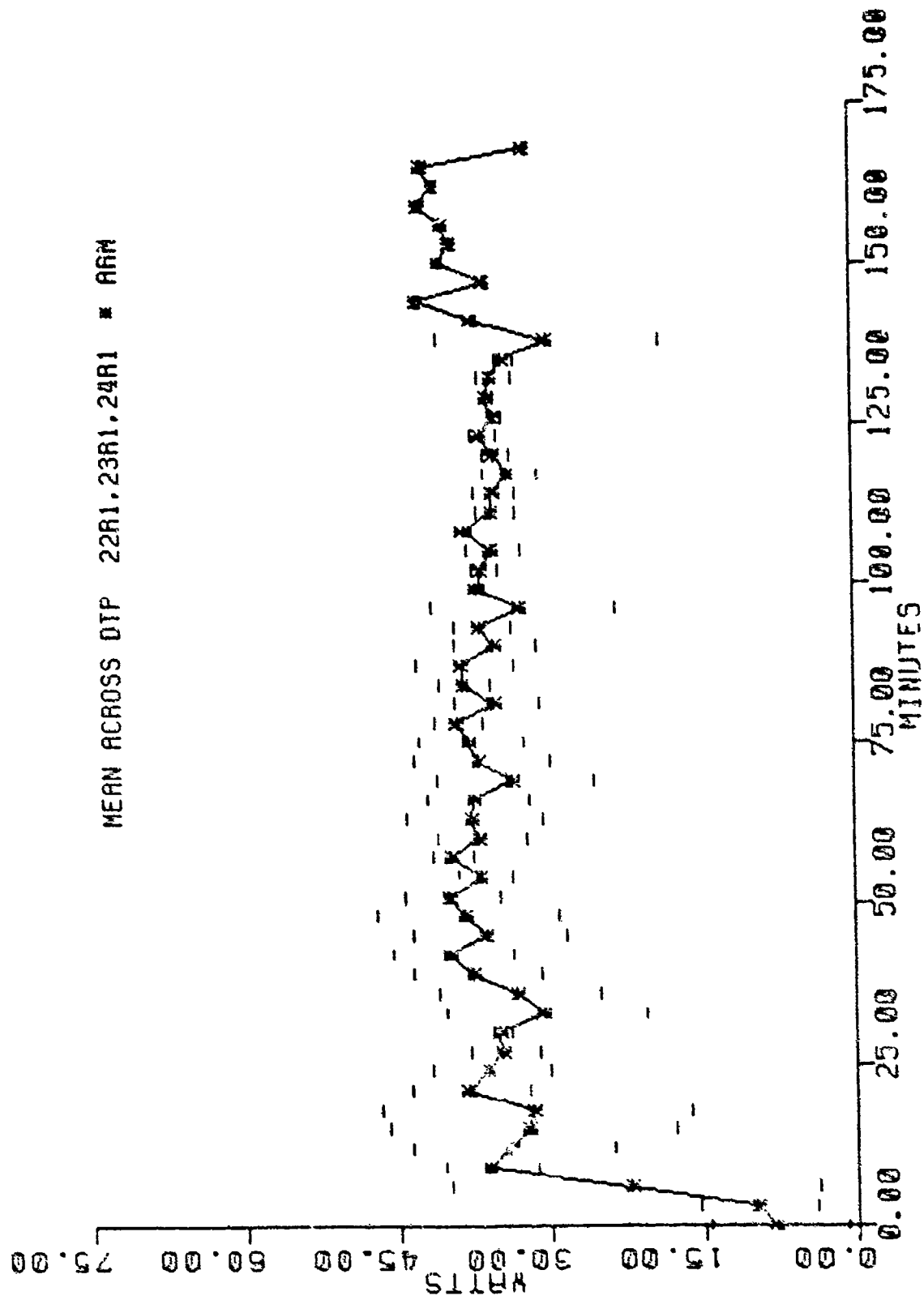


Figure 44. Segmental Subject-Averaged Rate of Heat Loss Profile for the Arm (ARM).

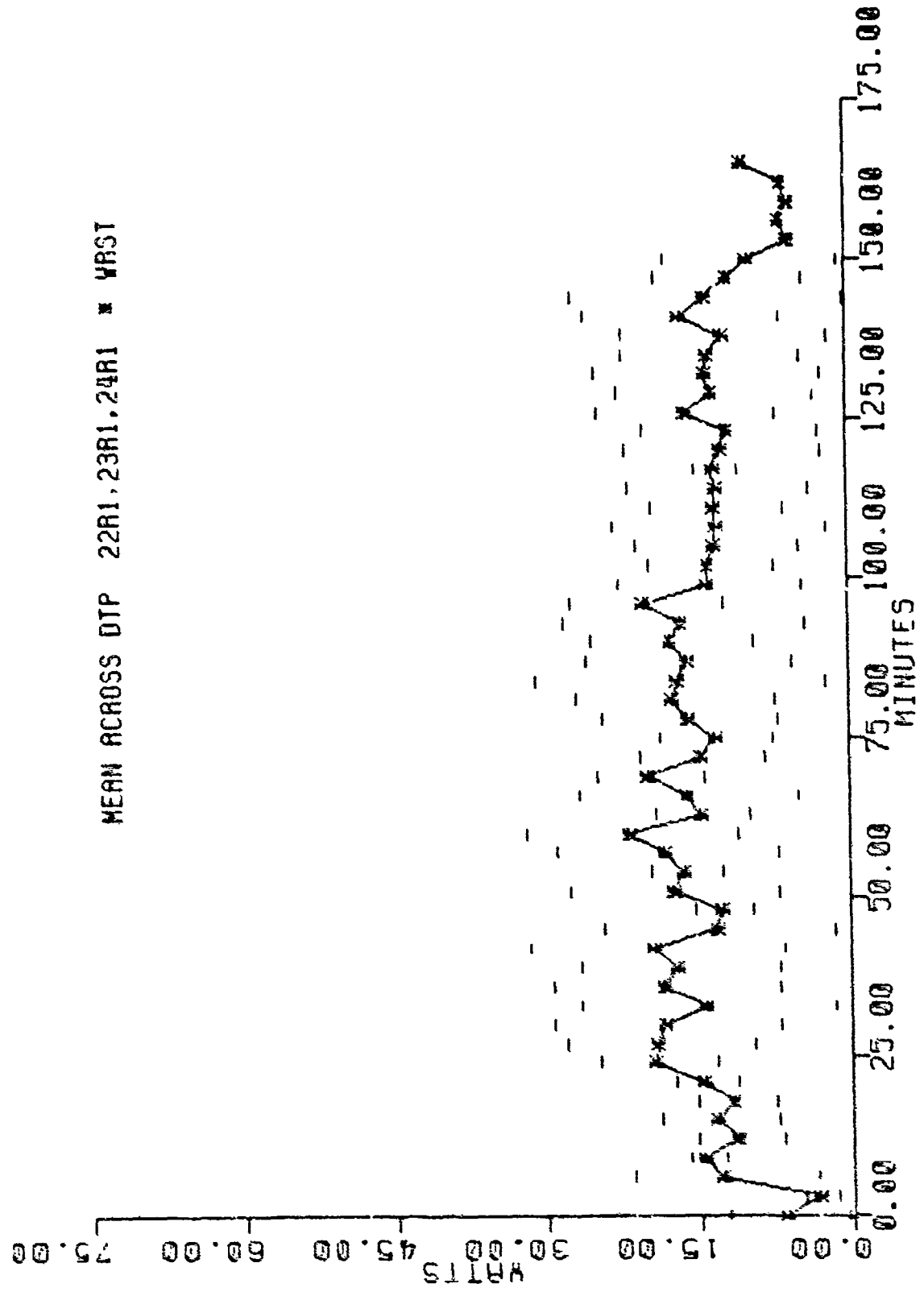


Figure 45. Segmental Subject-Averaged Rate of Heat Loss Profile for the Hand (WRST).

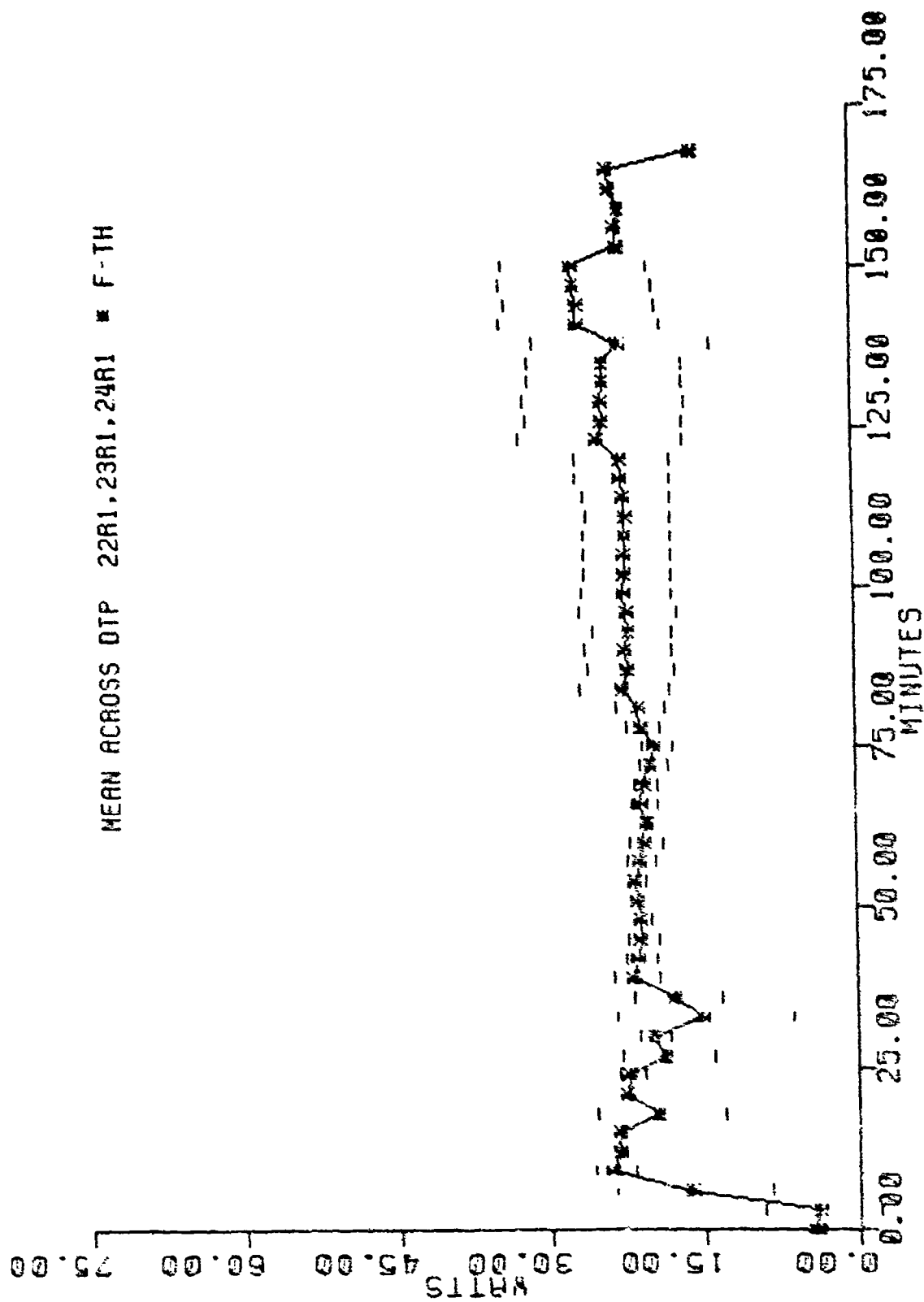


Figure 46. Segmental Subject-Averaged Rate of Heat Loss Profile for the Front Thigh (F-TH).

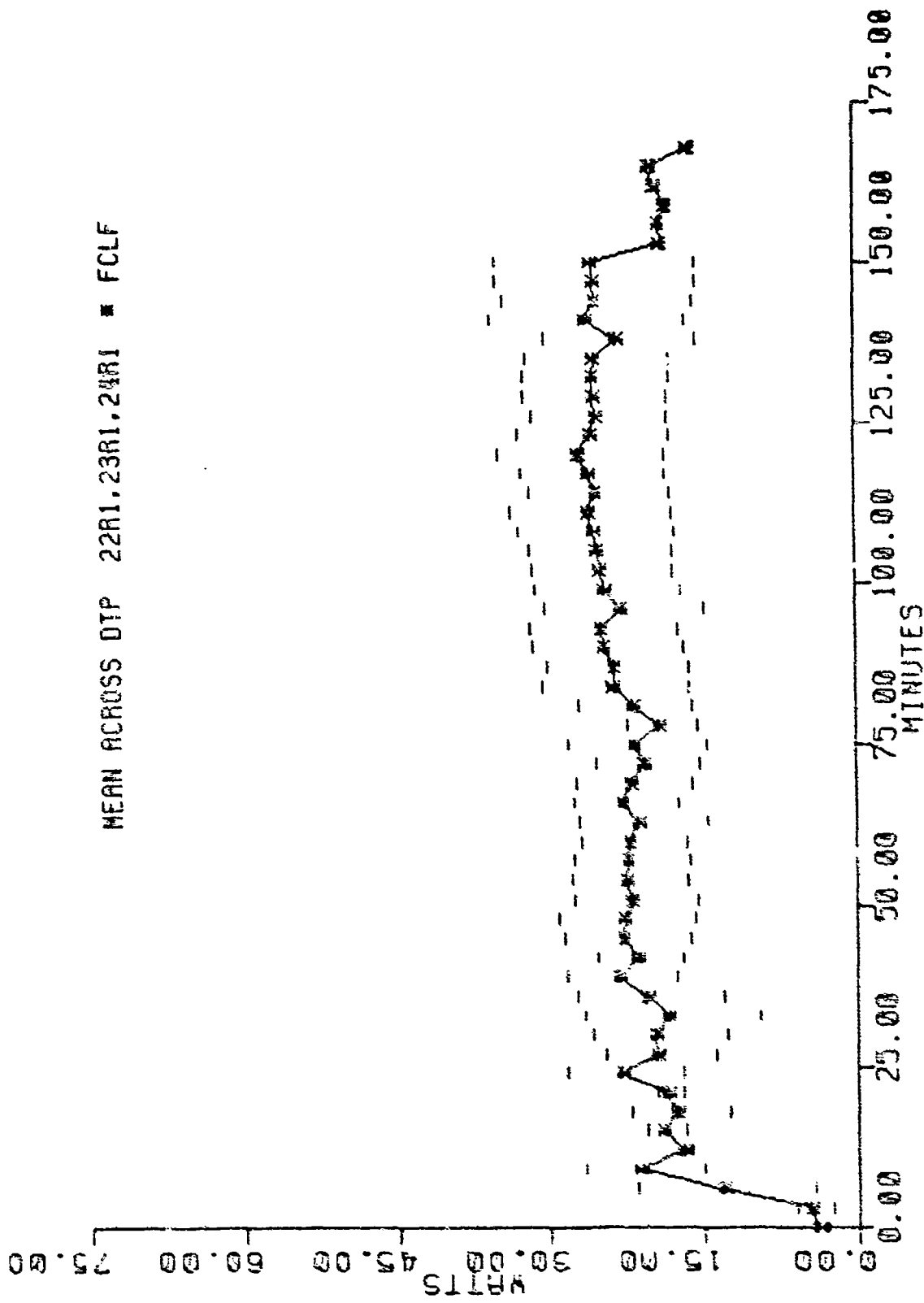


Figure 4/. Segmental Subject-Averaged Rate of Heat Loss Profile for the Front Calf (FCLF).

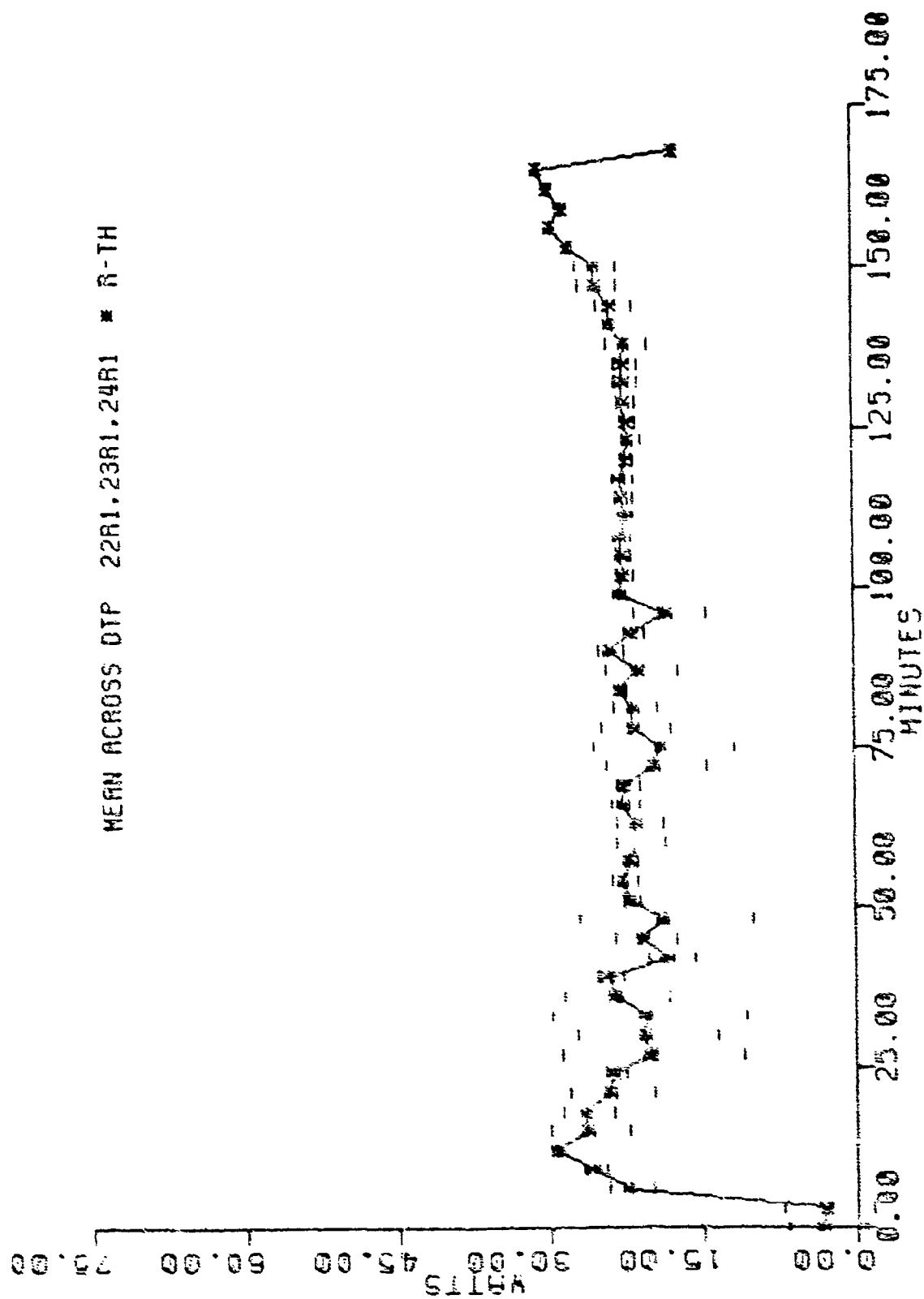


Figure 42. Sequential Subject-Averaged Rate of Heat Loss Profile for the Rear Thigh (R-TH).

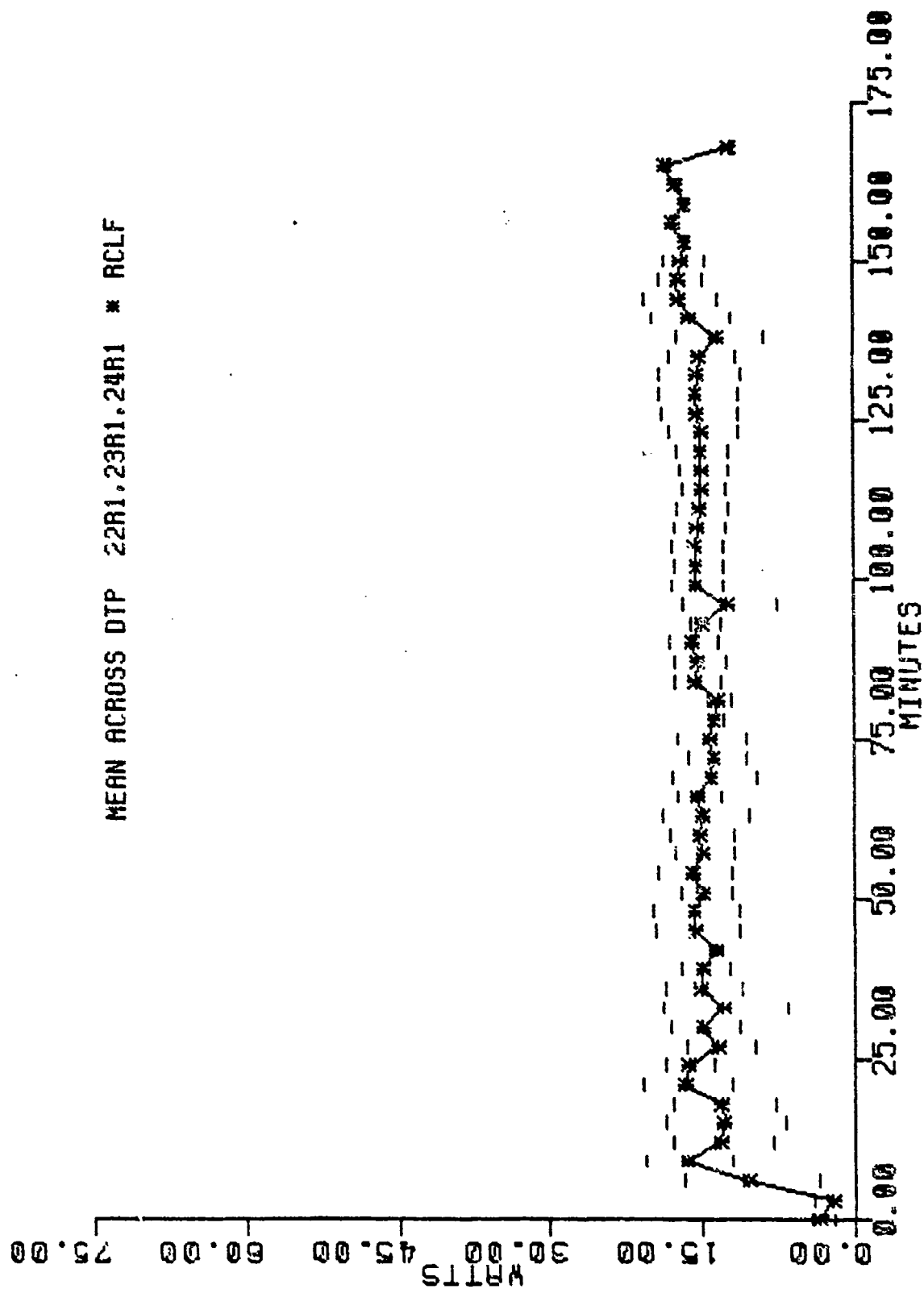


Figure 49. Segmental Subject-Averaged Rate of Heat Loss Profile for the Rear Calf (RCLF).

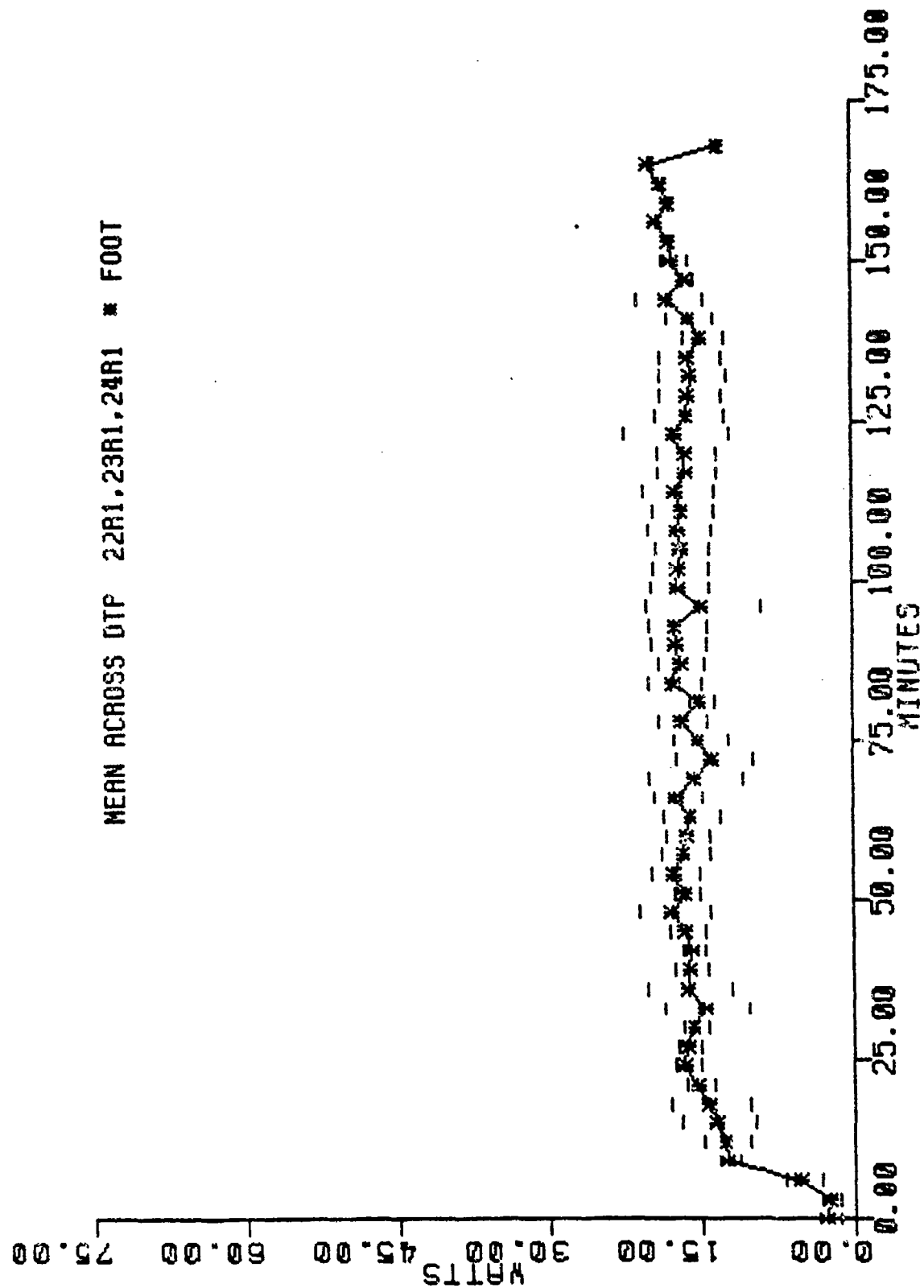


Figure 50. Segmental Subject-Averaged Rate of Heat Loss Profile for the Foot (FOOT).

## Description of Data Groups

Tables 2-4 list all of the data files we acquired which had been recorded with investigator calibrated instrumentation. As mentioned earlier, we employed subject-averaged (composite subject) data files in all of our developments to permit a general application to divers. Each of the data file groupings, which represent a composite subject, are listed below with a brief description deliniating the files included, the source of the data, any problems encountered, and whether or not we used the data (and if not, why).

Dashed lines denote a group change. Each group has been assigned a file for the storage of its composite data even though some of the groups were eliminated before any composite subject data was computed. These storage files were given the names which appear in the first column (Composite File Name) of the tables. These mean file names are used below to identify the groups, and the groups are listed in the order of appearance in Tables 2-4.

### RHL1AR1

The six subjects in this group were exposed to a 20 °C hyperbaric helium-oxygen environment at a pressure of 200 MSW while wearing only swim suits and resting in a sitting position [21]. These subjects participated in a respiratory heat loss study performed by the Navy Experimental Diving Unit. The segmental temperature and rate of heat loss plots, which compare the segmental profiles from each of the six subjects, revealed that the data recorded from subject 3 (RHL13R1) was uncharacteristic when compared to the five other subjects. Thus the data file RHL13R1 was excluded from the development of the composite subject. The mean subject profiles which are stored in RHL1AR1 were computed from subjects 1, 2, 4, 5, and 6, whose data is stored in files RHL11R1, RHL12R1, RHL14R1, RHL15R1, and RHL16R1, respectively.

The experimental heat flux data contained in these files was recorded in watts per meter squared. As a matter of accuracy, all of the segmental heat flux data from the individual subjects was converted to watts before beginning the subject averaging process. This was accomplished by multiplying the segmental data in  $W/M^2$  by the segmental surface area. Each subject's segmental surface area was determined by multiplying his recorded total body surface area by the respective Hody segmental surface area fraction (Table 1).

The RHL1AR1 data was employed in developing our segmental skin temperature predictive correlation for the twelve Hody segments (Fig. 2). This correlation is adapted from the eight region model proposed by Kerslake [2] and is described in detail in Chapter IV. This composite data was also used to develop convective heat transfer coefficients for the immersed diver subjects. This development was performed by extrapolating data from one environment to another by use of dimensionless heat transfer correlations.

#### RHL1AR2

The six subjects in this grouping were exposed to a 15 °C hyperbaric helium-oxygen environment at a pressure of 200 MSW while wearing only swim suits and resting in a sitting position [21]. These subjects were participants in the same respiratory heat loss study as the subjects in the RHL1AR1 grouping. The segmental temperature and rate of heat loss plots, which compare the segmental profiles from each of the six subjects, revealed no characteristic pattern among the subjects. The lack of similarity among these subjects suggested that the data produced by subject averaging would be unrepresentative of the group. Thus the data in files RHL12R2, RHL13R2, RHL14R2, RHL15R2, RHL16R2, and RHL17R2 were not used for any of our developments.

RHL1AG2

The two divers in this group were exposed to a 15 °C hyperbaric helium-oxygen environment at a depth of 200 MSW while clad in swim suits and resting in a sitting position [21]. The difference between this set of dives and the RHL1AR2 dives is that these subjects were breathing a heated helium-oxygen mixture at 20 °C, and the RHL1AR2 divers were breathing an unheated, 15 °C helium-oxygen mixture. Since these subjects were breathing warm gas, they could not be used in comparisons with the other helium-oxygen data. Thus, because of the comparison difficulties and the fact that the 15 °C ambient temperature was probably too cold, we decided not to use this data in any of our developments.

RHL1AW1

The five swim suited subjects of this group were exposed to a 20 °C hyperbaric helium-oxygen environment at a depth of 200 MSW while sitting on a bicycle ergometer and working at a fixed rate of 50 watts. These divers were also participants in the respiratory heat loss study performed by NEDU.

The plan for the development of the diver heat loss model first called for the development and verification of a resting model, followed by (data permitting) development of a numerical working diver model. Due to the small number of working studies performed under the same environmental conditions and at the same rates of work, we decided (in consultation with our Navy Medical Research and Development Command sponsor) to defer the development of the working model until more experimental data was available. As a result, our analysis of the working data has been limited to a basic decision of its usefulness.

The data found in RHL11W1, RHL13W1, RHL14W1, RHL15W1, and RHL16W1 could easily be converted to an average record. This composite data file could then

be employed for the purposes of adapting the resting segmental predictive skin temperature correlation and the convective heat transfer coefficients to the working case.

#### DTP1ART

This mean data file was generated from files DTP11RT, DTP12RT, DTP13RT, and DTP14RT. These studies were performed by the NCSC to evaluate their thermal data acquisition system. Each diver was dressed in the prototype DTP garment and submerged to a depth equivalent to 3 MSW in 5 °C water [13,22]. These air-breathing divers were then requested to remain at rest and in roughly a prone position for the duration of the dive. The plots which display the superimposed segmental profile of each diver showed a consistent pattern as a function of time among all the subjects. Initially the composite profiles displayed a sawtooth pattern which is characteristic of unsynchronized time records<sup>6</sup>. Examination of this composite segmental data indicated that not all of the constituent files were synchronized with a three minute time increment. Since the number of time records which were not synchronous was small compared to the total number of time increments, the unsynchronous time records were deleted from all computations. The corrected rate of heat loss data stored in DTP1ART is in the units of watts. Since the original data files were recorded in KCAL/M<sup>2</sup>·HR, the data was converted to watts before beginning the averaging operation. Readily available conversion factors and the individual subject's segmental surface area were used to change KCAL/M<sup>2</sup>·HR to watts. These segmental surface areas are computed in the same manner as described for the RHL1ARI file. This data was subsequently used to verify the heat loss model for a prone, resting, DTP clad diver.

---

<sup>6</sup>See Foreword for the connotation of time record.

DTP2AR1

The four subjects of this group were participants in a study performed by NCSC to evaluate a prototype DTP garment during air diving [22]. Each subject was clad in the prototype DTP garment and submerged in 5 °C water to a pressure equivalent to 3 MSW. The divers were to rest in a prone position until instructed otherwise. From the information provided about this series of dives [22], it was learned that subject number one's suit flooded very soon after immersion. Thus all data taken from subject 1 and contained in DTP21R1 was deleted. The segmental plots, which superimposed the segmental profile of each subject, did not indicate any irregularities among the divers. Thus the three subject's data that are contained in DTP22R1, DTP23R1, and DTP24R1 was averaged through use of Equation 2. As was the case with the original source files which make up the DTP1ART group, the constituent source files of the DTP2AR1 group were recorded in KCAL/M<sup>2</sup>·HR. As indicated earlier, all heat flux data was converted to units of watts before beginning the averaging process. For this group, the applied conversion factors were created from commonly available conversion factors and the segmental surface area of the appropriate subject. These segmental surface areas were computed from the total body surface area of each subject by using the Hody segmental surface area fractions (Table 1), as was the case in the RHL1AR1 section. This data was used to verify the heat loss model for a resting, DTP clad, air-breathing, submerged diver in water at a pressure and temperature of 3 MSW and 5 °C, respectively. The data presented here and in the DTP1ART file gave us two sets of similarly conditioned studies with which to verify our predictive diver heat loss model, therefore improving the statistical authenticity of the model.

DTP2AW2

The four subjects constituting this group participated in the same series of garment evaluation studies as the previous group and were exposed to the same environmental conditions. The only difference is that these divers worked on a vertical ergometer at a rate of 50 watts for six minutes followed by four minutes of rest. This sequence of work followed by rest was repeated throughout the experiment. The data found in DTP21W2, DTP22W2, DTP23W2, and DTP24W2 could be easily combined into a mean (composite) subject file. As was the case with the corresponding resting studies, the heat fluxes were recorded in  $\text{KCAL/M}^2\cdot\text{HR}$  and must be converted to watts before being processed into averages. This data would be useful in verifying a working model for a sitting subject who is intermittently working at a constant rate of 50 watts.

DTP2AW3

The four files in this group constitute the final dives performed in this series of NCSC garment evaluation studies [22]. Here the subjects worked under the same immersed conditions as the previous groups involved in the garment evaluations. The only difference between this group and the DTP2AW2 grouping is that, instead of working at a fixed rate, the subjects started at 50 watts but incrementally increased the ergometer work rate by 50 watts between successive cycles of work for six minutes and rest for four minutes until 150 watts had been completed. At that point, the subjects ceased working and rested for the duration of the study. Since the information provided on files DTP21W3, DTP22W3, DTP23W3, and DTP24W3 [22] indicated that no problems occurred during the dive, these files could be easily applied to generate an average (composite) record. As seen with the other groups involved in these garment evaluation studies, the heat loss data was recorded in  $\text{KCAL/M}^2\cdot\text{HR}$  and therefore must be converted to watts before being processed into averages.

These studies will not be very useful in developing an initial working model. This statement is made since the subjects performed at a higher rate of work than any other available files, and since these subjects quit working after reaching their maximum rate. This pattern is unique to this set of studies.

#### DTP3AR1

This set of dives was performed in a hyperbaric water environment at a depth of 21 MSW to further evaluate the prototype DTP garment. These files were provided to us by NEDU although the study was performed jointly by NEDU and NCSC [22]. The data in files DTP33R1, DTP34R1, DTP35R1, and DTP36R1 was all taken from air-breathing, DTP clad subjects who were exposed to 5 °C water at a hyperbaric pressure equivalent to 21 MSW and resting in a prone position. The segmental plots, which show the superimposed segmental profile of each subject, indicated that the data of subject 4 was consistently different from the other subjects. Thus the data in file DTP34R1 was excluded from the production of the composite files. When the segmental subject-averaged profiles were plotted, a great number of unsynchronous times were discovered. Due to the large number of data points and the number of files involved, the unsynchronized time records were realigned by decrementing each unsynchronous time value by one minute. The resulting files still had a few incongruous time records which were deleted. The subject-averaged values were computed by using the corrected files and are stored in DTP3AR1. As was the case with the original source files which make up the RHL1AR1 group, the constituent source files of the DTP3AR1 group were recorded in W/M<sup>2</sup>. Thus, the DTP3AR1 group's unit conversions were performed in the same manner described for the RHL1AR1 data. This data was used to verify the heat loss model for the prone, resting diver at 21 MSW even though it was necessary to correct the time records to obtain a representative data file. We used this average data in conjunction

with the other two DTP files (DTP1ART and DTP2AR1) to enhance the statistical significance of our model verification.

#### DTP3AW1

The five subjects of this composite file were also part of the 21 MSW garment evaluation study described in the DTP3AR1 section. These air-breathing, seated subjects were exposed to the 5 °C wet hyperbaric environment at a depth of 21 MSW. The difference between these dives and those of DTP3AR1 is that this data was taken from subjects who worked at a rate of 50 watts for six minutes and then rested for four minutes. These sitting subjects repeated the work/rest sequence for the duration of the study. Due to the large number of corrections that had to be applied to the resting studies (DTP3AR1) of this series, there is reason to believe that the data found in files DTP32W1, DTP33W1, DTP34W1, DTP37W1, and DTP38W1 will have many problems. With this in mind, the creation of the subject-averaged file (DTP3AW1) is likely to be rather involved. As described in the DTP3AR1 section, the heat flux values will need to be converted from watts per meter squared to watts. The conversion which was used with the DTP3AR1 data may also be applied here. This data could be used, if acceptable, to verify the working model for a sitting diver who is intermittently working at a fixed rate of 50 watts.

#### DTP4AR1

The three subjects in this group were not resting as implied by the name, but were performing light work of unknown magnitude. This data was taken from DTP clad, submerged subjects in 5 °C water at a depth of 3 MSW. These subjects, on command, would swim to a new position on the bottom of the tank and perform a timed manual dexterity test. The studies in this group were performed by NCSC to evaluate the DTP garment's ability to satisfy the mission

of providing suitable protection for six hours [31]. These operational tests were not designed to acquire heat transfer data, but were designed to evaluate the response of the suit and diver at the extremes of the suit capabilities [31]. This data, most probably, will not provide statistically significant results and would be very difficult to compare with the other data files since the rate of work was not quantized.

#### DTP4XYZ

The remaining eight files are single case tests in which the subjects performed specific tasks or were exposed to a sudden change in environment, such as total suit flooding or flooding of a hand. The fact that the protocols used in taking this data are, in general, different for each dive makes it impossible to group this data together and thus to obtain any statistical significance. As explained under the DTP4AR1 section, these studies were not performed to acquire heat transfer data, but to evaluate the response of the suit and the diver to unique situations. These dives were done as a check of the DTP garment's ability to meet its specified mission scenario [31].

#### Summary

This chapter has described the procedure used to create the mean (composite) subject files which were used in all verification and development phases of our resting, submerged diver heat loss model. As stated in the description of the first working data file which is presented (RHL1AW1), we have evaluated the available working data from the perspective of its usefulness in the development of a working diver model. We concluded from

this evaluation, with the concurrence of our Navy contract sponsor, that the adaptation of our resting diver heat loss model to the case of a working diver should be deferred until adequate experimental working data is available. As indicated previously, this conclusion is based on the fact that there are only two available working diver data sets that were performed in similar environments and at the same work rate and cycle (rest to work). However, these dives were conducted at two different depths (3 MSW in DTP2AW2 and 21 MSW in DTP3AW1), thus limiting the number of mean (composite) data files to each depth to one. The lack of statistical significance, when using such a small amount of data, would make any findings tenuous.

The four composite data files (RNL1AR1, DTP1ART, DTP2AR1, and DTP3AR1) are tabulated in Appendix B. The data files used to create these files and the other data of Tables 2-4 may be obtained from the Director of the F.G. Hall Environmental Laboratory, Duke University, only with the permission of the Naval Research and Development Command and the originating command.

### CHAPTER III

#### DEVELOPMENT OF THE DIVER MODEL

Our development of the diver heat loss model was performed in three distinct steps. The first task was to develop a geometrical representation of an average diver. The second objective was to derive a mathematical correlation for predicting the regional skin temperatures of our modeled subject. The final step was to develop a model for predicting the behavior of an assumed garment ensemble at any location on a prone, sitting, or standing diver. The development of the physical model and the definition of the problem and its solution are described in this chapter. The development of the regional predictive skin temperature correlation is described in Chapter IV, and the modeling of the physical behavior of the garment ensemble is presented in Chapter V.

#### The Physical Model

The model man, as shown in Figure 1, is fabricated from cylinders and spheres. Since both the head and the hand (when closed to conserve heat)

resemble spheres, they were treated as such; the seven remaining regions were modeled as cylinders. The proportions of each region were chosen to approximate the physical dimensions of a standard U.S. Air Force man as defined by Webb [23] and to produce regional surface area fractions comparable to those defined for the twelve segment Hody man in Table 1 and Figure 2.

The choice of the standard U.S. Air Force man [23] as the basis of the physical model was, in part, a result of the lack of complete anthropometric data found in the open literature. Webb's data [23], the only complete source found, was derived from a large population of U.S. Air Force men. We assumed that average Navy divers would conform to this Air Force data because all military personnel would be expected to be in a similar state of physical conditioning. The large number of subjects represented in Webb's standard man data suggested that accurate predictions would result from its use.

The dimensions chosen for the model man are displayed in Table 5. The height and total surface area, calculated to be 172.7 CM and 1.902 M<sup>2</sup>, respectively, compare favorably to the standard Air Force man's height of 175.5 CM and body surface area of 1.90 M<sup>2</sup>. The model man's regional surface area percentages are compared to those derived from Hody's segmental surface fractions (Table 1, in Table 6. Requiring our model man's dimensions to yield regional surface area fractions comparable to those of Hody's facilitated use of the available experimental data.

#### The Model and Its Solution

Our mathematical model for predicting diver regional heat loss and any required regional supplementary heating for a resting diver who is wearing

Table 5  
Model Man Dimensions

<u>Region ID #</u>	<u>Region Name</u>	<u>Shape</u>	<u>Diameter (M)</u>	<u>Characteristic Length (M)</u>	<u>Surface Area (M<sup>2</sup>)</u>
1	Head	sphere	0.206	0.206	0.1333
2	Torso	cylinder	0.300	0.353	0.3327
3	Abdomen	cylinder	0.300	0.353	0.3327
4	Thigh	cylinder	0.150	0.383	0.3610
5	Calf	cylinder	0.120	0.328	0.2474
6	Foot	cylinder	0.150	0.104	0.1334
7	Upper Arm	cylinder	0.096	0.223	0.1490
8	Lower Arm	cylinder	0.070	0.267	0.1174
9	Hand	sphere	0.123	0.123	0.0950
Total Body Surface Area (Sum of Regional Surface Areas)					1.902

Table 6  
Comparison of Model Man and Body's Man Regional Surface Area Percents

Region ID #	Region Name	Body Segment Name (ID #)	Regional Surface Area Percents	
			Model <sup>†</sup>	Body <sup>††</sup>
1	Head	Head (1)	7.0	7.0
2	Torso	Chest (2) + Upper Back (4)	17.5	17.5
3	Abdomen	Abdomen (3) + Lower Back (5)	17.5	17.5
4	Thigh	Front Thigh (8) + Rear Thigh (10)	19.0	19.0
5	Calf	Front Calf (9) + Rear Calf (11)	13.0	13.0
6	Foot	Feet (12)	7.0	7.0
7	Upper Arm	Arm (6)	7.8	14.0
8	Lower Arm		6.2	
9	Hand	Wrist (7)	5.0	5.0

<sup>†</sup>Model man regional surface area percents were calculated by: Regional surface area (Table 5) times 100.0 divided by the total body surface area (TBSA). The value of TBSA was 1.902 M<sup>2</sup> (Table 5).

<sup>††</sup>Body man regional surface area percents were computed by: Summing Body segment surface area fractions (Table 1) and then multiplying by 100.

a dry thermal protection garment is formulated as a function of the following parameters:

- a. Prescribed mean skin temperature. Regional skin temperatures are then calculated by means of specific predictive correlations which use this mean skin temperature as the independent argument.
- b. Ambient water temperature.
- c. Depth of immersion of the diver's shoulder.
- d. Garment thermal resistance characteristics.
- e. Gas with which suit is inflated to compensate for hydrostatic pressure.
- f. Hydrostatic suit squeeze due to local hydrostatic pressure, i.e., hydrostatic pressure relative to the locus of lung inflation. For ease of modeling, this is arbitrarily taken as the height of the shoulders of an erect diver (Fig. 1).
- g. Posture: prone, sitting, or standing.
- h. Allowable regional surface heat fluxes for resting man according to Burriess [33,34].
- i. Convective film coefficients calculated according to the empirical correlations which are discussed in Chapter V.

The numerical model synthesizes the parameters listed above to obtain an overall thermal conductance,  $U_i(j)$  (Eq. 4) for each node  $j$  of region  $i$  (Fig. 51), which is employed in Equation 5 for estimating the actual heat loss per unit length from each region were there no supplementary heating available.

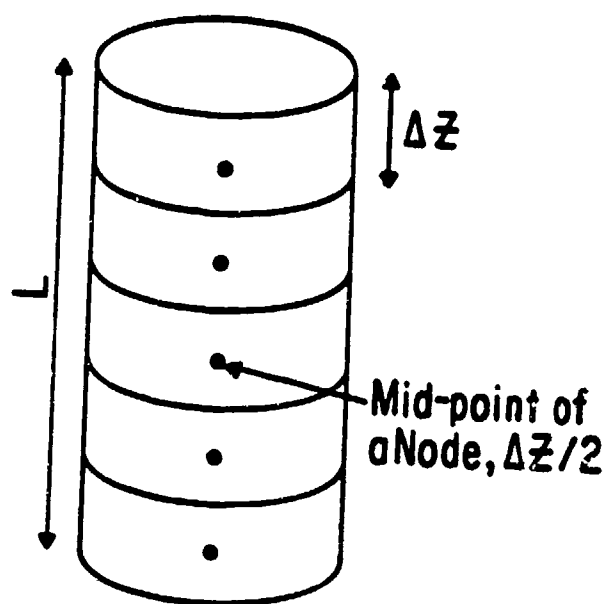


Figure 51. Vertical Cylindrical Region Divided into Five Nodes ( $j=5$ ).

$$U_i(j) = \sum_{k=1}^n R_k(j) \quad (4)$$

$$\dot{Q}_i(j) = U_i(j) S_i(j) (T_i - T_a) \quad (5)$$

- where:
- $U_i(j)$  = Overall heat transfer coefficient for node  $j$  of region  $i$
  - $R_k(j)$  = Thermal resistance of garment layer  $k$  surrounding node  $j$
  - $n$  = Number of garment layers covering all nodes of region  $i$
  - $\dot{Q}_i(j)$  = Rate of heat flow from node  $j$  of region  $i$
  - $S_i(j)$  = Skin surface area enclosed by node  $j$  of region  $i$
  - $T_i$  = Regional predicted skin temperature
  - $T_a$  = Ambient temperature

The regional predicted skin temperature,  $T_i$  (Eq. 5), is predicted as a function of the prescribed mean skin temperature by the predictive skin temperature correlation described in Chapter IV. The overall heat transfer coefficient ( $U_i(j)$ ), based on the skin surface area ( $S_i(j)$ ), is represented for each  $j$ th nodal element of the  $i$ th cylindrical region by:

$$U_i(j) = \frac{1}{\frac{1}{h_i(j)} + \frac{S_i(j) \cdot \ln(r_2/r_1)}{2\pi k_{ig} \cdot \Delta z} + \frac{S_i(j) \cdot \ln(r_3/r_2)}{2\pi k_{og} \cdot \Delta z} + \frac{S_i(j)}{S_o(j)h_o(j)}} \quad (6)$$

where:  $U_i(j)$  = Overall heat transfer coefficient for node  $j$  of region  $i$

$h_i(j)$  = Convective heat transfer coefficient for the gas layer between the skin surface and the undergarment of node  $j$  and region  $i$

$S_i(j)$  = Surface area of skin surface encircling node  $j$  of region  $i$

$r_1$  = Radius from regional center line to skin surface

$r_2$  = Radius from regional center line to undergarment/outer garment interface

$r_3$  = Radius from regional center line to outside surface of outer garment

$\Delta z$  = Nodal length

$k_{ig}$  = Thermal conductivity of inner garment

$k_{og}$  = Thermal conductivity of outer garment

$S_o(j)$  = Surface area of outer garment encircling node  $j$  of region  $i$

$h_o(j)$  = Convective heat transfer coefficient for the outer boundary layer on the surface of the outer garment of node  $j$  and region  $i$

The first thermal resistance term ( $1/h_i(j)$ ) accounts for the insulative effect that might be provided by a gas layer between the skin surface and an insulating garment. This would be considered a natural convection phenomenon

due to a microcirculation. However, the effect of this term is negligible since the assumed protective dry garment is subjected to hydrostatic suit squeeze below the chest level (in the case of our erect or sitting model from the shoulder crest down), thus minimizing this gas layer. The second term of Equation 6 may be replaced by an experimental value of garment thermal resistance that has been extrapolated to the ambient conditions of the suit entrapped gas and then further reduced for the local effect of suit compression (See Chapter V for details.). The third term of the denominator considers the contribution of the outer garment to the overall resistance. The assumed outer garment is a pre-crushed neoprene foam of 0.16 CM (1/16 inch) nominal thickness, worn primarily as a means of maintaining water tight integrity. The garment can be characterized as a solid sheet of neoprene rubber of comparable thickness because of the effects of the pre-immersion treatment on the foam material. The last thermal resistance term of Equation 6 is computed from dimensionless empirical convective heat transfer correlations that are defined in Chapter V.

$\dot{Q}_i(j)$ , as defined in Equation 5, is calculated for discrete nodes of a body region (Fig 51). These nodal rate of heat loss values are summed to obtain an overall regional rate of heat loss for the ambient environment under consideration. This computation models the rate of heat flow from the passive garment alone. The regional supplementary heating required to sustain a resting diver is estimated by subtracting a permissible regional rate of heat loss, as defined by Burriss [33,34], from the value calculated in the manner described above. These resultant values specify the rate of supplementary heating required for each region, the diver's overall heating requirement (obtained by summing the heating requirements of each region), and the relative heating intensity of each body region with respect to the total heating requirement.

The descriptive predictive model has been developed by assuming that the diver would wear some form of pressure compensated dry suit. Since all of the available experimental data was collected from immersed subjects clad in the Diver Thermal Protection (DTP) garment [22] whose thermal characteristics are known [12,13], we decided to develop our model with the DTP garment as the assumed dry suit design. Since the development of an overall heat transfer coefficient is dependent on the selected dry suit design, consideration of a suit which has characteristics different from those of the DTP garment requires that the resistance terms of Equation 6 be re-analyzed. This may be easily performed if the thermal characteristics of the garment at sea level are known and the variation of these parameters can be modeled as a function of temperature and pressure.

The DTP garment is configured as two different layers [22]. The innermost layer consists of a thin, cotton/wool long john underwear with wool socks and a M-400 Thinsulate<sup>7</sup> thermal undergarment which incorporates double layer boots [22]. Because of the significantly larger thermal resistance of the Thinsulate undergarment relative to the long john's [13], the long john underwear was neglected during the development of the overall heat transfer coefficient. The outer layer is the crushed neoprene foam garment.

---

<sup>7</sup>M-400 Thinsulate is a commercial trade name for a fibrous batt material made by the 3-M Corporation.

## CHAPTER IV

### DEVELOPMENT OF PREDICTIVE SKIN TEMPERATURE CORRELATION

It is a well established observation that the preferred mean weighted skin temperature of man at rest in a eutermic environment is  $33^{\circ}\text{C} \pm 1^{\circ}\text{C}$ . Associated with this resting state is a metabolic rate of about  $55 \text{ W/M}^2$ , the majority of which is emitted as waste heat and the remainder of which is utilized for metabolic processes [33-36]. Physiological laboratory studies have defined specific regional skin temperatures and rates of heat loss that are associated with this preferred mean skin temperature [33,34].

Kerslake [2] developed an algebraic model for predicting the temperature of any of eight different regions<sup>8</sup>, as a function of mean skin temperature, from extensive experimental studies of men in a nearly steady thermal state. The equations that he developed were of the form:

$$T_i = T_{skm} \pm A_i \cdot R \quad (7)$$

where:  $T_i$  = Skin temperature for region i

$T_{skm}$  = Mean skin temperature

$A_i$  = Distribution fraction for region i (Table 7)

$R$  = Temperature difference between trunk, and hand and foot

---

<sup>8</sup>See Foreword for the connotation of region and Kerslake region.

Table 7  
Kerslake's Curve Fitting Coefficients  $A_i$ <sup>†</sup>

<u>Region Index, i</u>	<u>Region Name</u>	<u><math>A_i</math></u>	<u>Corresponding Segmental Indices of Figure 2</u>
1	Head	0.27	1
2	Trunk	0.27	2, 3, 4, and 5
3	Lower Arm	-0.365	6
4	Hand	-0.73	7
5	Thigh	0.00	8 and 10
6	Calf	-0.365	9 and 11
7	Foot	-0.73	12
8	Upper Arm	0.00	6

<sup>†</sup>Data adapted from Kerslake [2]

Piironen and Takalo [37] conducted a series of physiological experiments with an instrumented suit calorimeter by which they determined both regional heat fluxes and skin temperatures for a variety of work rates and degrees of vasoconstriction. In their three experimental subjects, they found that maximum vasoconstriction occurred in the mean skin temperature range of 31-32 °C and that a 10% increase in metabolic heat production was observed whenever the minimum tissue conductance (maximum vasoconstriction) was attained. This observed increase in metabolic rate did not correlate with the onset of shivering thermogenesis. Shivering appeared only with a further lowering of the mean skin temperature below that required to attain the minimum tissue conductance. When shivering did occur, an associated increase in tissue conductance was indicated by the instrumented suit. Plots of the total body and regional experimental conductances from three resting subjects indicated that the minimum tissue conductance occurs at a mean skin temperature of 31.5 °C [37].

In designing an actively heated diver thermal protection garment of a limited energy supply, it would seem reasonable to allow peripheral vasoconstriction, but to avoid the onset of shivering and the associated increase in tissue conductance. Limits of thermal equilibrium are usually specified in terms of a minimum mean skin temperature and minimum temperatures for the hand and foot [11]. Supplementary heating of a diver may be required to maintain a specified minimum mean skin temperature, but most probably, at different regional rates to avoid compromising the regional skin temperatures. Therefore, a correlation for predicting regional skin temperature in the presence of peripheral vasoconstriction and as a function of mean skin temperature is most desirable for specifying minimum regional supplementary heating requirements.

## Development of Equations

Experimental data obtained from five nearly nude, sitting, resting divers exposed to a 20 °C helium-oxygen gas mixture at a pressure of 200 MSW was utilized to develop a Kerslake type algebraic equation for predicting Hody's twelve segmental temperatures (Fig. 2) rather than Kerslake's eight. This data was collected during a series of experimental dives conducted by the Navy Experimental Diving Unit to study respiratory heat loss under controlled hyperbaric conditions [21]. As described in Chapter II, the segmental data of these subjects was averaged to produce the mean subject file RHLIARI. Any further references to experimental data refer to data contained in the RHLIARI composite diver file. Hody's [24,25] twelve point mean skin temperature formula, Equation 8, was used in developing the predictive segmental skin temperature equations because all of the experimental data available for analysis had been recorded in the Hody format. Figure 2 illustrates these twelve sites and Table 1 defines the indices, nomenclature, abbreviations, and surface area fractions  $f$  for each of the twelve segments. The subscripts of Equation 8 correspond to the segmental indices appearing in Figure 2 and Table 1.

$$T_{skm} = 0.070T_1 + 0.085T_2 + 0.085T_3 + 0.090T_4 + 0.090T_5 + 0.140T_6 \\ + 0.050T_7 + 0.095T_8 + 0.065T_9 + 0.095T_{10} + 0.065T_{11} + 0.070T_{12} \quad (8)$$

Figures 52-63 each display a segment's temperature profile from the RHLIARI data and the Hody mean skin temperature calculated with Equation 8. Each graph is labeled with the abbreviated segment name (Table 1) that corresponds to the segment plotted; the abbreviation HMST indicates the Hody mean skin temperature. Each experimental curve was analyzed by the method of Least Squares [38], after incongruous data points were eliminated, to obtain

a linear regression equation for the time span of 35 to 90 minutes. This was selected as a representative quasi-steady time period. Figure 64 is a representative sample of the generated linear regression curves, which displays the linear regression lines for the abdomen (ABD) and the Hody mean skin temperature (HMSI). Subsequently, these linear regression representations of the experimental data were employed to facilitate the numerical development of the predictive segmental skin temperature correlations.

Our first task was to evaluate the suitability of Kerslake's equation for predicting regional skin temperatures under hyperbaric conditions. To obtain values of experimental temperature which correspond to the eight Kerslake regions, segmental values at the 84th minute of Figures 52-63 were weight averaged by using the Hody surface area fractions (Table 1) of the corresponding Hody segments. Table 8 illustrates the very good comparison between the respective regional weight averaged experimental temperatures and the temperatures that are predicted when the experimental Hody mean skin temperature is used as the argument in Equation 7. Three separate R values, defined in Table 8, were employed in Equation 7 to evaluate the accuracy of the Kerslake equation for predicting segmental skin temperatures of resting man under hyperbaric conditions. Table 8 also defines the weight averaging correlations for extrapolating twelve site data to eight sites.

Table 9, similar in form to Table 8, was prepared with data that was gathered from the linear regression equations which were fitted to the mean experimental data of five subjects. The analyses reflected in both Tables 8 and 9 were conducted with data obtained at the 84th minute when all of the subjects were deemed to have attained a quasi-steady state of thermal balance.

Figures 52-63. Representative Segmental Temperature and Body Mean Skin Temperature (HMST) Profiles. One figure for each of the 12 segments. Mean data taken from 200 MSW respiratory heat loss studies (RHL1AR1).

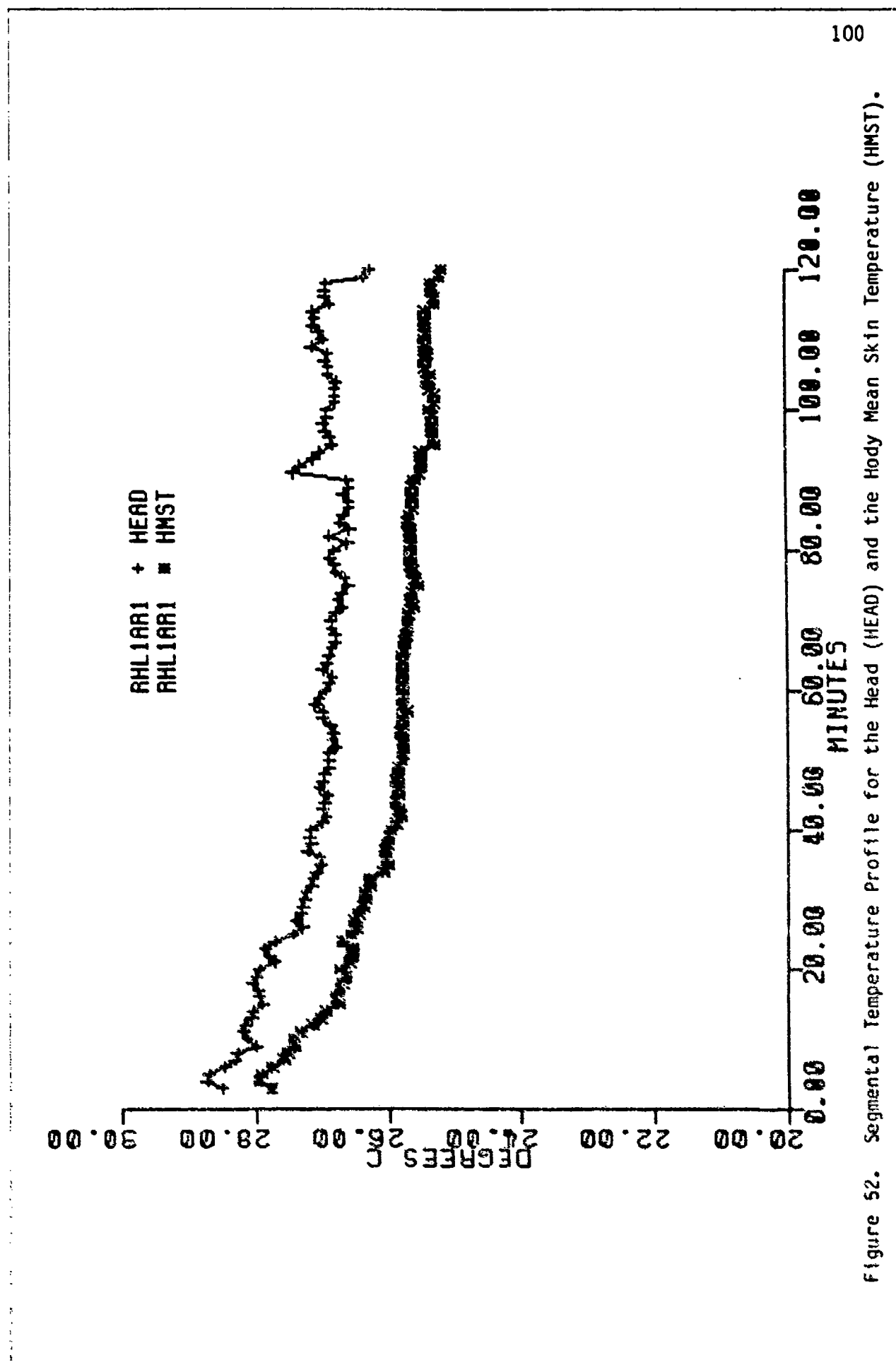


Figure 52. Segmental Temperature Profile for the Head (HEAD) and the Body Mean Skin Temperature (HMST).

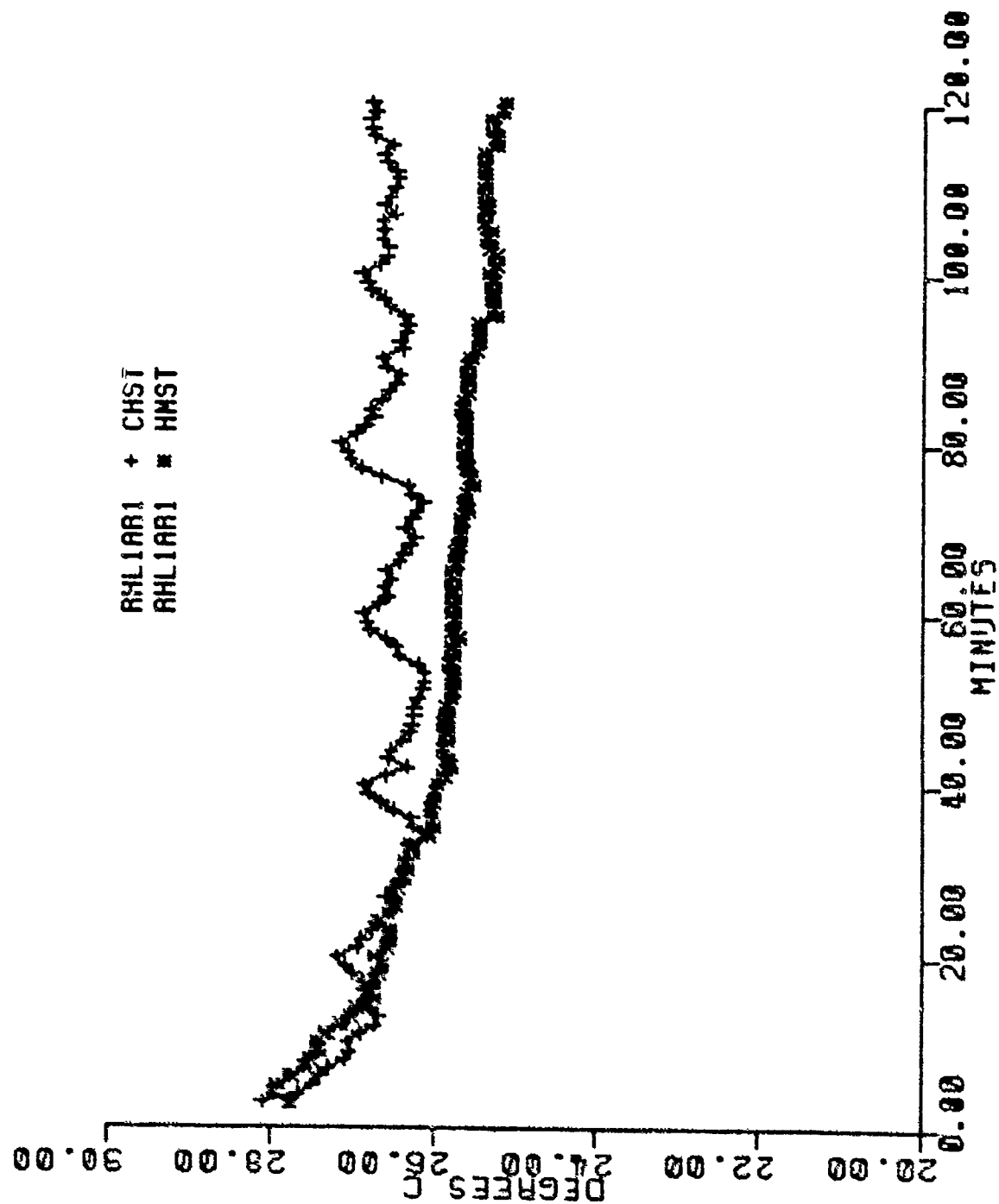


Figure 53. Segmental Temperature Profile for the Chest (CHST) and the Body Mean Skin Temperature (HMST).

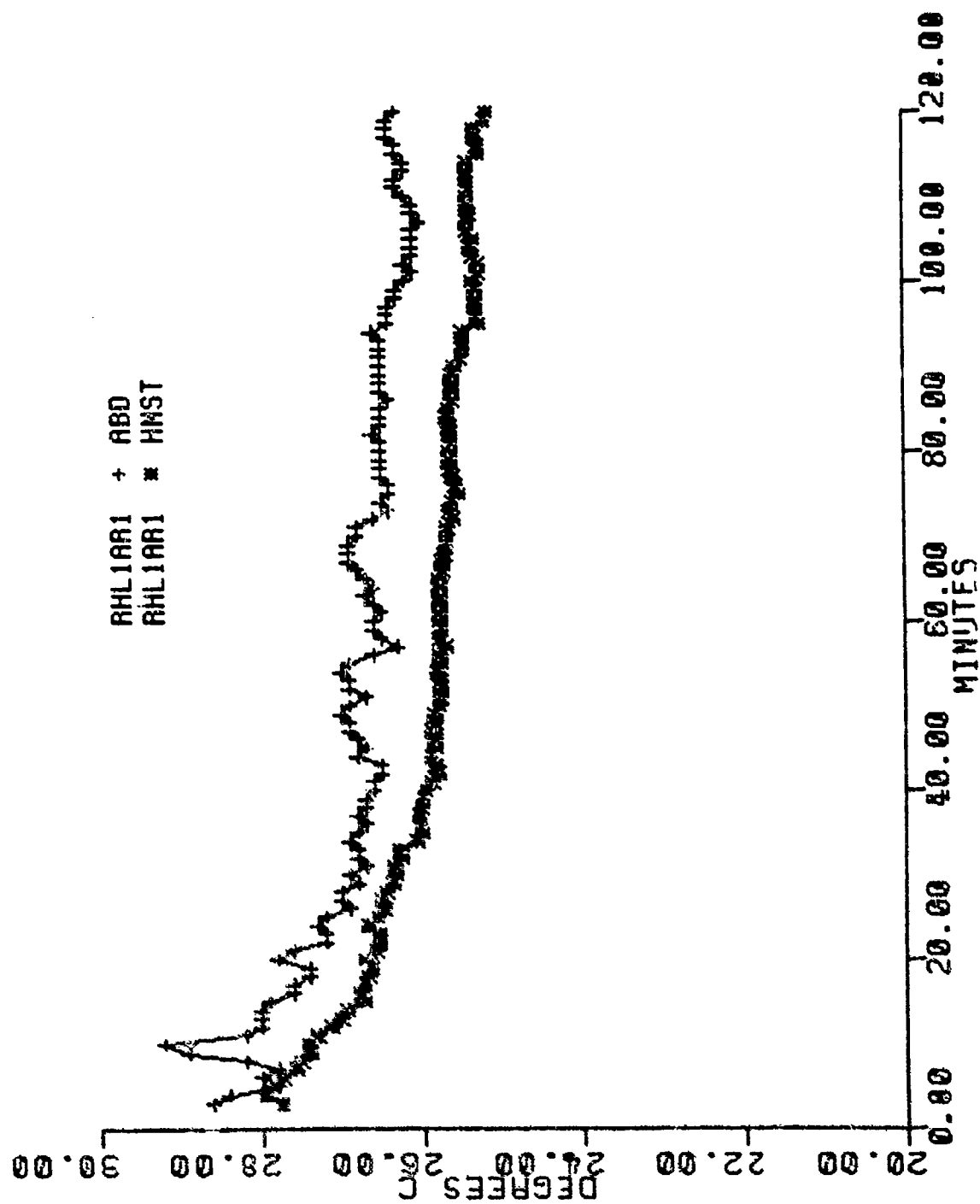


Figure 54. Segmental Temperature Profile for the Abdomen (ABD) and the Body Mean Skin Temperature (HMST).

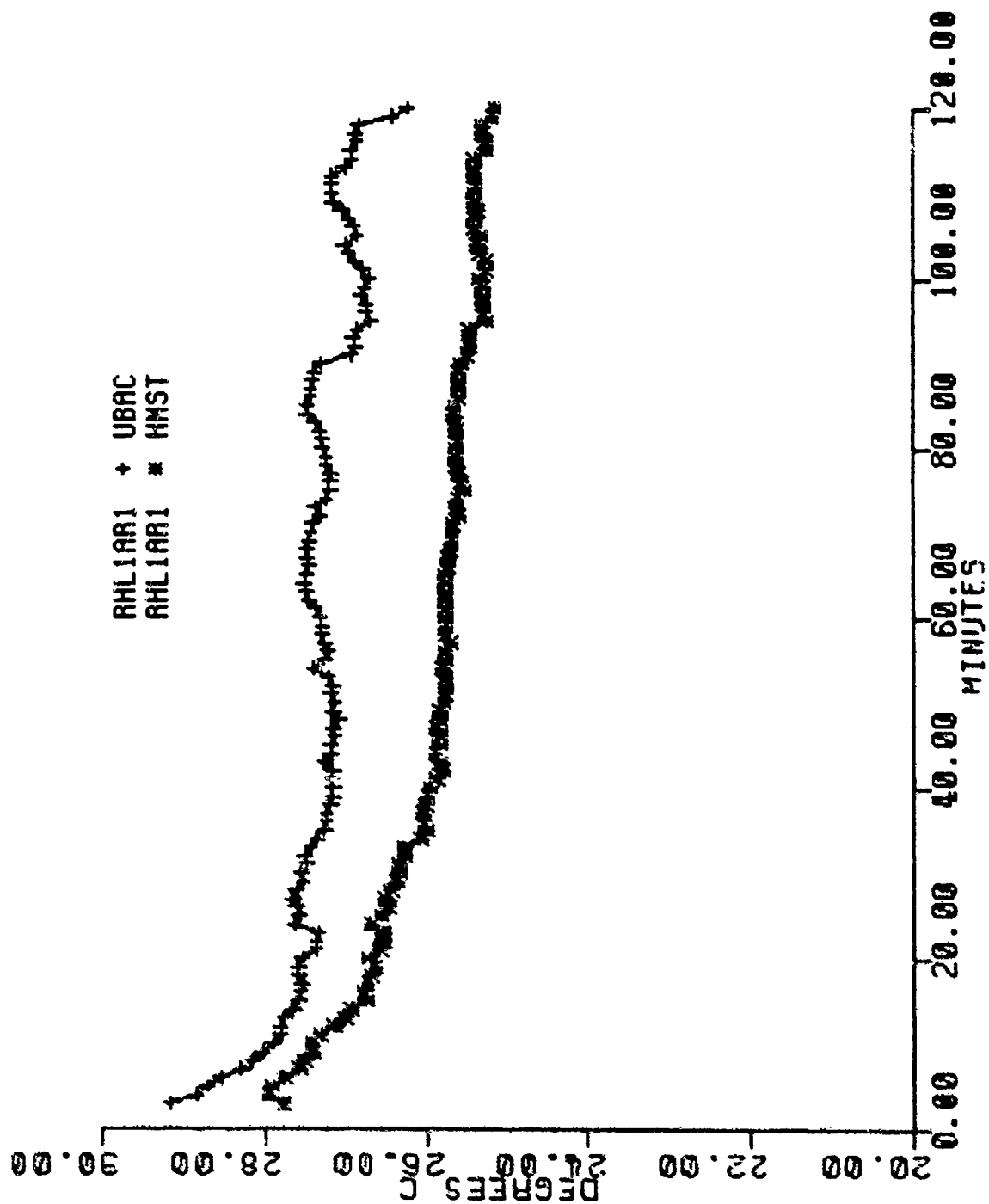


Figure 55. Segmental Temperature Profile for the Upper Back (UBAC) and the Body Mean Skin Temperature (HMST).

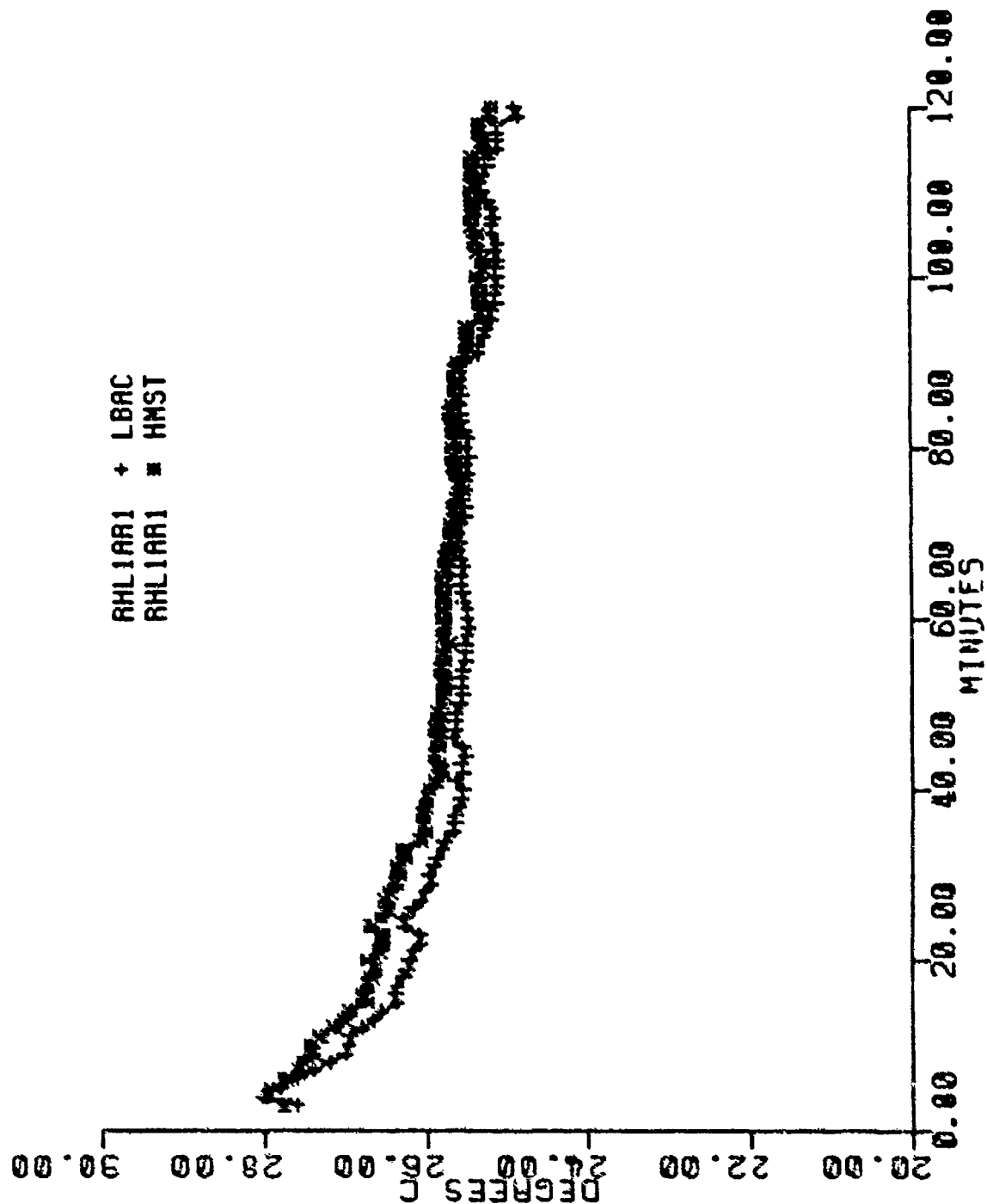


Figure 56. Segmental Temperature Profile for the Lower Back (LBAC) and the Body Mean Skin Temperature (HMST).

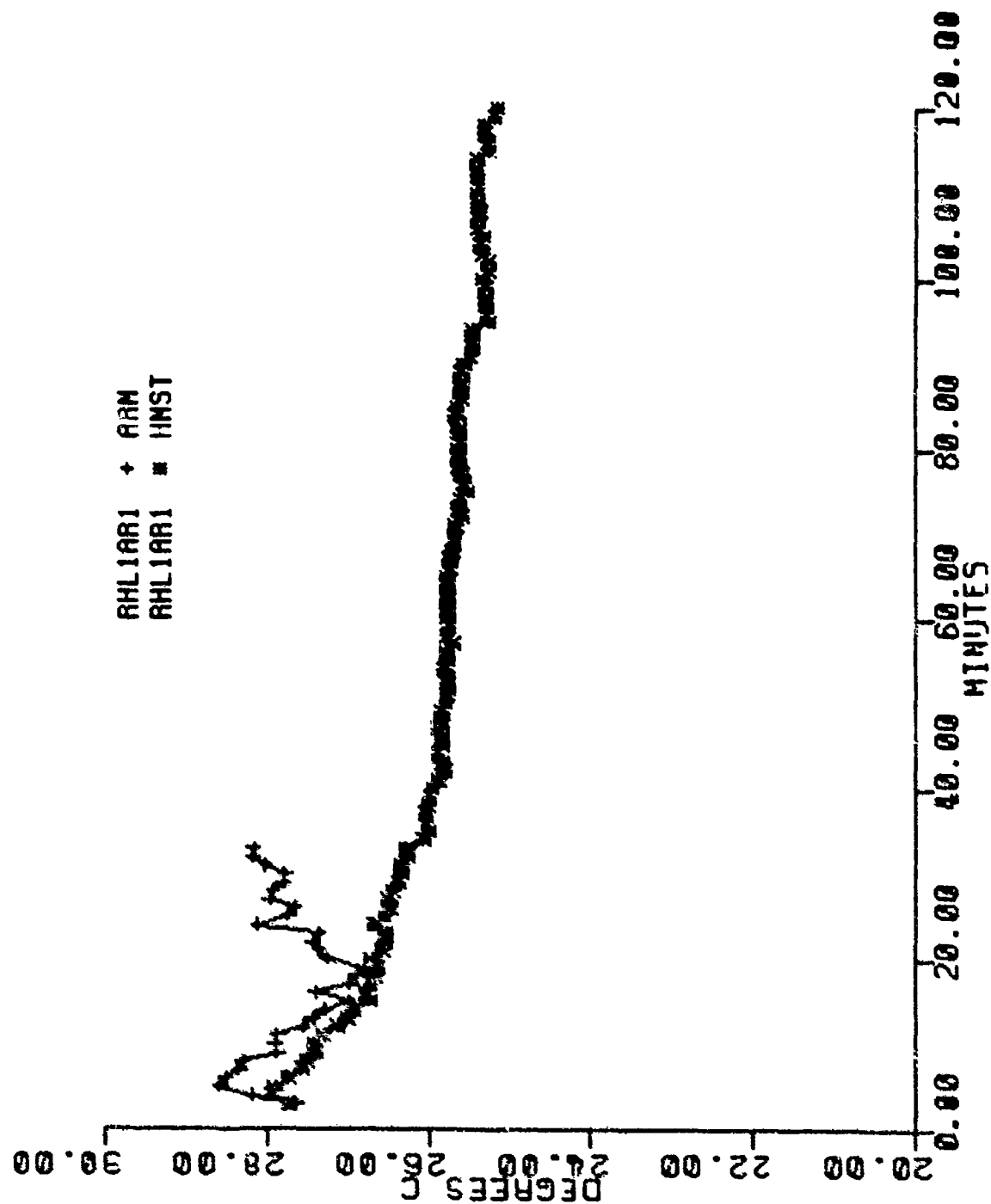


Figure 57. Segmental Temperature Profile for the Arm (ARM) and the Body Mean Skin Temperature (HMST).

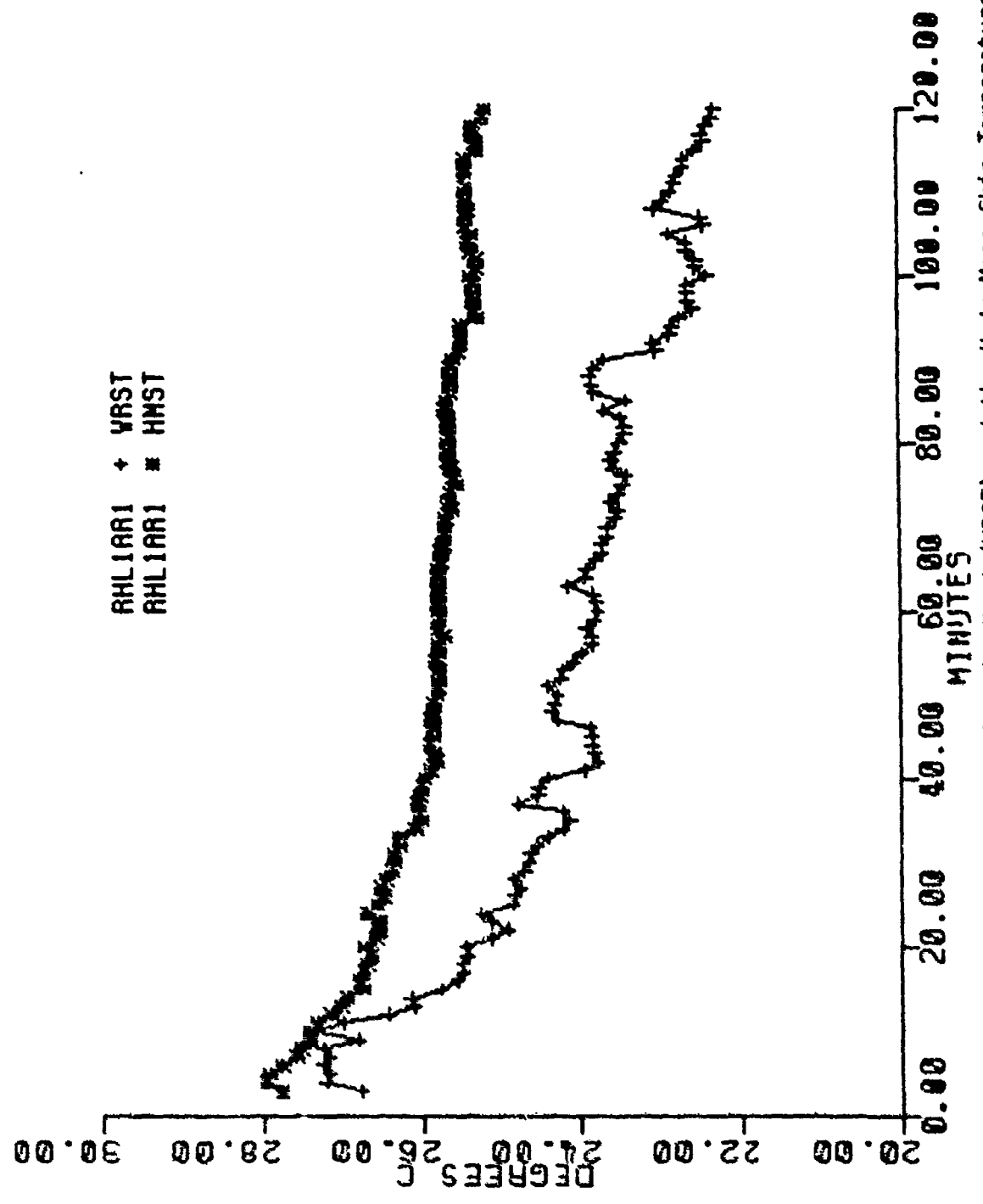


Figure 58. Segmental Temperature Profile for the Hand (WRST) and the Body Mean Skin Temperature (HMST).

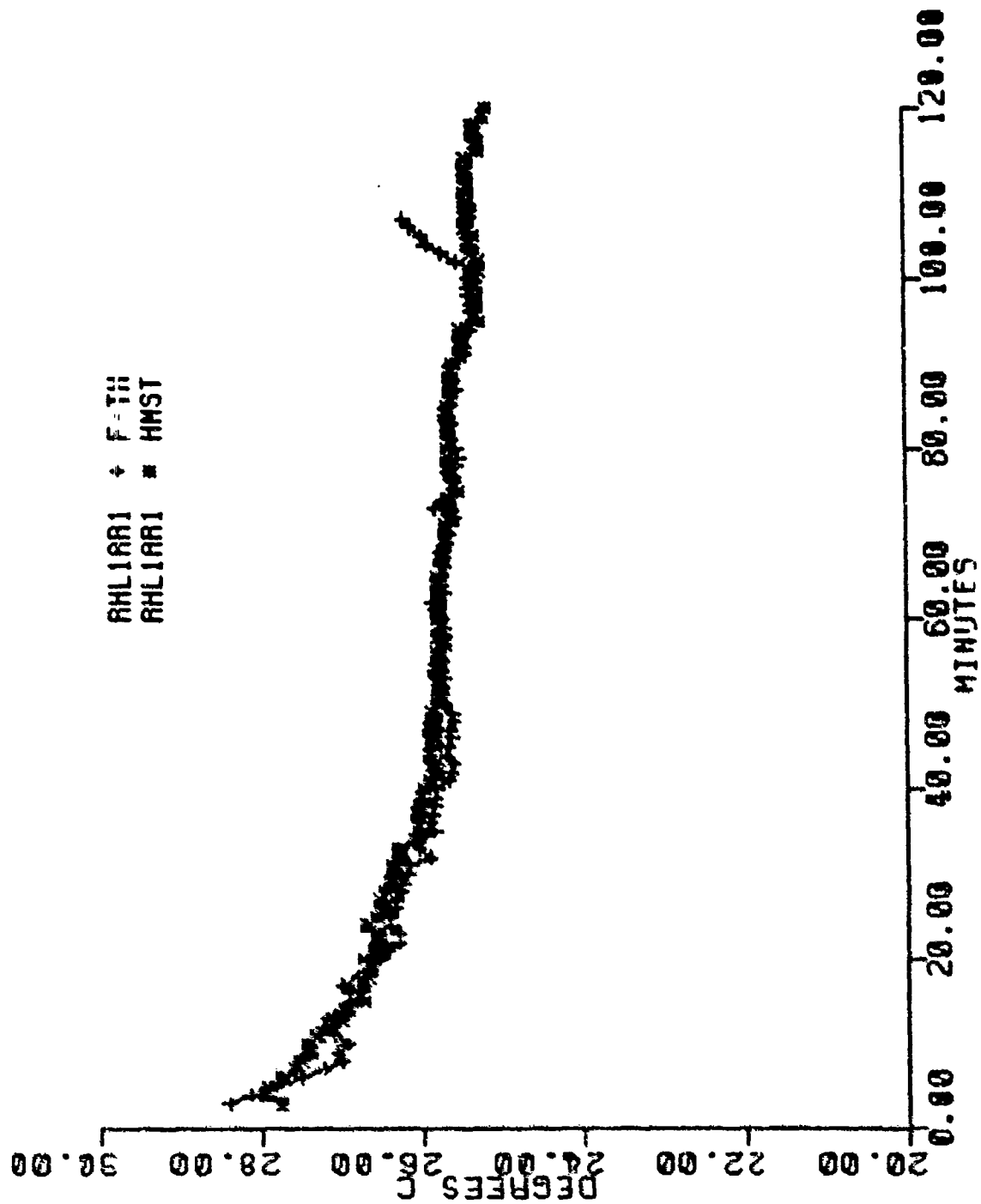


Figure 59. Segmental Temperature Profile for the Front Thigh (F-TH) and the Body Mean Skin Temperature (HMST).

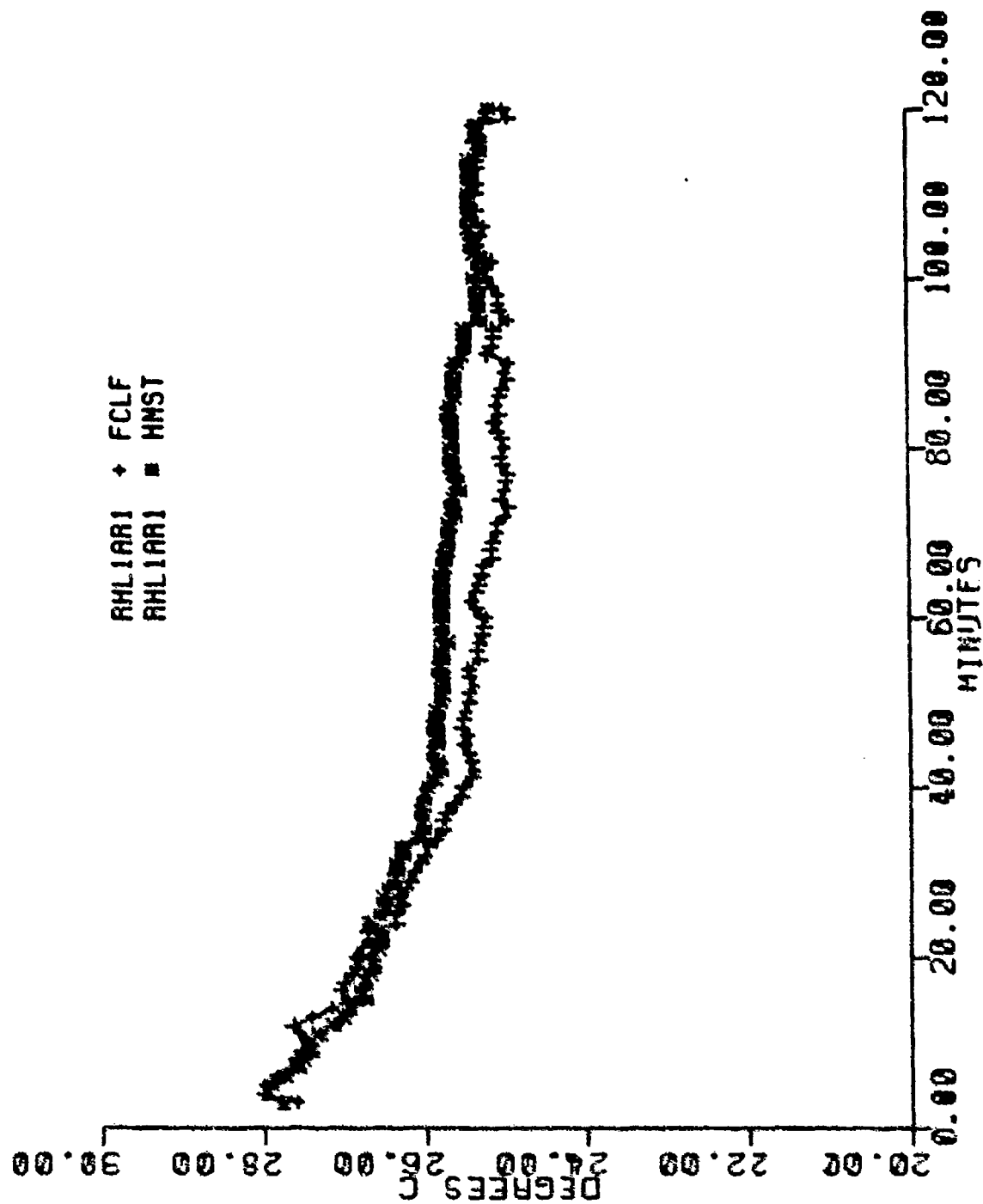


Figure 60. Segmental Temperature Profile for the Front Calf (FCLF) and the Body Mean Skin Temperature (HMST).

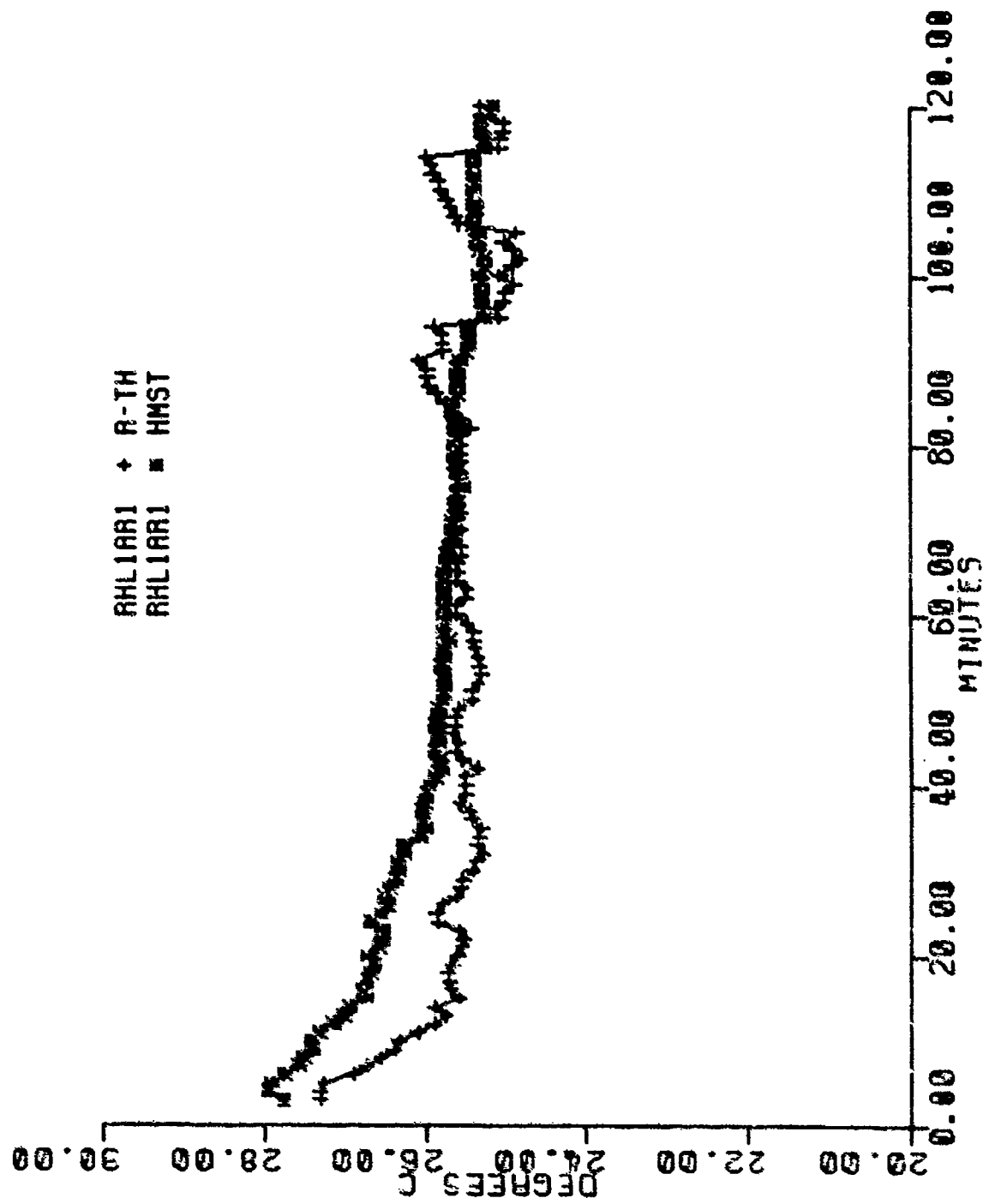


Figure 61. Segmental Temperature Profile for the Rear Thigh (R-TH) and the Body Mean Skin Temperature (HMST).

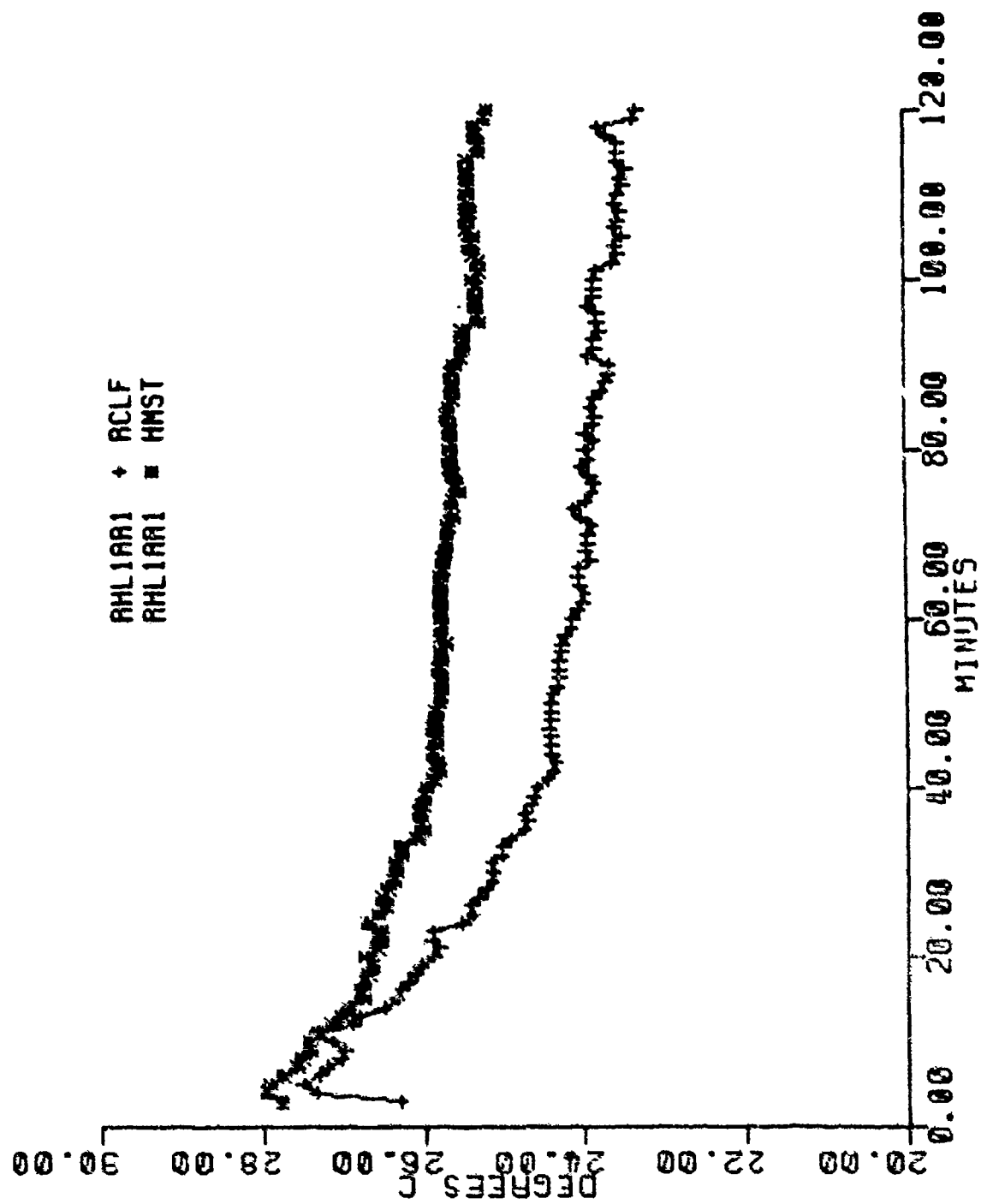


Figure 62. Segmental Temperature Profile for the Rear Calf (RCLF) and the Body Mean Skin Temperature (HMST).

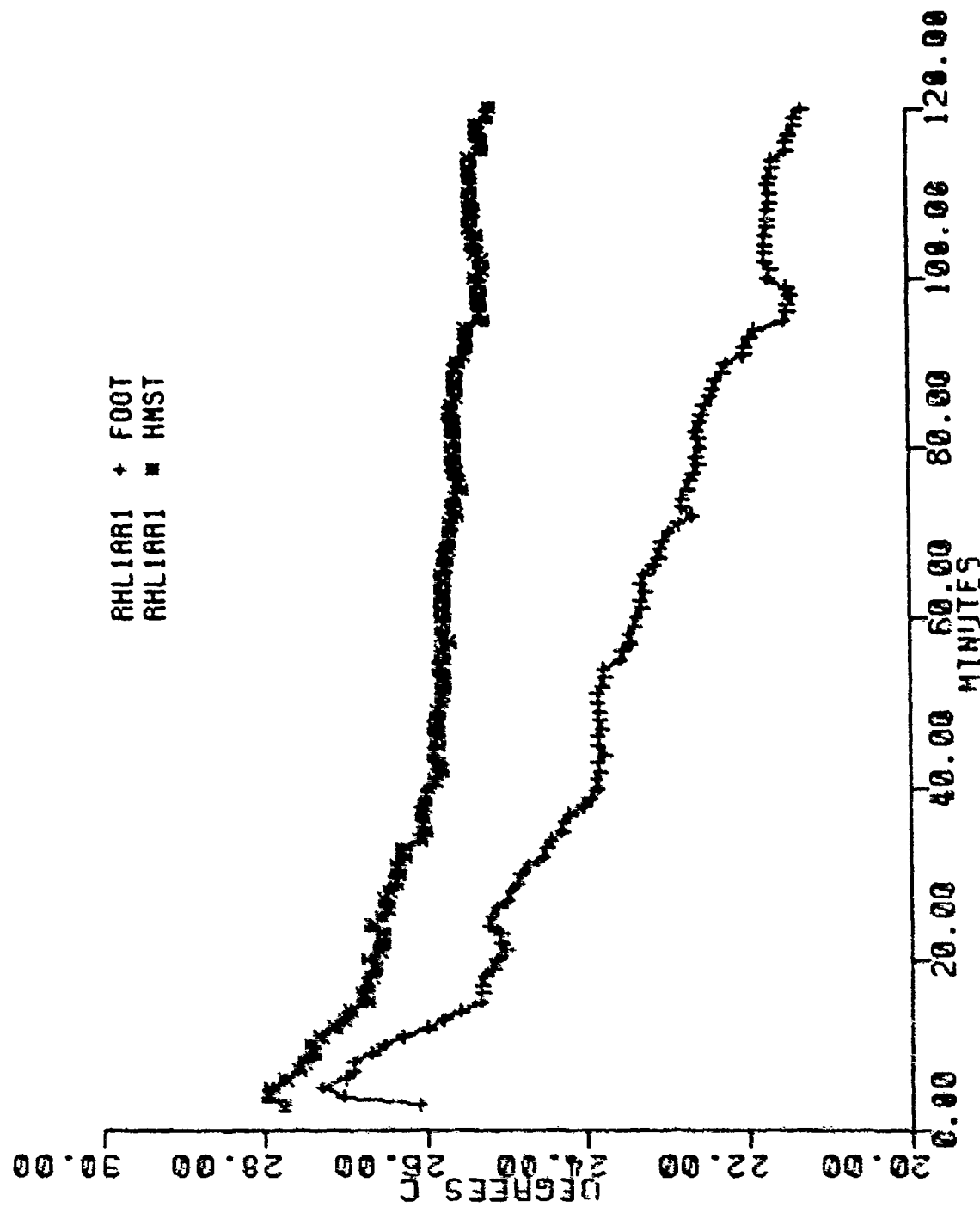


Figure 63. Segmental Temperature Profile for the Foot (FOOT) and the Body Mean Skin Temperature (HMST).

Figure 64. Representative Linearized Segmental Temperature for the Abdomen and Body Mean Skin Temperature Profiles. Linearized data for the abdomen taken from mean data of Figure 54 (RH11AR1).

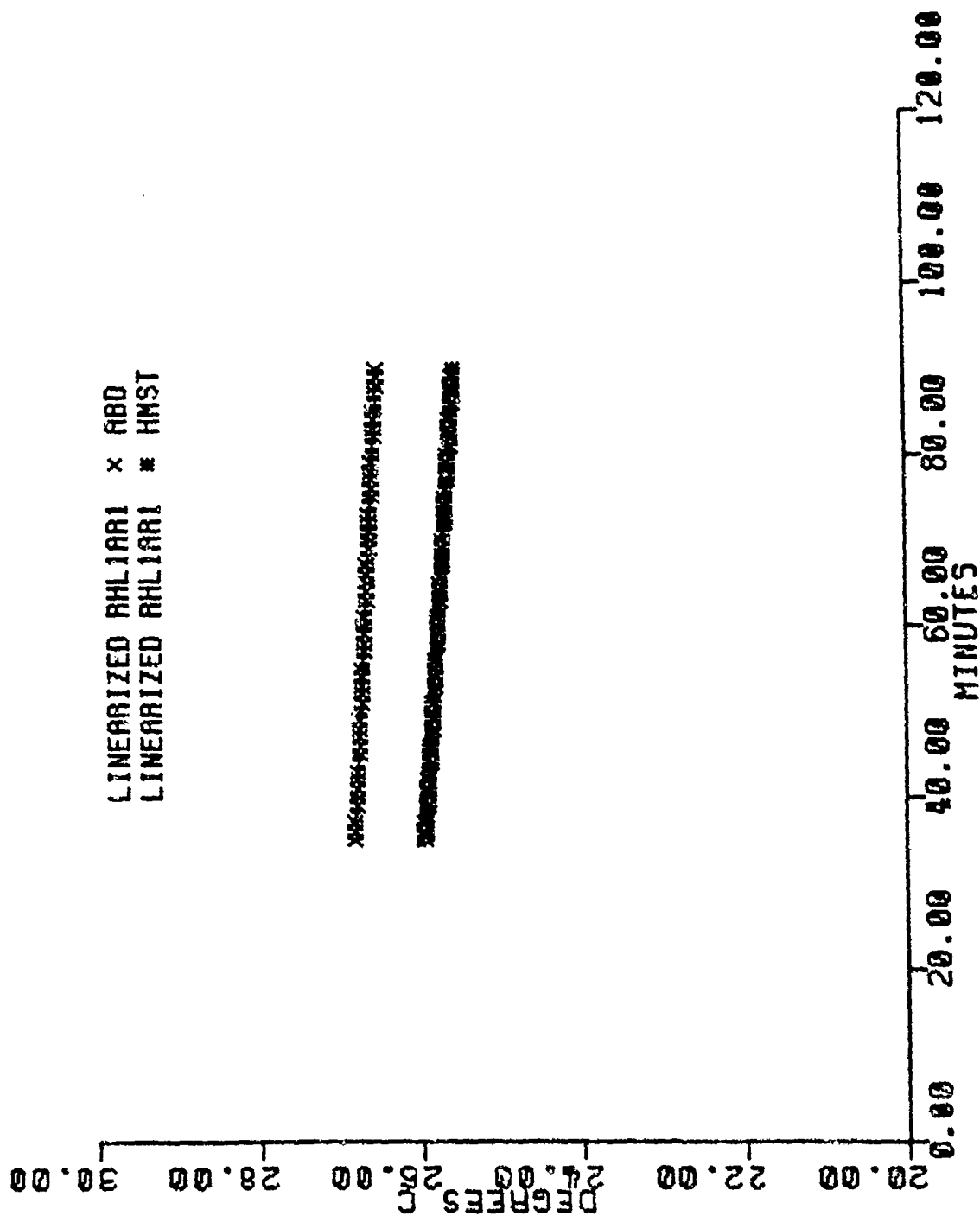


Figure 64. Linearized Abdominal (ABD) and Body Mean Skin (HMST) Temperatures.

Table 8

Comparison of Composite Experimental Temperatures Extracted From Figures 52-63 With Those Predicted With Kerslake's Equation (Eq. 7).<sup>†</sup> Experimental data recorded in the twelve segment format of Hody was extrapolated to Kerslake's format by the weight averaging correlations presented below.

Region	Experimental	<u>Temperatures in °C</u>		
		Predicted with R1, R2, and R3		
		R1	R2	R3
Head	26.67	26.60	26.45	26.76
Trunk	26.57	26.60	26.45	26.76
Lower Arm	26.32	24.41	24.61	24.20
Hand	23.67	23.15	23.56	22.74
Thigh	25.65	25.67	25.67	25.67
Calf	24.43	24.41	24.61	24.20
Foot	22.55	23.15	23.56	22.74
Upper Arm <sup>††</sup>	26.32	25.67	25.67	25.67

R Values Employed in Equation 1:

$$R1 = \text{Trunk} - (\text{Hand} + \text{Foot})/2.0 = 3.46$$

$$R2 = \text{Trunk} - \text{Hand} = 2.90$$

$$R3 = \text{Trunk} - \text{Foot} = 4.02$$

Weight averaging correlations:

$$\text{Trunk} = (0.085 \text{ CHST} + 0.085 \text{ ABD} + 0.090 \text{ UBAC} + 0.090 \text{ LBAC})/0.350$$

$$\text{Thigh} = (0.095 \text{ F-Th} + 0.095 \text{ R-TH})/0.190$$

$$\text{Calf} = (0.065 \text{ FCLF} + 0.065 \text{ RCLF})/0.130$$

<sup>†</sup>The comparison is predicated on the mean of data collected during the 84th minute of the experimental series. The Hody mean skin temperature (T<sub>skm</sub> of Equation 7) was calculated by means of Equation 8 as 25.67 °C.

<sup>††</sup>Experimental data recorded from the lower arm was utilized since none was recorded for the upper arm.

Table 9

Comparison of Composite Experimental Temperatures Estimated by Means of Respective Linear Regression Equations Which Were Derived From Figures 52-63 With Those Predicted With Kerslake's Equation (Eq. 7).<sup>†</sup> Experimental values estimated from Hody's twelve segment format were extrapolated to Kerslake's format by the weight averaging correlations presented below.

Region	Experimental	<u>Temperatures in °C</u>		
		Predicted with R1, R2, and R3		
		R1	R2	R3
Head	26.65	26.53	26.39	26.68
Trunk	26.51	26.53	26.39	26.68
Lower Arm	25.10	24.32	24.51	24.12
Hand	23.55	23.04	23.43	22.66
Thigh	25.55	25.59	25.59	25.59
Calf	24.37	24.32	24.51	24.12
Foot	22.49	23.04	23.43	22.66
Upper Arm <sup>††</sup>	26.10	25.59	25.59	25.59

R Values Employed in Equation 1:

$$R1 = \text{Trunk} - (\text{Hand} + \text{Foot})/2.0 = 3.49$$

$$R2 = \text{Trunk} - \text{Hand} = 2.96$$

$$R3 = \text{Trunk} - \text{Foot} = 4.02$$

Weight Averaging Correlations:

$$\text{Trunk} = (0.085 \text{ CHST} + 0.085 \text{ ABD} + 0.090 \text{ UBAC} + 0.090 \text{ LBAC})/0.350$$

$$\text{Thigh} = (0.095 \text{ F-TH} + 0.095 \text{ R-TH})/0.190$$

$$\text{Calf} = (0.065 \text{ FCLF} + 0.065 \text{ RCLF})/0.130$$

<sup>†</sup>The comparison is developed for the 84th minute of the experimental series. The Hody mean skin temperature (T<sub>skm</sub> of Equation 7) was calculated by means of Equation 8 as 25.59 °C.

<sup>††</sup>Linearized experimental data of the lower arm was utilized since no experimental data was recorded for the upper arm.

The excellent comparison between the tabulated regional values in the first column of Tables 8 and 9 supports our assumption that the linear regression equations accurately represent the experimental profiles for the span of 35 to 90 minutes. Also, we observed the best comparison between the experimental and predicted values of Table 8 when the constant  $R_1$  was employed in Equation 7 to predict the Kerslake regional temperatures.

Eight graphs of the absolute temperature difference between the averaged experimental temperature and that predicted by Kerslake's correlation, Equation 7, were plotted by using the respective linear regression equations to determine the segmental skin temperatures as a function of time. The value of mean skin temperature employed in Equation 7 was determined by means of Equation 8 for each minute of time from the experimental temperatures which were estimated by the linear regression equations.  $R$  in Equation 7 was defined as being equivalent to  $R_1$  of Tables 8 and 9 and was calculated at each time interval prior to its use in Equation 7. The temperature averaging scheme which was used to obtain the equivalent Kerslake regional values from the linearized experimental data was the same as that defined in Tables 8 and 9. Review of these graphs revealed that for the entire period of analysis (35 to 90 minutes) the experimental temperature of the trunk, thigh, and calf agreed to within  $\pm 0.5^\circ\text{C}$  of that predicted by Equation 7. The same agreement was observed for the head and hand for 90% of the time span, and for 70% of the period for the foot. The Kerslake predicted upper and lower arm values were compared to the linearized experimental data of the arm (See Table 7.). The absolute temperature difference between the predicted value for the upper arm and the experimental value for the arm varied between  $0.5$  and  $0.8^\circ\text{C}$  throughout the time span; for the lower arm, the absolute temperature difference observed was considerably larger, i.e., greater than  $1.50^\circ\text{C}$  throughout the entire time span. We do not understand the exact cause of the

poor comparison between the predicted and linearized experimental skin temperatures for the upper and lower arm when such a good correspondence was observed for the other body regions. We suspect that the lack of similar regions between which to compare may have contributed to the noted incongruity. Regardless of the results of the upper and lower arm comparison, the good agreement noted for the principal regions confirms the hypothesis of extrapolating Kerslake's predictive equation for eight regions (Table 7) to the twelve segment map of Hody (Fig. 2 and Table 1).

To adapt Kerslake's algebraic model to the Hody twelve segment map, it was necessary to compute curve fitting coefficients,  $A(i)$ , from Equation 9, which is a transposition of Equation 7.

$$A(i) = \frac{(T(i) - T_{skm})}{R1} \quad (9)$$

where:  $A(i)$  = Distribution fraction for segment  $i$

$T(i)$  = Linearized experimental temperature for segment  $i$

$T_{skm}$  = Linearized Experimental Hody mean skin temperature

$R1$  = 2.946

We substituted into Equation 9 values of  $T(i)$ ,  $T_{skm}$ , and  $R1$ , all of which had been evaluated at the midpoint of the selected time span of 35 to 90 minutes. We then solved for the respective values of  $A(i)$  which are tabulated in Table 10.

Although the numerical analysis was based upon data which was obtained from shivering men with mean skin temperatures ( $T_{skm}$ ) of approximately 26 °C, we propose that the modified Kerslake correlation, Equation 10, can be used with the tabulated values of Table 10 to estimate the twelve segmental skin temperatures of a vasoconstricted but non-shivering diver whose mean skin temperature is between 31 and 32 °C.

Table 10

## Distribution Fractions for Predictive Skin Temperature Correlations

Time = 63 minutes

R1 = 2.946

<u>Segment ID #, i</u>	<u>Segment Name</u>	<u>Distribution Fraction A(i)</u>
1	Head	0.36
2	Chest	0.27
3	Abdomen	0.30
4	Upper Back	0.52
5	Lower Back	-0.08
6	Arm	0.22
7	Hand	-0.64
8	Front Thigh	-0.04
9	Front Calf	-0.16
10	Rear Thigh	-0.06
11	Rear Calf	-0.55
12	Foot	-0.86

$$T(i) = T_{skm} + A(i) \cdot R_1 \quad (10)$$

where:  $T(i)$  = Predicted temperature for segment  $i$

$T_{skm}$  = Body mean skin temperature

$A(i)$  = Distribution fraction for segment  $i$  (Table 10)

$R_1 = 2.946$

The application of Equation 10 to the Body mean skin temperature ( $T_{skm}$ ) range of 31 to 32 °C is by extrapolation. Ideally, this proposed application should be tested experimentally under physiological conditions analogous to those for which it is intended. Realistically, no such experimental data is currently available.

#### Authentication of the Model

The mean subject data which had been obtained during several evaluations of the Navy's prototype DTP garment (DTP1AR1, DTP2AR1, DTP3AR1; see Chapter II.) were used to evaluate the accuracy of the predictive temperature correlation. The subjects in these evaluations had mean skin temperatures which approached those observed in the respiratory heat loss studies (RHL1AR1) and were observed to be both shivering and pronouncedly vasoconstricted. We assumed that if our predicted segmental skin temperatures compared favorably with those found in the experimental data files, then we could presume that the correlation would yield reasonably accurate segmental temperatures at the more conservative mean skin temperature range of 31 to 32 °C.

The modified Kerslake correlation was derived with skin temperature data taken from five seated, resting subjects in a hyperbaric helium-oxygen environment at ambient conditions of 20 °C and 200 MSW [21] because this data

correlated well when comparing one subject to another and when it was free of segmental anomalies. Visual inspection of graphs prepared from data recorded during the three available immersed studies (DTP1ART, DTP2AR1, DTP3AR1) exhibited aberrant temperatures associated with the head, hand, and foot for a number of the experimental subjects. The deviation of data from its mean is a very important consideration in making statistical inferences when the number of experimental subjects is small. For this reason, the most statistically accurate predictive segmental skin temperature correlations should be obtained from the hyperbaric data (RHL1AR1) despite significant respiratory heat loss in addition to losses attributed to surface convection and radiation. We ignored any effect that respiratory heat loss may have produced on the peripheral vasomotor state of these hyperbaric subjects because of the observation that the peripheral thermoreceptors play the major role in regulating metabolic heat production without apparent adjustment for cooling through the respiratory tract [21].

To examine the accuracy of the modified Kerslake correlation to represent the entire quasi-steady period of thermal equilibrium (35 to 90 minutes) chosen from the hyperbaric records, we calculated  $T(i)$  for each minute of time by means of Equation 10 and the parameters of Table 10. The independent variable  $T_{skm}$  was computed with Equation 8 from segmental temperatures which were determined from the experimental linearized equations (derived from data in the RHL1AR1 file). Finally, each predicted segmental temperature was compared to the equivalent linearized experimental value for the same instant of time and an absolute temperature difference was obtained. These computations were conducted twice: once with  $R1$  of Equation 10 equal to a constant as defined in Table 10, and then with  $R1$  computed at each instant of time. The results of these comparisons are summarized in Table 11. Also tabulated for both the variable and constant  $R1$  cases is the percentage of the

Table 11

Percentage of the Total Number of Compared Points (56) Over the Span of 35 to 90 Minutes Which Have Absolute Temperature Differences  $\leq 0.50^{\circ}\text{C}$  and  $\leq 0.25^{\circ}\text{C}$ . Evaluations for both  $R1$  constant and  $R1$  as a function of time are presented.

Segment Name	<u>Percentages</u>			
	$R1 = \text{constant}$		$R1 = R1(\text{time})$	
	$\leq 0.25^{\circ}\text{C}$	$\leq 0.50^{\circ}\text{C}$	$\leq 0.25^{\circ}\text{C}$	$\leq 0.50^{\circ}\text{C}$
Head	100	100	76.8	100
Chest	69.6	100	100	100
Abdomen	100	100	100	100
Upper Back	80.4	100	100	100
Lower Back	100	100	100	100
Arm	100	100	83.9	100
Hand	100	100	100	100
Front Thigh	100	100	100	100
Front Calf	100	100	100	100
Rear Thigh	69.6	100	62.5	100
Rear Calf	91.1	100	100	100
Foot	30.4	63	100	100

total number of compared points which had absolute differences of  $\leq 0.50$  °C and  $\leq 0.25$  °C. For R1 evaluated as a function of time, the predicted skin temperature for each segment is always within 0.50 °C of the corresponding linearized experimental value. When R1 is constant, all segments except the foot compare within 0.50 °C; however, the foot satisfies the 0.50 °C criteria for 63% of the time considered.

Further authentication of the modified Kerslake correlation was conducted with the actual experimental data from which the correlation was derived (RHL1AR1) and with three sets of experimental segmental temperatures, collected as described by Zumrick [30], from immersed divers during NCSC evaluations of the DTP garment [22] (DTP1ART, DTP2AR1, DTP3AR1). DTP1ART's and DTP2AR1's data were obtained from divers immersed in water at a depth equivalent to 3 MSW, and DTP3AR1's data was obtained from divers submerged to a depth equivalent to 21 MSW. The number of experimental subjects in each of the four studies (RHL1AR1, DTP1ART, DTP2AR1, and DTP3AR1) were 5, 4, 3, and 3, respectively.

The authentication process was conducted with a normalized temperature (Eq. 11) which permits comparison of experimental studies with different mean skin ( $T_{skm}$ ) and ambient ( $T_a$ ) temperatures.

$$TN(i) = \frac{T(i) - T_a}{T_{skm} - T_a} \quad (11)$$

where:  $TN(i)$  = Normalized skin temperature for segment  $i$

$T(i)$  = Predicted or experimental skin temperature for segment  $i$

$T_a$  = Experimental ambient temperature

$T_{skm}$  = Experimental Body mean skin temperature

Mean segmental temperature profiles, which were prepared for each experimental study, were analyzed for a period of 75 minutes. This period began at the 30th minute of each experimental record after the suggestion of Piantadosi et al. [22] that transitory effects of peripheral vasoconstriction were, by then, complete. Each data file was analyzed at discrete time intervals where a normalized temperature for each of Hody's twelve segments was calculated. The normalized temperatures were calculated by Equation 11 with a mean skin temperature ( $T_{skm}$ ) value determined by Equation 8 from the mean experimental data. With this same value of  $T_{skm}$ , segmental predicted temperatures were calculated for the same time interval by means of Equation 10 and the parameters defined in Table 10. The normalized predicted skin temperature was then determined with Equation 11. Both the experimental and the predicted normalized temperatures were averaged over time and are tabulated in Tables 12-15 for data files RHL1AR1, DTP1ART, DTP2AR1, and DTP3AR1, respectively. The standard deviation, determined when the normalized temperatures were time averaged, is also listed for each of the twelve segments. To quantify the accuracy of the predictive correlation for estimating the actual experimental temperatures, the time averaged predicted  $\overline{T_N(i)}_{PREP}$  and experimental normalized  $\overline{T_N(i)}_{EXP}$  temperatures were employed to calculate a percent difference with the normalized experimental temperature as the computational base (Eq. 12). This percent difference is also tabulated in Tables 12-15. A negative percent difference indicates that the normalized experimental temperature is greater than the predicted value as shown below.

Table 12

Time Averaged (Mean) Normalized Temperatures for Each of Hody's Twelve Segments Computed From the Mean Temperature Profiles of Experimental File RHL1AR1 and the Equivalent Predicted Normalized Temperature Which was Estimated by Equations 10 and 11. The percent difference between the segmental predicted and experimental time averaged, normalized temperatures was computed by Equation 12.

Time Averaged T<sub>skm</sub>: 25.70 °C, Std. Dev.: 0.2464

Time Averaged T<sub>a</sub>: 20.03 °C, Std. Dev.: 0.3162

Normalized Temperatures

<u>Segment</u>	Experimental		Predicted		% Diff.
	Mean	Std. Dev. <sup>†</sup>	Mean	Std. Dev. <sup>†</sup>	
Head	1.208	4.24E-02	1.188	1.21E-02	-1.66
Chest	1.146	7.41E-02	1.141	9.03E-03	-0.44
Abdomen	1.160	3.63E-02	1.157	1.01E-02	-0.26
Upper Back	1.268	4.89E-02	1.271	1.75E-02	0.24
Lower Back	0.963	1.64E-02	0.958	2.59E-03	-0.52
Arm	1.121	4.16E-02	1.115	7.45E-03	-0.54
Hand	0.642	7.36E-02	0.666	2.15E-02	3.74
Front Thigh	0.993	2.70E-02	0.979	1.43E-03	-1.41
Front Calf	0.924	3.21E-02	0.916	5.37E-03	-0.87
Rear Thigh	0.963	5.13E-02	0.969	2.04E-03	0.62
Rear Calf	0.719	4.83E-02	0.713	1.84E-02	-0.83
Foot	0.526	1.31E-01	0.551	2.89E-02	4.75

<sup>†</sup>E format notation is equivalent to scientific notation; i.e., E-02 = 10<sup>-2</sup>.

Table 13

Time Averaged (Mean) Normalized Temperatures for Each of Hody's Twelve Segments Computed From the Mean Temperature Profiles of Experimental File DTP1ART and the Equivalent Predicted Normalized Temperature Which was Estimated by Equations 10 and 11. The percent difference between the segmental predicted and experimental time averaged, normalized temperatures was computed by Equation 12.

Time Averaged T<sub>skm</sub>: 27.77 °C, Std. Dev.: 0.7740

Time Averaged T<sub>a</sub>: 4.04 °C, Std. Dev.: 0.1316

Normalized Temperatures

<u>Segment</u>	Experimental		Predicted		% Diff.
	Mean	Std. Dev. <sup>†</sup>	Mean	Std. Dev. <sup>†</sup>	
Head	0.903	6.53E-02	1.045	1.61E-03	15.73
Chest	1.111	4.03E-02	1.034	1.03E-03	- 6.93
Abdomen	1.131	1.84E-02	1.037	1.24E-03	- 8.31
Upper Back	1.155	4.28E-02	1.065	2.28E-03	- 7.79
Lower Back	1.084	1.01E-02	0.990	6.18E-04	- 8.67
Arm	1.090	1.56E-02	1.027	1.03E-03	- 5.78
Hand	1.116	3.16E-02	0.925	2.86E-03	-17.56
Front Thigh	0.712	8.51E-02	0.995	2.76E-04	39.75
Front Calf	0.933	2.56E-02	0.980	5.52E-04	5.04
Rear Thigh	0.877	2.28E-02	0.993	5.52E-04	13.23
Rear Calf	0.938	1.47E-02	0.932	2.49E-03	- 0.64
Foot	0.907	3.25E-02	0.893	3.81E-03	- 1.54

<sup>†</sup>E format notation is equivalent to scientific notation; i.e., E-02 = 10<sup>-2</sup>.

Table 14

Time Averaged (Mean) Normalized Temperatures for Each of Hody's Twelve Segments Computed From the Mean Temperature Profiles of Experimental File DTP2AR1 and the Equivalent Predicted Normalized Temperature Which was Estimated by Equations 10 and 11. The percent difference between the segmental predicted and experimental time averaged, normalized temperatures was computed by Equation 12.

Time Averaged T<sub>skm</sub>: 28.58 °C, Std. Dev.: 1.2525

Time Averaged T<sub>a</sub>: 4.77 °C, Std. Dev.: 0.0500

Normalized Temperatures

<u>Segment</u>	Experimental		Predicted		% Diff.
	Mean	Std. Dev. <sup>†</sup>	Mean	Std. Dev. <sup>†</sup>	
Head	0.980	3.87E-02	1.045	2.26E-03	6.63
Chest	0.937	1.15E-02	1.033	1.68E-03	10.25
Abdomen	0.977	9.36E-03	1.037	1.77E-03	6.14
Upper Back	1.194	3.21E-02	1.065	3.29E-03	-10.80
Lower Back	1.102	1.62E-02	0.990	4.76E-04	-10.16
Arm	1.103	1.73E-02	1.027	1.30E-03	- 6.89
Hand	0.985	6.16E-02	0.921	4.02E-03	- 6.50
Front Thigh	0.868	1.15E-02	0.995	3.91E-04	14.63
Front Calf	1.018	2.04E-02	0.980	8.29E-04	- 3.73
Rear Thigh	0.863	1.42E-02	0.993	3.91E-04	15.06
Rear Calf	0.905	2.37E-02	0.932	3.43E-03	2.98
Foot	0.983	7.71E-03	0.893	5.39E-03	- 9.16

<sup>†</sup>E format notation is equivalent to scientific notation; i.e., E-02 = 10<sup>-2</sup>.

Table 15

Time Averaged (Mean) Normalized Temperatures for Each of Hody's Twelve Segments Computed From the Mean Temperature Profiles of Experimental File DTP3AR1 and the Equivalent Predicted Normalized Temperature Which was Estimated by Equations 10 and 11. The percent difference between the segmental predicted and experimental time averaged, normalized temperatures was computed by Equation 12.

Time Averaged T<sub>skm</sub>: 26.64 °C, Std. Dev.: 0.6198

Time Averaged T<sub>a</sub>: 4.25 °C, Std. Dev.: 0.3600

Normalized Temperatures

<u>Segment</u>	Experimental		Predicted		% Diff.
	Mean	Std. Dev. <sup>†</sup>	Mean	Std. Dev. <sup>†</sup>	
Head	0.576	5.90E-02	1.047	8.50E-04	81.77
Chest	1.133	1.83E-02	1.036	7.18E-04	- 8.56
Abdomen	1.091	5.80E-02	1.039	7.87E-04	- 4.77
Upper Back	1.273	4.46E-02	1.068	1.20E-03	- 16.10
Lower Back	1.154	2.84E-02	0.989	3.21E-04	- 14.30
Arm <sup>††</sup>					
Hand	0.966	4.08E-02	0.916	1.73E-03	- 5.18
Front Thigh	0.959	3.04E-02	0.995	7.87E-04	3.86
Front Calf	1.155	3.25E-02	0.979	5.56E-04	- 15.24
Rear Thigh	0.845	5.30E-02	0.992	3.21E-04	17.40
Rear Calf	0.930	5.45E-02	0.928	1.40E-03	- 0.22
Foot	0.283	1.86E-02	0.887	2.20E-03	213.43

<sup>†</sup>E format notation is equivalent to scientific notation; i.e., E-02 = 10<sup>-2</sup>.

<sup>††</sup>Insufficient data recorded from the arm to permit comparative analysis.

$$\% \text{ Diff}(i) = \left( \frac{\overline{\text{TN}}(i)_{\text{PRED}} - \overline{\text{TN}}(i)_{\text{EXP}}}{\overline{\text{TN}}(i)_{\text{EXP}}} \right) \cdot 100 \quad (12)$$

where:  $\% \text{ Diff}(i)$  = Percent difference for segment  $i$

$\overline{\text{TN}}(i)_{\text{PRED}}$  = Time averaged predicted temperature for segment  $i$

$\overline{\text{TN}}(i)_{\text{EXP}}$  = Time averaged experimental temperature for segment  $i$

Table 12 displays the percent differences for all regions except the head, hand, front thigh, and foot to be less than 1% for the RHL1ARI data. This result was expected since the modified Kerslake correlations were developed with this data. Table 13, which is based upon experimental file DTP1ART, shows percent differences within 10% for all regions except the head (15.73%), hand (17.56%), front thigh (39.75%), and rear thigh (13.23%). The larger error associated with the front thigh is probably an anomaly since considerably better agreement is found for the front thigh in the two other submerged studies that were analyzed (Tables 14 and 15). Table 14, which is derived from experimental file DTP2AR1, shows percent differences which are less than or equal to 15% for all regions.

During the 21 MSW submerged evaluation of the DTP garment (Table 15, from data file DTP3AR1), insufficient data was recorded from the arm to permit comparative analyses. The percent differences associated with the head (81.77%) and the foot (213.43%) were obviously anomalous when compared to the significantly better values for the head and foot in Tables 13 and 14. A review of the DTP3AR1 data revealed that erroneous data was collected from the head and foot over much of the 75 minute period of interest.<sup>9</sup> Only those data

---

<sup>9</sup>The 75 minute period of time, which begins at the 30th and ends at the 105th minute of each experimental file, was chosen to establish a representative common period of exposure among the four experimental files considered.

points which could be assumed to be representative of the experimental phenomenon were considered in the analyses reflected in Table 15.

Unfortunately, the small number of usable data points heavily biases the results obtained. Of all the sets of experimental data, that recorded during the 21 meter evaluation of the DTP garment was the least congruous.

In considering the results of our analyses, it should be noted that all of the experimental data within the selected time period (30 to 105 minutes) was employed in computing the time averaged normalized temperatures. Examination of the mean experimental data also revealed the presence of questionable data points, particularly for the head, hand, and foot. Piantadosi et al. [22] suggests that some of the observed anomalies, artificially high heat flux values, were due to an influx of cold water around poorly sealed areas of the dry suit's outer garment. Leaks occurred between the suit sleeve and glove, which compromised the suit's insulation in this area, and air often collected in the garment's hood, which precipitated leakage around the hood-face seal [22].

We concluded from these results that the modified Kerslake equation (Eq. 10 and Table 10) can be employed to predict segmental skin temperatures over a mean skin temperature range of 26 to 28 °C. Extrapolation of the correlation to T<sub>skm</sub> values above this envelope is probably reasonable, but is dependent upon levels of vasoconstriction and shivering - two variables over which we had no control during data acquisition or the numerical analyses. Ideally, actual experimental data would confirm the validity of the extrapolation to other T<sub>skm</sub> values. Furthermore, it is apparent from the tabulated comparisons of time averaged, normalized predicted and experimental skin temperatures (Tables 13-15) that the modified Kerslake correlation approximates the principal segments' temperatures within a 15% error.

The regional predicted skin temperatures of our model ( $T_r$  of Eq. 5) are derived from these predicted segmental skin temperatures ( $T(i)$  of Eq. 10 with Table 10).<sup>10</sup> Table 16 displays each model man region with the corresponding body segments. For the regions that have two corresponding segments (See Table 16.), the predicted segmental skin temperatures (Eq. 10 with Table 10) are weight averaged with the corresponding body segmental surface area fractions (Table 1) to obtain the regional predicted skin temperature. Equation 13 shows an example (the torso) of the weight averaging equation which is used to find the regional predicted skin temperature.

$$T_2 = \frac{W(2)T(2) + W(4)T(4)}{W(2) + W(4)} \quad (13)$$

where:  $T_2$  = Temperature of region 2, the torso (Fig. 1)

$W(i)$  = Body surface area fraction for segment  $i$  (Table 1)

$T(i)$  = Segmental predicted skin temperatures for segment  $i$ ;  
computed from Equation 10 with Table 10

$i=2$  indicates segment 2, chest

$i=4$  indicates segment 4, upper back

The regional predicted skin temperature is equal to the segmental predicted skin temperature for regions that exhibit a one to one correspondence with a segment (for example, the head; see Table 16.)

---

<sup>10</sup>See Foreword for connotation of segment and region.

Table 16

## Model Man Region Names, Indices, and Corresponding Body Segments

Regional Index	Region Name	Region Abbreviation	Corresponding Body Segment Indices (Table 1) (segment name)
1	Head	HEAD	1 (head)
2	Torso	TORSO	2 (chest), 4 (upper back)
3	Abdomen	ABDOMEN	3 (abdomen), 5 (lower back)
4	Thigh	THIGH	8 (front thigh), 10 (rear thigh)
5	Calf	CALF	9 (front calf), 11 (rear calf)
6	Foot	FOOT	12 (foot)
7	Upper Arm	UP ARM	6 (arm)
8	Lower Arm	LOW ARM	6 (arm)
9	Hand	HAND	7 (hand)

## CHAPTER V

### DEVELOPMENT OF OVERALL HEAT TRANSFER COEFFICIENT

As indicated in Chapter III, the overall heat transfer coefficient,  $U_i(j)$  (Eq. 6), has been developed by using the thermal characteristic of the DTP garment as being representative of a pressure compensated dry suit. The analysis presented below is also valid for dry suit configurations which behave similarly to the DTP garment, but appropriate garment characteristics would have to be substituted for those associated with the DTP garment.

Equation 6 is presented below to facilitate the discussion.

$$U_i(j) = \frac{1}{\frac{1}{h_i(j)} + \frac{S_i(j) \cdot \ln(r_2/r_1)}{2\pi k_{ig} \cdot \Delta z} + \frac{S_i(j) \cdot \ln(r_3/r_2)}{2\pi k_{og} \cdot \Delta z} + \frac{S_i(j)}{S_o(j)h_o(j)}} \quad (6)$$

As stated previously, the first term of Equation 6 is neglected since we assume that the suit is always subjected to a hydrostatic pressure differential, below the shoulder level, which causes the garment to rest on the skin surface. Thus, hypothetically, no gas layer can exist between the skin and undergarment. Since the DTP suit's outer garment is constructed of a 0.16 CM thick crushed neoprene foam, the outer garment can be modeled as solid

neoprene with the same nominal thickness of 0.16 CM (1/16 inch). Thus, the outer garment can be treated as being incompressible and impermeable to the breathing gases and water. Substituting the skin surface area of a nodal element,  $S_i(j)$  (Eq. 14), into the third term of Equation 6 ( $R_{OG}$ ) and canceling

$$S_i(j) = 2\pi r_1 \Delta z \quad (14)$$

where:  $S_i(j)$  = Nodal skin surface area ( $M^2$ )

$r_1$  = Radius from regional center line to skin surface (M)

$\Delta z$  = Nodal height

the  $2\pi\Delta z$  term in both the numerator and denominator yields Equation 15.

$$R_{OG} = \frac{r_1 \cdot \ln(r_3/r_2)}{k_{og}} \quad (15)$$

The natural logarithm in Equation 15 corrects for the surface area variation of a cylinder.

#### Resistance of the Outer Boundary Layer

Substituting the nodal skin surface area,  $S_i(j)$  (Eq. 14), and the outer surface area of the crushed neoprene garment,  $S_o(j)$  (Eq. 16), into the last

$$S_o(j) = 2\pi r_3 \Delta z \quad (16)$$

where:  $S_o(j)$  = Nodal skin surface area of outer surface of the outer garment ( $M^2$ )

$r_3$  = Radius from regional center line to the outside surface to the outer garment (M)

$\Delta z$  = Nodal height

term of Equation 6 ( $R_{OBL}$ ) and canceling the  $2\pi\Delta z$  term in both the numerator and denominator yields Equation 17.

$$R_{OBL} = \frac{r_1}{r_3 h_0} \quad (17)$$

Since the empirical film coefficients (presented below) were derived from experimental data which was recorded at one location per region, these values are assumed to be regional averages. Thus, the nodal indicator, 'j', of  $h_0(j)$  in Equation 6 has been dropped.

#### Convective heat transfer coefficient ( $h_0$ )

The experimental respiratory heat loss data (RHL1AR1) was utilized to obtain empirical correlations for the mixed mode convective film coefficient ( $h_0$ ). The correlations are expressed in terms of a dimensionless Nusselt number as a function of the Grashof number and Prandtl number product. Figures 65-67 are plots of the logarithm (base 10) of the Nusselt number versus the logarithm (base 10) of the Grashof number and Prandtl number product. Figure 65 displays the data derived from the RHL1AR1 file for the torso (TORSO), abdomen (ABDOMEN), upper arm (UP ARM), lower arm (LOW ARM), calf (CALF), and foot (FOOT) (Fig. 1.). Since these regions may be taken as vertical cylinders for a sitting subject, Figure 65 also displays the curve generated from the classical empirical free convection correlation for vertical cylinders (theory)  $\overline{Nu} = 0.59 \cdot (GrPr)^{0.25}$  [39]. Figures 66 and 67 present the data derived from the RHL1AR1 file for the thigh (THIGH), and the head (HEAD) and hand (HAND), respectively. For a sitting subject, the thigh is treated as horizontal cylinders, and the head and hand are considered to be spheres. Figures 66 and 67 also display the curve produced from the classical

Figures 65-67. Composite Experimental, Classical Empirical Correlation for Natural Convection (THEORY) and Our Empirically Derived Correlation (FITTED) for Vertical Cylinders, Horizontal Cylinders and Spheres. Log of Nusselt number plotted against the log of the Grashof number and Prandtl number product.

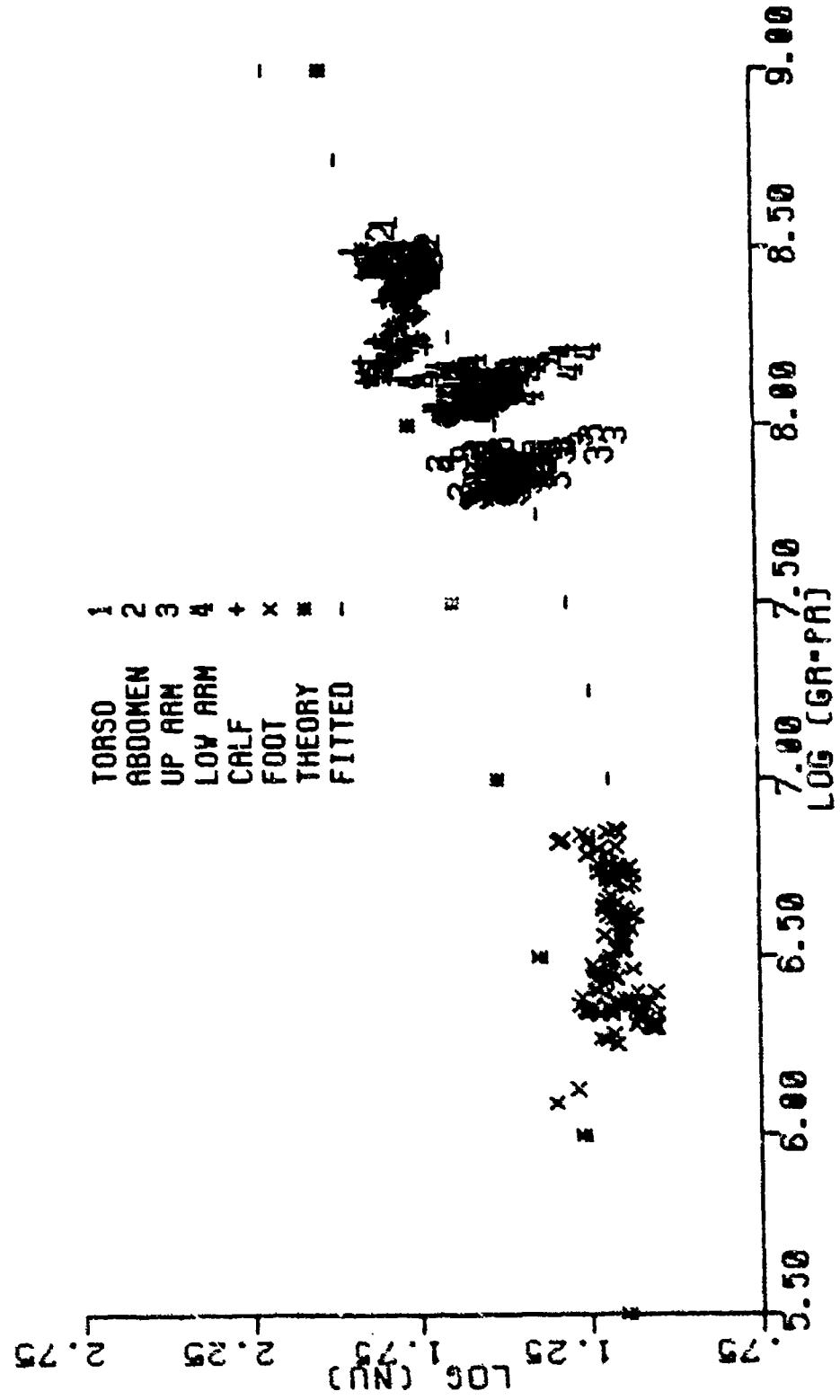


Figure 65. Log of Nusselt Number Versus Log of Grashof Number and Prandtl Number Product for Vertical Cylinder.

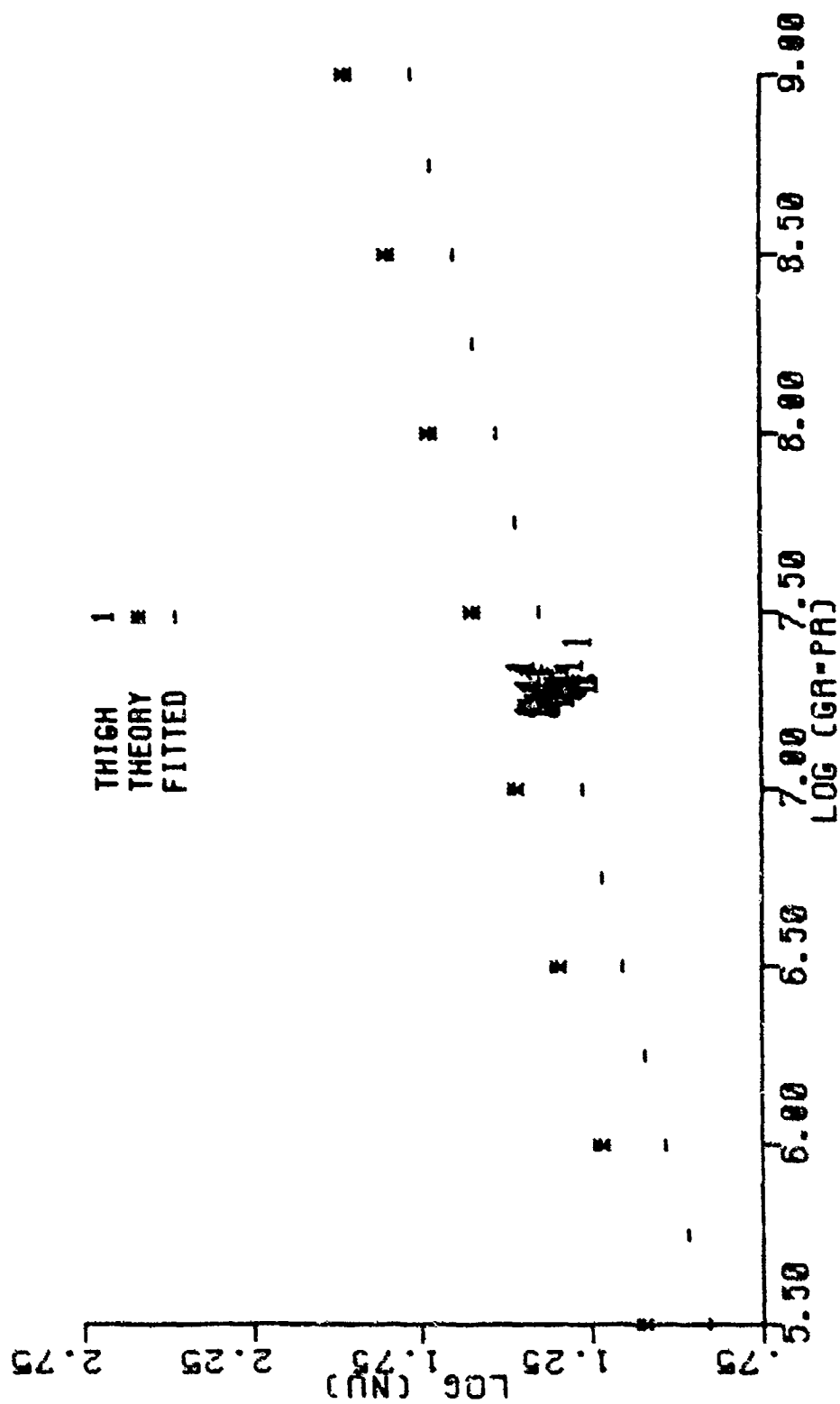


Figure 66. Log of Nusselt Number Versus Log of Grashof Number and Prandtl Number Product for Horizontal Cylinder.

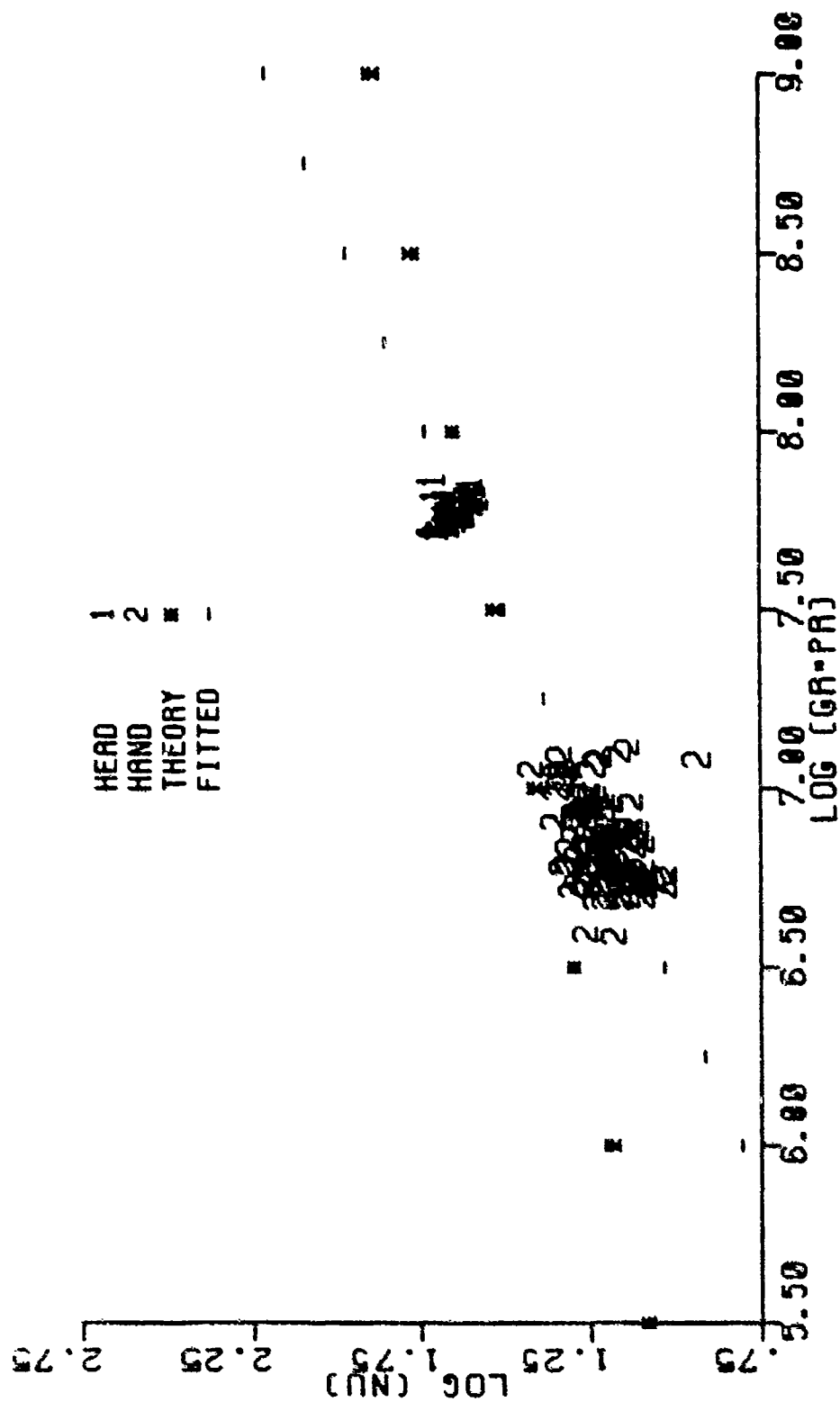


Figure 67. Log of Nusselt Number Versus Log of Grashof Number and Prandtl Number Product for Sphere.

empirical correlation for free convection (theory) for horizontal cylinders,  $\overline{Nu} = 0.53 \cdot (GrPr)^{0.25}$  [39], and spheres,  $\overline{Nu} = 2.0 + 0.43 \cdot (GrPr)^{0.25}$  [40,41], respectively.

Since the RHLIARI data was recorded from sitting, resting subjects exposed to a 20 °C hyperbaric 95% helium - 5% oxygen environment at a pressure equivalent to 200 MSW, the properties necessary to determine these dimensionless parameters were determined at a constant depth of 200 MSW and at an average film temperature of 22.15 °C. The film temperature was taken as the arithmetic mean between the regional skin and the ambient temperatures; this average film temperature was the mean of the highest and lowest film temperatures during the 120 minute duration of the experimental studies. The specific heat,  $C_p$ , and the density,  $\rho$ , were interpolated from data tabulated in the U.S. Navy Diving Gas Manual [42]. The viscosity,  $\mu$ , and thermal conductivity,  $k$ , were determined for a binary mixture by using the Wilke correlation [43] in the viscosity equation and the Lindsay and Bromley [43] formulation in the thermal conductivity equation. The constituent properties of helium and oxygen were interpolated as a function of temperature and pressure from values in the U.S. Navy Diving Gas Manual [42]. Appendix C contains example calculations for the viscosity,  $\mu$ , thermal conductivity,  $k$ , and the other properties mentioned above.

The experimental data in file RHLIARI is stored in the twelve segment format of Hody (Fig. 2), but the regions mentioned above refer to the nine regions of the model man (Fig. 1).<sup>11</sup> To convert the data in RHLIARI to the nine region model man format, the experimental segments corresponding to a model man's region were weight averaged with the Hody surface area fractions which correspond to the equivalent model region. (See Eq. 13 for an example.)

---

<sup>11</sup>See Foreword for the connotation of segment and region.

The differences between the Nusselt correlations derived from experimental data and the classical empirical curves, displayed in Figures 65-67, are attributed to a forced convection component superimposed on the natural convection. We could not evaluate the accuracy of accepted mixed mode convective heat transfer correlations since no information concerning forced draft gas currents was recorded during the experiments. Since no velocity information of any kind was recorded during these experiments, empirical correlations (Table 17) were derived from the composite experimental data of Figures 65-67. The equation for vertical cylinders (Table 17) was derived by fitting a parabola to the data of the torso, abdomen, upper arm, lower arm, and foot. The data from the calf was dropped because it was considered aberrant when compared, in dimensionless form, to the other vertical cylindrical regions (Fig. 65). As a result, we assumed that the calf obeyed our derived correlation for a vertical cylinder. This anomaly is possibly a result of the transition from a vertical to a horizontal cylinder that occurs at the knee for a sitting subject. Figure 66 displays the single set of data available for a horizontal cylinder. Since this data is too far removed from the classical empirical curve to simply use the classical empirical equation, we decided that it would be reasonable to assume that the experimental data follows a line parallel to the classical empirical line. Therefore, the formula for the horizontal cylinders was defined as a line with a slope matching that of the classical empirical line, but with a different y-intercept. The equation for spheres presented in Table 17 is the result of fitting a straight line between the two sets of data shown in Figure 67. Figures 65-67 also display the corresponding empirical correlation (FITTED) which is defined in Table 17.

Because of the poor agreement between the experimental data and the classical empirical free convection equations, we consider that our empirical

Table 17

## Empirical Convective Heat Transfer Correlations

Region	Geometrical Model	Correlation
Torso	Vertical Cylinder	$\log \overline{Nu} = a_2 (\log (GrPr))^2 + a_1 \log (GrPr) + a_0$
Abdomen		$a_2 = 0.1817$
Upper Arm		$a_1 = -2.4128$
Lower Arm		$a_0 = 9.1934$
Foot		
Calf		
Thigh	Horizontal Cylinder	$\log \overline{Nu} = a_1 \log (GrPr) + a_0$
		$a_1 = 0.2486$
		$a_0 = -0.4483$
Head	Sphere	$\log \overline{Nu} = a_1 \log (GrPr) + a_0$
Hand		$a_1 = 0.46486$
		$a_0 = -1.9726$

correlations (Table 17) are a more accurate representation of the experimental events than the classical empirical equations for free convection. Therefore, our empirical correlations (Table 17) have been employed to estimate the resistance due to the outer boundary layer ( $R_{OBL}$  of Eq. 17) in the overall heat transfer coefficient.

#### Undergarment Thermal Resistance

For the case of a diver who is wearing a pressure compensated dry suit, the predominant thermal resistance is provided by an undergarment which is fabricated of either a fibrous material or an insulative foam. The experimental data which was used in these developments was collected from resting subjects who were wearing the DTP suit with an undergarment fabricated of fibrous material (M-400 Thinsulate made by 3-M Corporation). We assumed that if the model was correct for the fibrous material, it also could be utilized for other suit ensembles which satisfy the same basic assumptions. The thermal resistance of this fibrous undergarment varies because of permeation by the ambient environmental gas inside the dry suit and compression (suit squeeze) which results from a local hydrostatic pressure differential between the interior of the garment and the surrounding water.

Although the variation in the properties of Thinsulate have not been evaluated under hyperbaric conditions, tests have been performed at 1 ATA with air and other gases [13]. These tests revealed that Thinsulate's insulative quality, as well as that of similar porous materials, is due primarily to its ability to entrap gas without the establishment of micro-convective currents within the material. For this reason, we assumed that the principal mode of heat loss through the undergarment is conduction. We further assumed that the

experimental thermal resistance data obtained in air can be extrapolated to any hyperbaric environment by multiplying the experimental air data by the ratio of the thermal conductivities of the air and the ambient hyperbaric environment (Eq. 18). The assumed method of extrapolation correlates well with experimental findings in helium at a pressure of 1 ATA [13]. This method of computation yields the baseline specific thermal resistance ( $R'$ )<sup>12</sup> of the undergarment at any depth of immersion (evaluated at the shoulder crest) and for any compensating suit gas.

$$R'_{TH}(0) = R'_a \left( \frac{k_a}{k_g} \right) \quad (18)$$

where:  $R'_{TH}(0)$  = Specific thermal resistance of Thinsulate which has been corrected for effects of the entrapped gas at ambient conditions

$R'_a$  = Specific thermal resistance of Thinsulate at sea level in air at 21.1 °C (2.27 CLO/CM) as determined by Audet, Orner, and Kupferman [12]

$k_a$  = Thermal conductivity of air at sea level and 21.1 °C

$k_g$  = Thermal conductivity of entrapped gas at ambient conditions

The immersed upright diver is subjected to a differential pressure because of the linearly increasing hydrostatic head. This differential pressure is zero at the neckline and approximately 13.8 kilopascals (2 PSIG) at the feet of a standing man. Audet et al. [12] developed a method of predicting the change in specific thermal resistance,  $R'$  (CLO/CM of thickness), as a function of the change in material density because of this hydrostatic pressure differential. They assumed that the density change in

---

<sup>12</sup>Specific thermal resistance ( $R'$ ) is defined in terms of CLO/CM of thickness. 1 CLO = 0.18 M<sup>2</sup>·HR°C/KCAL or in SI units, 0.155 M<sup>2</sup>°C/W.

the material was directly proportional to the change in thickness. Furthermore, they assumed that the degradation in  $R'$  as a function of the change in density (thickness) in fibrous batt materials (Thinsulate) was analogous to that which was observed in foam garment insulating materials. The behavior that they observed in these foam insulating materials (high density foams) indicated that, as the density increased (thickness decreased), the specific thermal resistance ( $R'$ ) decreased linearly. Adopting this model for the change in the specific thermal resistance of the Thinsulate undergarment, Figure 68 was derived from experimental data obtained by Audet et al. [12]. At a compressive pressure of 2 PSIG, the Thinsulate had a specific thermal resistance of 2.11 CLO/CM and the thickness had been reduced by 60%. The decimal percent change in  $R'$  (DPCSR) which corresponds to the 2.11 CLO/CM value is calculated by Equation 19 to be 0.07048, and the 60% change in thickness corresponds to a decimal percent change in thickness (DPCT) of 0.60 (Eq. 20).

$$DPCSR = \frac{R'_0 - R'}{R'_0} \quad (19)$$

where: DPCSR = Decimal percent change in specific thermal resistance

$R'_0$  = Uncompressed specific thermal resistance. This was taken from Audet et al. to be 2.27 CLO/CM at an uncompressed thickness of 1.63 CM.

$R'$  = Specific thermal resistance at elevated pressure; at 2 PSIG it is equal to 2.11 CLO/CM

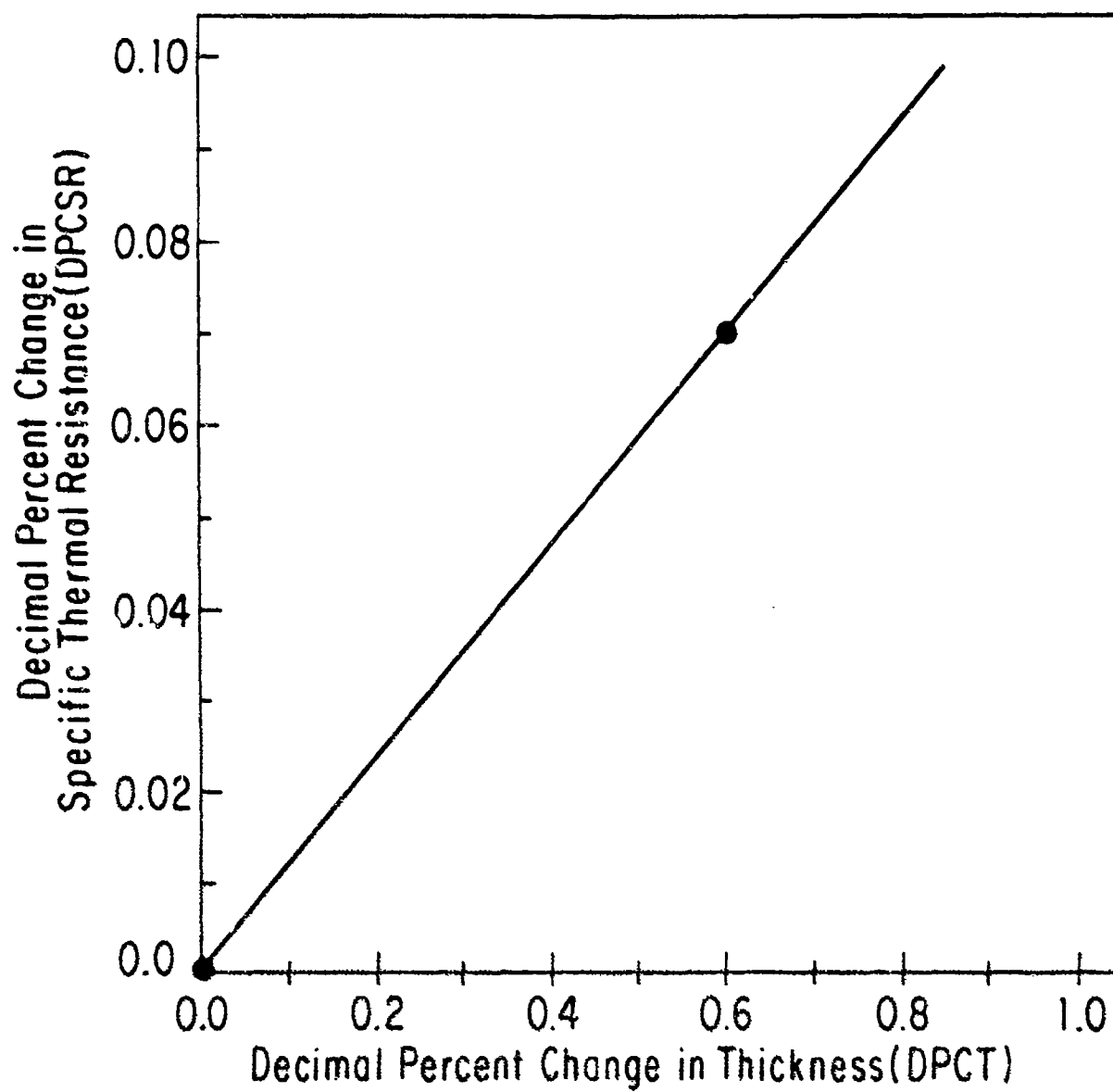


Figure 68. Linear Relationship Describing the Undergarment's Specific Thermal Resistance Change as a Function of Change in Thickness.

$$DPCT = \frac{t_0 - t}{t_0} \quad (20)$$

where: DPCT = Decimal percent change in thickness

$t_0$  = Uncompressed thickness (1.63 CM)

$t$  = Thickness after compression

In determining the gradient plotted in Figure 68, it was assumed that, in the uncompressed state, the Thinsulate has no degradation in specific thermal resistance or in thickness. The slope (DR) of the line (Fig. 68) which passes from (0.0,0.0) to (0.60,0.07048) was determined to be 0.1175. This line illustrates the hypothesis that, as the undergarment thickness is decreased, the specific thermal resistance is also decreased linearly. Therefore, the specific thermal resistance corrected for hydrostatic suit squeeze may be predicted at any depth below the shoulders between 0.0 CM and 136.8 CM (2.0 PSIG) by the derived equation:

$$R'_{TH}(Z) = R'_{TH}(0) (1 - [DR \cdot DPCT(Z)]) \quad (21)$$

where:  $R'_{TH}(Z)$  = Specific resistance of Thinsulate at Z CM below the shoulders

$R'_{TH}(0)$  = Specific resistance of Thinsulate at the shoulder crest

DR = 0.1175, which is the slope of the line (Fig. 68) that describes the decimal percent change in specific thermal resistance (DPCSR) versus the decimal percent change in thickness (DPCT)

DPCT(Z) = Decimal percent change in thickness of the undergarment at Z CM below the shoulders

The variation in the decimal percent change in thickness (DPCT) for the fibrous batt material (Thinsulate), as a result of the hydrostatic head which

is measured from the shoulders, is predicted by either of the following empirical equations:

$$\text{DPCT} = 2.358 \times 10^{-2} \cdot Z, \quad (22)$$

For  $Z \leq 17.11$  CM (0.25 PSIG).

$$\text{DPCT} = 0.343 + 3.784 \times 10^{-3} \cdot Z - 1.345 \times 10^{-5} \cdot Z^2, \quad (23)$$

For  $17.11$  CM (0.25 PSIG)  $< Z \leq 136.84$  CM (2.0 PSIG).

$Z$  is the depth in CM below the shoulder crest. Equations 22 and 23 were fitted to experimental data (Fig. 69) which was taken on flat samples by Audet et al. [12]. The dashed line in Figure 69 indicates that a break point was assumed at 0.25 PSIG as a result of our analysis of the experimental data of Audet et al., which is reproduced in Figure 70. This figure displays the percent change in thermal resistance (CLO) as a function of suit compressive pressure (PSIG). Inspection of Figure 70 reveals a rather sharp gradient between 0.25 PSIG and the origin, but shows that the rate of percent change in thermal resistance as a function of the imposed pressure moderates at pressures above 0.25 PSIG. This observation suggests that there should be a similar break point in the curves plotted in Figure 69 for the percent change in thickness as a function of the compressive load. Therefore, we assumed a linear rate of change in the Thinsulate's thickness between 0.0 PSIG and 0.25 PSIG with a more moderate curvilinear rate from 0.25 PSIG to 0.44 PSIG. We determined the break point of Figure 69 as that point of intersection between an extension of the line between the experimental data points at 0.44 PSIG and 0.50 PSIG and the constant compressive pressure intercept at 0.25 PSIG. The thermal resistance values ( $R$  in CLO) obtained by using Equations 22 or 23, 21, and 24 for the pressure range of 0.0 to 0.44 PSIG compare to within 10% of those displayed in Figure 70.

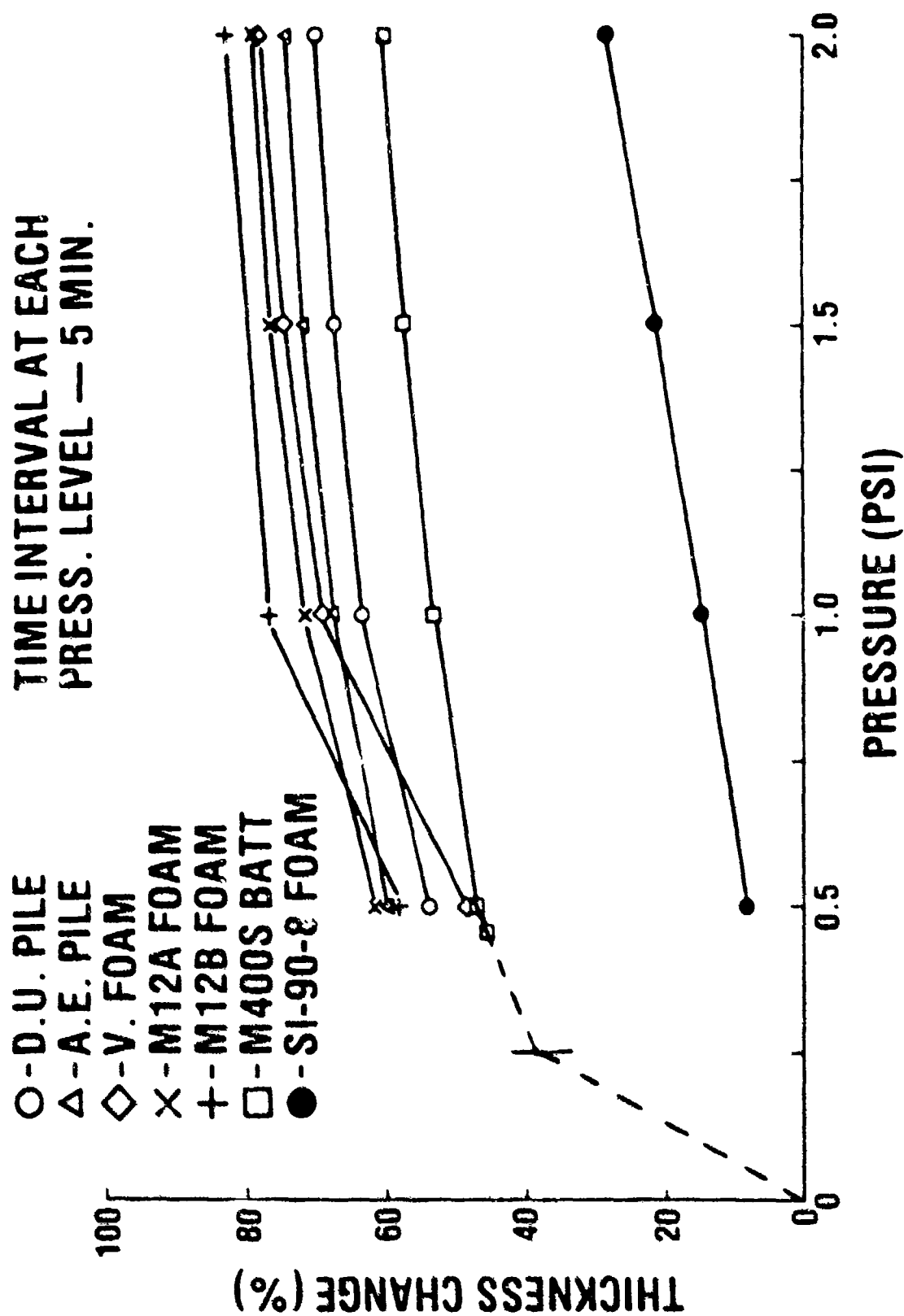


Figure 69. Percent Change in Thickness as a Function of Compressive Pressure. Re-drawn from a graph presented by Audet, Orner, and Kupferman [12].

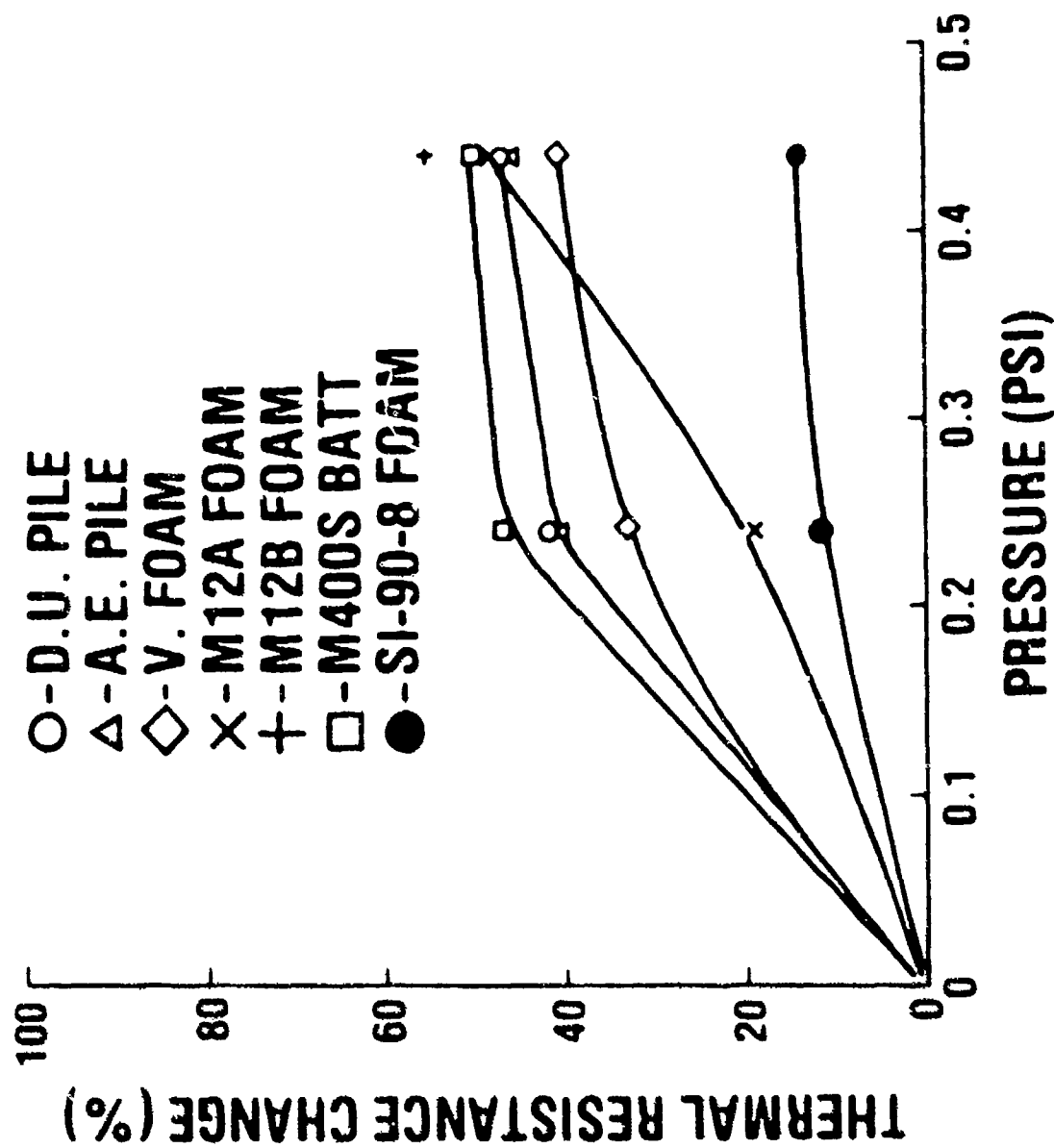


Figure 70. Percent Change in Thermal Resistance as a Function of Compressive Pressure. Re-drawn from a graph presented by Audet, Orner, and Kupferman [12].

$$R_{TH} = R'_{TH}(Z) (t_i - (t_i \cdot DPCT)) \quad (24)$$

where:  $R_{TH}$  = Thermal resistance of Thinsulate undergarment (CLO)

$R'_{TH}(Z)$  = Specific thermal resistance of Thinsulate undergarment (CLO/CM)

$t_i$  = Uncompressed thickness of undergarment (CM)

DPCT = Decimal percent change in thickness from Equation 22 or 23

To correct the specific thermal resistance of a nodal element for the effects of the suit entrapped gas and hydrostatic suit squeeze, the following procedure is used. First, the undergarment's uncompressed  $R'$  value of 2.27 CLO/CM [12] at sea level in 21.1 °C air is corrected for the effects of the suit entrapped gas at the ambient conditions (Eq. 18). This corrected  $R'$  value is then used as the shoulder crest value in Equation 21. To evaluate the decimal percent change in thickness (DPCT) at the node's depth below the shoulders, the dimensions of the body regions (Table 5) and the posture of the subject are considered. Depending upon the magnitude of this depth ( $Z$ ), either Equation 22 or 23 is utilized. The resulting value for the decimal percent change in thickness (DPCT) is then substituted into Equation 21. This value represents the specific thermal resistance after it has been corrected for the effects of the ambient entrapped gas and the reduction in thickness of the undergarment due to hydrostatic suit squeeze. The undergarment's thermal resistance is now computed by converting  $R'_{TH}(Z)$  (CLO/CM) to a thermal resistance (CLO) through multiplication by the undergarment's estimated thickness at a depth of  $Z$  CM below the shoulders (Eq. 24). The  $R_{TH}(Z)$  value in CLO's is then converted to SI units ( $R_{TH}$ ) (See footnote 12 on page 143.) and substituted into Equation 25.

$$R_{UG} = \frac{r_1 \cdot R_{TH} \cdot \ln(r_2/r_1)}{\Delta r} \quad (25)$$

where:  $R_{UG}$  = Thermal resistance of the undergarment corrected for suit entrapped gas and hydrostatic pressure ( $M^2^{\circ}C/W$ )

$R_{TH}$  = Thermal resistance of undergarment at ambient conditions

$\Delta r$  =  $r_2 - r_1 = t_i \cdot DPCT$

$t_i$  = 1.63 CM which is the uncompressed undergarment thickness [12]

DPCT = Decimal percent change in undergarment thickness from Equations 22 or 23

The natural logarithm in Equation 21 corrects the  $R_{TH}$  value for the effects of the region's curved surface.

#### Overall heat transfer coefficient

Neglecting any insulation which might have been contributed by a gas layer between the skin and undergarment because of suit squeeze, Equation 6 is rewritten below by substituting  $R_{UG}$  (Eq. 25),  $R_{OG}$  (Eq. 15), and  $R_{OBL}$  (Eq. 17) for terms 2 through 4, respectively.

$$U_i(j) = \frac{1}{\frac{r_1 \cdot R_{TH} \cdot \ln(r_2/r_1)}{\Delta r} + \frac{r_1 \cdot \ln(r_3/r_2)}{k_{og}} + \frac{r_1}{r_3 h_o}} \quad (26)$$

---

## CHAPTER VI

### THE INTERACTIVE MODEL PROGRAM

The regional temperature prediction correlations (Chapter IV) and the overall heat transfer coefficient formulation (Chapter V) have been synthesized into a numerical model for predicting the regional heat loss and required regional supplementary heating of a resting, immersed diver. The body geometry is that described in Chapter III. The numerical model assumes that the predicted regional temperatures (Eq. 10 with Table 10 and Eq. 13) are uniform over the entire regional surface and that there is no thermal interaction between any of the regions. This model program assumes that the diver will be in a prone, sitting, or standing posture while wearing the U.S. Navy's prototype Diver Thermal Protection garment that was described in Chapter III. Further, the initial model is restricted to a breathing gas of air. This limitation was necessary because all of the available experimental data from which the model was developed was obtained with air as the breathing gas; however, this does not restrict the model to only air diving. The model, as programmed, should yield reasonable results with other breathing gases under the presumption that the thermal conductivity of these gases as a function of temperature and pressure can be predicted. The program computes

the regional supplementary heating requirement by subtracting the regional allowable heat flux from the corresponding regional predicted heat flux value. The regional allowable heat fluxes which are used by the model program are those attributed to Burriss [33,34] and are tabulated in Table 18.

The model program allows the user to perform the heat loss computations for the entire region as a whole or for many finite difference nodes when the region is vertical. When a region approximates a horizontal cylinder or a sphere, the program assumes that the resistance of these regions may be accurately estimated by using thermophysical properties which are determined at the lateral midline (Fig 71).

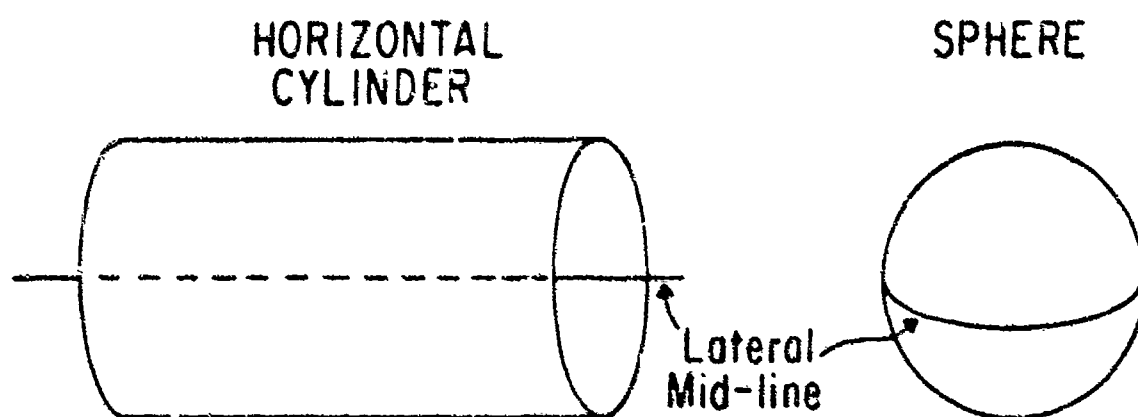


Figure 71. Lateral Mid-lines for Horizontal Cylinder and Sphere.

Table 18

Regional Allowable Heat Fluxes  
Excerpted from Burriss [33,34]

<u>Region ID #</u>	<u>Region Name</u>	<u>Allowable Heat Flux (W/M<sup>2</sup>)</u>
1	Head	23.30
2	Torso	60.00
3	Abdomen	49.70
4	Thigh	42.40
5	Calf	85.00
6	Foot	97.00
7	Upper Arm	98.90
8	Lower Arm	125.25
9	Hand	265.86

The thermal resistance of vertical regions when considered to be single nodes are computed with properties that are determined at the midpoint of their height (Fig. 72). When the vertical regions are divided into discrete nodal elements, the thermal resistance is determined for each node separately by using properties that are determined at the respective nodal depth (Fig. 72).

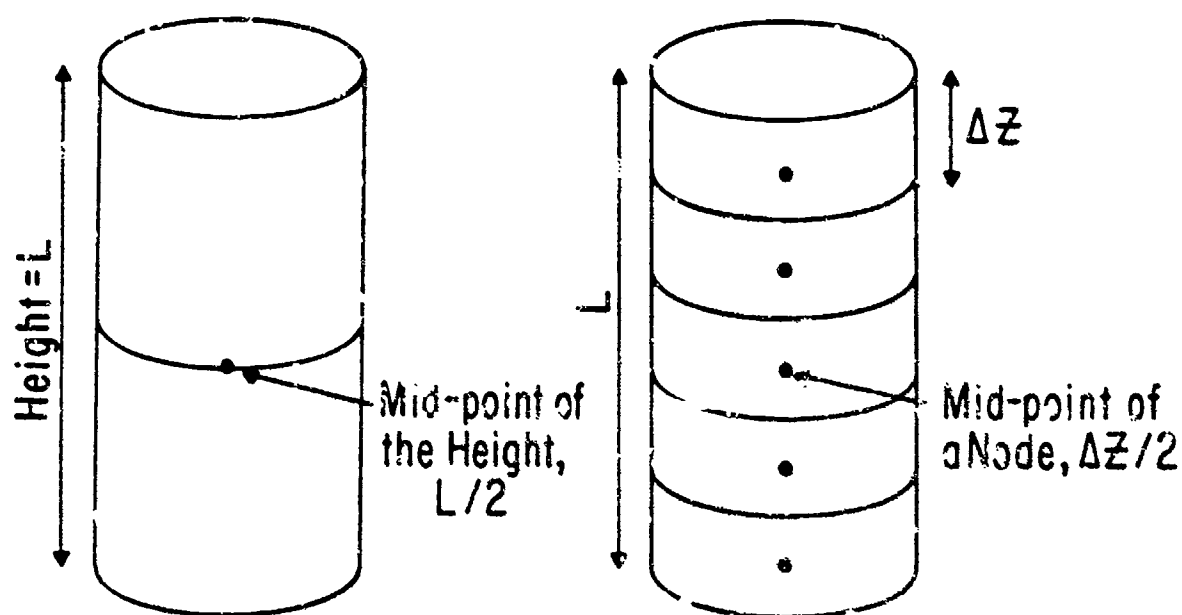


Figure 72. Single Nodal Element for a Vertical Body Region and Multi-nodal Element for a Vertical Body Region.

The model program consists of ten modules which are named Main, REINIT, OHTC, F(T), CHTC, TR, PRED, TC, PLOTD, and PLOTN. Documentation describing the use of the interactive model program is contained in Appendix D; each module is flow charted in Appendix E. Appendix F contains a complete source code listing of each module. Each module is listed below with a brief description of its function (See Appendices E and F for details.), and an explanation of the source (derivation) of any properties which are introduced in the model. Appendix G is a sample calculation which illustrates the computations that are performed in executing a simple production mode run (See Appendix D for explanation.). A summary of all the data that is used by the program is included at the front of Appendix G.

#### Main Program

The Main module acts as a controller which governs the sequence of execution. It collects all of the information that is necessary to define the problem and then proceeds to call the other modules, as required, to compute the nodal (one or many) heat loss(es). The regional rate of heat loss is determined by summing the nodal rates of heat loss and the regional supplementary heating requirement is then computed by subtracting a regional rate of allowable heat loss from this predicted regional rate of heat loss. This module synthesizes the information provided to determine which mode of execution to follow. If the user indicates the production mode, then a design value of the mean skin temperature and of the ambient temperature must be entered. If a research run is indicated, the program allows the user to compare predicted and experimental values of temperature, heat flux, overall heat transfer coefficient, normalized temperature, and Biot number. The

questions asked and the consequences of the possible responses are described in Appendix D, and the mechanics of the program's execution is described in the flow chart (Appendix E) and the source code listing (Appendix F). All of the properties that are defined in the Main module have been previously described in Chapters III, IV, V, and VI.

#### REINIT

This function subroutine is provided to allow the operator to return to the program-assigned values. The Main module allows the DTP garment properties (Chapter III) and thicknesses (Chapter III), the regional allowable heat fluxes (Chapter III and VI), and the overall heat transfer coefficient biasing factors (which will be described in Chapter VII) to be dynamically altered. This routine returns these values to their program-assigned values. See questions 5 thru 8 of the Question Flow section of Appendix D for the program-assigned values and the method of altering these values.

#### OHTC

This subroutine determines the overall heat transfer coefficient for a specified node with the method and equation that are described in Chapter V. The values for  $R_{OG}$  (Eq. 15) and  $R_{UG}$  (Eq. 25) are determined in this module. The value for  $R_{OBL}$  (Eq. 17) is found by using the Secant Method [44,45] for estimating the temperature of the outside surface of the outer garment ( $T_3$ ). The Secant algorithm utilizes the module  $F(T)$  to ascertain whether the estimated value of  $T_3$  is correct. Until the energy

balance of Function  $F(T)$  is approximately equal to zero, the Secant algorithm continues to iterate for  $T3$ .

The value for the convective heat transfer coefficient ( $h_0$  of Eq. 17) is computed at temperature  $T3$  with module CHTC. All properties that are used in this module are defined in the Main module. Because of the limits imposed on air diving by the U.S. Navy [46], we have restricted the model program to depths  $\leq 250$  FSW (76.2 MSW, 111.37 PSIG), and the ambient temperature must be  $< 1.0$  °C to remain within the limits defined for the boundary layer fluid properties.

### $F(T)$

This is a function subroutine which calculates the heat flux which passes through the complete garment ensemble and compares it with the heat flux that only passes through the undergarment and outer garment ( $F(T)$  in Eq. 27). These computations are carried out by assuming that the temperature of the outside surface of the outer garment ( $T$ ) is  $T3$  as passed from subroutine OHTC.

$$F(T) = \frac{(T_1 - T_a)}{RUG + ROG + \frac{r_1}{r_3 \cdot \text{CHTC}(T, r_3)}} - \frac{(T_1 - T)}{RUG + ROG} \quad (27)$$

where:  $T$  = Temperature  $T_3$ , passed from the Secant Method computation of Function OHTC

$T_1$  = Temperature of skin surface ( $^{\circ}\text{C}$ )

$T_a$  = Ambient temperature ( $^{\circ}\text{C}$ )

$RUG$  = Thermal resistance of undergarment

$ROG$  = Thermal resistance of outer garment

$r_1$  = Radius of body region

$r_3$  = Radius to outside of outergarment

$\text{CHTC}(T, r_3)$  = Function subroutine which estimates the convective heat transfer coefficient at temperature  $T$  and radius  $r_3$

All of the properties needed by Equation 27 are passed from module OHTC. If the estimated temperature  $T$  is correct,  $F(T)$  will equal zero.

#### CHTC

The module CHTC determines the convective heat transfer coefficient for the outer (water) boundary layer ( $h_o$ ) by using our derived empirical equations (Table 17) which are described in Chapter V. The subroutine first determines whether the region is a vertical or horizontal cylinder, or a sphere. For both the horizontal cylinders and spheres, the characteristic length (CL) is defined to be twice the radius of the outer garment ( $R_3$ ). The vertical cylinders use the height as the characteristic length as they are defined in

Table 5 of Chapter III. A value for the Grashof number and Prandtl number product (GrPr) is now determined with Equation 28.

$$\text{GrPr} = \alpha \cdot \text{CL}^3 \cdot (T_3 - T_a) \quad (28)$$

where:  $T_3$  = Temperature of outside surface of outer garment ( $^{\circ}\text{C}$ )

$T_a$  = Ambient temperature ( $^{\circ}\text{C}$ )

$$\alpha = \frac{g\beta\rho^2C_p}{\mu k} \left( \frac{1}{\text{M}^3\text{C}} \right), \text{ described below}$$

The property grouping,  $\alpha$  (Eq. 28), is determined with Equation 29.

$$\alpha = \log^{-1} [9.80714 (\log (T_f))^{0.12733}] \quad (29)$$

where:  $\alpha = \frac{g\beta\rho^2C_p}{\mu k}$

$g$  = Acceleration of gravity,  $9.81 \text{ M/SEC}^2$

$\beta$  = Volumetric coefficient of expansion ( $^{\circ}\text{K}^{-1}$ ) for water

$\rho$  = Density of water ( $\text{KG/M}^3$ )

$C_p$  = Specific heat at constant pressure ( $\text{J/KG}^{\circ}\text{K}$ ) for water

$\mu$  = Dynamic viscosity ( $\text{KG/M} \cdot \text{SEC}$ ) for water

$k$  = Thermal conductivity of water ( $\text{W/M}^{\circ}\text{K}$ )

$T_f$  = Film temperature ( $^{\circ}\text{K}$ ) =  $\frac{T_3 + T_a}{2.0}$

$T_3$  = Outside surface temperature of outer garment ( $^{\circ}\text{K}$ )

$T_a$  = Ambient temperature ( $^{\circ}\text{K}$ )

$\log^{-1} x = 10^x$

The constants 9.80714 and 0.12733 of Equation 29 are curve fitting coefficients that were determined when a power curve was fitted to the data of

Table 19 which was excerpted from Holman [40].  $\log^{13} T$  and  $\log \alpha$  of Table 19 correspond to  $x$  and  $y$ , respectively, in Equation 30.

$$y = ax^b \quad (30)$$

Table 19

$\alpha$  as a Function of Temperature  
Excerpted from Holman [40]

<u>T (°C)</u>	<u>log T</u>	<u><math>\alpha</math> (1/M<sup>3</sup>°C)</u>	<u>log <math>\alpha</math></u>
4.444	0.6478	$1.91 \times 10^9$	9.281
10.000	1.0000	$6.34 \times 10^9$	9.80209
15.555	1.1919	$1.08 \times 10^{10}$	10.033
21.111	1.3245	$1.46 \times 10^{10}$	10.164

This curve fit was performed with the HP-65 Stat PAC 1 routine Stat 1-24A [47] for power curve fitting. The determined value of  $\alpha$  (Eq. 29) is substituted into Equation 28, which yields an estimate for the product of the Grashof and Prandtl numbers. This value of  $GrPr$  is substituted into the appropriate equation of Table 17 to produce an estimate for the Nusselt number which is associated with the garment water interface.

$$Nu = \frac{h_0 CL}{k} \quad (31)$$

where:  $Nu$  = Nusselt number (dimensionless)

$h_0$  = Convective heat transfer coefficient

$CL$  = Characteristic length (M)

$k$  = Thermal conductivity of water (W/M°K) at the film temperature ( $T_f$ )

---

<sup>13</sup>log is to base 10.

Solving Equation 31 for the convective heat transfer coefficient ( $h_o$ ) requires a value for the thermal conductivity of water. This is determined by Equation 32 which is a curve that is fitted to tabulated thermal conductivity data that was excerpted from Holman [40] (Table 20).

$$k = 0.56662 + T \cdot 1.7977 \times 10^{-3} \quad (32)$$

where:  $k$  = Thermal conductivity of water (W/M°C)

$T$  = Film temperature (°C)

This fresh water thermal conductivity is used because all of the available immersed experimental data was recorded from divers who were submerged in fresh water and because the thermal conductivity of resting or slowly moving sea water may be approximated by that of fresh water [48].

Table 20

Thermal Conductivity of Water as a Function of Temperature  
Excerpted from Holman [40]

<u>T (°C)</u>	<u>k (W/M°C)</u>
0.000	0.566
4.444	0.575
10.000	0.585
15.555	0.595
21.111	0.604

Equation 32 was fitted to the data of Table 20 with the HP-65 Stat PAC 1 routine Stat 1-22A [47] for linear regression. Substituting the thermal conductivity value that is estimated by Equation 32 into Equation 31 allows the convective heat transfer coefficient ( $h_o$ ) to be determined.

## TR

This subroutine predicts an estimate of the model man's regional skin temperature by weight averaging the corresponding predicted segmental temperatures (Eq. 13 and Eq. 10 with Table 10 of Chapter IV). Table 16 of Chapter IV displays the correspondence between the model man's regions and the experimental segments which were used in developing the predicted temperature correlations of Equations 13 and 10 with Table 10.

## PRED

This subroutine predicts a segmental skin temperature by using Equation 10 with the constants of Table 10 (See Chapter IV.). These segmental skin temperatures are the values which are weight averaged in Function TR, above.

## TC

Module TC determines the thermal conductivity of air for use in Equation 18 of Chapter V. The value is interpolated from tabulated air data, which was excerpted from the U.S. Navy Diving Gas Manual [42], as a function of temperature and pressure. The two-dimensional interpolation routine was taken from Carnahan, Luther, and Wilkes [49]. Because of the limits imposed on air diving by the U.S. Navy [46], we have restricted the model program to depths  $\leq$  250 FSW (76.2 MSW, 111.37 PSIG), and the ambient temperature must be

< 1.0 °C to remain within the limits defined for the boundary layer fluid properties.

#### PLOTD

This subroutine takes dimensional temperatures, heat fluxes, and overall heat transfer coefficients (both experimental and predicted) and graphs them as a function of time. This data is generated whenever predicted and experimental data are compared. These graphs are produced with the Digital Equipment Corporation's (DEC) PLXY-11M plotting routines [50] and are printed on a DEC LXY11 Printer/Plotter (Printronix P300).

#### PLOTN

The PLOTN module uses the experimental and predicted temperatures, heat fluxes, and overall heat transfer coefficients to compute dimensionless, normalized temperatures,  $TN$  (Eq. 33), and Biot numbers [40],  $BI$  (Eq. 34).

$$TN = \frac{T_i - T_a}{T_{skm} - T_a} \quad (33)$$

where:  $TN$  = Regional normalized experimental or predicted skin temperature

$T_i$  = Regional experimental or predicted skin temperature

$T_a$  = Experimental ambient temperature

$T_{skm}$  = Body mean skin temperature (Eq. 8); determined with the experimental data

$$BI = \frac{U_i r_1}{k_g} \quad (34)$$

where: BI = Experimental or predicted Biot number [40]

$U_i$  = Experimental or predicted overall heat transfer coefficient

$r_1$  = Radius from the region's center line to the skin surface

$k_g$  = Thermal conductivity of the entrapped breathing gas (air);  
determined at the experimental or predicted film temperature

These experimental and predicted normalized temperatures and Biot numbers are then graphed as a function of the time. Each plot (normalized temperature or Biot number) shows both the experimental and the predicted values. These plots are produced in a manner similar to that described in the PLOTD section.

---

## CHAPTER VII

### MODEL VERIFICATION, CONCLUSIONS, AND RECOMMENDATION

#### Empirical Correlation of the Model

Inspection of Equation 5 (Chapter III) indicates that the rate of heat loss from each of the hypothetical nodal elements ( $\dot{Q}_i(j)$ ) is computed as the product of the respective nodal surface area ( $S_i(j)$ ), overall heat transfer coefficient per unit of skin area ( $U_i(j)$ ), and the temperature differential between the regional skin surface ( $T_i$ ) and the ambient environment ( $T_a$ ). The data analysis performed in Chapter IV revealed that Equation 10 would predict the segmental skin temperatures ( $T(i)$ ) with an accuracy of 15% for the mean skin temperature range of 26 to 29 °C and that the regional values ( $T_i$ ) are predicted by weight averaging the segmental values. Table 6 displays the good agreement which exists between the surface area percentages of our model man (Fig. 1) and the accepted experimental surface area percentages of Hody, thus indicating the accuracy of the model man's dimensions (Table 5). To complete the model, we investigated the accuracy of the empirical  $U_i(j)$  term of Equation 26 by comparing its predictions for each region (Fig. 1) with a representative experimental overall heat transfer coefficient for the same

region. This comparison is expressed in the form of a dimensionless Biot number (BI), Equation 34, which is repeated below.

$$BI = \frac{U_i r_1}{k_g} \quad (34)$$

Expressing the overall heat transfer coefficient in this dimensionless form neutralizes the influence of the ambient temperature and pressure on the ensemble's thermal conductance and thus, permits the comparison of experimental data collected at various ambient depths and temperatures. As may be seen in Equations 26, 18, 21, and 24, the effects of the ambient temperature and pressure are restricted to the first term of the denominator of our empirical expression for  $U_i(j)$  (Eq. 26). Inspection of Equations 18 and 21 indicates that any variation in the undergarment's thermal resistance due to the ambient pressure and temperature is primarily caused by changes in the thermal conductivity of the gas with which the suit is pressure compensated. The other terms of the denominator of Equation 26 are considered essentially invariant over the ambient temperature and pressure range in which the immersed experiments (DTP1ART, DTP2ARI, DTP3ARI; see Chapter II.) were conducted.

To determine regional biasing factors for correcting the hypothetical overall conductance of Equation 26, we employed experimental data that was collected during three evaluations of the DTP garment (DTP1ART, DTP2ARI, DTP3ARI). The instrumentation system which was utilized for data collection was analogous to that described by Zumrick [30] and was calibrated with the technique which was developed by Nuckols [19]. Two of the evaluation studies (DTP1ART and DTP2ARI) were conducted with divers immersed in water at a pressure equivalent to 3 MSW, and the third (DTP3ARI) was conducted at a pressure equivalent of 21 MSW. The number of experimental subjects in each of

the three studies (DTP1ART, DTP2AR1, and DTP3AR1) was 4, 3, and 3, respectively. For each experimental study, representative segmental temperature and rate of heat loss profiles (stored in DTP1ART, DTP2AR1, and DTP3AR1) were prepared by numerically averaging the data from the diver subjects at each time interval. This process is described in detail in Chapter II. The ambient temperature of the water ranged between 2 and 5 °C. Except for the head and feet, the garment ensemble worn by these prone, resting divers consisted of a fibrous batt (Thinsulate) undergarment of 1.63 CM nominal thickness at 1 ATA and an outer garment of crushed foam neoprene which has a nominal thickness of 0.16 CM. The head was covered by a conventional neoprene hood and the feet were insulated by a double thickness of the fibrous batt material. The passive protection garment was pressure compensated with air at a pressure equivalent to the ambient hydrostatic pressure at the shoulder crest. All three of the test series are documented in Chapter II.

To obtain experimental values that are equivalent to the nine region model (Fig. 1) from the segmental data of the composite data records (DTP1ART, DTP2AR1, DTP3AR1), experimental values of temperature and rate of heat loss from the corresponding Hody segments were averaged by using the corresponding Hody weighting factors (Table 1) (See Table 16.). From these profiles and a knowledge of the ambient temperature, experimental overall conductance ( $U_i(j)$ ) profiles were derived as a function of time. These conductance profiles were then converted to Biot number profiles with Equation 34. To discount any transitory effects of peripheral vasoconstriction, each of the experimental Biot number profiles was examined for a period of 75 minutes beginning at the 30th minute, after the suggestion of Piantadosi et al. [22]. Similarly, predicted conductances, as a function of time, were calculated for the same time period by means of Equation 26 and plotted as predicted Biot numbers.

Both the experimental and the predicted regional Biot number profiles were averaged over time and are tabulated in Tables 21, 22, and 23 for DTP1ART, DTP2AR1, and DTP3AR1 data files, respectively. The standard deviations that were determined when the profiles were time averaged are also listed for each region. The head data is not displayed in these tables because of the anomalies found in the experimental profiles for this region. To determine the accuracy of the predictive correlation (Eq. 26), the time averaged predicted and experimental Biot numbers ( $\overline{BI}$ ) were used in Equation 35 to calculate a percent difference. These regional percent difference values for the three DTP studies are also tabulated in Tables 21, 22, and 23. Negative values indicate that the experimental Biot number is greater than the predicted.

$$\% \text{ DIFF}_i = \left( \frac{\overline{BI}_{i\text{PRED}} - \overline{BI}_{i\text{EXP}}}{\overline{BI}_{i\text{EXP}}} \right) \cdot 100 \quad (35)$$

where:  $\% \text{ DIFF}_i$  = Percent difference for region  $i$

$\overline{BI}_{i\text{PRED}}$  = Time averaged predicted Biot number for region  $i$

$\overline{BI}_{i\text{EXP}}$  = Time averaged experimental Biot number for region  $i$

Because of the large percent differences ( $\% \text{ DIFF}$ ) that are displayed in Tables 21 through 23, biasing factors were obtained for each region by averaging the time averaged experimental and predicted Biot numbers of Tables 21, 22, and 23; calculating a decimal percent difference (DP) in a manner analogous to Equation 35; and determining the biasing factor by means of Equation 36. The study-averaged values of the experimental and predicted Biot numbers for all model regions, except the head, and their respective biasing factors (BF) are tabulated in Table 24.

$$\text{BF} = \frac{1}{1 + \text{DP}} \quad (36)$$

Table 21

Time Averaged (Mean) Biot Numbers for Each Model Region (Fig. 1)  
 Computed From the Composite Profiles of Experimental File DTP1ART  
 and the Equivalent Predicted Biot Number. Percent difference  
 between the respective regional experimental and predicted time  
 averaged Biot numbers.

		<u>Biot Numbers</u>				
<u>ID</u>	<u>Region</u>	Experimental		Predicted		% Diff.
		Mean	Std. Dev. <sup>†</sup>	Mean	Std. Dev. <sup>†</sup>	
1	Head					
2	Torso	3.65E+01	4.20E+00	1.01E+01	1.00E-03	-72.3
3	Abdomen	2.30E+01	1.43E+00	1.01E+01	2.93E-03	-56.1
4	Thigh	1.93E+01	2.08E+00	5.32E+00	1.16E-03	-72.4
5	Calf	1.42E+01	8.15E-01	4.36E+00	8.15E-04	-69.3
6	Foot	2.16E+01	7.80E-01	2.96E+00	2.13E-04	-86.3
7	Upper Arm	7.32E+00	8.18E-01	3.59E+00	4.56E-04	-51.0
8	Lower Arm	5.34E+00	5.96E-01	2.75E+00	4.90E-04	-48.5
9	Hand	1.17E+01	1.00E+00	4.44E+00	1.54E-03	-62.1

<sup>†</sup>E format notation is equivalent to scientific notation; i.e., E-02 = 10<sup>-2</sup>.

Table 22

Time Averaged (Mean) Biot Numbers for Each Model Region (Fig. 1)  
 Computed From the Composite Profiles of Experimental File DTP2AR1  
 and the Equivalent Predicted Biot Number. Percent difference  
 between the respective regional experimental and predicted time  
 averaged Biot numbers.

		<u>Biot Numbers</u>				
		Experimental		Predicted		% Diff.
<u>ID</u>	<u>Region</u>	Mean	Std. Dev. <sup>†</sup>	Mean	Std. Dev. <sup>†</sup>	
1	Head					
2	Torso	2.07E+01	3.82E+00	1.01E+01	2.39E-03	-51.2
3	Abdomen	2.27E+01	1.38E+00	1.01E+01	2.51E-03	-55.5
4	Thigh	1.58E+01	1.61E+00	5.33E+00	1.02E-03	-66.3
5	Calf	1.43E+01	1.38E+00	4.37E+00	9.95E-04	-69.4
6	Foot	1.45E+01	1.32E+00	2.96E+00	3.73E-04	-79.6
7	Upper Arm	9.14E+00	6.62E-01	3.60E+00	8.29E-04	-60.6
8	Lower Arm	6.67E+00	4.82E-01	2.76E+00	8.27E-04	-58.6
9	Hand	1.67E+01	2.95E+00	4.45E+00	2.53E-03	-73.4

<sup>†</sup>E format notation is equivalent to scientific notation; i.e., E-02 = 10<sup>-2</sup>.

Table 23

Time Averaged (Mean) Biot Numbers for Each Model Region (Fig. 1)  
 Computed From the Composite Profiles of Experimental File DTP3AR1  
 and the Equivalent Predicted Biot Number. Percent difference  
 between the respective regional experimental and predicted time  
 averaged Biot numbers.

		<u>Biot Numbers</u>				
		Experimental		Predicted		% Diff.
<u>ID</u>	<u>Region</u>	Mean	Std. Dev. <sup>†</sup>	Mean	Std. Dev. <sup>†</sup>	
1	Head					
2	Torso	2.25E+01	3.88E+00	1.01E+01	8.95E-03	-55.1
3	Abdomen	2.30E+01	3.45E+00	1.01E+01	9.50E-03	-56.1
4	Thigh	2.06E+01	1.48E+00	5.32E+00	4.27E-03	-74.2
5	Calf	1.35E+01	2.02E+00	4.36E+00	3.31E-03	-67.7
6	Foot	7.67E+01	2.26E+01	2.96E+00	1.56E-03	-96.1
7	Upper Arm <sup>††</sup>			3.59E+00	2.69E-03	
8	Lower Arm <sup>††</sup>			2.75E+00	1.93E-03	
9	Hand	1.82E+01	1.65E+01	4.44E+00	6.43E-03	-75.6

<sup>†</sup>E format notation is equivalent to scientific notation; i.e., E-02 =  $10^{-2}$ .

<sup>††</sup>Insufficient data recorded from the arm to permit comparative analysis.  
 Mean experimental values of Table 24 were obtained by averaging the time  
 averaged Biot numbers of records DTP1ART and DTP2AR1, contained in  
 Tables 21 and 22, respectively.

Table 24

Mean Experimental and Predicted Biot Numbers Averaged From the Respective Biot Numbers of Tables 21, 22, and 23 From Files DTP1ART, DTP2AR1, and DTP3AR1, Respectively.

Recommended biasing factors computed by Equation 36.

ID	Region	<u>Biot Numbers</u>		<u>Biasing Factor</u>
		Mean Experimental <sup>†</sup>	Mean Predicted <sup>†</sup>	
1	Head			Same as ID 2
2	Torso	2.66E+01	1.01E+01	2.63
3	Abdomen	2.29E+01	1.01E+01	2.27
4	Thigh	1.86E+01	5.32E+00	3.50
5	Calf	1.40E+01	4.36E+00	3.21
6	Foot	3.76E+01	2.96E+00	12.70
7	Upper Arm <sup>††</sup>	8.23E+00	3.59E+00	2.29
8	Lower Arm <sup>††</sup>	6.01E+00	2.75E+00	2.19
9	Hand	1.55E+01	4.44E+00	3.49

<sup>†</sup>E format notation is equivalent to scientific notation; i.e., E-02 = 10<sup>-2</sup>.

<sup>††</sup>Mean experimental values obtained by averaging the time averaged Biot numbers of records DTP1ART and DTP2AR1, contained in Tables 21 and 22, respectively.

The hypothetical  $U_i(j)$  value obtained from Equation 26 should be multiplied by its respective regional biasing factor prior to being used in estimating the actual heat loss from a resting diver (Eq. 5). For the case of the head, we suggest that the biasing factor associated with the torso be applied since the vasomotor reflex of the torso and abdomen better approximate that of the head and neck than does that of the limbs. Because it was highly incongruous, none of the experimental head data collected during the three immersed DTP evaluations was considered in our analysis. Subjects often reported that air collected in the hood during the experiments, thus compromising the inherent thermal insulation and precipitating leakage around the hood-face seal. The large biasing factor associated with the foot in Table 24 is a result of the large differences in the experimental values among the three DTP studies. The wide differences in the experimental data is considered to be anomalous.

#### Discussion and Recommendation

The three DTP garment tests which were used for determining the overall heat transfer coefficient biasing factors of Table 24 were conducted as pragmatic evaluations of the garment ensemble. These tests were never intended to serve the dual role of providing physiological heat loss and skin temperature data for thermal modeling. The experiments in total involved only ten subjects, hardly a reliable statistical base from which to draw definitive conclusions. Furthermore, several problems cited in reference 22 appear to have plagued the subjects throughout all of the suit tests. Inadequate sealing of the dry suit's outer garment, in particular a leaking joint between the suit and glove, was a common complaint of the experimental subjects.

Another source of concern was the hood worn with the breathing mask. It collected air and, as a result, compromised the integrity of the hood-face seal by permitting leakage into the suit. Our discussions with the principal investigators of these tests indicated that the dry suit may have been under inflated for much of the experimental immersions because of problems associated with the breathing mask configuration. The principal investigators thought that this condition, commonly called suit squeeze, may have reduced the overall insulation of the garment ensemble by hydrostatically compressing the insulative undergarment. Their conjecture seems to be supported by the results of more recent evaluations of an improved version of the same diving suit. Naval Coastal Systems Center investigators found that the total body insulation provided by the suit was substantially increased when the problems noted above were corrected [51].

Recognizing the limitations and constraints associated with the cited data, we suggest that the biasing factors of Table 24 be employed with the model presented until better correlating factors can be obtained from data collected during controlled experiments. Although the biasing factors were developed by using the results of studies wherein the subjects remained primarily prone, we recommend their application for a resting diver, regardless of his posture. The variation of the local overall conductance due to posture is considered when the hypothetical value of  $U_1(j)$  is computed by Equation 26. Our predictive model may be easily transferred to other garment configurations if the characteristics of the suit materials are known and if they satisfy the same assumptions as developed for the DTP ensemble.

Additional experiments need to be conducted not only for the prone, resting diver, but also for the sitting and standing diver while at rest. Special care should be taken during these experiments to obtain reproducible conditions among the experiments, particularly with respect to posture and

ambient environmental conditions. Such experiments will result in statistically reliable data and better correlations for the overall heat transfer coefficient from divers in conventional attitudes. As well, basic experiments should be performed to investigate the velocity field which exists around the diver for the various postures cited to permit a more definitive development of the outer garment film coefficient. Although this investigation deals only with a model for a resting diver, we recommend the conduct of similar experiments at various work rates in order to develop well-authenticated predictive models for working divers. We decided (in consultation with our Navy Medical Research and Development Command sponsor) to defer the development of the working model until more experimental data was available. This decision was reached because of the lack of available working experimental data recorded in similar ambient environments and at the same rate of work.

Since it can be argued that some body regions are more like truncated cones than cylinders, we have examined the effects of using a truncated cone rather than a cylinder as a body region. Based on information that is presented by Webb [23] and on personal observation, it seems reasonable to assume that the thigh is the most probable body region to be defined as a truncated cone. Table 25 displays median data which was taken from reference 23 for the circumference of the upper and lower thigh. The radii that correspond to each of these circumferences is also presented.

Table 25

Geometrical Data for the Thigh  
Adapted from Data Presented by Webb [23]

	<u>Circumference</u>		<u>Radius (R) in CM</u>
	Inches	CM	$R = \text{Circumference}/2\pi$
Upper Thigh	25.1	63.75	10.15
Lower Thigh	17.0	43.18	6.87

Length of Thigh = 38.3 CM, from Table 5

To compare the improvement in the model that might be attained by using a cone instead of a cylinder for the thigh, the effects of these geometries on the predictive heat loss model must be examined. Inspection of Equation 26 indicates that, except for the resistance of the Thinsulate undergarment ( $R_{TH}$ ), the thermal conductivity of outer garment ( $k_{og}$ ), and the convective heat transfer coefficient ( $h_o$ ); all of the terms in the denominator are solely functions of the various radii. The thermal conductivity of the outer garment,  $k_{og}$ , is assumed to be constant and is only a function of the thickness. The thermal resistance of the undergarment,  $R_{TH}$ , was empirically derived from experiments which were performed with flat samples, and the logarithm of the ratio of radii (Eq. 26) is intended to correct for the curvature associated with its application to a cylinder. The convective heat transfer coefficients,  $h_o$ , were derived from geometry independent information except for the characteristic length, which appears in both the Grashof and Nusselt numbers. For vertical regions, this length could be arbitrarily defined as either the vertical height,  $L$ , or the slant height,  $S$ , of Figure 73. For horizontal regions, this length is a characteristic diameter. From these findings, it is apparent that the effects of the change in geometry are restricted to changes in the radii and the associated slant height.

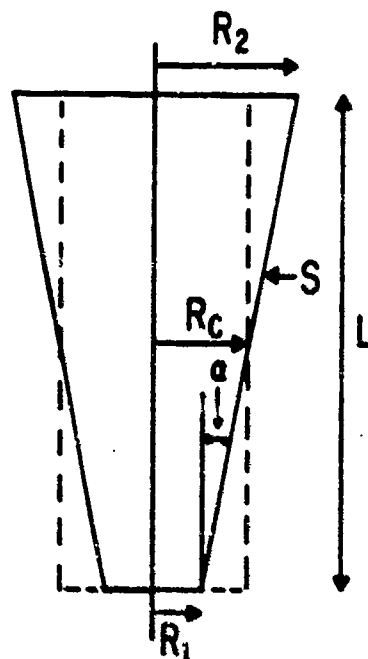


Figure 73. Representative Region Presented as a Truncated Cone.

To examine the possibility of approximating a cone with a cylinder, we assumed that the surface area and the vertical height must remain the same as cited by Webb [23]. This assumption results from the hypothesis that, irregardless of the shapes assumed for the various regions, the model man must continue to approximate an average Navy diver. Therefore, the height and surface area of the regions must remain unchanged. Equation 37 is written by equating the surface area of a cylinder and a truncated cone. For the purposes of this comparison, end effects are neglected.

$$2\pi R_c L = \pi(R_1 + R_2) \sqrt{(R_2 - R_1)^2 + L^2} \quad (37)$$

where:  $R_c$  = Radius of a cylinder

$L$  = Vertical height

$R_1$  = Smaller radius (Fig. 73)

$R_2$  = Larger radius (Fig. 73)

Dividing both sides of Equation 37 by  $2\pi L$  yields Equation 38.

$$R_c = \frac{R_1 + R_2}{2} \cdot \frac{\sqrt{(R_2 - R_1)^2 + L^2}}{L} \quad (38)$$

Equation 38 indicates that a cone may be approximated by a cylinder of radius  $\frac{R_1 + R_2}{2}$  if the square root term divided by  $L$  (in Eq. 39) is approximately equal to one. Substituting the upper and lower thigh radii (Table 25) for  $R_2$  and  $R_1$ , respectively, into Equation 39 yields a value of  $\cos \alpha$  equal to 0.9964.

$$\cos \alpha = \left( \frac{\sqrt{(R_2 - R_1)^2 + L^2}}{L} \right)^{-1} \quad (39)$$

where:  $\cos \alpha$  = Cosine of angle  $\alpha$  in Figure 73

$R_2$  = 10.15 CM (Table 25)

$R_1$  = 6.87 CM (Table 25)

$L$  = 38.3 CM (Table 25)

The value of 0.9964 from Equation 39 corresponds to an angle  $\alpha$  of approximately 4.86°. Since this angle is small, it is reasonable to assume that the thigh may be treated as a cylinder without introducing any significant error in our predictive model. The thigh is probably the region

that is least like a cylinder, therefore, we also assume that all other possible conical regions may be treated as cylinders without causing significant errors in our predictive model. Since pressure is considered to act uniformly in all directions at a particular depth, we can assume that the pressure would act on the inclined surface of a cone normal to the unit area. Thus, the hydrostatic head at a given depth below the shoulder crest would result in the same net compression on the inclined surface of the cone as the cylinder. This indicates that the ratios of the radii would be the same with either geometry. From this additional consideration, we conclude that use of conical geometries for certain regions would be of little merit in increasing the accuracy of our model as it is now defined.